

# UNCLASSIFIED

AD NUMBER
AD461713
NEW LIMITATION CHANGE
TO Approved for public release, distribution unlimited
FROM Distribution authorized to U.S. Gov't. agencies and their contractors; Administrative/Operational Use; NOV 1964. Other requests shall be referred to U.S. Air Force Flight Dynamics Laboratory, Attn: Research and Technology Division, Wright-Patterson AFB, OH 45433.
AUTHORITY
AFFDL ltr, 21 Oct 1974

THIS PAGE IS UNCLASSIFIED

UNCLASSIFIED

AD\_ 4 6 1 7 1 3

DEFENSE DOCUMENTATION CENTER

FOR

SCIENTIFIC AND TECHNICAL INFORMATION

CAMERON STATION ALEXANDRIA, VIRGINIA



UNCLASSIFIED

NOTICE: When government or other drawings, specifications or other data are used for any purpose other than in connection with a definitely related government procurement operation, the U. S. Government thereby incurs no responsibility, nor any obligation whatsoever; and the fact that the Government may have formulated, furnished, or in any way supplied the said drawings, specifications, or other data is not to be regarded by implication or otherwise as in any manner licensing the holder or any other person or corporation, or conveying any rights or permission to manufacture, use or sell any patented invention that may in any way be related thereto.

461713

CATALOGED BY: DDC

461713

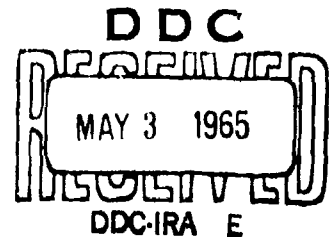
AFFDL-TR-64-161

HIGH TEMPERATURE INVESTIGATION OF VARIOUS  
CREW ESCAPE CONCEPTS FOR THE  
REENTRY FLIGHT REGIME

TECHNICAL REPORT NO. AFFDL-TR-64-161  
November 1964

AF Flight Dynamics Laboratory  
Research and Technology Division  
Air Force Systems Command  
Wright Patterson Air Force Base, Ohio

Project No. 1362, Task No. 136203



(Prepared under Contract No. AF33(615)-1131 by General Dynamics|Astronautics  
a Division of General Dynamics Corporation, San Diego, California;  
C. J. Cohan, G. Campbell, W. Herman, W. Nugent and J. Heathman, authors)



## NOTICES

When Government drawings, specifications, or other data are used for any purpose other than in connection with a definitely related Government procurement operation, the United States Government thereby incurs no responsibility nor any obligation whatsoever; and the fact that the Government may have formulated, furnished, or in any way supplied the said drawings, specifications, or other data, is not to be regarded by implication or otherwise as in any manner licensing the holder or any other person or corporation, or conveying any rights or permission to manufacture, use, or sell any patented invention that may in any way be related thereto.

Qualified users may obtain copies of this report from Defense Documentation Center.

Foreign announcement and dissemination of this report is not authorized.

DDC release to OTS is not authorized. The distribution of this report is limited because the report contains technology identifiable with items on the strategic embargo lists excluded from export or re-export under U. S. Export Control Act of 1949 (63 Stat. 7) as amended (50 U.S.C. App. 2020.2031) as implemented by AFR 400-10.

Copies of this report should not be returned to the Research and Technology Division, Wright-Patterson Air Force Base, Ohio, unless return is required by security considerations, contractual obligations, or notice on a specific document.

# FOREWORD

This report describes the work accomplished in an investigation of crew escape concepts for maximum temperature capability during the reentry flight regime by General Dynamics/Astronautics, San Diego, California, under Air Force Contract Number AF 33(615)-1131. The program was conducted for the Recovery and Crew Station Branch of the Air Force Flight Dynamics Laboratory, Research and Technology Division, Air Force Systems Command, Wright-Patterson Air Force Base, Ohio. Mr. R. Sheldon was the program engineer for the Laboratory.

The objective of the program was to investigate single-place reentry escape system concepts and their associated separation techniques permitting successful escape from a lifting type flight vehicle operating at its maximum temperature capability during the reentry flight regime. This is part of a continuing effort to obtain escape systems design criteria under Project 1362, "Crew Escape for Flight Vehicles", and Task 136203, "Aeronautical Crew Escape Techniques".

General Dynamics/Astronautics Project Leader was Mr. C. J. Cohen. Other key Astronautics personnel assigned to the project were Mr. W. Egli, configuration design; Mr. F. Plummer, escape rocket analysis; Mr. G. Campbell and Mr. W. Herman, performance analysis and aerodynamics; Mr. G. Schadt, aerodynamic heating; Mr. A. Eugent and Mr. J. Heathman, separation interface and disconnect techniques. The contractor's report number is GD/A-JOB-64-076.

This technical report has been reviewed and is approved.

THELSON J. BAKER  
Asst. for Research and Technology  
Vehicle Equipment Division  
AF Flight Dynamics Laboratory

## ABSTRACT

This report presents the results of an analysis of escape system separation techniques from a maximum heating re-entry trajectory. Four escape capsule concepts applicable to a lifting type flight vehicle were considered. These are (1) a separable-nose ballistic body; (2) a separable-nose lifting body; (3) a pod capsule; (4) a turnaround capsule. The objective of the study was to determine the applicability of these capsules and various thermal protection schemes to providing escape capability from the maximum heating point of a typical lifting re-entry trajectory. The compatibility of escape techniques developed at the maximum heating point with providing escape capability throughout the complete mission profile was also investigated. It was determined that all concepts except the turnaround capsule could provide escape capability throughout the mission. Separation interface structural criteria and disconnect techniques applicable to the four capsule configurations are presented.

## TABLE OF CONTENTS

1	INTRODUCTION	1
2	CONFIGURATIONS AND MISSIONS	2
	2.1 Primary Flight Vehicle	2
	2.2 Escape Capsules	5
3	AERODYNAMIC CHARACTERISTICS	18
	3.1 Hypersonic Aerodynamics	18
	3.2 Supersonic Aerodynamics	20
	3.3 Subsonic Aerodynamics	21
	3.4 Interference Effects	22
4	ANALYSIS TECHNIQUES	54
	4.1 Trajectory Performance	54
	4.2 Aerodynamic Heating	59
5	SEPARATION PROPULSION	64
	5.1 Escape Rocket Design Data	64
	5.2 Escape Rocket Requirements	70
	5.3 Escape Rocket Installation	77
	5.4 Escape Rocket Cooling Requirements	84
6	PERFORMANCE ANALYSIS	90
	6.1 Ballistic Body Capsule	91
	6.2 Lifting Body Capsule	124
	6.3 Pod Capsule	169
	6.4 Turnaround Capsule	202
7	SEPARATION INTERFACE AND DISCONNECT TECHNIQUES	231
	7.1 Vehicle Definitions	231
	7.2 Separation Interface	235
	7.3 Escape Capsule Application	252
8	CONCLUSIONS AND RECOMMENDATIONS	278
	8.1 Conclusions	278
	8.2 Recommendations	280
	REFERENCES	281
	BIBLIOGRAPHY	283

## LIST OF FIGURES

<u>Figure No.</u>	<u>Title</u>	<u>Page</u>
1.	Primary Flight Vehicle Configuration	3
2.	Hypersonic Aerodynamic Characteristics - Primary Flight Vehicle	4
3.	Boost and Re-Entry Trajectory - Primary Flight Vehicle	6
4.	Primary Flight Vehicle Leading Edge Temperature History	7
5.	Primary Flight Vehicle - Recovery Ceiling	8
6.	Human Tolerance Limits to Acceleration	10
7.	Ballistic Body Configuration	14
8.	Lifting Body Configuration	15
9.	Turnaround Capsule Configuration	16
10.	Pod Capsule Configuration	17
11.	Ballistic Body Hypersonic Longitudinal Characteristics	25
12.	Ballistic Body Hypersonic Pitch Stability Derivatives	26
13.	Ballistic Body Hypersonic Lateral - Directional Derivatives	27
14.	Ballistic Body Hypersonic Rolling Velocity Derivatives	28
15.	Ballistic Body Hypersonic Yawing Velocity Derivatives	29
16.	Lifting Body Hypersonic Longitudinal Characteristics	30
17.	Lifting Body Hypersonic Pitch Stability Derivatives	31
18.	Lifting Body Hypersonic Lateral - Directional Derivatives	32
19.	Lifting Body Hypersonic Rolling Velocity Derivatives	33
20.	Lifting Body Hypersonic Yawing Velocity Derivatives	34
21.	Pod Capsule Hypersonic Longitudinal Characteristics	35
22.	Pod Capsule Hypersonic Pitch Stability Derivatives	36
23.	Pod Capsule Hypersonic Lateral - Directional Derivatives	37
24.	Pod Capsule Hypersonic Rolling Velocity Derivatives	38
25.	Pod Capsule Hypersonic Yawing Velocity Derivatives	39
26.	Turnaround Capsule Hypersonic Longitudinal Characteristics, $40^\circ < \alpha < 180^\circ$	40
27.	Turnaround Capsule Hypersonic Longitudinal Characteristics, $-20^\circ < \alpha < 40^\circ$	41
28.	Turnaround Capsule Hypersonic Pitch Stability Derivatives	42
29.	Turnaround Capsule Hypersonic Lateral - Directional Derivatives	43
30.	Turnaround Capsule Hypersonic Rolling Velocity Derivatives	44
31.	Turnaround Capsule Hypersonic Yawing Velocity Derivatives	45
32.	Ballistic Body - Supersonic Aerodynamic Characteristics	46
33.	Lifting Body - Supersonic Aerodynamic Characteristics	47

<u>Figure No.</u>	<u>Title</u>	<u>Page</u>
34.	Pod Capsule - Supersonic Aerodynamic Characteristics	48
35.	Ballistic Body - Subsonic Aerodynamic Characteristics	49
36.	Lifting Body - Subsonic Aerodynamic Characteristics	50
37.	Pod Capsule - Subsonic Aerodynamic Characteristics	51
38.	Ballistic Body Flow Field Interference	52
39.	Pod Hypersonic Interference	53
40.	Autopilot Schematic - Turnaround Capsule	57
41.	Pitch Roll Mixer Schematic	58
42.	Boundary Layer Schematic	61
43.	Effect of Transition Reynolds Number on Temperature	62
44.	Solid Rocket Impulse to Weight Characteristics for Several Operational Short Burn Time Configurations	67
45.	Comparison of Typical Escape Rocket Size vs Number Required ( $F_{TOTAL} = 40K \#$ )	69
46.	Escape Rocket Thrust Characteristics - 40,000 Lbs.	72
47.	Escape Rocket Thrust Characteristics - 25,000 Lbs.	73
48.	Effect of Retro-Rocket Velocity Increment on Re-Entry Conditions	75
49.	Ballistic Body Capsule Escape Rocket Installation	79
50.	Lifting Body Capsule Escape Rocket Installation	81
51.	Turnaround Capsule Escape Rocket Installation	82
52.	Separable Pod Escape Rocket Installation	83
53.	Thermodynamic Model - Rocket Motor Heating	85
54.	Temperature Characteristics in Region of Separation Rockets	89
55.	Ballistic Capsule Angle of Attack Response - Effect of Pitch Damping	99
56.	Ballistic Capsule Dynamic Response - Effect of Thrust Moments	100
57.	Ballistic Capsule Load Factor Characteristics - Effect of Thrust Moments	101
58.	Ballistic Capsule Separation Characteristics - Effect of Thrust Moments	102
59.	Ballistic Capsule Dynamic Response - Effect of Lateral - Directional Disturbances	103
60.	Ballistic Capsule Load Factor and Separation Characteristics Effect of Thrust Level	104
61.	Ballistic Capsule Dynamic Response - Effect of Longitudinal Center of Gravity	105
62.	Effect of Wing Loading on Ballistic Body Escape Trajectories	106
63.	Primary Flight Vehicle - Temperature History Leading Edge	107

<u>Figure No.</u>	<u>Title</u>	<u>Page</u>
64.	Ballistic Capsule Separation Temperature History - Run 6	108
65.	Ballistic Capsule Separation Temperature History - Run 7	109
66.	Ballistic Capsule Separation Temperature History - Run 8	110
67.	Ballistic Capsule Temperature History - Complete Trajectory - Zero Lift	111
68.	Ballistic Body - Orbit Escape Trajectory Characteristics	113
69.	Ballistic Body Capsule - Orbit Re-Entry Trajectories	114
70.	Ballistic Body - Recovery Ceiling	115
71.	Ballistic Body - On-The-Pad Escape Trajectory Characteristics	117
72.	Ballistic Body - Landing Escape Trajectory Characteristics	118
73.	Ballistic Body - Maximum Dynamic Pressure Escape Trajectory Characteristics - Effect of Thrust Moment	120
74.	Ballistic Body - Maximum Dynamic Pressure Escape Trajectory Characteristics - Effect of Reaction Controls	121
75.	Ballistic Body - Maximum Dynamic Pressure Escape Trajectory Characteristics - Separation Distance	122
76.	Ballistic Body - Maximum Dynamic Pressure Escape Trajectory Characteristics - Effect of Initial Pitch Rate	123
77.	Lifting Body Capsule Dynamic Response - Effect of Aerodynamic and Reaction Control Pitch Damping	135
78.	Lifting Body Dynamic Response - Effect of Aerodynamic, Thrust Gimbal and Reaction Pitch Damping	136
79.	Lifting Body Motion Characteristics - Nominal Trajectory	137
80.	Lifting Body Load Factor Characteristics Including Thrust Moments - Nominal Trajectory	138
81.	Lifting Body Separation Characteristics - Nominal Trajectory	139
82.	Lifting Body Dynamic Response - Effect of High Trim Angle of Attack	140
83.	Lifting Body Dynamic Response - Effect of Lateral - Directional Disturbances	141
84.	Lifting Body Load Factor and Separation Characteristics - Effect of Thrust Level	142
85.	Lifting Body Dynamic Response - Effect of Longitudinal Center of Gravity	143
86.	Lifting Body Separation Characteristics - Effect of Thrust Angle	144
87.	Lifting Body Trajectories - Effect of Angle of Attack Variation	145
88.	Effect of Wing Loading and Trim Alpha on Lifting Body Escape Trajectories	146
89.	Lifting Body Separation - Leading Edge Temperature Histories Effect of Aerodynamic Control, Reaction Control and Thrust Gimbaling	147

<u>Figure No.</u>	<u>Title</u>	<u>Page</u>
90.	Lifting Body Separation - Lower Flap Temperature History - Trajectory 3	148
91.	Lifting Body Capsule Separation - Leading Edge and Lower Surface Temperature Histories - Effect of Trim Angle	149
92.	Lifting Body Separation - Temperature Histories - Nominal Trajectory 6	150
93.	Lifting Body Separation - Leading Edge and Side Flap Temperature Histories - Effect of Initial Sideslip Angle, Trajectory 8	151
94.	Lifting Body Leading Edge Temperature Histories - Effect of Fixed Angle of Attack	152
95.	Lifting Body Leading Edge Temperature Histories - Effect of Varying Angle of Attack	153
96.	Lifting Body - Leading Edge Heating - Effect of Wing Loading - Final Trim Alpha = $15^{\circ}$	154
97.	Lifting Body - Leading Edge Heating - Effect of Wing Loading - Final Trim Alpha = $30^{\circ}$	155
98.	Lifting Body - Orbit Escape Trajectory Characteristics	157
99.	Lifting Body Capsule - Orbit Re-Entry Trajectory	158
100.	Lifting Body - Recovery Ceiling	159
101.	Lifting Body - On-The-Pad Escape Trajectory Characteristics	161
102.	Lifting Body - On-The-Pad Escape Trajectory Characteristics Effect of Control Type and Trim Angle	162
103.	Lifting Body - Landing Approach Escape Trajectory Characteristics	163
104.	Lifting Body - Landing Approach Escape Trajectory Effect of Control Type and Trim Angle	164
105.	Lifting Body - Maximum Dynamic Pressure Escape Trajectory Characteristics - Effect of Control Type	166
106.	Lifting Body - Maximum Dynamic Pressure Escape Trajectory Characteristics - Effect of Trim Angle and Initial Pitch Rate	167
107.	Lifting Body - Maximum Dynamic Pressure Escape Trajectory Characteristics	168
108.	Pod Capsule Dynamic Response - Nominal Trajectory	177
109.	Pod Capsule Load Factor Characteristics - Effect of Thrust Level	178
110.	Pod Capsule Separation Characteristics - Effect of Thrust Level	179
111.	Pod Capsule Dynamic Response - Effect of Thrust Moment and Thrust Gimbal	180
112.	Pod Capsule Dynamic Response Effect of Aerodynamic Damping	181



<u>Figure No.</u>	<u>Title</u>	<u>Page</u>
113.	Pod Capsule Dynamic Response - Effect of Lateral - Directional Disturbances	182
114.	Pod Capsule Separation Characteristics - Effect of Thrust Angle	183
115.	Pod Capsule Dynamic Response - Effect of Trim Angle of Attack and Center of Gravity Location	184
116.	Effect of Wing Loading and Trim Alpha on Pod Capsule Escape Trajectories	185
117.	Pod Capsule Temperature Histories - Nominal Run - Nose, Lower Flap and Upper Surface	186
118.	Pod Capsule Temperature Histories - Nominal Run - Lower Surface	187
119.	Pod Capsule Temperature Histories - Run 11 Upper and Lower Surface	188
120.	Pod Capsule - Effect of Wing Loading - Trim Alpha = $14^{\circ}$	189
121.	Pod Capsule - Orbit Escape Trajectory Characteristics	191
122.	Pod Capsule - Orbit Re-Entry Trajectories	192
123.	Pod Capsule - Recovery Ceiling	193
124.	Pod Capsule - On-The-Pad Escape Trajectory Characteristics	195
125.	Pod Capsule - On-The-Pad Escape Trajectory Characteristics Effect of Control Type and Thrust Moments	196
126.	Pod Capsule - Landing Approach Escape Trajectory Characteristics - Effect of Control Type	197
127.	Pod Capsule - Landing Approach Escape Trajectory Characteristics	198
128.	Pod Capsule - Maximum Dynamic Pressure Escape Trajectory Characteristics	200
129.	Pod Capsule - Maximum Dynamic Pressure Escape Trajectory Characteristics, Effect of Control Type and Thrust Moments	201
130.	Turnaround Capsule Dynamic Response - Nominal Trajectory	210
131.	Turnaround Capsule Load Factor Characteristics - Nominal Trajectory	211
132.	Turnaround Capsule Separation Characteristics - Nominal Trajectory	212
133.	Turnaround Capsule Dynamic Response - Effect of Flap Deflection Point	213
134.	Turnaround Capsule Dynamic Response - Effect of Lateral - Directional Disturbances	214
135.	Turnaround Capsule Dynamic Response - Effect of Aerodynamic and Reaction Control Pitch Dumping	215

<u>Figure No.</u>	<u>Title</u>	<u>Page</u>
136.	Turnaround Capsule Dynamic Response - Effect of Command Pitch Rate and Thrust Moments	216
137.	Turnaround Capsule Dynamic Response - Effect of Longitudinal Center of Gravity	217
138.	Turnaround Capsule Dynamic Response - Effect of Thrust Level, Thrust Angle and Burning Time	218
139.	Turnaround Capsule Load Factor and Separation Characteristics - Effect of Thrust Level, Thrust Angle and Burning Time	219
140.	Effect of Wing Loading on Turnaround Capsule Escape Trajectories	220
141.	Heat Shield Temperature History - Run 1 - Turnaround Capsule	221
142.	Lower Surface Temperature Histories - Run 2 - Turnaround Capsule	222
143.	Flap Temperature Histories - Run 1 and Run 6 - Turnaround Capsule	223
144.	Heat Shield Temperature - Long Time Trajectory - Turnaround Capsule	224
145.	Turnaround Capsule - Orbit Escape Trajectory Characteristics	226
146.	Turnaround Capsule - Orbit Re-Entry Trajectories	227
147.	Turnaround Capsule - Recovery Ceiling	228
148.	Turnaround Capsule - Maximum Dynamic Pressure Escape Trajectory Characteristics	229
149.	Turnaround Capsule - Subsonic Escape Trajectory Characteristics	230
150.	Typical Hot Truss Cross Section	232
151.	Radiation Cooled Panel Attachment	233
152.	Structural Temperature History at Explosive Disconnect	238
153.	Explosive Charge Heat Transfer Model	239
154.	Ignition System Schematic	241
155.	Lifting Body and Ballistic Body Structural Disconnect	243
156.	Turnaround Body Structural Disconnect	245
157.	Turnaround Body Shear Joint	246
158.	Tension Failure Disconnect	247
159.	Electrical & Electronic Disconnect	249
160.	Centrifugal Clutch and Control Disconnect	250
161.	Fluid and Environmental Supply Disconnect	251
162.	Ballistic Capsule Separation Forces	253
163.	Ballistic Body - Load Normal to Guides - Thrust Build Up = 550,000 Lb/Sec.	254

<u>Figure No.</u>	<u>Title</u>	<u>Page</u>
164.	Ballistic Body - Load Normal to Guides - Thrust Build-Up = 775,000 Lbs/Sec.	255
165.	Ballistic Body - Translation Distance	257
166.	Ballistic Body - Rotation Characteristics	258
167.	Ballistic Body Capsule - Separation Interface Design	259
168.	Lifting Body - Load Normal to Guides	261
169.	Lifting Body - Translation Distance	263
170.	Lifting Body - Rotation Characteristics	264
171.	Lifting Body Capsule - Separation Interface Design	265
172.	Turnaround Capsule - Separation Interface Design	266
173.	Turnaround Capsule - Load Time History	269
174.	Pod Side Frame Geometry and Forces	271
175.	Pod Capsule - Separation Interface Design	274
176.	Pod Capsule - Loading Diagram	276
177.	Pod Capsule - Load Time History	277

## LIST OF TABLES

I.	Typical Parameter Range for Escape Type Solid Propellant Rockets	65
II.	Selected Escape Rocket Characteristics	66
III.	Properties of Separation Rocket Modules for Ballistic Capsule	74
IV.	Properties of Separation Rocket Modules for Lifting Body Capsule	74
V.	Thermodynamic Properties	86
VI.	Summary of Conditions for Ballistic Body Re-Entry Trajectory Runs	98
VII.	Summary of Conditions for Ballistic Body Orbit Trajectory Runs	112
VIII.	Summary of Conditions for Ballistic Body Subsonic Trajectory Runs	116
IX.	Summary of Conditions for Ballistic Body Supersonic Trajectory Runs	119
X.	Summary of Conditions for Lifting Body Re-Entry Trajectory Runs	134
XI.	Summary of Initial Conditions for Lifting Body Orbit Trajectory Runs	156
XII.	Summary of Conditions for Lifting Body Subsonic Trajectory Runs	160
XIII.	Summary of Initial Conditions for Lifting Body Supersonic Trajectory Runs	165
XIV.	Summary of Conditions for Pod Capsule Re-Entry Trajectory Runs	176
XV.	Summary of Initial Conditions for Pod Capsule Orbit Trajectory Runs	190
XVI.	Summary of Conditions for Pod Capsule Subsonic Trajectory Runs	194
XVII.	Summary of Initial Conditions for Pod Capsule Supersonic Trajectory Runs	199
XVIII.	Summary of Conditions for Turnaround Re-Entry Trajectory Runs	209
XIX.	Summary of Initial Conditions for Turnaround Capsule Orbit Trajectory Runs	225
XX.	Frame Weight Estimate - Primary Vehicle With Pod Capsule	272

## SECTION 1

## INTRODUCTION

Previous Air Force studies involving the re-entry flight regime of moderate L/D, low orbital flight vehicles, have proposed as a crew escape system, for the flight vehicle, various versions (lifting, ballistic and combinations thereof) of the separable-nose escape system concept. Due to the predominate influence of high performance requirements upon the design philosophy of the total flight vehicle, it has been a characteristic of these proposed re-entry escape systems to have a high ballistic coefficient,  $W/C_{DA}$  or to possess a higher wing loading than the primary flight vehicle. In addition, the stability requirements of the lifting type separable-nose escape concepts often dictate a high trim angle for the escape system, which upon separation from a flight vehicle performing at a lower angle of attack results in large capsule oscillations and high transient heating rates. If the primary flight vehicle is operating at or near its maximum temperature capability, it is readily conceivable that the resultant escape environment will exceed the capabilities of those escape concepts utilizing the heat protective structure of the primary flight vehicle.

The present study was conducted to determine what separation techniques, if any, can be utilized to permit safe escape under the severe aerodynamic heating conditions described above. In addition, the performance was investigated to determine if the separation techniques evolved at the re-entry escape point led to escape capsule recovery capability greater than that of the primary flight vehicle and also to determine the compatibility of the re-entry escape system techniques with respect to providing escape throughout the mission profile of the primary flight vehicle. A final aspect of the study was an investigation to determine the availability of realistic structural design techniques at the escape capsule/primary flight vehicle separation interface.

---

Manuscript released by the author October 1964 for publication as an RTD Technical Report.

## SECTION 2

## CONFIGURATIONS AND MISSIONS

## 2.1 PRIMARY FLIGHT VEHICLE

2.1.1 CONFIGURATION. The primary flight vehicle considered in the present study is a single-place boost glide vehicle assumed to be based on current state-of-the-art technology. A sketch of the primary vehicle is presented in Figure 1 from which it can be seen that it is similar to the Dynasoar vehicle and the primary flight vehicle presented in Reference 1. The vehicle has a low,  $73^\circ$  sweep delta wing with a fuselage mounted above the wing. The wing leading edge has a diameter of .5 feet. The vertical tails are mounted on the upper surface of the wing at the tips. The pilot is housed in conventional aircraft manner in the fuselage forebody. This configuration is such that it can accommodate any of the four proposed escape concepts which will be introduced in Section 2.2 with minor configuration modifications.

The primary flight vehicle is assumed to have a wing loading of 30 psi and be radiation cooled. The details of the primary flight vehicle structure will be discussed in Section 7.1.

The hypersonic aerodynamic data assumed for the primary flight vehicle are presented in Figure 2. It was assumed that these data were invariant throughout the hypersonic regime. The variations in aerodynamic characteristics which do occur in the hypersonic regime are of no particular significance to the present study.

The surface material was assumed to be constant over the vehicle except at the nose. The nose uses a higher temperature capability material since it is at the stagnation point and experiences more severe aerodynamic heating. This is consistent with present re-entry glider design philosophy, e.g., Dynasoar. Excluding the nose therefore, the peak surface temperature will occur at the wing leading edge over the region of available trim angle of attack.

2.1.2 MISSION. The primary flight vehicle is boosted by a vertical take-off rocket into a low altitude earth orbit. As a re-entry vehicle it was assumed that the glider had trim capability between maximum lift and maximum lift-to-drag. The re-entry corridor therefore is between a maximum lift trajectory at zero bank angle and a maximum lift-to-drag ratio trajectory at a bank angle of 45 degrees. This latter trajectory yields approximately the maximum lateral range capability.

The initial re-entry maneuver is assumed to be accomplished in the following manner. The vehicle re-enters the atmosphere trimmed to maximum lift at zero bank angle. This orientation is held through the initial pullout. When a flight path angle of zero degrees is achieved the bank angle is adjusted so that the vehicle flies a constant altitude transition trajectory until it intersects the desired equilibrium glide trajectory.

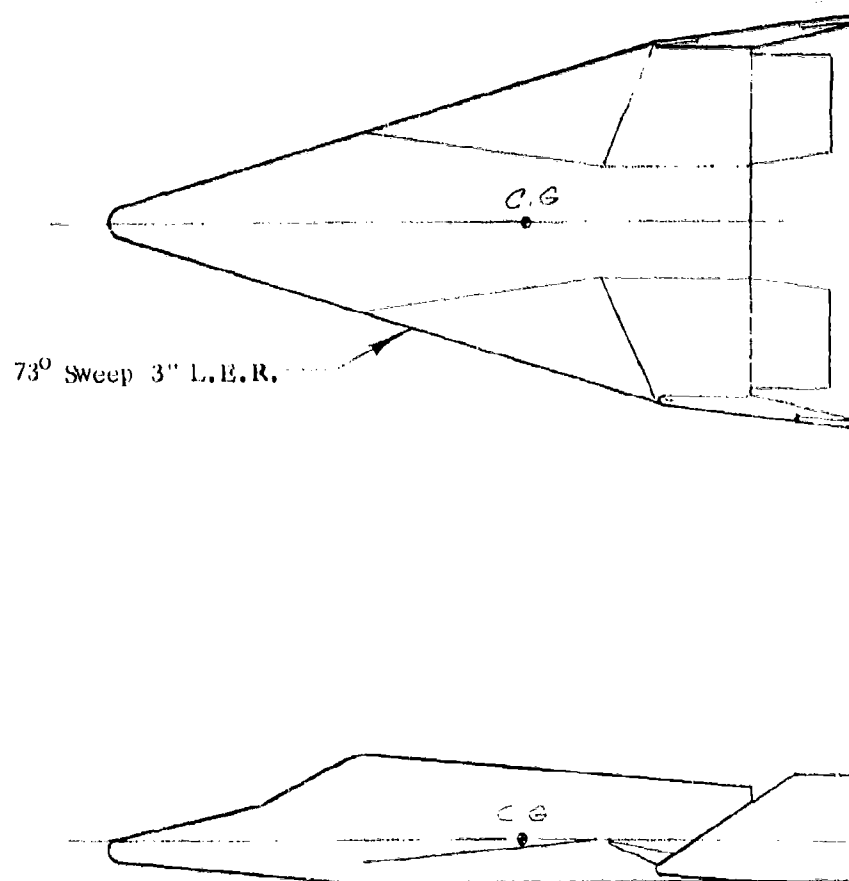


Figure 1 Primary Flight Vehicle Configuration

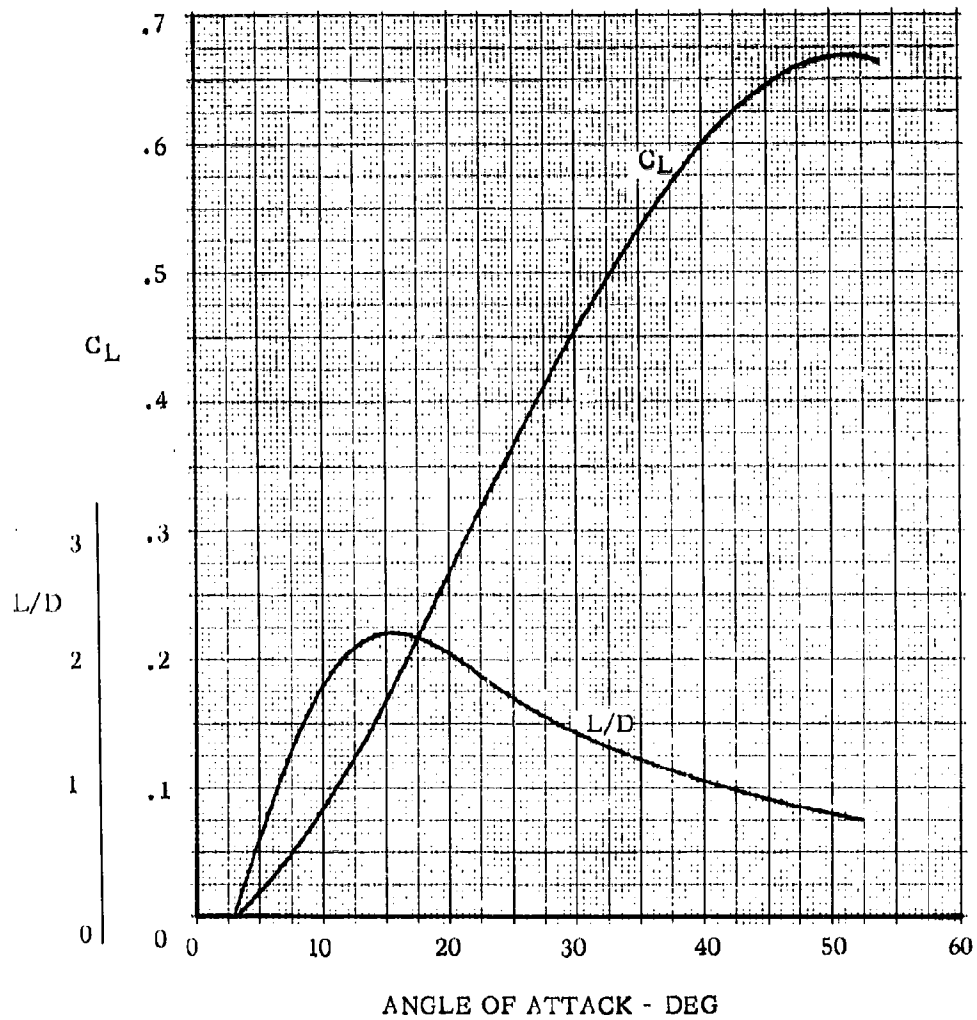


Figure 2 Hypersonic Aerodynamic Characteristics - Primary Flight Vehicle



The primary flight vehicle boost and re-entry trajectories are presented in Figure 3. The re-entry trajectories were calculated using the aerodynamic data presented in Figure 2.

The maximum lift-to-drag ratio,  $45^\circ$  bank angle trajectory, is the maximum heating trajectory. The leading edge temperature history corresponding to this trajectory is presented in Figure 4. It is seen that the peak leading edge temperature is  $3460^\circ\text{R}$  occurring at the following flight conditions:

$$\gamma = -.14 \text{ degrees}$$

$$V = 21913 \text{ fps}$$

$$H = 221241$$

This flight condition was used as the initial condition for the re-entry escape performance studies which will be discussed in Section 6.0.

The maximum dynamic pressure during boost is 825 psf occurring at a velocity of 1800 fps at an altitude of 43,000 ft.

The recovery ceiling of the primary flight vehicle is presented in Figure 5. The recovery ceiling is defined as the locus of maximum apogee altitudes from which the vehicle can recover to level flight without violating its structural load factor of maximum temperature capability. In the present primary flight vehicle the recovery ceiling was determined by aerodynamic heating considerations. The recovery ceiling was calculated assuming a constant angle of attack re-entry. A maximum lift coefficient of .667 was used. Improvements in recovery ceiling capability can be achieved by modulating the lift. However, since the primary flight vehicle recovery ceiling is being used in the present study as a basis for comparison between the various escape capsules, the constant angle of attack maneuver is believed to be adequate.

## 2.2 ESCAPE CAPSULES

2.2.1 GENERAL ESCAPE CAPSULE CRITERIA. An escape capsule for a boost-glide vehicle such as considered in the present study serves two purposes. During normal flight it serves as the crew and sensitive equipment protective compartment and as the control center of the vehicle. The crew compartment is designed primarily to accomplish this function. The second purpose of an escape capsule is, as the name implies, to serve as an escape system for the primary vehicle. Design requirements dictated by escape generally serve as constraints on the design of the crew compartment as the vehicle control center.

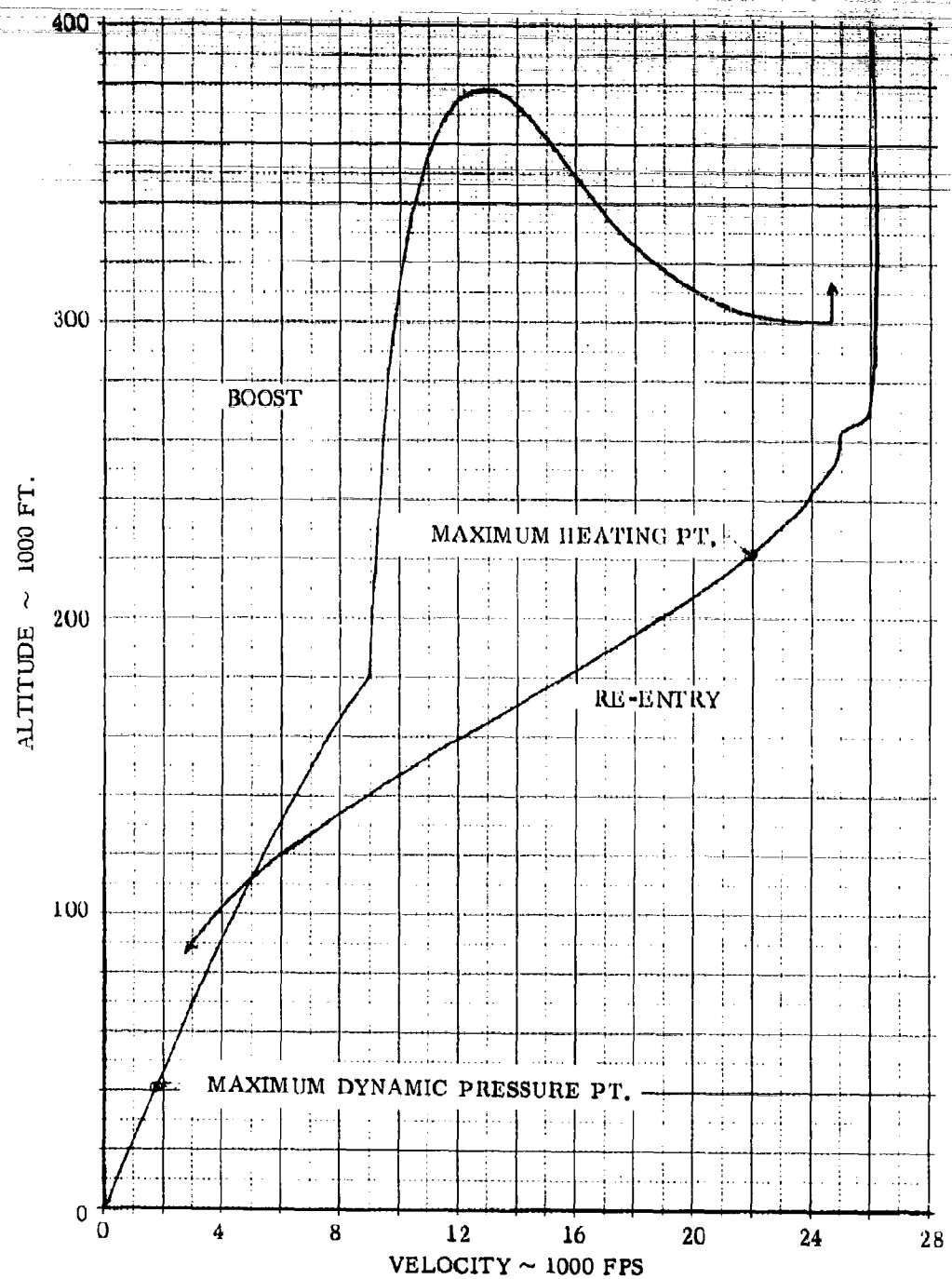


Figure 3 - Boost and Re-Entry Trajectory - Primary Flight Vehicle

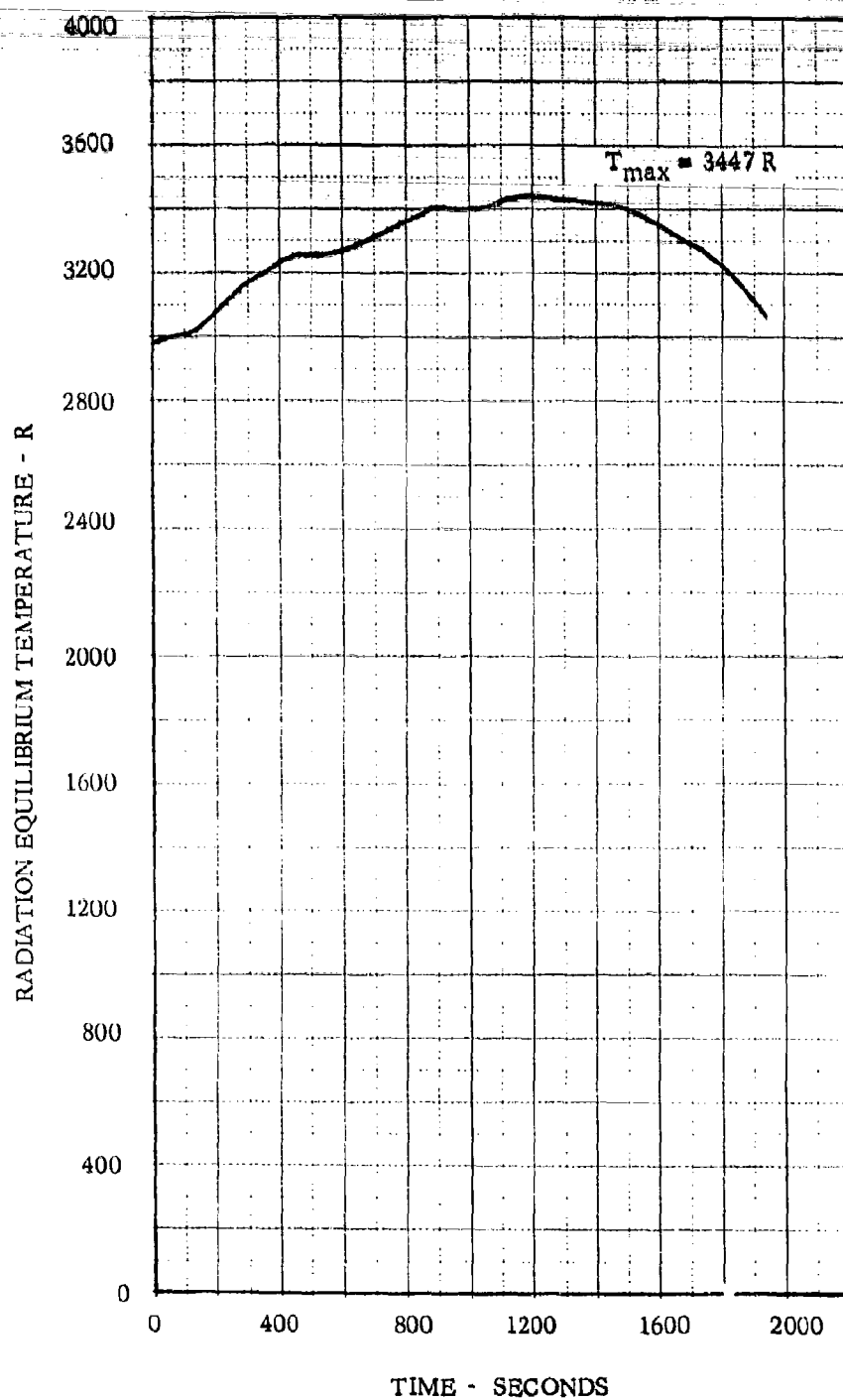


Figure 4 - Primary Flight Vehicle Leading Edge Temperature History

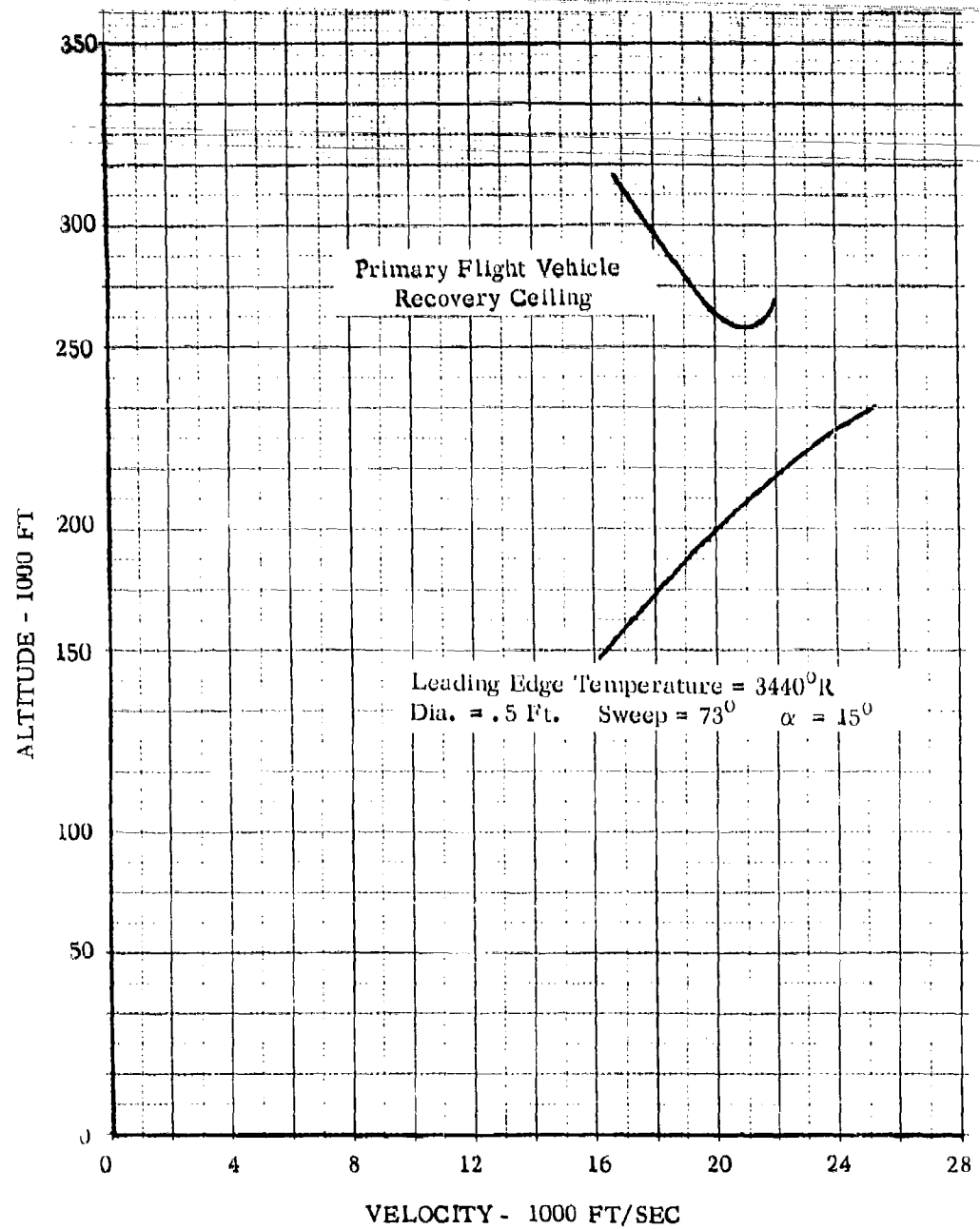


Figure 5 - Primary Flight Vehicle - Recovery Ceiling

An escape capsule for the primary flight vehicle of the present study should meet the following general criteria:

1. The capsule should be capable of providing successful escape throughout the mission profile.
2. The capsule should not compromise the glider's ability to withstand air loads, and/or heating loads.
3. The capsule should not significantly compromise the performance or stability characteristics of the primary-flight vehicle.
4. The capsule should be aerodynamically stable and capable of completely automatic flight throughout the mission profile since the capability of the pilot cannot be assured during emergency situations.
5. The capsule vehicle separation interface should minimize separation interference effects.
6. The capsule should have provisions for a safe impact and in the case of water impact, flotation devices.
7. The capsule should operate within the human tolerance limits to high accelerations and tumbling. For the present study the acceleration limits presented in Figure 6 were assumed and a maximum tumbling limit of 60 RPM was used.
8. The capsule should have provisions for an emergency lift support system.

2.2.2 STABILIZATION AND CONTROL. The studies of Reference 1 have indicated the requirement for an active stabilization and control system for escape capsules. This system is required to permit orientation while in orbit and to insure that at no time during flight will human endurance, structural strength or heating limitations be exceeded.

Outside the atmosphere, stabilization and control is achieved with reaction jet controls. For the present study an  $I_{sp}$  of 135 was used for the reaction controls. The thrust level varied with each configuration and will be described below.

Within the atmosphere stabilization is accomplished aerodynamically. Stability can be inherent in the basic configuration design or can be achieved with the use of extendable aerodynamic surfaces. Control within the atmosphere can be achieved either with aerodynamic controls, (i. e., deflecting surfaces) or reaction controls. However, the use

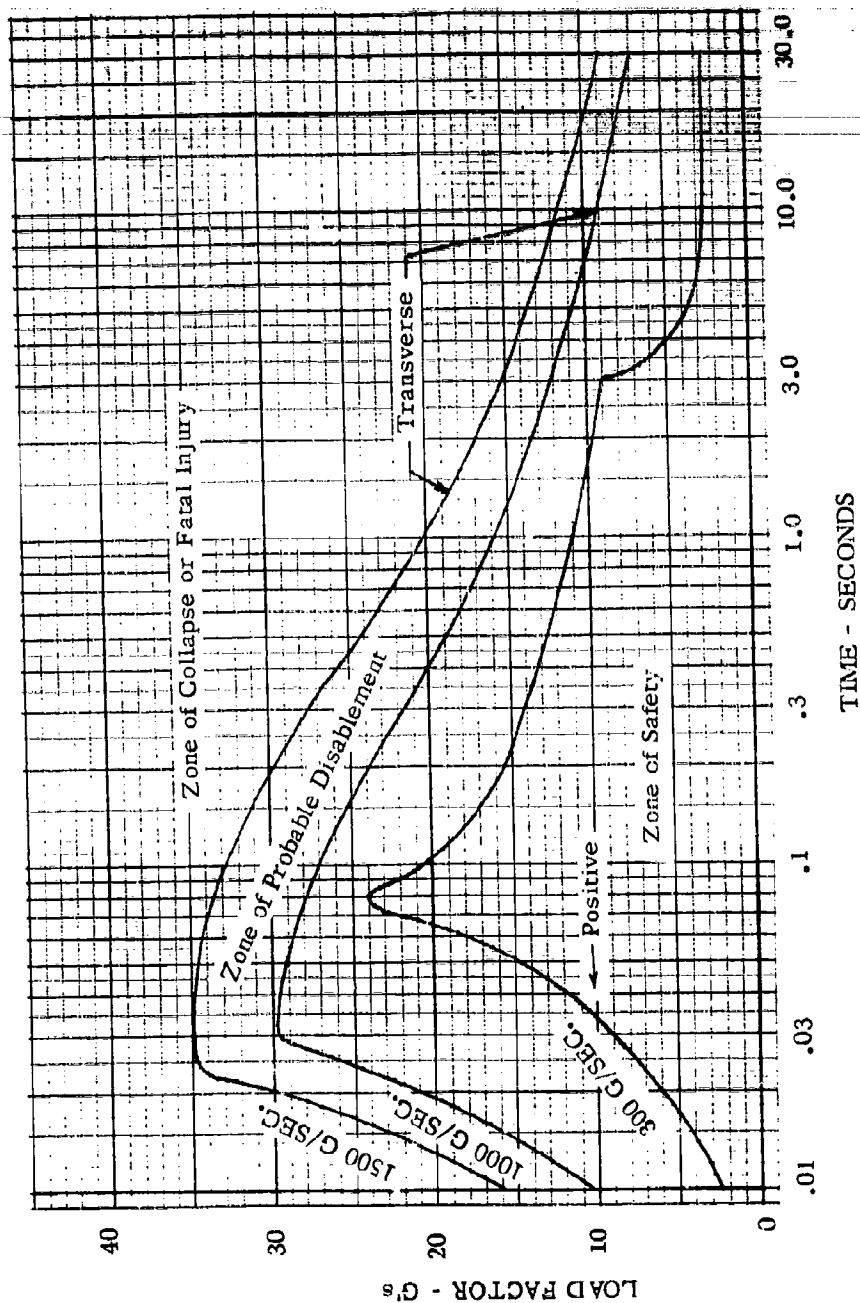


Figure 6 - Human Tolerance Limits to Acceleration

of reaction controls at high dynamic pressure generally requires large thrust forces. The use of variable deflection aerodynamic surfaces may be required to vary trim angle and/or increase drag as well as serving as the damping control. From the standpoint of simplicity, however, which should be an objective of any escape system design, aerodynamic control surfaces having only one or two fixed positions would be desirable. In the present study the applicability of both types of control throughout the mission are investigated.

Flap controls were used as the aerodynamic control; however, the qualitative results obtained with these controls would be applicable also for other types of aerodynamic controls, e.g., booms.

**2.2.3 ESCAPE CAPSULE CONFIGURATIONS.** One of the primary factors affecting the design of re-entry vehicle is the severe aerodynamic heating environment. There are two principal methods of protection from this aerodynamic heating. These are mass transfer (i.e., ablation) or radiation cooling. In ablation heat protection schemes a large part of the heat input to the vehicle is used to melt the ablation material. In order to reduce the weight of ablation material the vehicle should have high drag.

In utilizing the radiation cooling concept the convective heat flux to the body is maintained at such a level that the body is kept within its prescribed temperature limits by the radiation away from the body. This approach is limited by the temperature limits of materials suitable for use on the vehicle surface. The use of this heat protection scheme is generally limited to lifting type vehicles since only these type vehicles achieve radiation equilibrium temperatures within the limits of present state-of-the-art surface materials. Reducing the vehicle wing loading results in higher altitude trajectories which reduces the convective heat transfer.

In many re-entry vehicle designs a combination of these two heat protection schemes is used since the temperature characteristics vary over the surface of the vehicle.

In the present study both of these heat protection techniques have been incorporated in the four escape capsule concepts which were investigated. These configurations will be described below and their structural aspects will be discussed in Section 7.1. The configurations as described below were used in the performance analysis. During the investigation of the separation interface and disconnects it was found necessary to make minor modifications in the basic configurations. These modifications would have some effect on the quantitative aerodynamic characteristics and performance, but would not change the basic escape techniques to be used.

**2.2.3.1 Separable - Nose Ballistic Body.** This configuration which is shown in Figure 7 is a blunt configuration which utilizes an ablation heat shield for thermal protection. The blunt nose of this design will degrade the performance capability of the primary flight vehicle but is included in this study to serve as a baseline vehicle for the evaluation of the various other concepts to be investigated in this program.

This configuration is very similar to the ballistic configuration of Reference 1 and much of the information of Reference 1 has been incorporated into the present investigation. The weight, inertia and center of gravity data as taken from Reference 1 and used in the performance study are presented in Figure 5.

The ballistic body configuration has both aerodynamic and reaction controls. The reaction controls consist of hydrogen peroxide reaction jets located as shown in Figure 7.

Trailing edge flaps are used to provide aerodynamic stability and control and also to increase the drag during re-entry in order to minimize the total heat input. The lower flap has been split into two parts in order to eliminate rocket exhaust impingement on the surfaces. It is assumed that these surfaces are deflected automatically to pre-selected positions which are a function of the position in the primary flight vehicle trajectory. When considering aerodynamic damping in the performance studies it was necessary to use one of the flaps as a damping control.

**2.2.3.2 Separable - Nose Lifting Body.** This configuration, shown in Figure 8, utilizes the basic re-radiative structure of the primary flight vehicle as its thermal protection system. For this reason, the lifting body capsule has the same temperature limits as the primary flight vehicle. This configuration is very similar to the lifting body configuration of Reference 1, and much of the information of Reference 1 has been incorporated into the present investigation. The weight, inertias and center of gravity of this configuration as taken from Reference 1 and used in the performance studies are presented in Figure 8.

The lifting body configuration has both aerodynamic and reaction controls. The aerodynamic controls consist of four flaps located around the body as shown in Figure 8. The two side flaps are used to provide directional stability and the upper and lower flaps are used for longitudinal stability and control. It is assumed that these flaps are deflected automatically to pre-selected positions which are a function of the position in the trajectory. It was found during the course of the investigation that the nominal side flaps shown in Figure 8 were insufficient to provide adequate directional stability. For this reason the effects of 30% larger side flaps were considered. This aspect is discussed in more detail in Section 3.0 where the aerodynamic characteristics of the vehicle are presented.

Reaction control is provided by six reaction jets as shown in Figure 8. Two of the six reaction controls are used for yaw control and the other four are used as both pitch and roll control. A value of 40 lbs. of thrust per nozzle was used with a specific impulse of 135 seconds.

**2.2.3.3 Separable - Nose Turnaround Capsule.** This configuration, shown in Figure 9, utilizes the basic re-radiative structure of the primary flight vehicle with the addition of an ablation heat shield at the separation plane. This configuration is similar to the body portion of the lifting body configuration described above. During normal flight the heat shield is enclosed within the fuselage of the primary flight vehicle. Upon separation during an escape, the capsule is turned around so that the ablation heat shield is in front. The



purpose of examining this configuration is to evaluate a vehicle which has high temperature capability during an escape maneuver as a result of using a blunt ablation heat shield but does not compromise the lift-to-drag ratio performance of the primary flight vehicle. The nominal weight, inertia and center of gravity data used in the performance studies are presented in Figure 9.

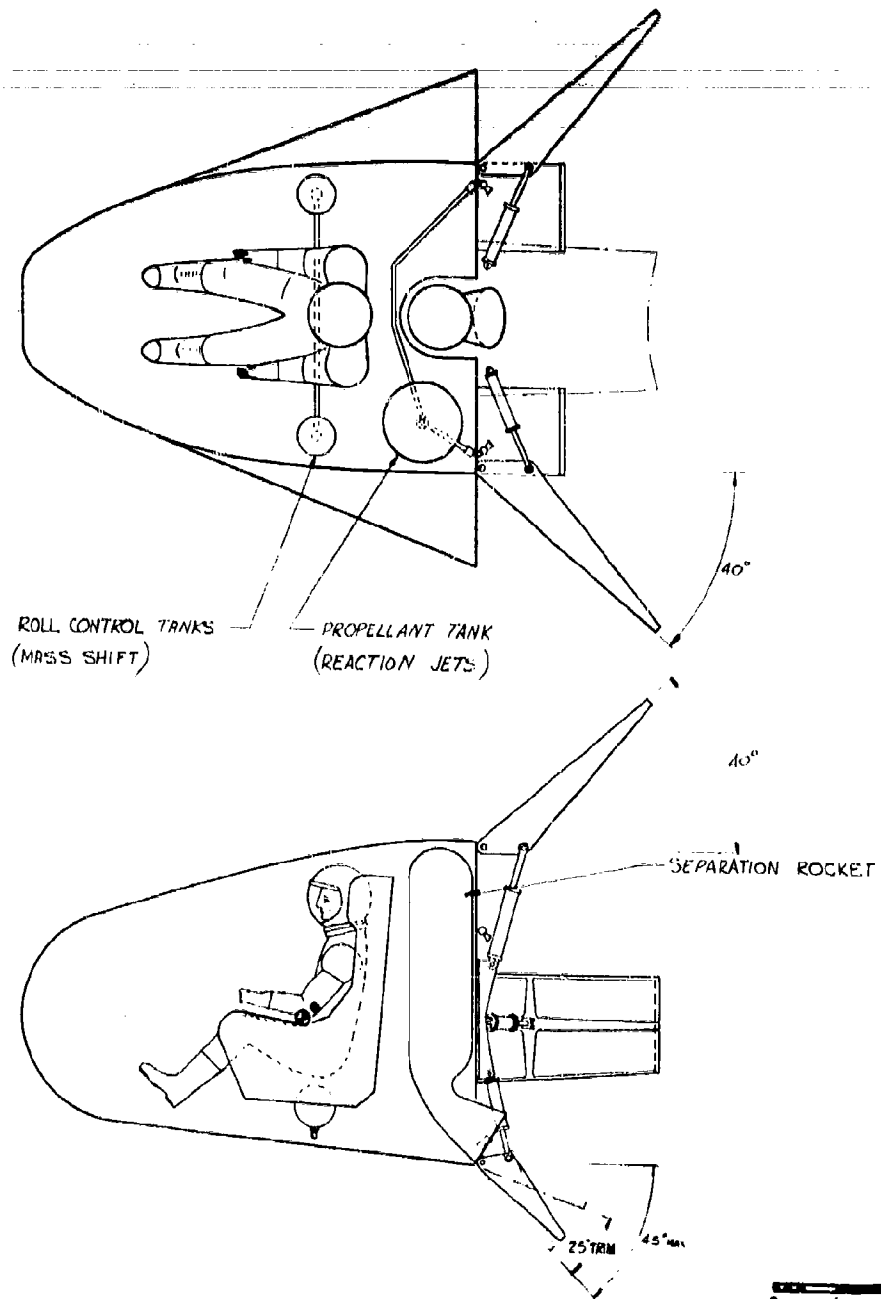
The turnaround configuration has both aerodynamic and reaction controls. The aerodynamic controls consist of three flaps located around the body as shown in Figure 9. The aerodynamic surfaces are required for stability within the atmosphere. Since the flaps are required after the configuration is turned around their hinge line is located at the end of the flap nearest the heat shield. With this arrangement, aerodynamic heating and loading considerations preclude opening the flap until the configuration has turned past ninety degrees.

The reaction control jets are located as shown in Figure 9. Two reaction jets are used to provide control in each of the three planes. A value of 40 lbs. of thrust per nozzle was used for the yaw and roll controls and a value of 80 lbs. for the pitch controls. A specific impulse value of 135 seconds was used.

2.2.3.4 Separable Pod. This configuration shown in Figure 10 consists of the crew cabin portion of the forward fuselage and utilizes the re-radiative structure of the primary flight vehicle for its top surface and an ablation heat shield for its bottom surface. The ablation heat shield is enclosed within the vehicle's fuselage during normal flight. The nominal weight, inertia and center of gravity data used in the performance studies are presented in Figure 10.

The pod configuration utilizes both aerodynamic and reaction controls. The aerodynamic controls consist of five flaps located around the configuration as indicated in Figure 8. Two lower flaps were used to allow a space for the expansion of the rocket exhaust. The two side flaps are used to provide directional stability and the upper and lower flaps are used for longitudinal stability and control. It is assumed that these flaps are deflected automatically to pre-selected deflections. There is a delay in the deflection of the lower flap to allow the pod to clear the primary vehicle.

Six reaction jets as shown in Figure 10 are used for reaction control. Two of the reaction controls are used for control of each of the motions, pitch, roll and yaw. A value of 40 lbs. of thrust per nozzle was used with a specific impulse of 135 seconds.



1 REACTION

2 REACTION

0 1 2 3 4 5 Feet

1

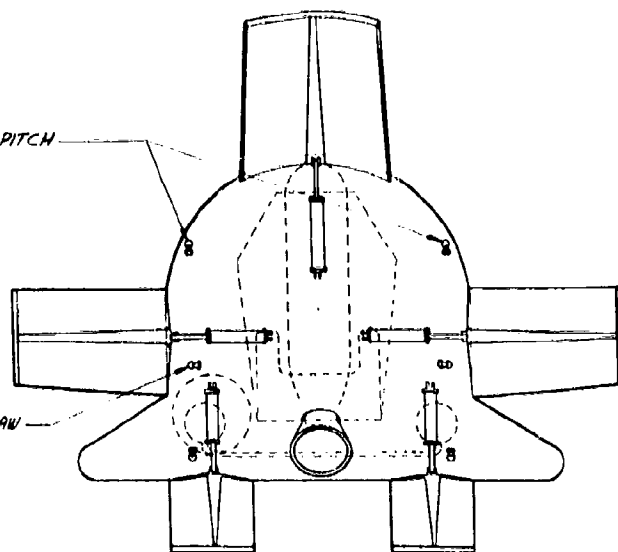
2

VEHICLE DATA	
REFERENCE AREA - PLANFORM	57 SQ. FT
SIDE FLAP AREA - EACH	6.03 SQ. FT
UPPER FLAP AREA	8.1 SQ. FT
LOWER FLAP AREA - TOTAL	4.9 SQ. FT
REFERENCE LENGTH ALONG BODY	7.25 FT
WEIGHT (PRIOR TO THRUSTING)	2680 LB
WEIGHT (AFTER THRUSTING)	2500 LB
$I_{xx}$	190 SLUG · FT <sup>2</sup>
$I_{yy}$	541 " "
$I_{zz}$	530 " "
$I_{xy}$	+56.7 " "

SEPARATION ROCKET DATA	
THRUST (NOM)	40,000 LB
TOTAL IMPULSE	40,000 LB · SEC
PROPELLANT	SOLID
SPECIFIC IMPULSE (S.I.)	220 LB/LB · SEC
THROAT AREA	5.8 SQ. IN.
EXPANSION RATIO	3 : 1
CHAMBER PRESSURE	1000 PSI

4 REACTION JETS - PITCH

2 REACTION JETS - YAW



0 1 2 3 4 5 FEET

Figure 1. Ballistic Body Configuration

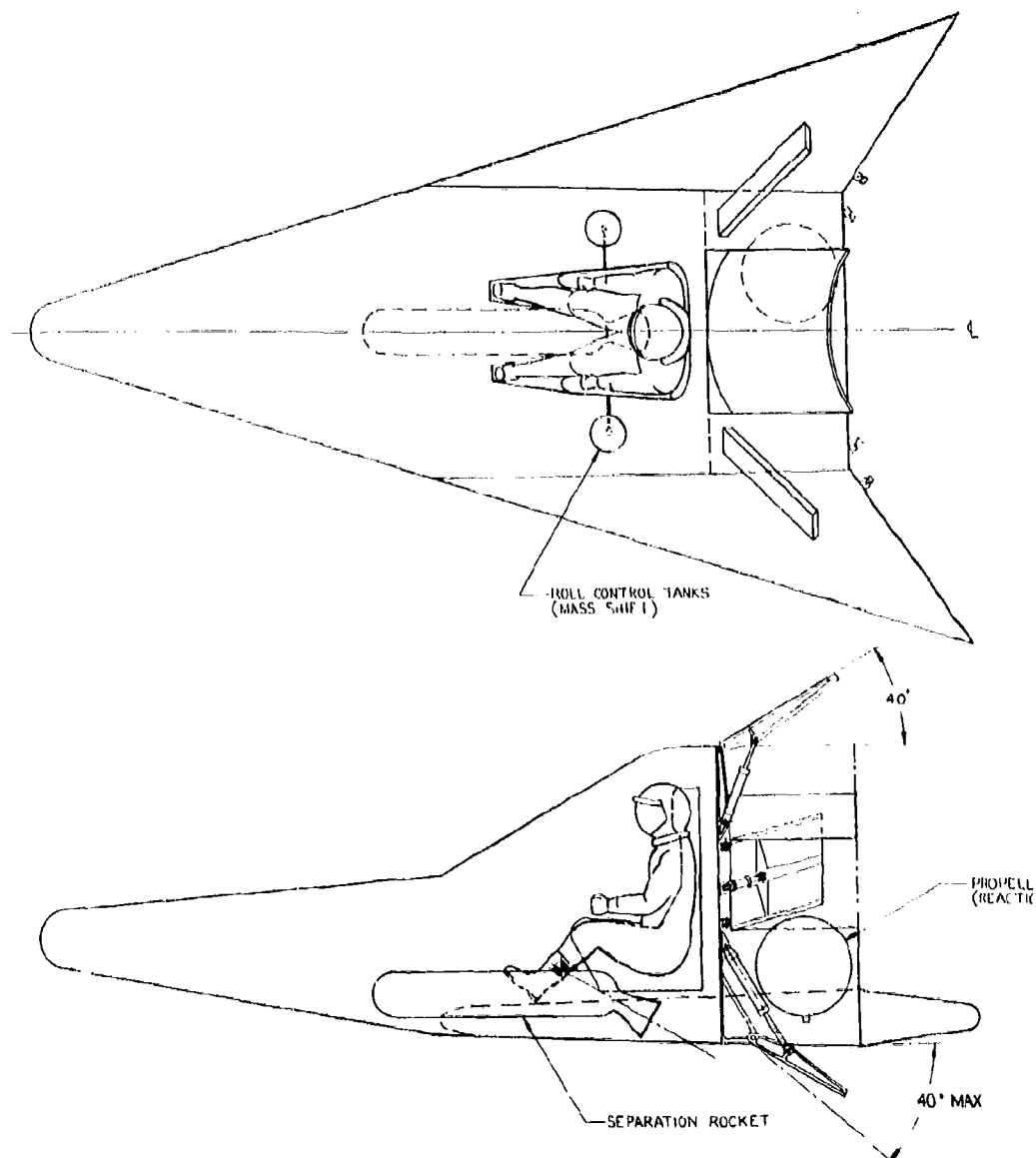
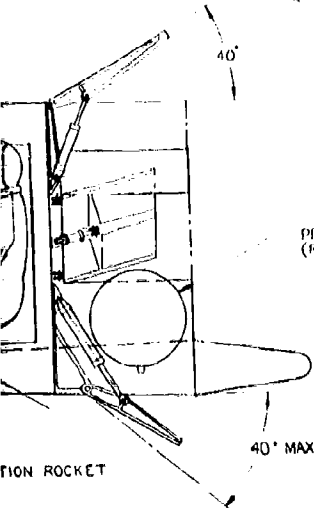
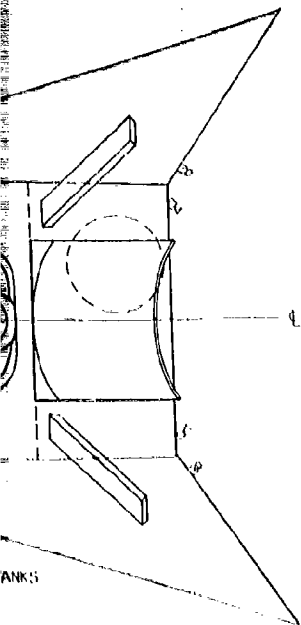


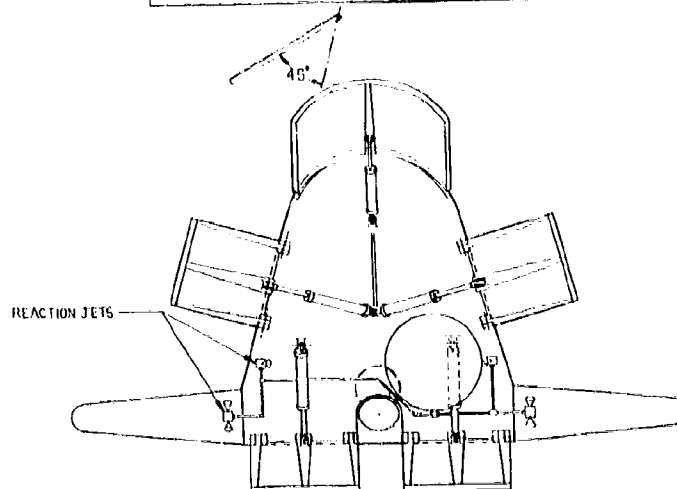
Figure 8 Lifting Body Configuration

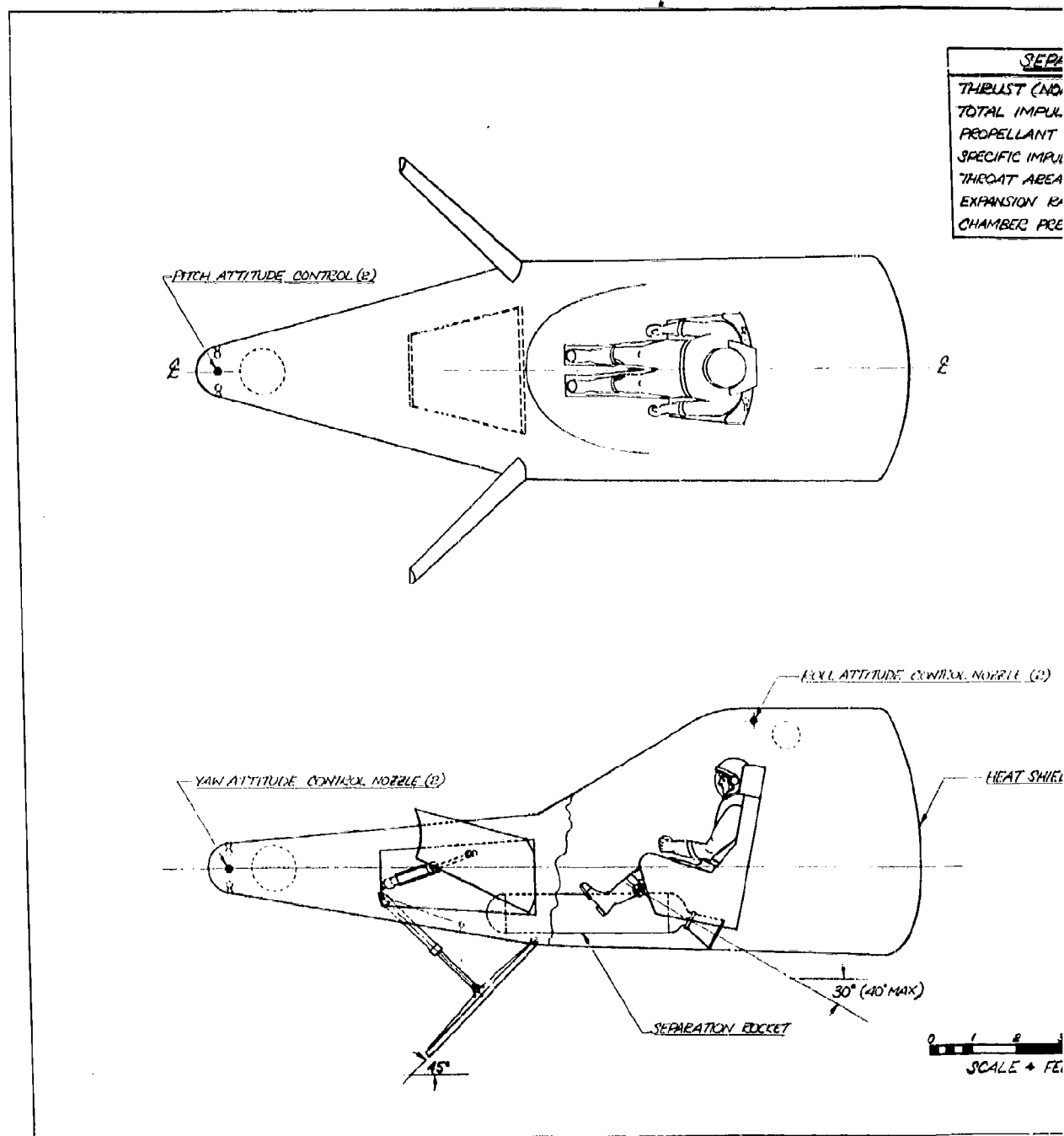


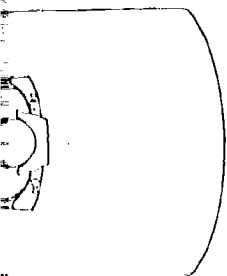
0 1 2 3 4 5 FEET

VEHICLE DATA	
REFERENCE AREA - PLANFORM	88 SQ FT
SIDE FLAP AREA - EACH	3.8 SQ FT
UPPER FLAP AREA	94 SQ FT
LOWER FLAP AREA - TOTAL	60 SQ FT
REFERENCE LENGTH ALONG BODY $\ell$	15.1 FT
WEIGHT (PRIOR TO THRUSTING)	2613 LB
WEIGHT (AFTER THRUSTING)	2500 LB
$I_{xx}$	236 SLUG-FT <sup>2</sup>
$I_{yy}$	971 " "
$I_{zz}$	956 " "
$I_{xy}$	-34 " "

SEPARATION ROCKET DATA	
THRUST (NOMINAL)	25,000 LBS
TOTAL IMPULSE	25,000 LB SEC
PROPELLANT	SOLID
SPECIFIC IMPULSE (SL)	220 LB/LB/SEC
THROAT AREA	5.7 SQ INS
EXPANSION RATIO	3 : 1
CHAMBER PRESSURE	1,000 PSI



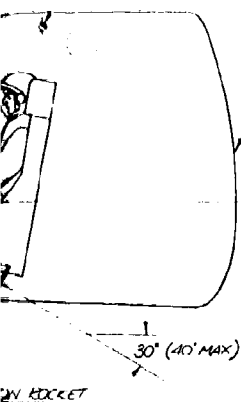




SEPARATION ROCKET DATA	
THRUST (NOMINAL)	25000 LB
TOTAL IMPULSE	25000 LB SEC
PROPELLANT	SOLID
SPECIFIC IMPULSE (SL)	220 LG/LB/RC
THROAT AREA	3.7 IN <sup>2</sup>
EXPANSION RATIO	3:1
CHAMBER PRESSURE	1000 LB/IN <sup>2</sup>

VEHICLE DATA	
REFERENCE AREA - PLANFORM	57.3 FT <sup>2</sup>
SIDE FLAP AREA - EACH	5.2 FT <sup>2</sup>
LOWER FLAP AREA	10.0 FT <sup>2</sup>
REFERENCE LENGTH ALONG BODY Z	15.91 FT
HEIGHT PRIOR TO THRUSTING	2613 LB
HEIGHT AFTER THRUSTING	2500 LB
I <sub>xx</sub>	999 SLUG-FT <sup>2</sup>
I <sub>yy</sub>	136 SLUG-FT <sup>2</sup>
I <sub>zz</sub>	865 SLUG-FT <sup>2</sup>
I <sub>xy</sub>	-205 SLUG-FT <sup>2</sup>

ROLL ATTITUDE CONTROL NOZZLE (2)



SCALE - FEET

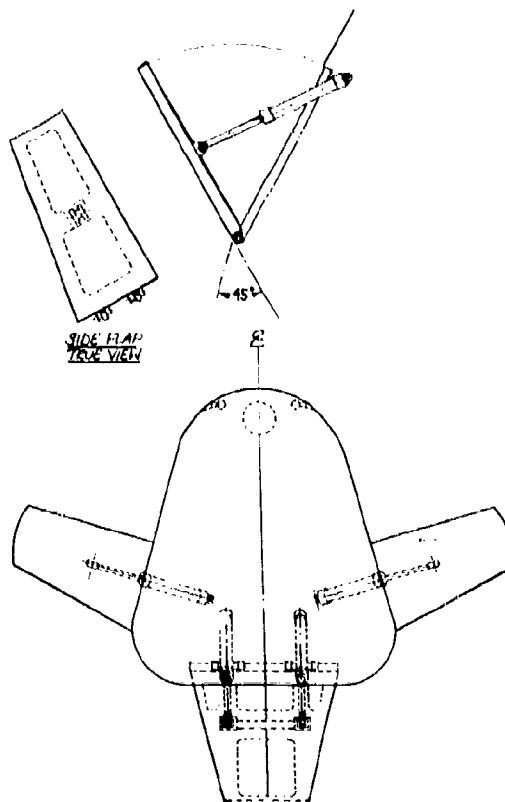


FIGURE 9 - TURNAROUND CAPSULE CONFIGURATION

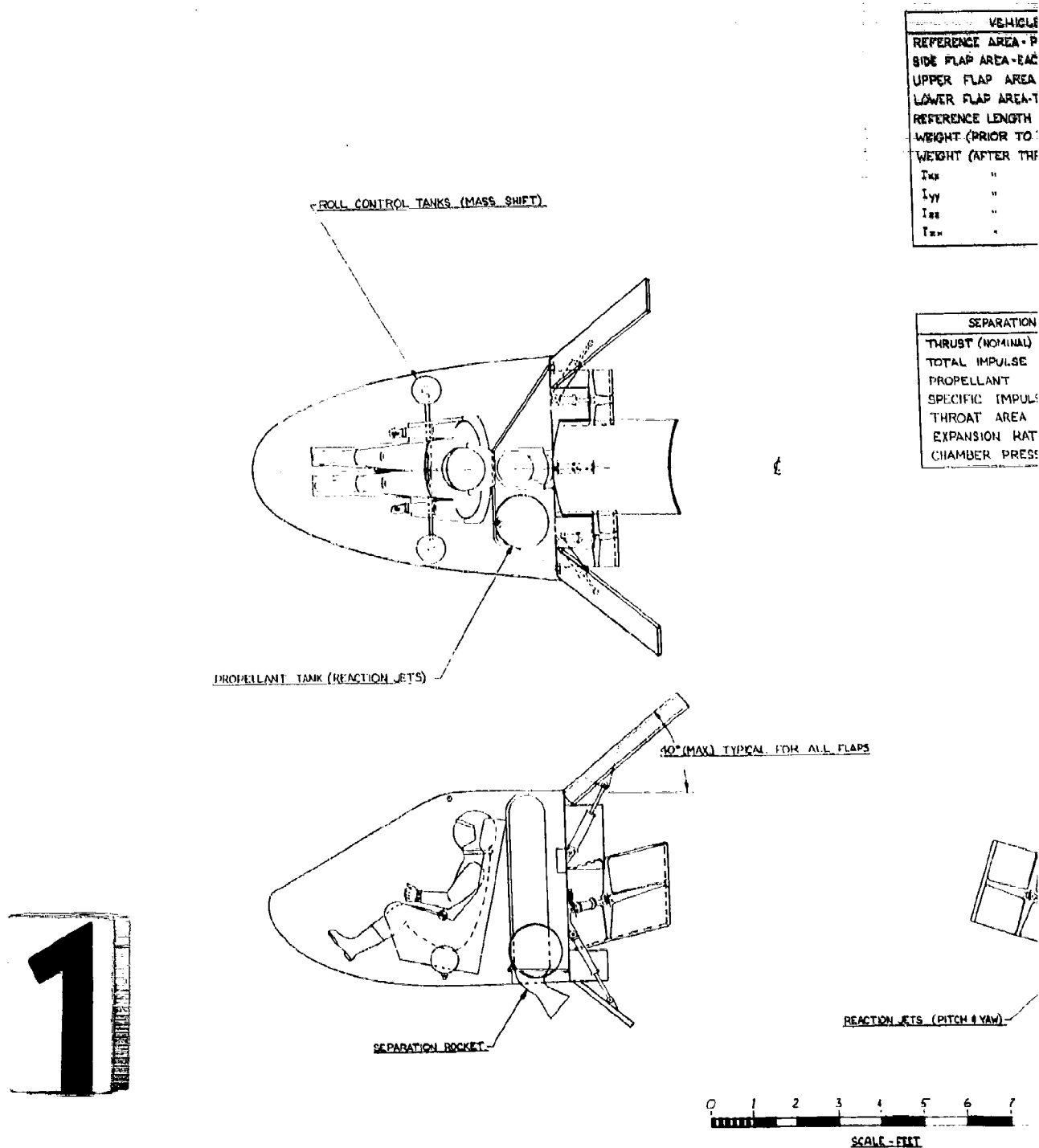
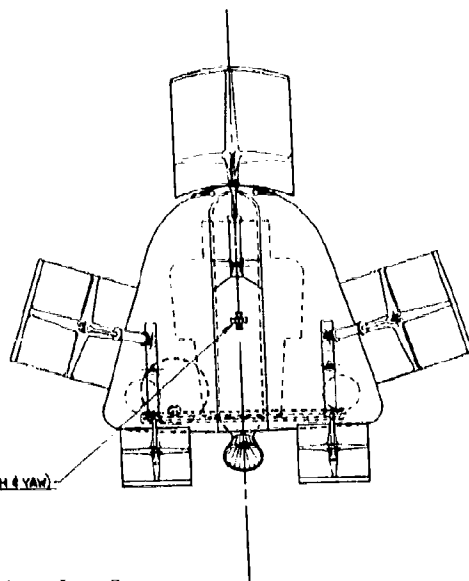


Figure 10 Pod Capsule Configuration



VEHICLE DATA	
REFERENCE AREA - PLATFORM	274 FT <sup>2</sup>
SIDE FLAP AREA - EACH	6.0 FT <sup>2</sup>
UPPER FLAP AREA	7.9 FT <sup>2</sup>
LOWER FLAP AREA - TOTAL	4.55 FT <sup>2</sup>
REFERENCE LENGTH ALONG BODY $L$	7.92 FT
WEIGHT (PRIOR TO THRUSTING)	2680 LB
WEIGHT (AFTER THRUSTING)	2500 LB
$I_{xx}$	190 SLUG-FT <sup>2</sup>
$I_{yy}$	591 SLUG-FT <sup>2</sup>
$I_{zz}$	530 SLUG-FT <sup>2</sup>
$I_{xy}$	+567 SLUG-FT <sup>2</sup>

SEPARATION ROCKET DATA	
THRUST (NOMINAL)	40,000 LB
TOTAL IMPULSE	40,000 LB-SEC
PROPELLANT	SOLID
SPECIFIC IMPULSE (S.I.)	250 LB/LB/SEC
THROAT AREA	5.8 IN <sup>2</sup>
EXPANSION RATIO	3:1
CHAMBER PRESSURE	100 PSI



REACTION JETS (PITCH & YAW)

SCALE - FEET



## SECTION 3

## AERODYNAMIC CHARACTERISTICS

## 3.1 HYPERSONIC AERODYNAMICS

3.1.1 TECHNIQUES. Hypersonic aerodynamic data was calculated using the Modified Newtonian Impact theory. An unpublished IBM 7090 computer program was utilized to determine the steady state and stability derivatives for the configurations without flaps. Input for this program consisted of defining the configuration as a series of flat plate segments and calculating the centroids, areas, and direction cosines of each segment. The output of this program was curve fitted and used as input to an unpublished IBM 7090 computer program which computes total vehicle aerodynamic characteristics including flap effects. The flap contributions were determined by curve fitting data of flap shadow area and centroid location as a function of flap deflection and angle of attack. This data was then used to determine the trim capability and stability derivatives of the four configurations with the flap sizes and c. g. locations as shown in Figures 7 through 10.

The body alone aerodynamic data, the flap areas and centroid locations were curve fitted and used as input to the three and six degree of freedom trajectory programs utilized in the performance investigation.

## 3.1.2 RESULTS.

3.1.2.1 Ballistic Body Capsule. Hypersonic aerodynamic data for the ballistic body are presented in Figures 11 through 15. Moments are referenced about the 62% point of the centerline length of the vehicle body. The lateral directional stability derivatives are referenced about the body axis and the longitudinal data are referenced about the stability axis. The upper flap was used for trim control and aerodynamic damping for the hypersonic performance studies.

Pitching moment characteristics show the vehicle is longitudinally stable and can be trimmed between 1 degree and 15 degrees angle of attack for flap configurations as presented in Figure 11. The pitch derivatives corresponding to these flap configurations are presented in Figure 12.

It should be noted that the lateral-directional stability derivatives presented in Figures 13, 14, and 15 are dependent upon the side flaps and not the upper or lower flaps. All curves are presented for a side flap deflection of  $40^\circ$ . The vehicle is directionally stable, as shown in Figure 13, however the dihedral effect is positive, indicating that the vehicle is unstable in the spiral mode. This spiral instability could be corrected by relocating the flaps so the flap centroid was above the center of gravity.

3.1.2.2 Lifting Body Capsule. Hypersonic aerodynamic data for the lifting body are presented in Figures 16 through 20. Moments are referenced about the 63.7% point of the vehicle body centerline. The lateral-directional stability derivatives are referenced about the body axis and the longitudinal data are referenced about the stability axis. The lower flap was used for trim control and aerodynamic damping in the hypersonic performance studies.

Pitching moment characteristics, as presented in Figure 16, show the vehicle is longitudinally stable and can be trimmed between 0 degrees and 30 degrees angle of attack. The dashed curve represents the change in trim characteristics with the use of an approximately 30% larger side flap necessitated by directional stability considerations as noted below. Because of side flap orientation on the vehicle body, the flap contributes a positive pitching moment and the vehicle will trim at approximately 3 degrees higher angle of attack than the smaller flap at the same deflection. The pitch derivatives corresponding to these flap configurations are presented in Figure 17.

The lateral-directional stability derivatives are presented in Figures 18, 19, and 20. All curves are presented for a side flap deflection of 45 degrees. The vehicle is directionally unstable with the small side flap, however, by increasing the flap area approximately 30% the directional stability was increased as noted on Figure 18 by the dashed curve. The vehicle is stable in the spiral mode as indicated by the dihedral effect,  $C_{l\beta}$ .

3.1.2.3 Pod Capsule. Hypersonic aerodynamic data for the pod configuration are presented in Figures 21 through 25. Moments are referenced about the 51.6% point of the vehicle centerline. The lateral-directional stability derivatives are referenced about the vehicle body axis and the longitudinal data are referenced about the stability axis. The lower flap is used for trim control and aerodynamic damping in the hypersonic performance studies.

Longitudinal data are presented in Figure 21. The vehicle is longitudinally stable and can be trimmed from approximately 5 degrees to 14 degrees angle of attack for the flap configurations presented.

The lateral-directional stability derivatives are presented in Figures 23 through 25. All curves are presented for a side flap deflection of 40 degrees. The vehicle is directionally stable but is unstable in the spiral mode. This spiral instability could be corrected by relocating the side flaps.

3.1.2.4 Turnaround Capsule. Hypersonic aerodynamic data for the turnaround configuration data are presented in Figures 26 through 31. Moments are referenced about the 59.7% point of the vehicle centerline. Because of the large variation in angle of attack, all data presented are referenced about the vehicle body axis. The lower flap is used for trim control and aerodynamic damping in the hypersonic performance studies.

Figure 26 presents the longitudinal data from an angle of attack of 180 degrees to 40 degrees. The sketch above the curves in Figure 26 shows the sign convention being used for aerodynamic data presentation. The solid curves represent data with all flaps in the closed position. This data is used for the initial phase of the turnaround maneuver. The dashed curves represent data with all flaps extended to 45 degrees. An extrapolation of data to approximately 190 degrees angle of attack indicates the vehicle would be in a trimmed condition at that point, however, the vehicle is longitudinally unstable and any small disturbance would start turnaround in the direction of the disturbance. Figure 27 is a continuation of longitudinal data after the vehicle has completed turnaround. Trim can be accomplished from approximately 1 degree to 20 degrees with lower flap deflections between 30 and 45 degrees. With the lower flap deflected to 15 degrees, the vehicle will trim at approximately 50 degrees angle of attack, however, this data is not presented at high angles as it is unlikely that trim will be required in this attitude. The vehicle is longitudinally stable for all trim conditions after turnaround.

The lateral-directional stability derivatives are presented in Figures 29, 30, and 31. All curves are presented for a side flap deflection of 45 degrees. The vehicle is directionally stable and is stable in the spiral mode as indicated in Figure 29.

### 3.2 SUPERSONIC AERODYNAMICS

3.2.1 TECHNIQUES. Supersonic aerodynamic data for the ballistic body and lifting body configurations were determined by using the data presented in Reference 1 for fixed flap deflection angles as a basis. Flap characteristics were based on experimental data on similar configurations (e.g., References 2 through 5) and the basic data of Reference 1 was then corrected to yield the aerodynamic characteristics for the configurations without flaps. This data, along with the flap data, was used as input to an unpublished IBM 7090 computer program which computed the aerodynamic characteristics for the complete vehicles at various angles of attack, flap deflections and Mach numbers.

Because the pod configuration and the ballistic body are similar, the supersonic aerodynamic data were determined for the pod capsule by using a ratio of the hypersonic characteristics for the two configurations as follows:

$$C_{i_{pod}} = C_{i_{BB}} \left( \frac{C_{i_{pod} - hypersonic}}{C_{i_{BB} - hypersonic}} \right) \quad (1)$$

where

$C_{i_{pod}}$  - Pod aero coefficient without flaps @ M

$C_{i_{BB}}$  - Ballistic body aero coefficient without flaps @ M

$C_{i_{pod} - hypersonic}$  - Hypersonic pod aero coefficient without flaps

$C_{i_{BB} - hypersonic}$  - Hypersonic ballistic body aero coefficient without flaps

Flap characteristics of the ballistic body were used for the pod configuration. The above-mentioned computer program was utilized to determine aerodynamic characteristics for the complete pod configuration.

Aerodynamic data for the trajectories were determined by using the flap characteristics and the body alone data as input for the three degree of freedom trajectory program.

A preliminary analysis of the supersonic characteristics of the turnaround capsule indicated that it was more stable (in the heat shield forward position) than at hypersonic speeds. Consequently, it would be unstable in the sharp nose forward attitude as at hypersonic speeds and tend to turn around. Since it was felt that a turnaround maneuver executed at maximum dynamic pressure would achieve load factors in excess of human tolerances, the maximum dynamic pressure performance was calculated using the hypersonic aerodynamic characteristics described above. These data would yield optimistic load factor characteristics. If they yielded excessive load factors, then the use of supersonic aerodynamic data would only make the situation worse.

### 3.2.2 RESULTS

3.2.2.1 Ballistic Body. Supersonic aerodynamic data for the ballistic body configuration are presented in Figure 32. This data is referenced about the stability axis and moments are referenced about the 62% point of the vehicle centerline. The vehicle can be trimmed between approximately -3 degrees and +10 degrees angle of attack for the flap deflections as presented, and the vehicle is longitudinally stable. For the supersonic trajectory analysis the lower flap is utilized for trim control and aerodynamic damping.

3.2.2.2 Lifting Body. Lifting body supersonic data is presented in Figure 33. Data is referenced about the stability axis and moments are referenced about the 63.7% point of the vehicle centerline. The vehicle can be trimmed between approximately -10 degrees and +10 degrees angle of attack for the flap deflections as presented. This configuration is longitudinally stable. The upper flap was used as trim control and aerodynamic damping for the trajectory analysis in the supersonic flight regime.

3.2.2.3 Pod Capsule. Figure 34 presents the supersonic aerodynamic data for the pod configuration. Data is referenced about the stability axis and moments are referenced about the 51.6% point of the vehicle centerline. This configuration is longitudinally stable and can be trimmed between approximately -3 degrees and +9 degrees angle of attack. The lower flap was used as trim control and aerodynamic damping for the trajectory analysis.

### 3.3 SUBSONIC AERODYNAMICS

3.3.1 TECHNIQUES. Subsonic aerodynamic data for the ballistic body and lifting body configurations were determined by extrapolating the supersonic body alone data on

the basis of experimental data of similar configurations such as presented in References 6 through 8. Subsonic flap characteristics were determined in the same manner as for the supersonic data. The computer program was then utilized to determine the aerodynamic characteristics of the complete configurations.

Subsonic aerodynamic data for the pod configuration was determined by ratioing the ballistic body data as was done at supersonic speeds. The ballistic body subsonic flap data was used in calculating the data for the complete pod configuration.

Subsonic aerodynamic data was not generated for the turnaround capsule since it was felt that the gross trajectory characteristics resulting from a turnaround maneuver would only be slightly affected by the difference in aerodynamic characteristics between hypersonic and subsonic speeds.

3.3.2 RESULTS. Figure 35 through 37 present the subsonic aerodynamic for the three configurations. All data are referenced about the stability axis and moment reference points are the same as noted in Section 3.2.2 for each respective configuration.

3.3.2.1 Ballistic Body. The ballistic body data is presented in Figure 35. The vehicle is stable and can be trimmed between approximately -3 degrees and +12 degrees angle of attack. The lower flap was used as trim control and aerodynamic damping in the trajectory analysis.

3.3.2.2 Lifting Body. Figure 36 presents the subsonic data for the lifting body. The vehicle can be trimmed between approximately +1 degrees and +23 degrees angle of attack for the flap deflections presented and the vehicle is longitudinally stable. The upper flap was used as trim control and aerodynamic damping.

3.3.2.3 Pod Capsule. Figure 37 presents subsonic data for the pod configuration. The vehicle is stable above an angle of attack of -30 degrees and can be trimmed between -1 degree and +15 degrees angle of attack. The lower flap was used for trim control and aerodynamic damping in the trajectory analysis.

#### 3.4 INTERFERENCE EFFECTS.

Previous experience with separating bodies, e.g. escape capsules, airplane mounted missiles, two stage missiles etc. have indicated that aerodynamic interference between the two bodies can have a significant effect on the separation performance. These effects are quite difficult to treat on an exact basis due to the complex nature of the flow field and the fact that it is transient in nature.

The type of interference effects varies depending upon whether separation is nose separation, or separation of a portion of the vehicle aft of the nose. With nose separation, interference effects only occur in the aft regions of the body. For separation of a portion of the vehicle aft of the nose the separating portion is subject to the flow field of the nose.

Reference 9 presents the results of an analytical and experimental investigation of separation dynamics including aerodynamic interference effects. This reference concludes that for nose separation in which there is a distinct separation plane, e.g. no flaps overhanging the remainder of the configuration, there are no interference effects on the separating nose. Based on this information it was concluded that there was no significant aerodynamic interference effects on either the lifting body capsule or the turnaround capsule.

The ballistic body capsule however, has flaps which overhang the after-body and it is therefore subject to aerodynamic interference effects.

The interference results from the flow field which develops over the after-body interacting with the flaps. The interference effects were analyzed at hypersonic speeds only for the upper flap which is the largest. This yields a conservative estimate of the interference effects since it produces the largest pitching moments. In actuality the interference effects would be less since the interference pitching moment on the lower flap would offset the upper flap to some extent.

A schematic of the flow field model used in the analysis is given in Figure 38. A detached shock forms ahead of the afterbody and intersects with the flap resulting in an increase in pressure and hence a disturbing moment. It was assumed that the pressure coefficient behind the shock at the point of intersection with the flap was 1.42, based on free stream conditions. Since the shock moves across the flap as a function of time the interference effects are transient. The interference pitching moments were calculated as a function of time and the results integrated to determine an effective pitch rate of .1 rad/sec. in a nose down direction. This pitch rate was incorporated into the hypersonic flight dynamics studies as a measure of the aerodynamic interference effects.

The free stream dynamic pressure is much higher at the maximum dynamic pressure point than in the hypersonic regime which will tend to increase the magnitude of the interference effects. In the performance studies for the maximum dynamic pressure escape condition the effects of initial pitch rates as high as 1.75 rad/sec were investigated.

The pod capsule is located within the flow field of the nose of the primary vehicle which results in aerodynamic interference effects during separation. Upon separation, the pod capsule must traverse this body flow field of the body were analyzed at hypersonic speeds using the analytical model shown in Figure 39. The configuration is such that the capsule tends to have a nose down pitching moment when acting in the flow field from the body nose. In order to determine a conservative value of the nose down

moment it was assumed that only the forward upper surface of the capsule contributed an aerodynamic moment. If all the surfaces were included the nose down moment would be decreased. The nose down moment was such that it gave a pitch acceleration of  $10 \text{ deg./sec.}^2$ . The capsule is in the body flow field for about .3 seconds which would yield an angular velocity of 3.0 degrees per second. This interference effect was incorporated into the hypersonic flight dynamics studies by assuming an initial angular velocity of  $-.1 \text{ rad/sec.}$  at maximum dynamic pressure the effect of higher initial angular rates which would result from the higher dynamic pressure were investigated in the performance studies.



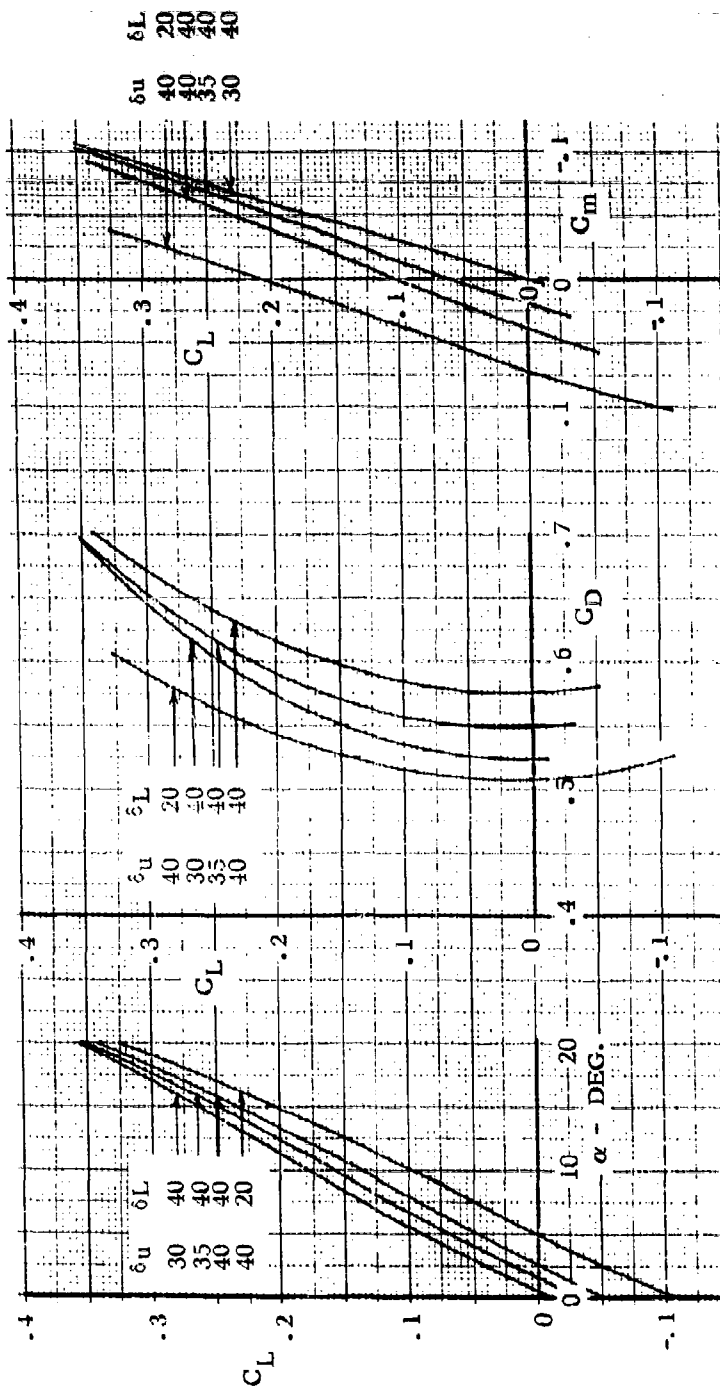


Figure 11 - Ballistic Body Hypersonic Longitudinal Characteristics

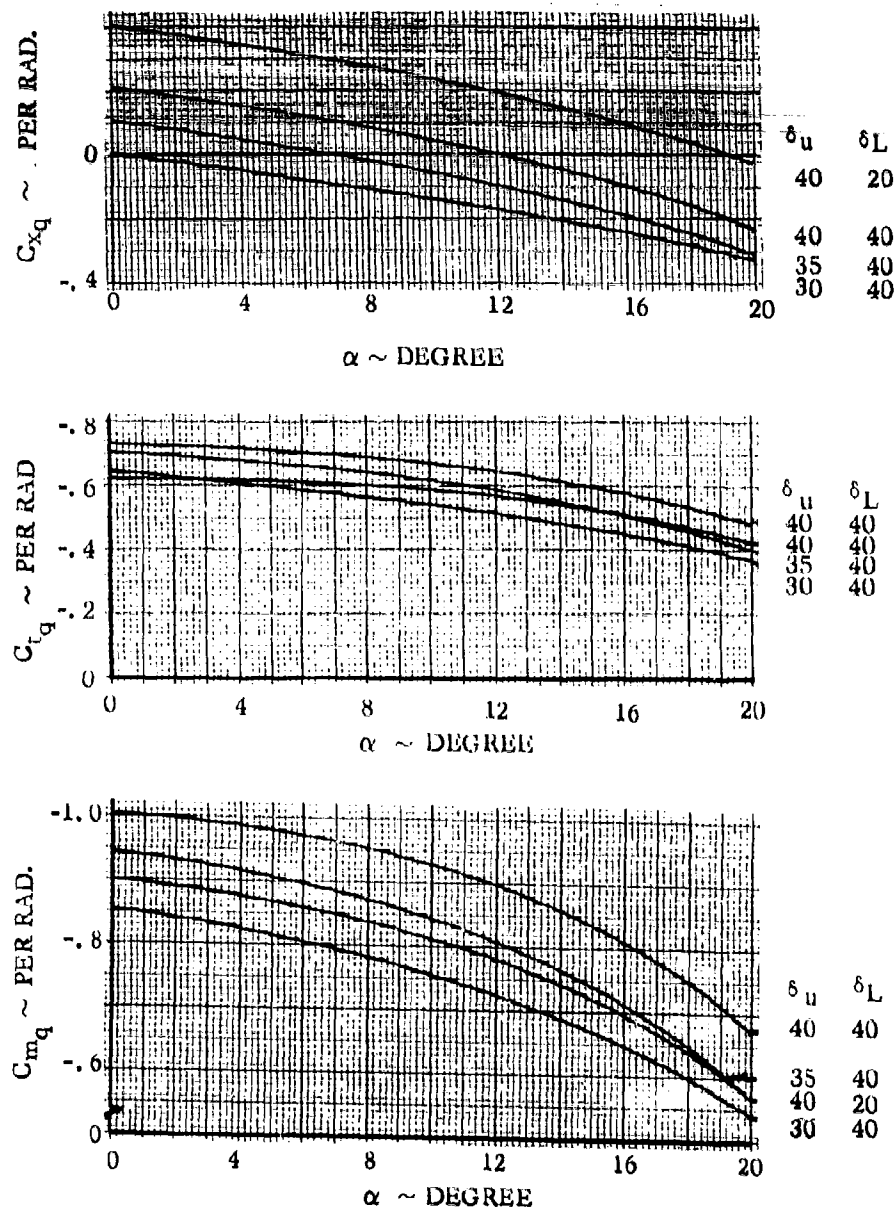


Figure 12 - Ballistic Body Hypersonic Pitch Stability Derivatives

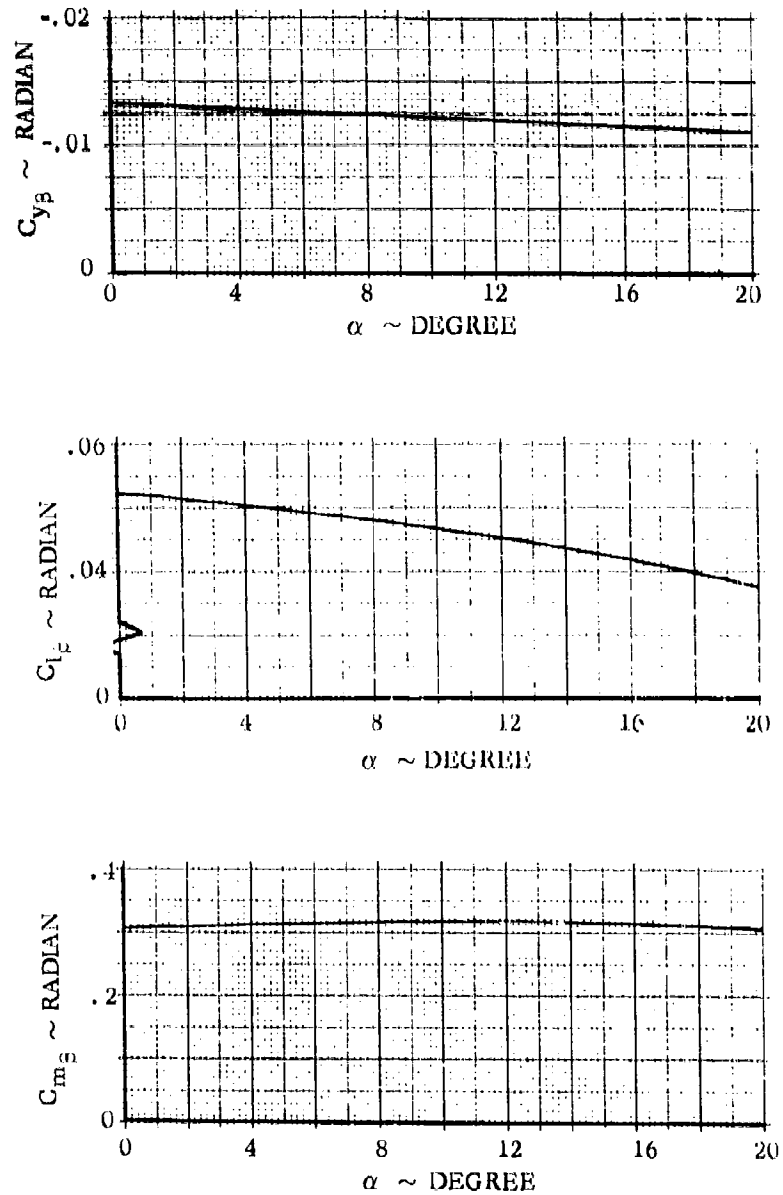


Figure 13 - Ballistic Body Hypersonic Lateral - Directional Derivatives

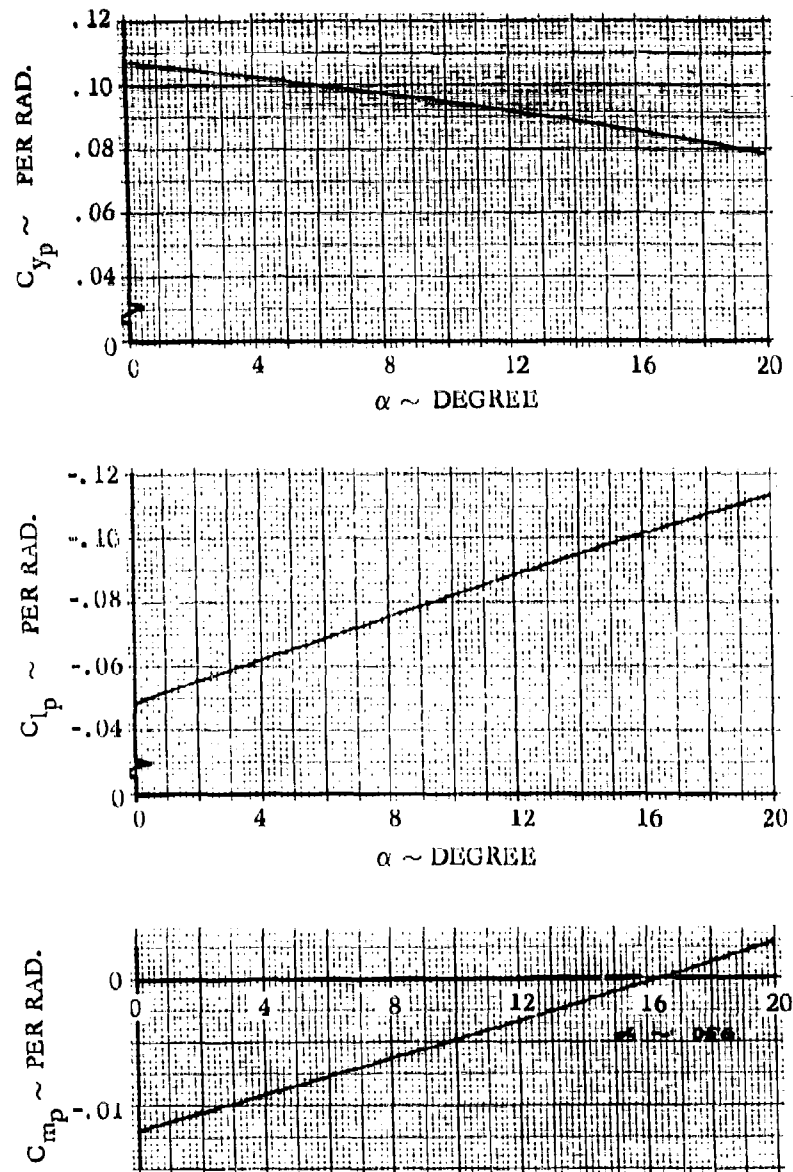


Figure 14 - Ballistic Body Hypersonic Rolling Velocity Derivatives

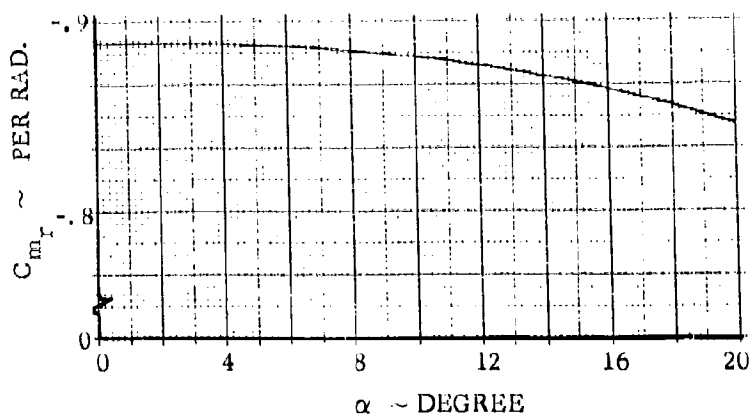
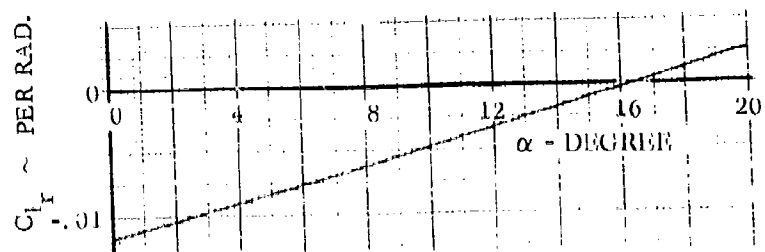
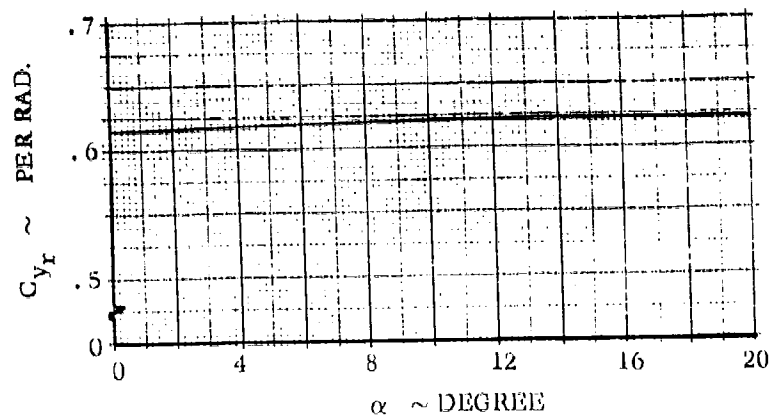


Figure 15 - Ballistic Body Hypersonic Yawing Velocity Derivatives

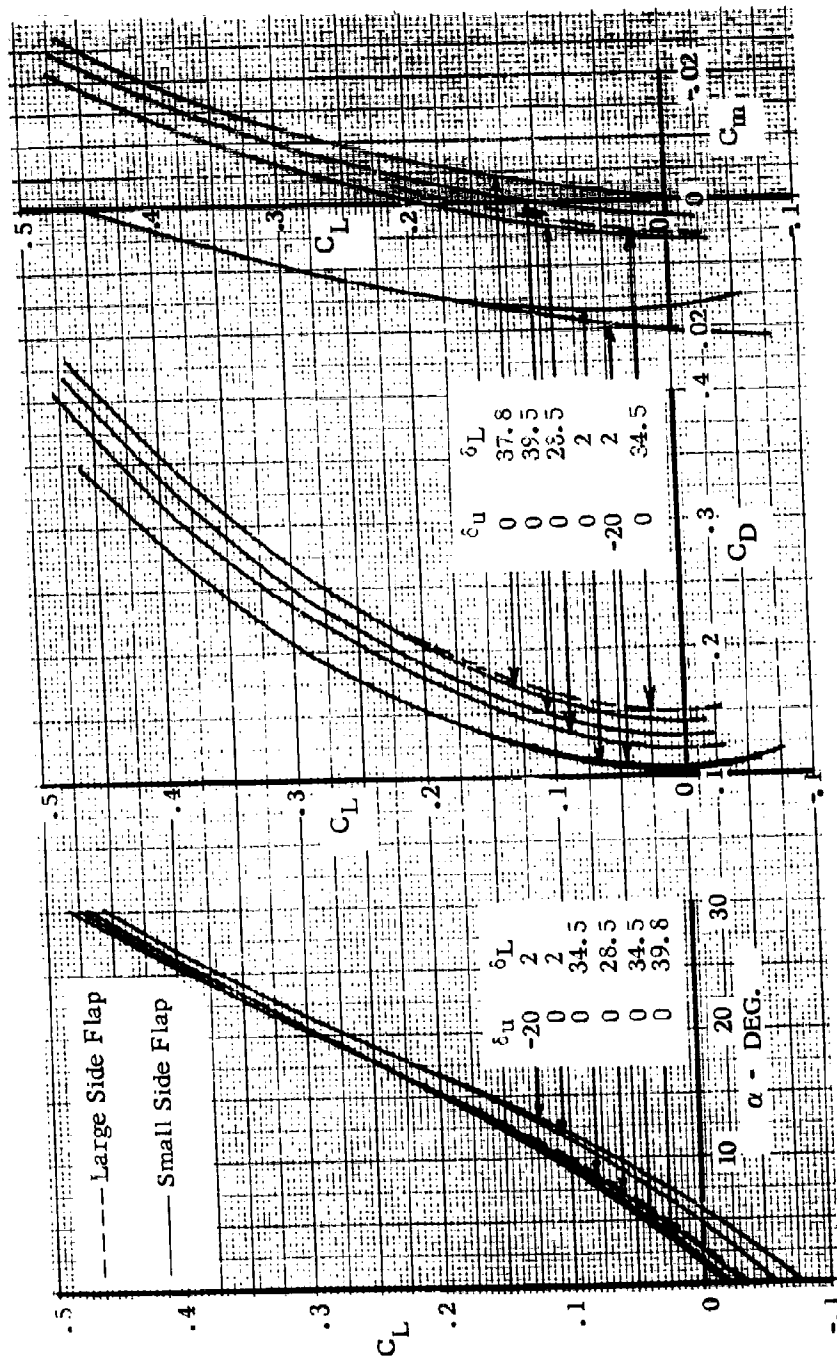


Figure 16 - Lifting Body Hypersonic Longitudinal Characteristics

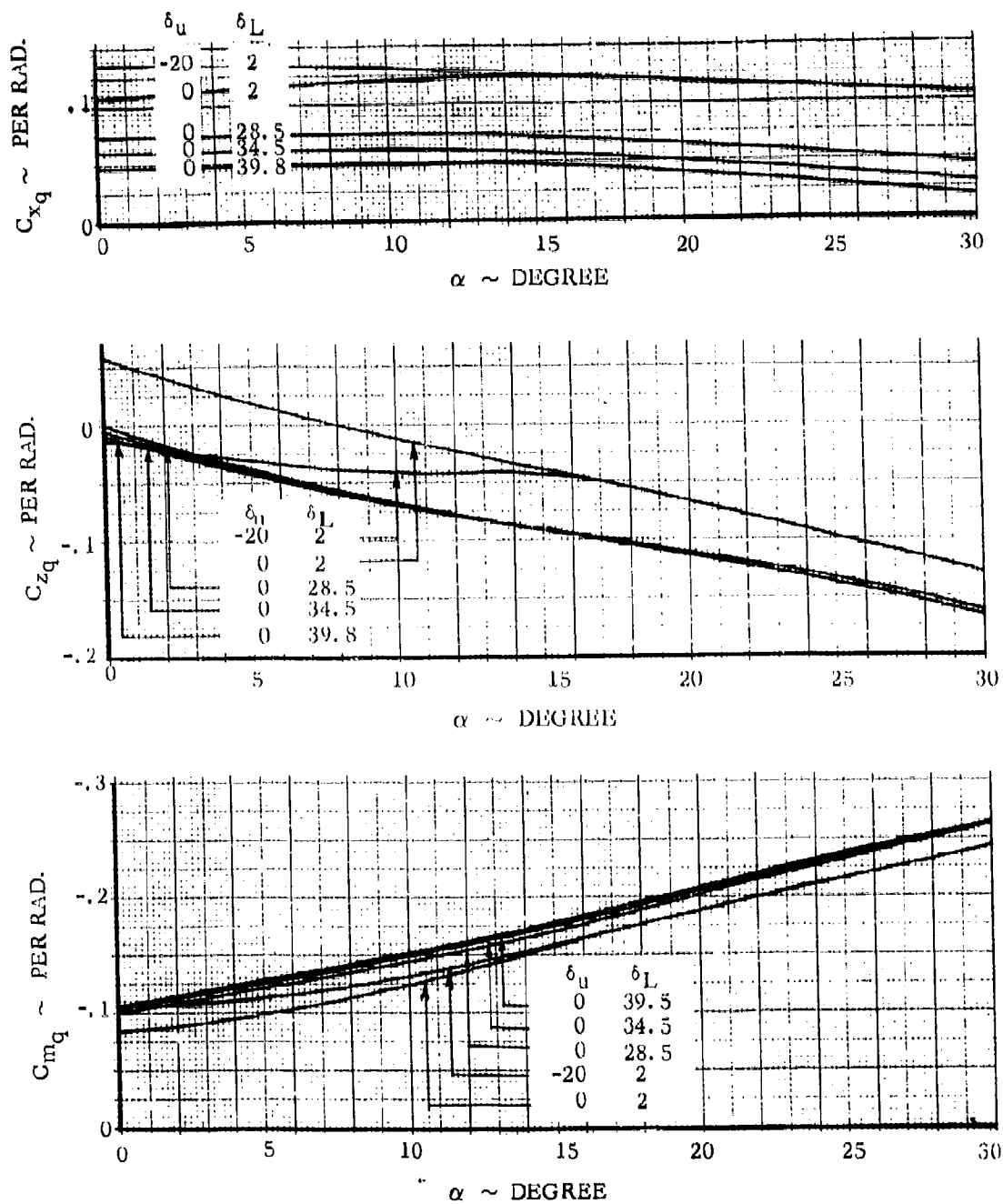


Figure 17 - Lifting Body Hypersonic Pitch Stability Derivatives

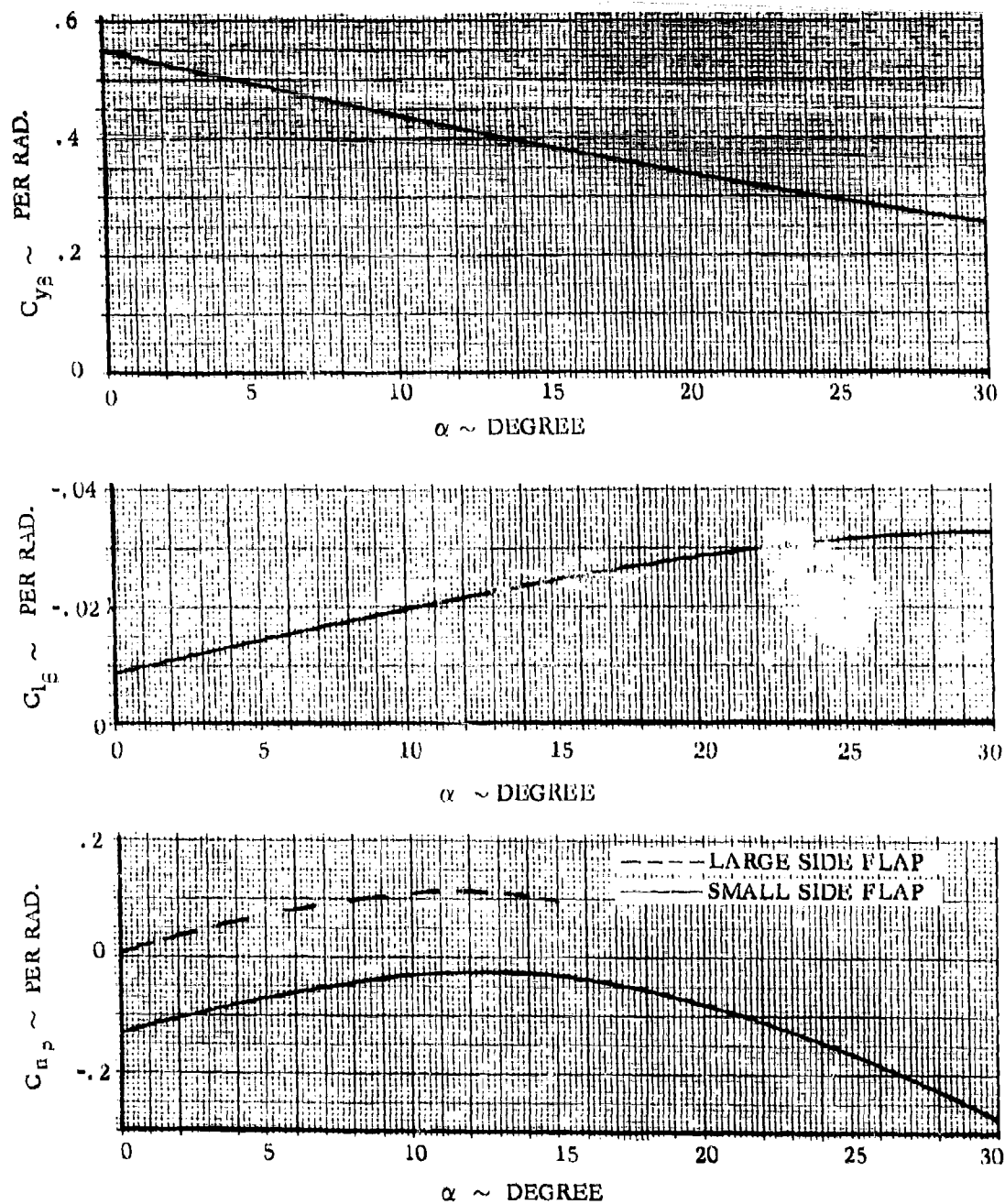


Figure 18 - Lifting Body Hypersonic Lateral - Directional Derivatives



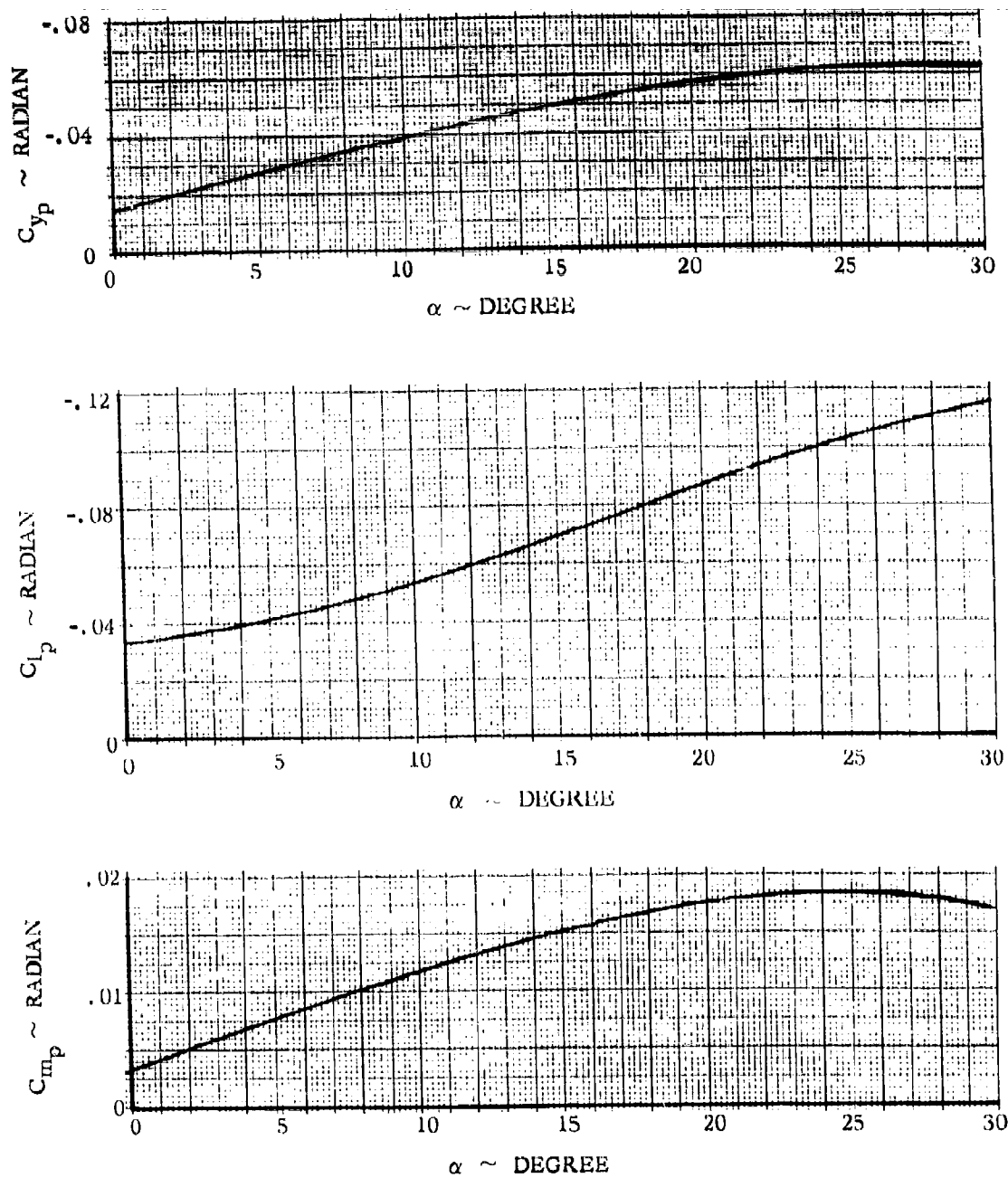


Figure 19 - Lifting Body Hypersonic Rolling Velocity Derivatives

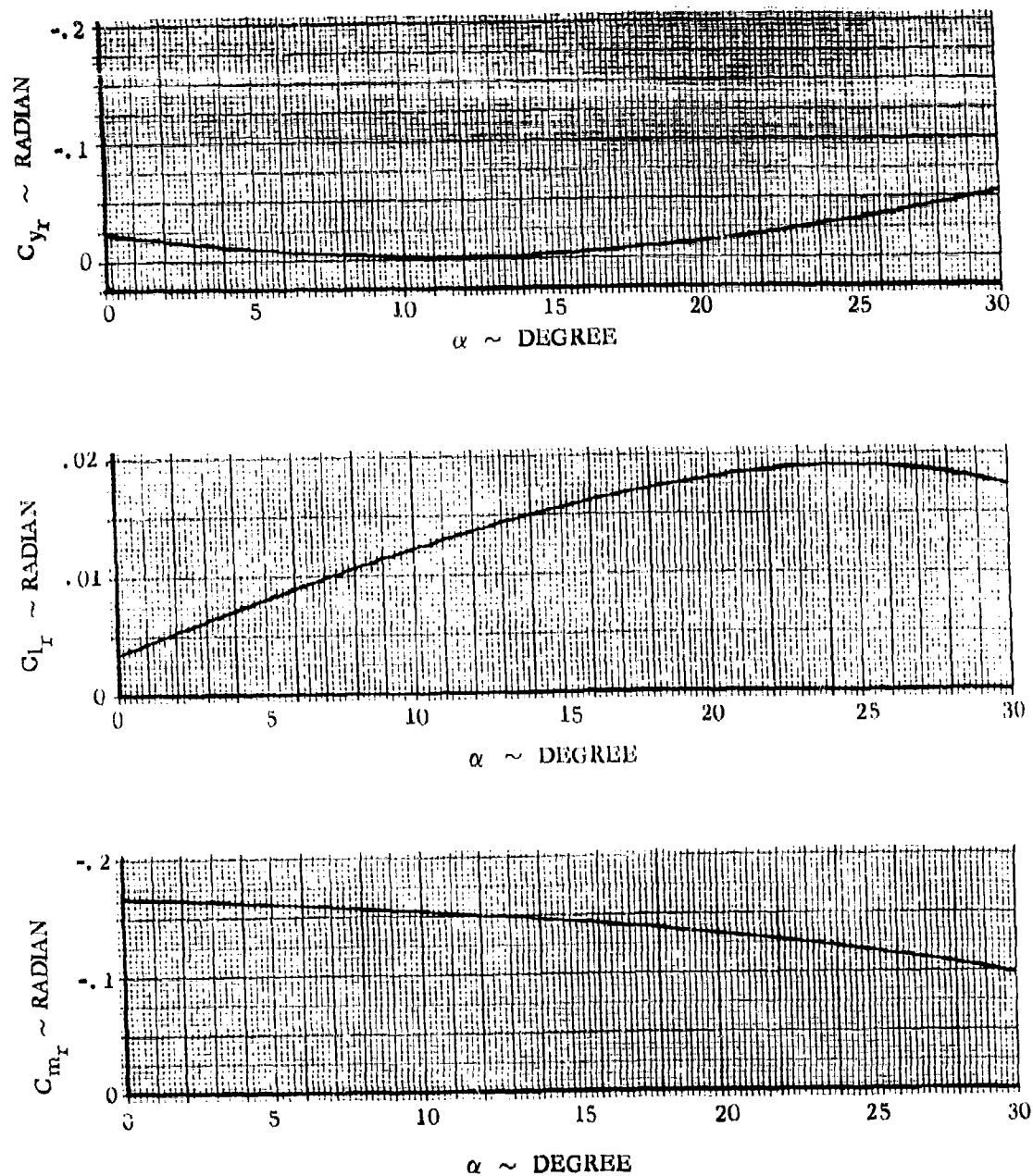


Figure 20 - Lifting Body Hypersonic Yawing Velocity Derivatives

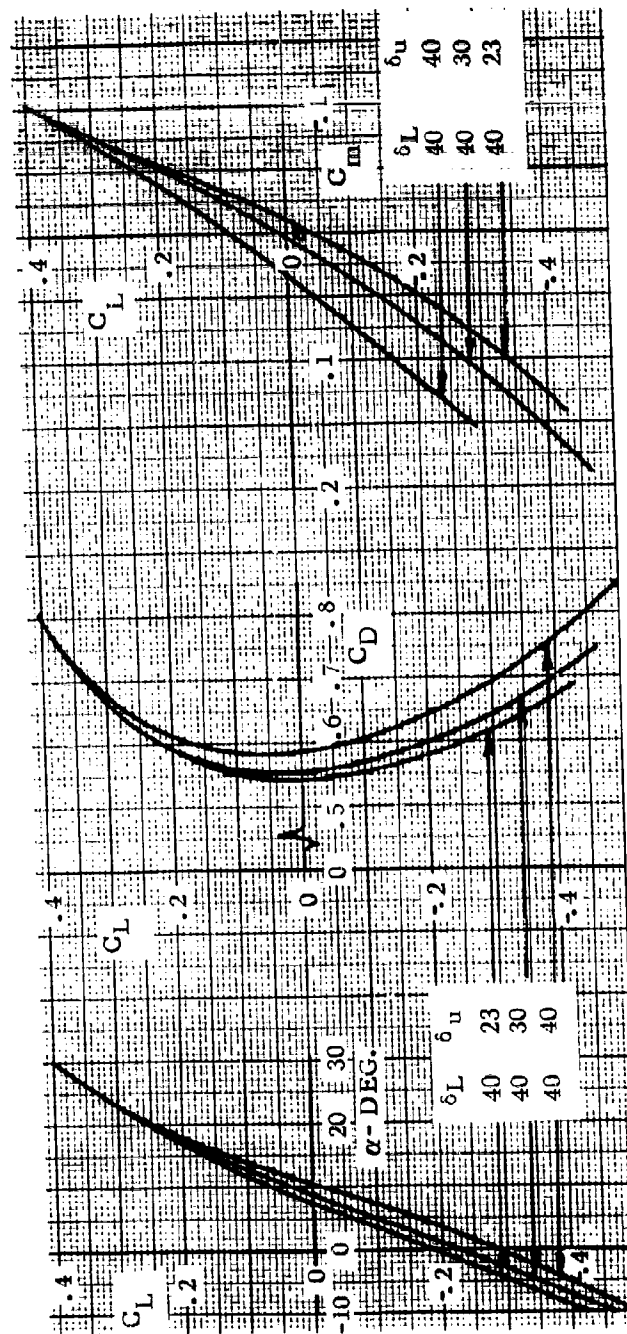


Figure 21 - Pod Capsule Hypersonic Longitudinal Characteristics

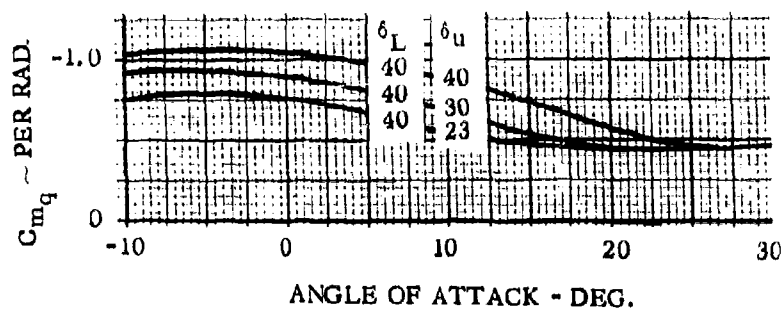
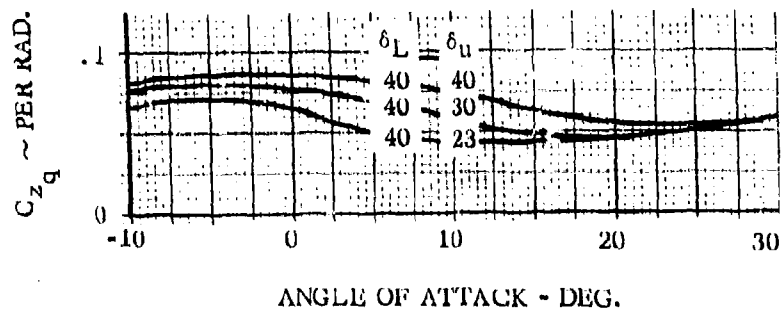
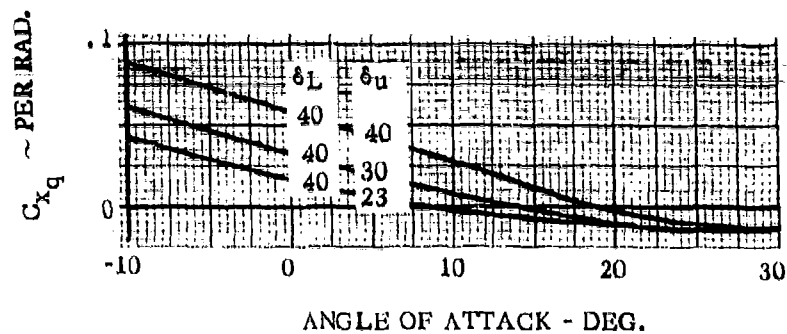


Figure 22 - Pod Capsule Hypersonic Pitch Stability Derivatives

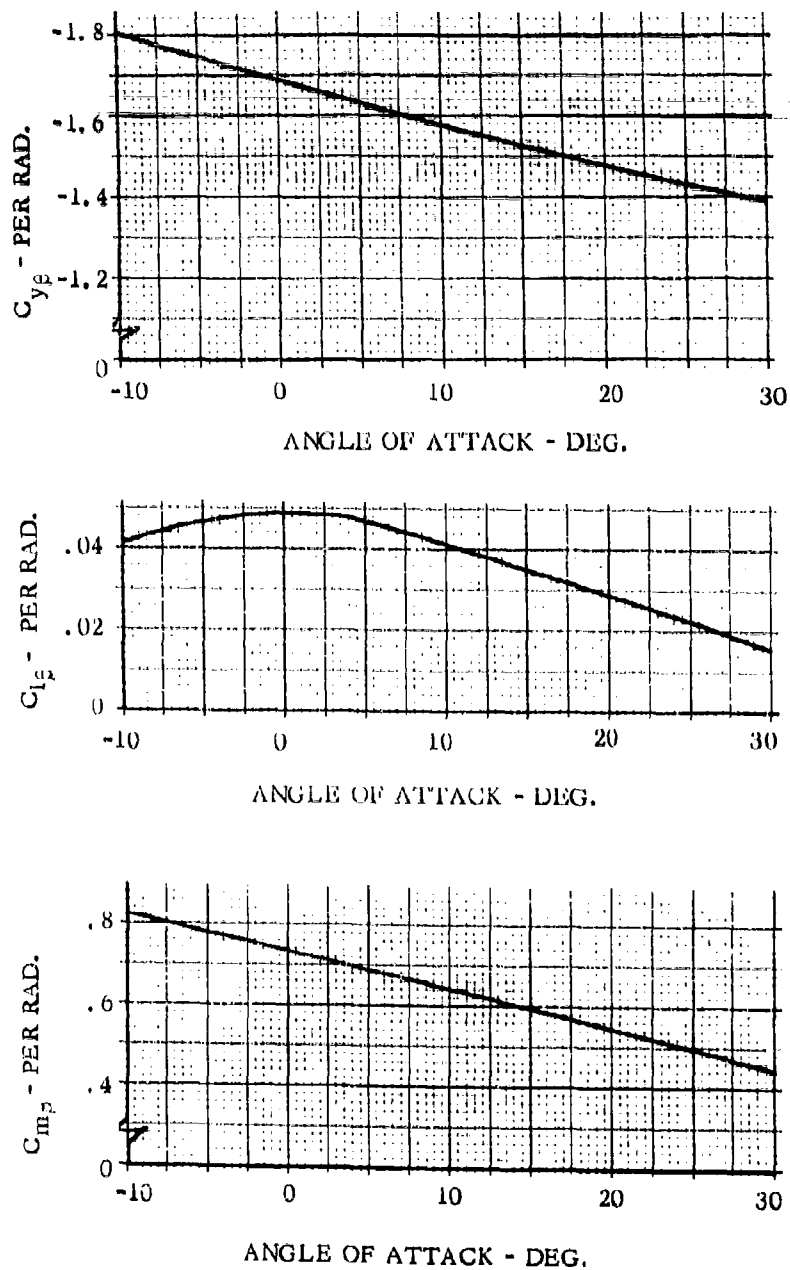


Figure 23 - Pod Capsule Hypersonic Lateral - Directional Derivatives

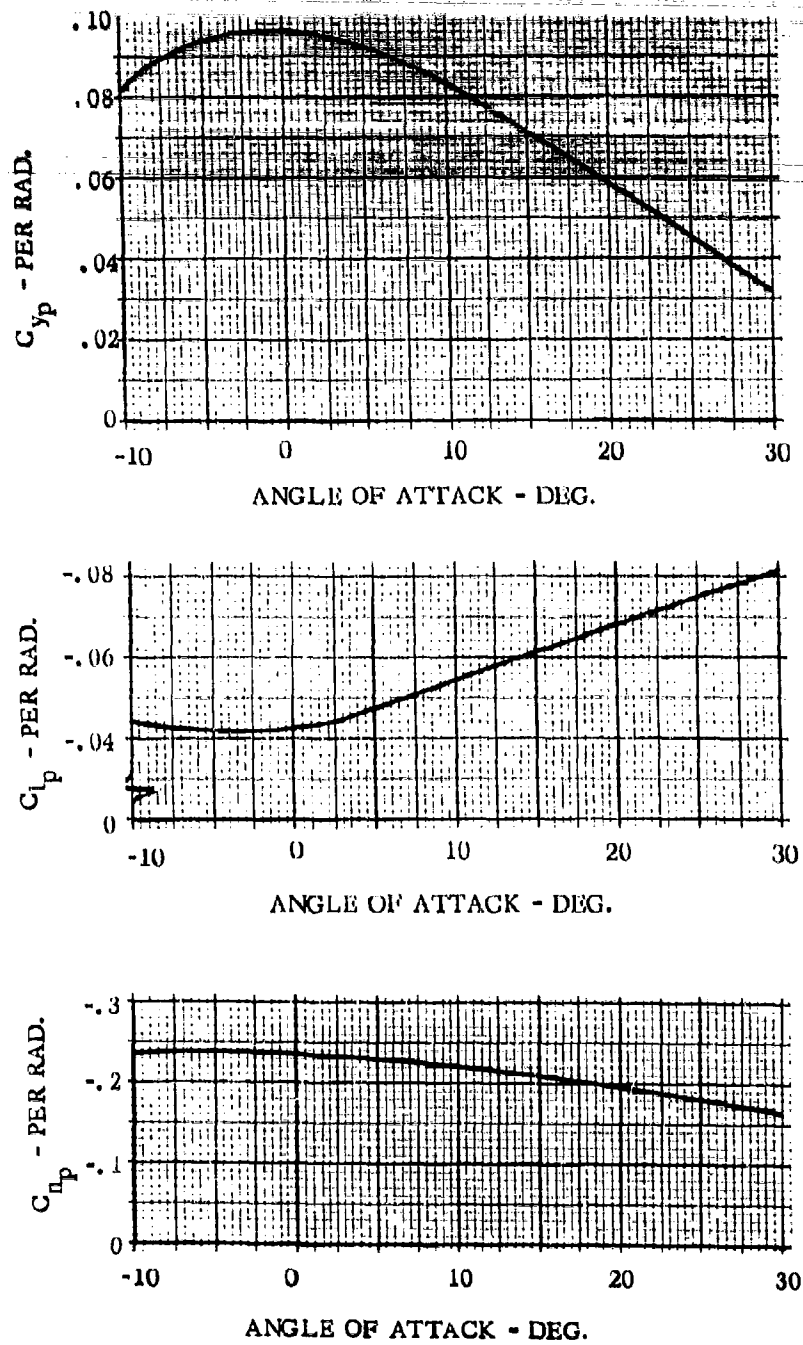


Figure 24 - Pod Capsule Hypersonic Rolling Velocity Derivatives

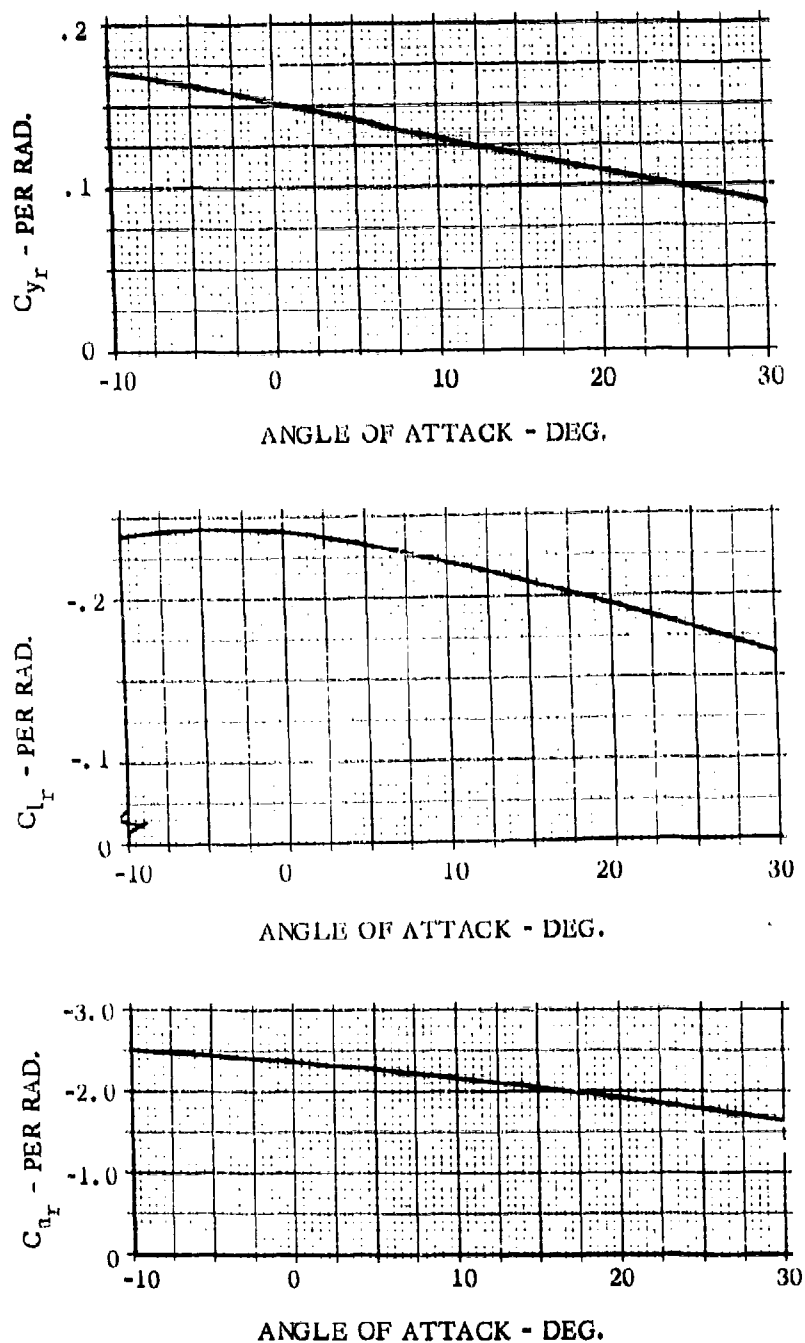


Figure 25 - Pod Capsule Hypersonic Yawing Velocity Derivatives

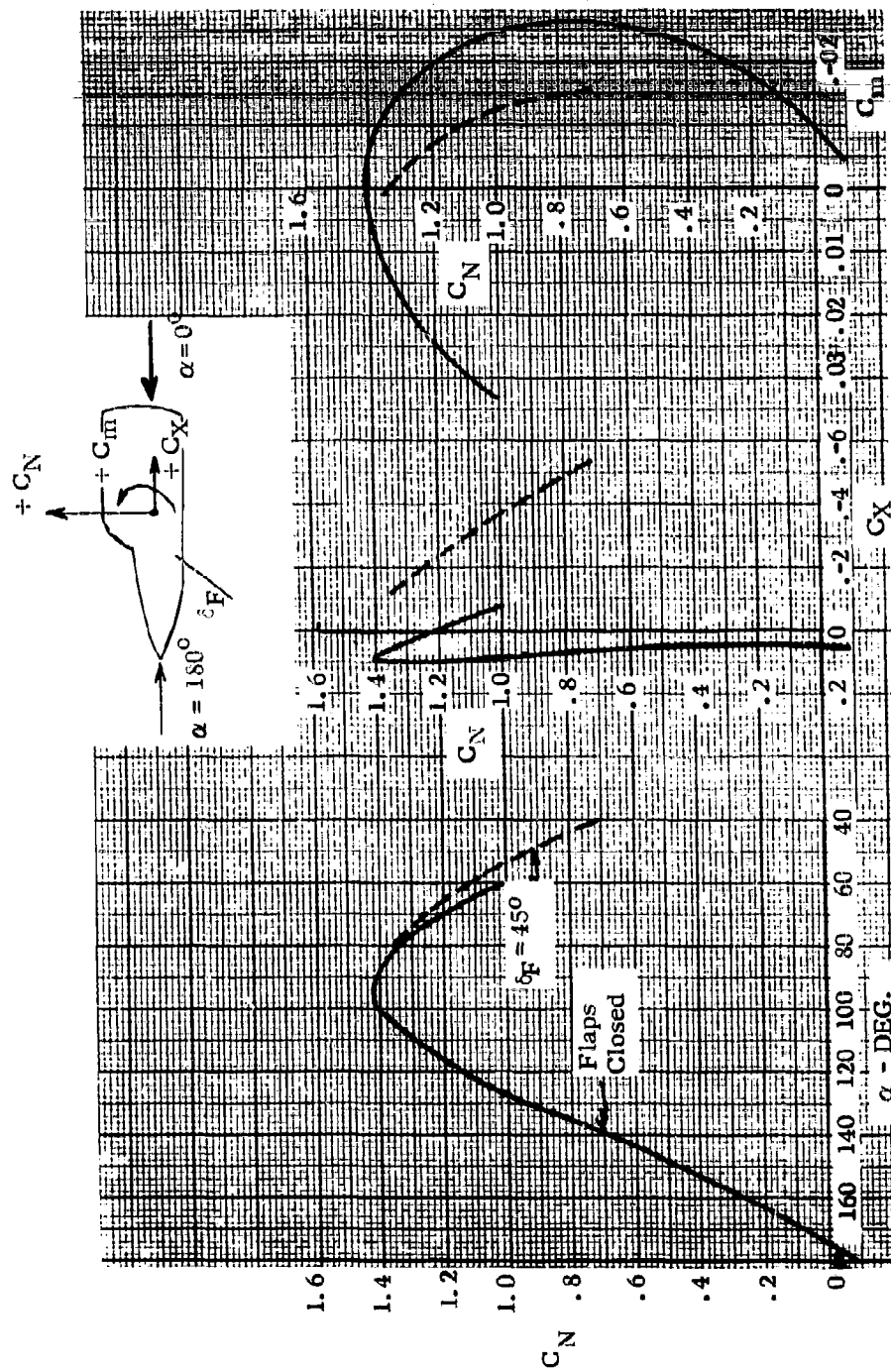


Figure 26 - Turnaround Capsule Hypersonic Longitudinal Characteristics,  $40^\circ < \alpha < 180^\circ$



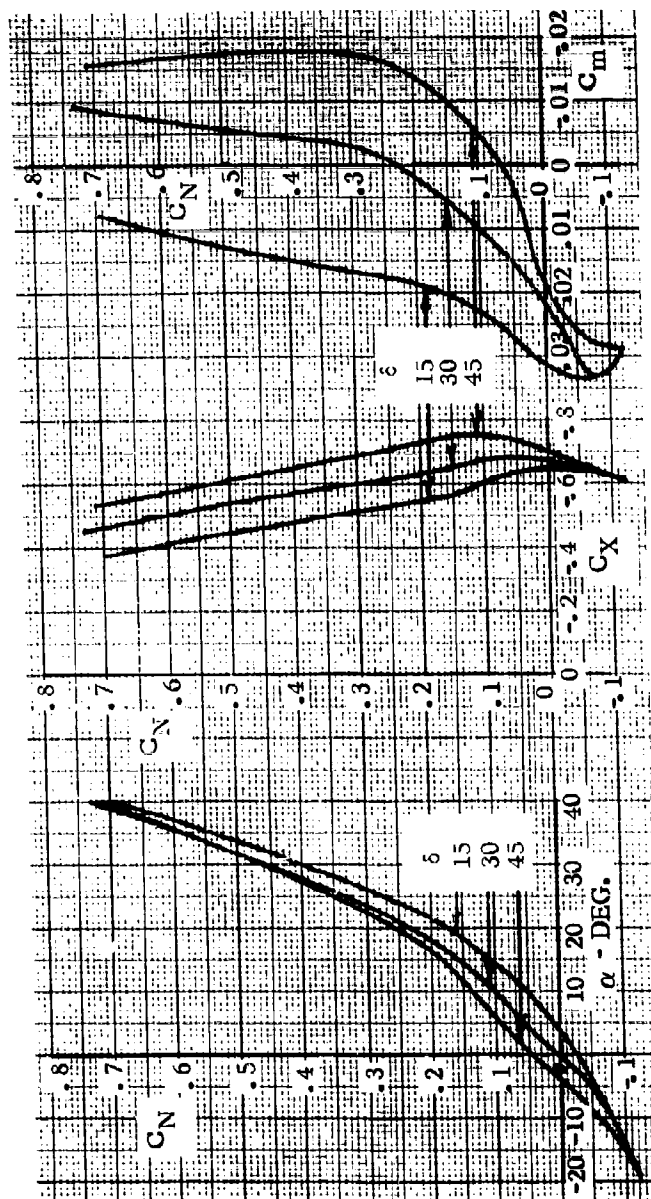


Figure 27 - Turnaround Capsule Hypersonic Longitudinal Characteristics,  $-20^\circ < \alpha < 40^\circ$

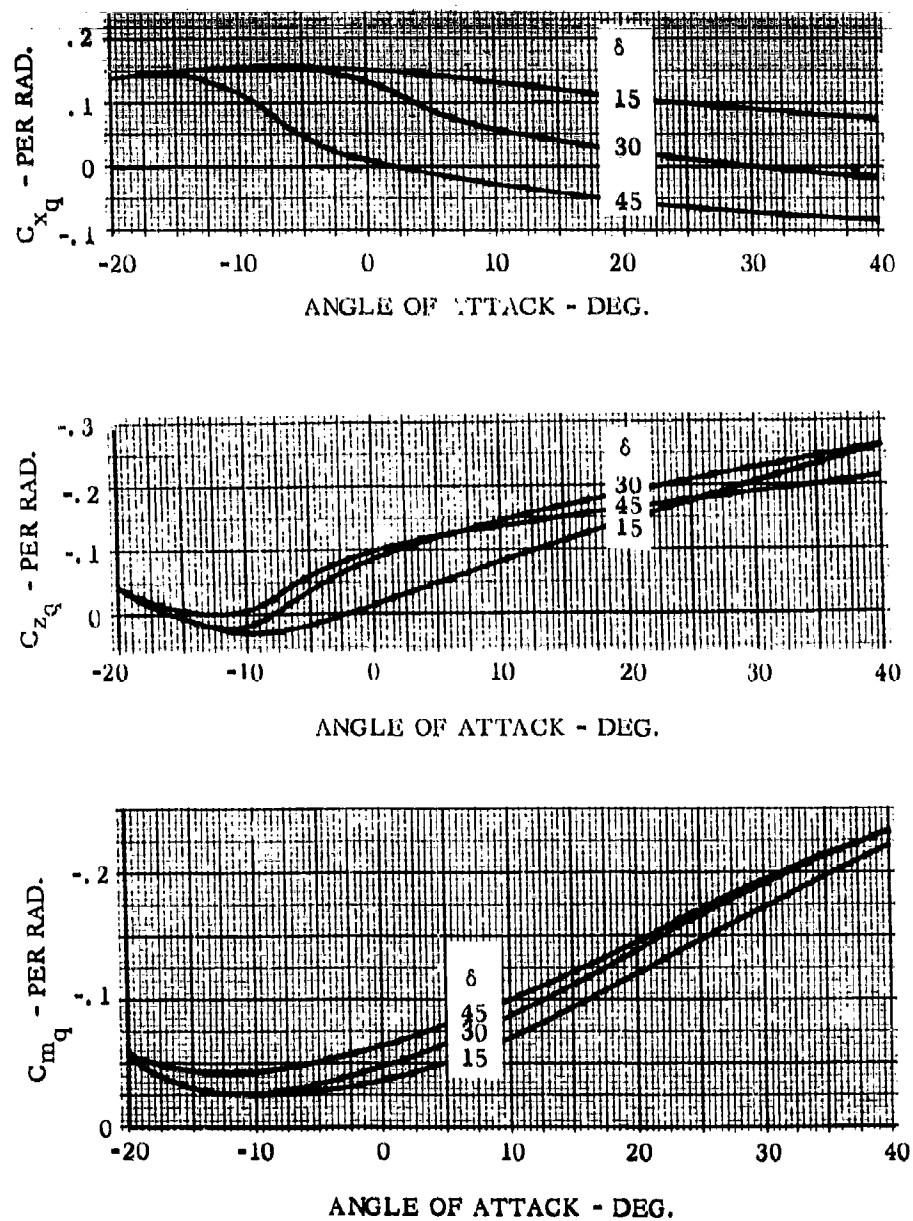


Figure 28 - Turnaround Capsule Hypersonic Pitch Stability Derivatives

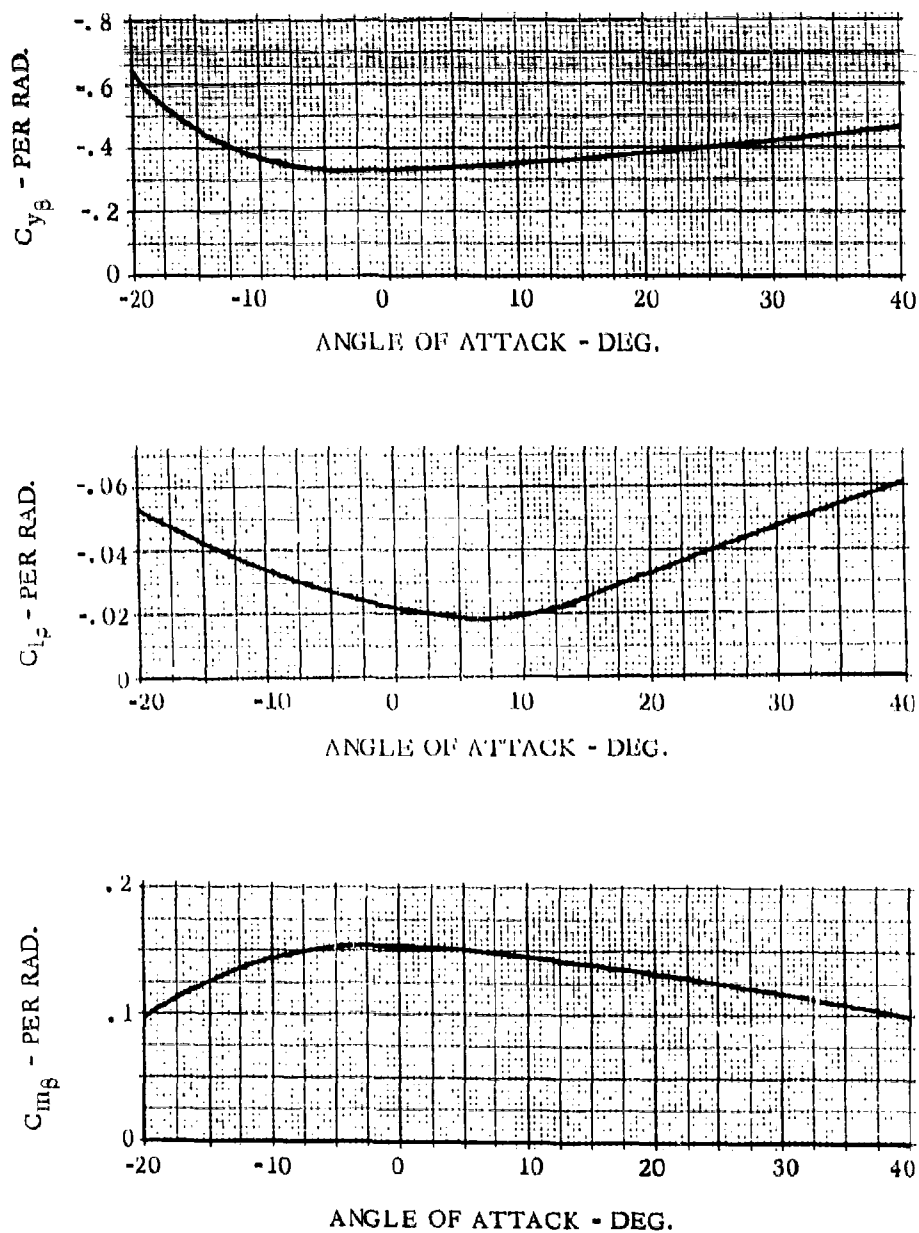


Figure 29 - Turnaround Capsule Hypersonic Lateral - Directional Derivatives

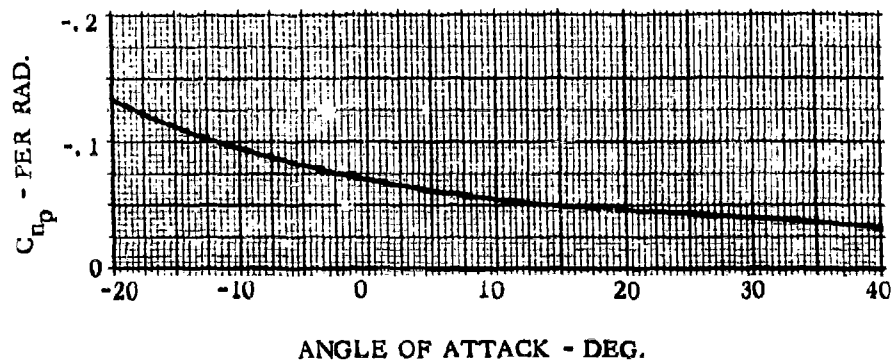
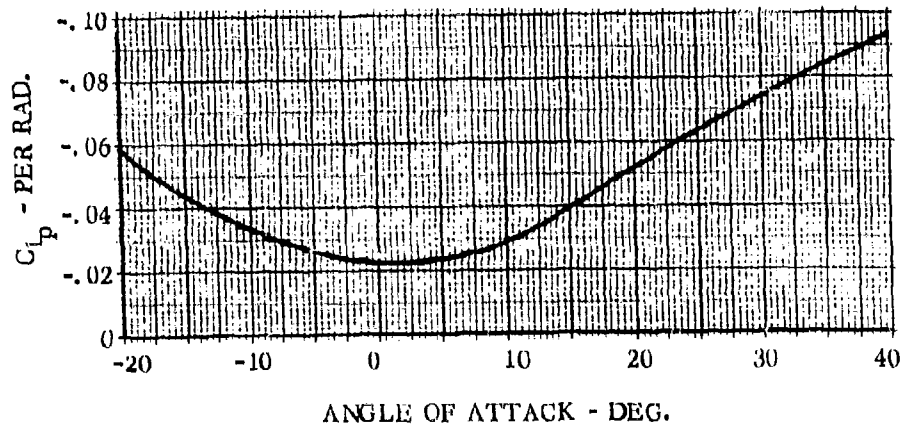
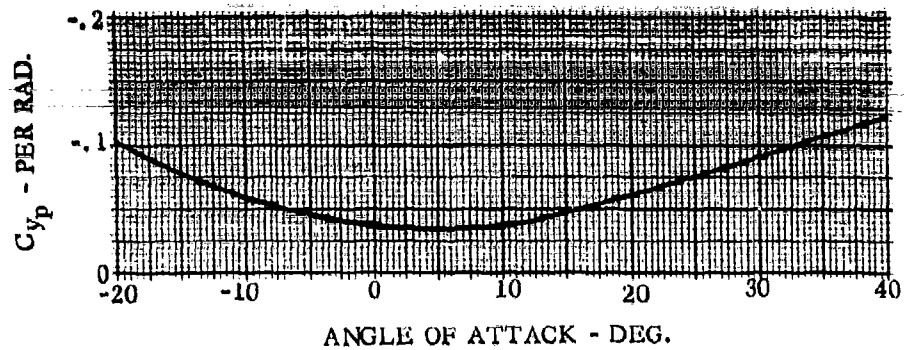


Figure 30 - Turnaround Capsule Hypersonic Rolling Velocity Derivatives

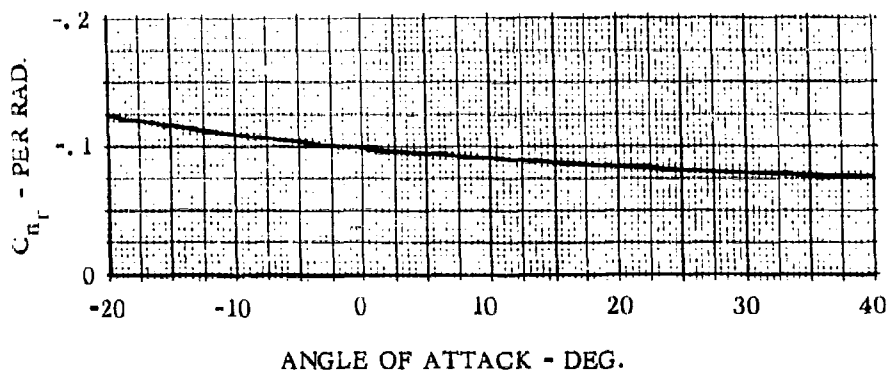
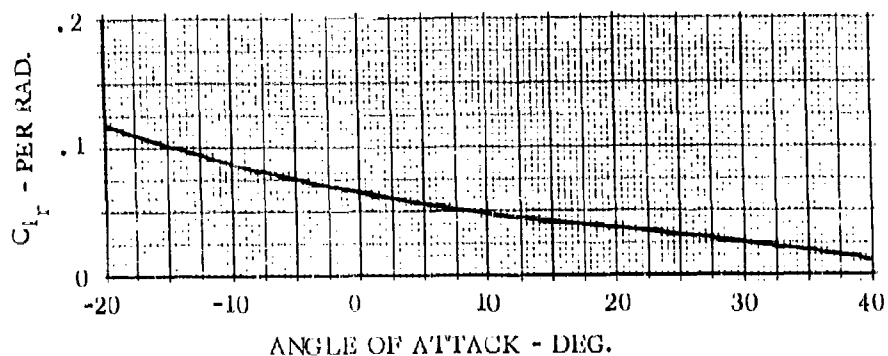
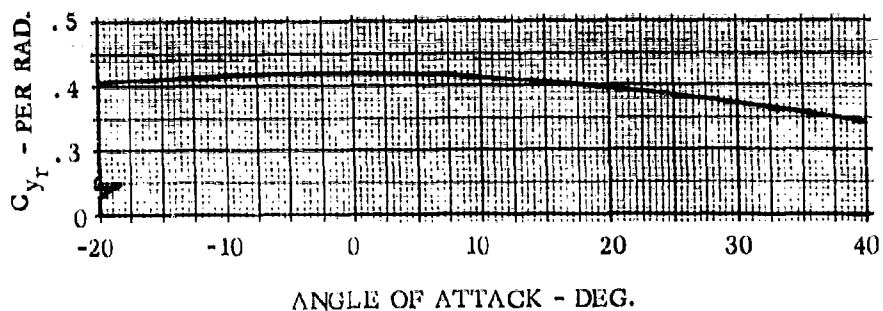


Figure 31 - Turnaround Capsule Hypersonic Yawing Velocity Derivatives

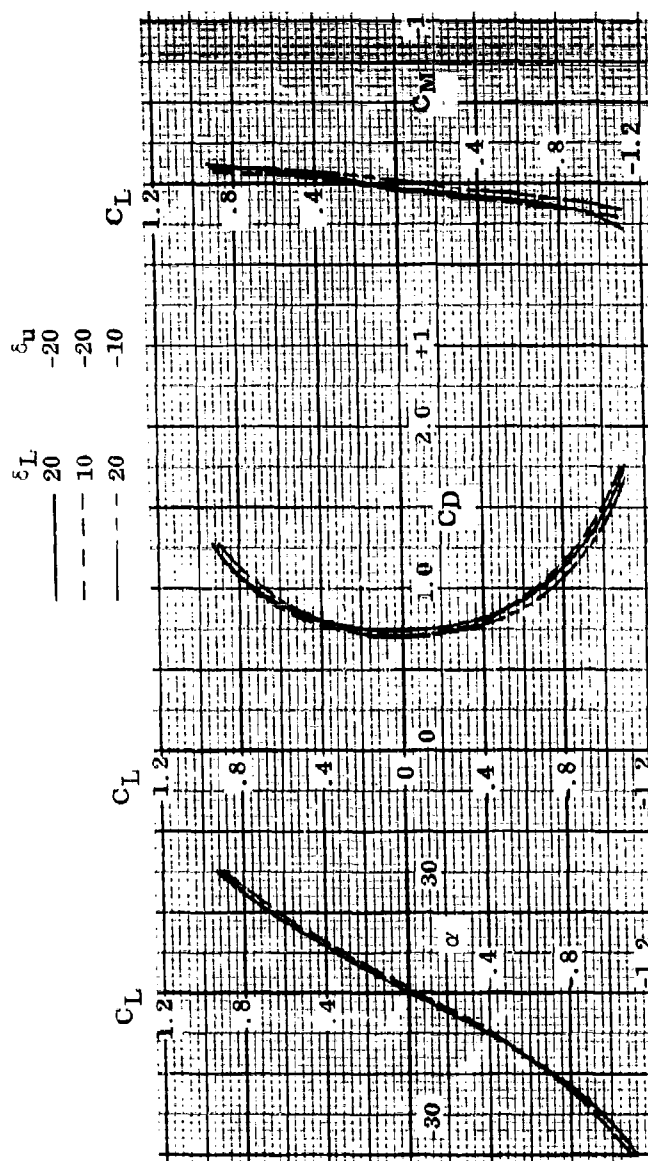


Figure 32-Ballistic Body - Supersonic Aerodynamic Characteristics

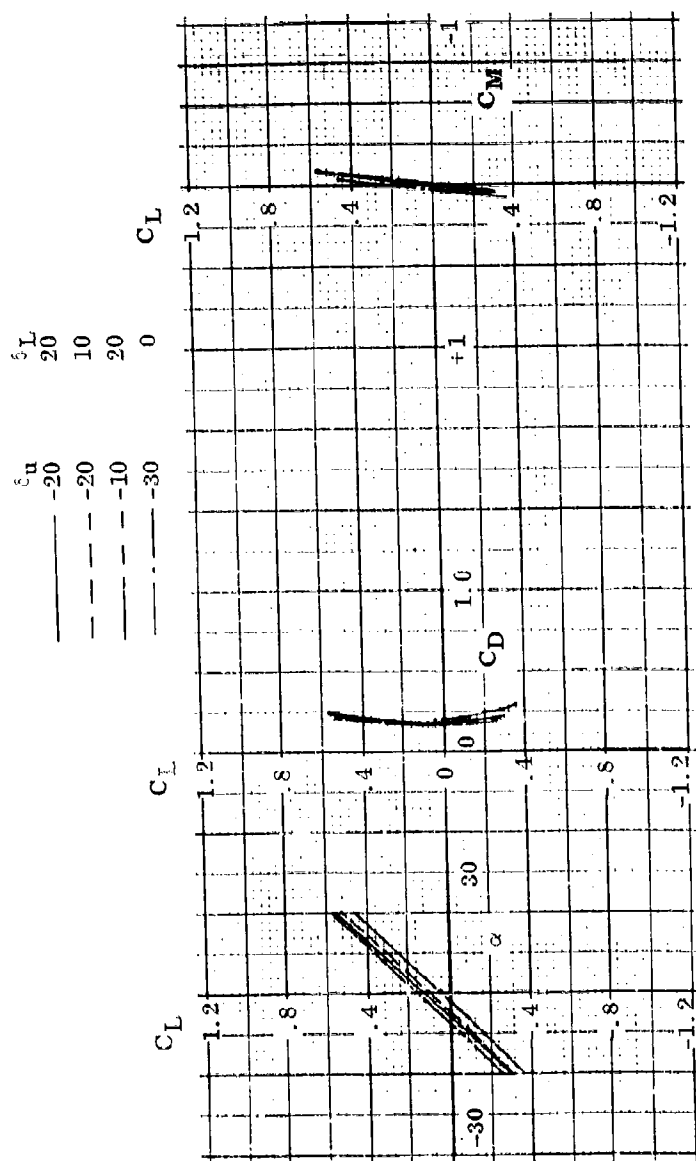


Figure 33 - Lifting Body - Supersonic Aerodynamic Characteristics

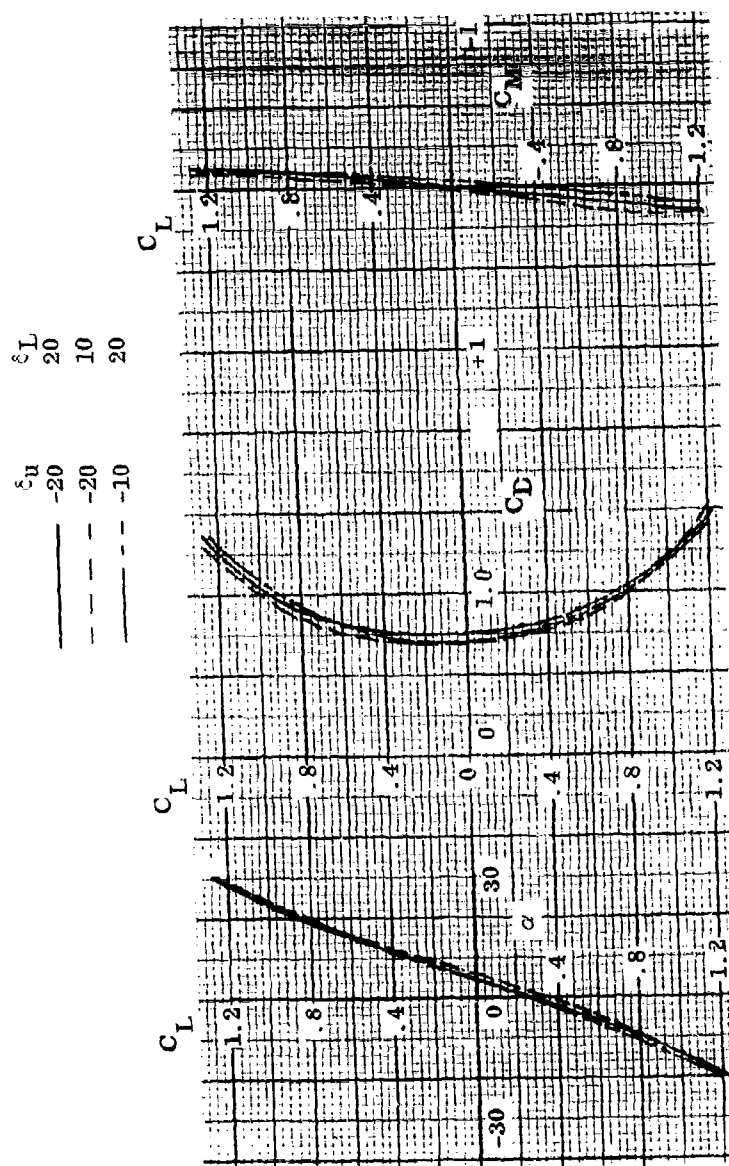


Figure 34 - Pod Capsule - Supersonic Aerodynamic Characteristics



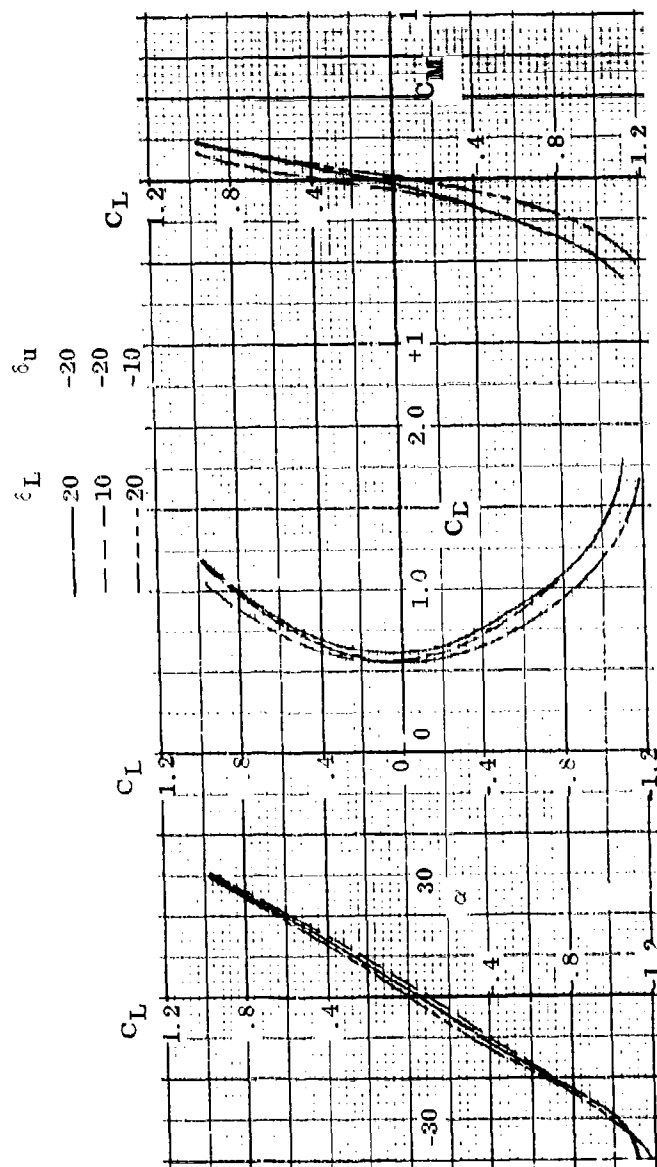


Figure 35 - Ballistic Body - Subsonic Aerodynamic Characteristics

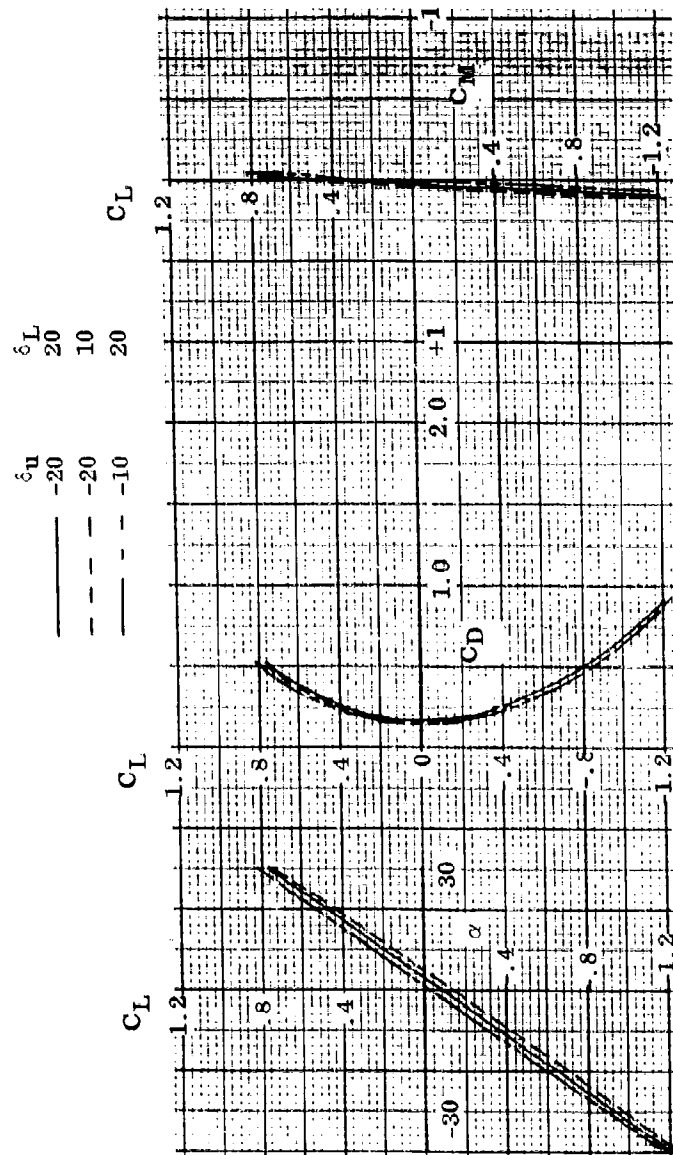


Figure 36- Lifting Body - Subsonic Aerodynamic Characteristics

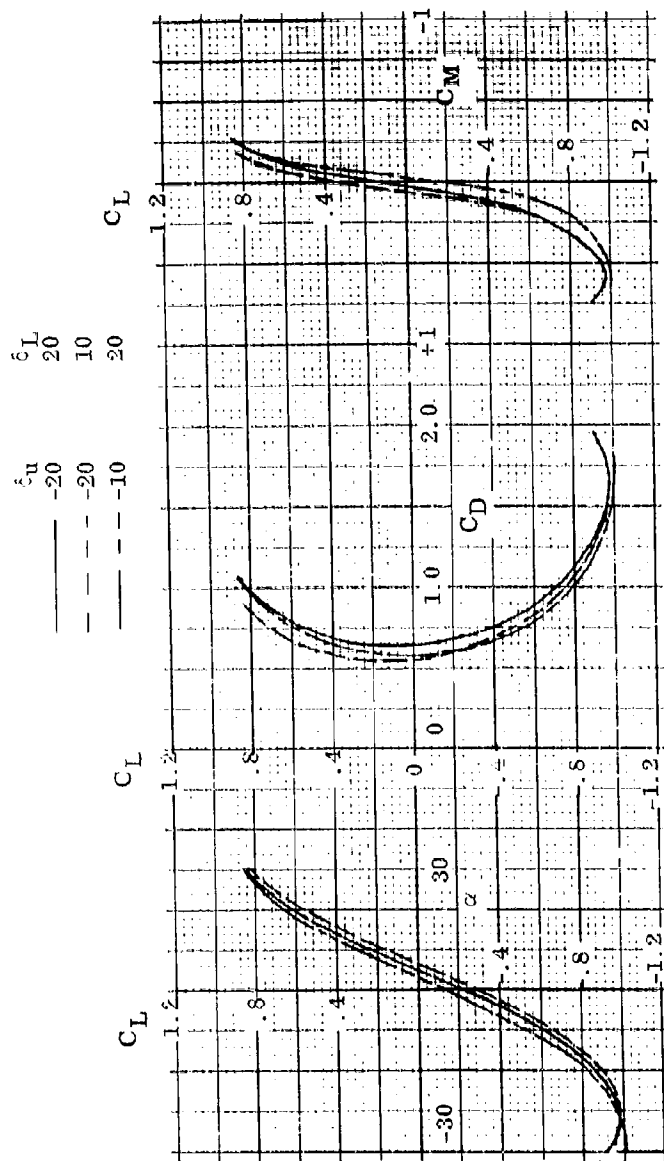


Figure 37- Pod Capsule - Subsonic Aerodynamic Characteristics

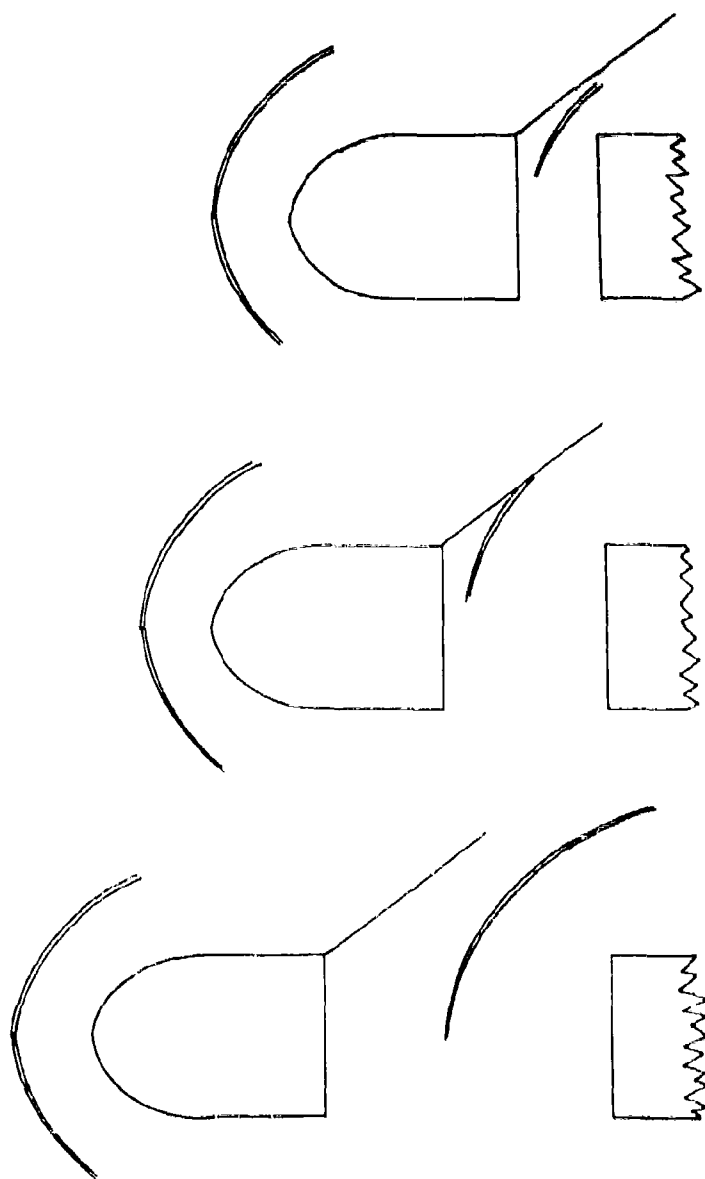
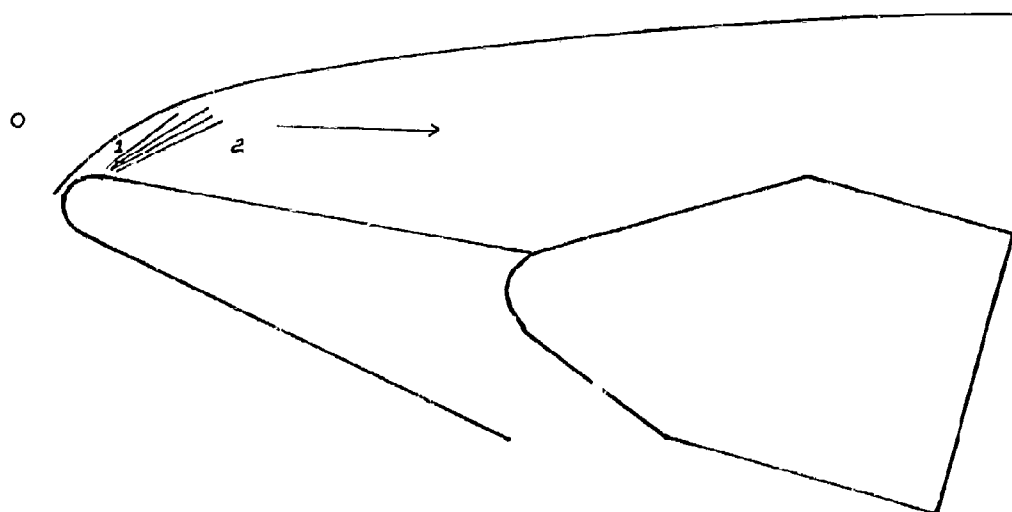


Figure 38 - Ballistic Body Flow Field Interference



FLOW REGION	MACH NO.	FLOW DEFLECTION	q
0	20.	0	65
1	4.4	22°	312
2	7.85	- 2°	33

Figure 39 - Rod Hypersonic Interference

## SECTION 4

### ANALYSIS TECHNIQUES

This section will discuss the analyses techniques used in computing trajectory performance and aerodynamic heating.

#### 4.1 TRAJECTORY PERFORMANCE

4.1.1 TWO DEGREE OF FREEDOM PROGRAM. A modification of an existing General Dynamics/Astronautics IBM 7090 digital computer, two degree of freedom trajectory analyses program was used in the present study. It was used in determining preliminary separation trajectories, long time escape trajectories and recovery ceiling characteristics. The basic program is a point mass non-rotating earth trajectory program. For use in this escape study the following modifications were introduced:

1. A constant value of escape rocket thrust for a preselected burning time.
2. Initial bank angle and preselected roll rate to a desired final bank angle.
3. Trim lift coefficient as a function of time.

The output of this program consists of time histories of position, velocity, angles and load factor.

4.1.2 SIX DEGREE OF FREEDOM. For analysis of separation techniques at the re-entry escape condition a six degree of freedom IBM 7090 trajectory analysis computer program was utilized.

4.1.2.1 Basic Program. The basic program consists of a series of subroutines that can be readily adapted to the peculiarities of each individual configuration. A basic data package is prepared that consists of aerodynamic characteristics, thrust data, inertias, autopilot controls, and vehicle reference data. These inputs will be discussed in more detail as the various subroutines are discussed.

Because of the short times used for separation, a flat earth has been utilized. The program will handle unlimited attitude (Euler angles), aerodynamic angles, and flight path angles which are computed from body axis velocities. Initial conditions at separation are input to the program and variables such as initial velocity, altitude, flight path angle, angle of attack, and angular rates can be simulated.

The main or driver subroutine consists of a series of call statements that put program control in the other subroutines. The first subroutine that is called is the input where all input is read and stored in the computer.

The navigation subroutine computes vehicle attitude, aerodynamic angles, flight path, separation distances, and total velocity by a modified Gill integration subroutine. This type integration method allows an unlimited number of simultaneous integrations. The time increment for integration can be varied during the run as a function of elapsed time from separation. Separation distances of the escape vehicle are computed from the undisturbed flight path of the parent vehicle.

An atmosphere subroutine computes density, gravity, pressure ratio and dynamic pressure as a function of altitude.

Mass, inertias, and center of gravity position are varied as a function of weight remaining during and after separation thrust. Separation thrust is calculated by using a mass flow variation with time and ISP as a function of altitude as input.

The autopilot subroutine will be discussed in detail in Section 4.1.2.2.

The aerodynamic subroutine is based on Modified Newtonian impact theory. Aerodynamic characteristics of the configuration without controls are curve fitted as a function of angle of attack. Surface contributions are based on computed local direction cosines of velocity and the surface normal. The flap characteristics are input as a function of shadow area and angle of attack at various deflections. Total vehicle aerodynamic forces and moments are then calculated for the desired flap deflections, which are input to this subroutine from the autopilot section of the program.

This program allows several options for the separation trajectory. Thrust moments may or may not be included. For the thrust moment option, moments are calculated based on the thrust angle, thrust vector location, and center of gravity location which are program inputs, or in the case of the center of gravity is a function of vehicle weight. Thrust gimbaling (used to reduce thrust moments) is also a program option and the thrust angle is then determined by the autopilot.

Vehicle motion may be controlled by either fixed aerodynamic surfaces, aerodynamic damping, or reaction controls. Combinations of fixed aerodynamic surfaces and reaction controls or aerodynamic damping and reaction controls may be utilized. Surface angles for damping and reaction control operation are determined by the autopilot. The locations and direction cosines of the reaction control thrust are input to the program.

4.1.2.2 Autopilot. In investigating the separation characteristics of the various vehicles, it was required to simulate autopilots with varying degrees of complexity. Since the purpose of the present study was not to generate the details of a control system, the intention was to use the autopilots and control systems as described in Reference 1 as far as practical. The turnaround vehicle required a more sophisticated autopilot, and is described in detail. Differences in the autopilots for the other configurations will be noted where applicable.

Figure 40 is a block diagram of the turnaround autopilot simulation. Three parallel body axis channels are shown, which are the roll, pitch, and yaw axis channels.

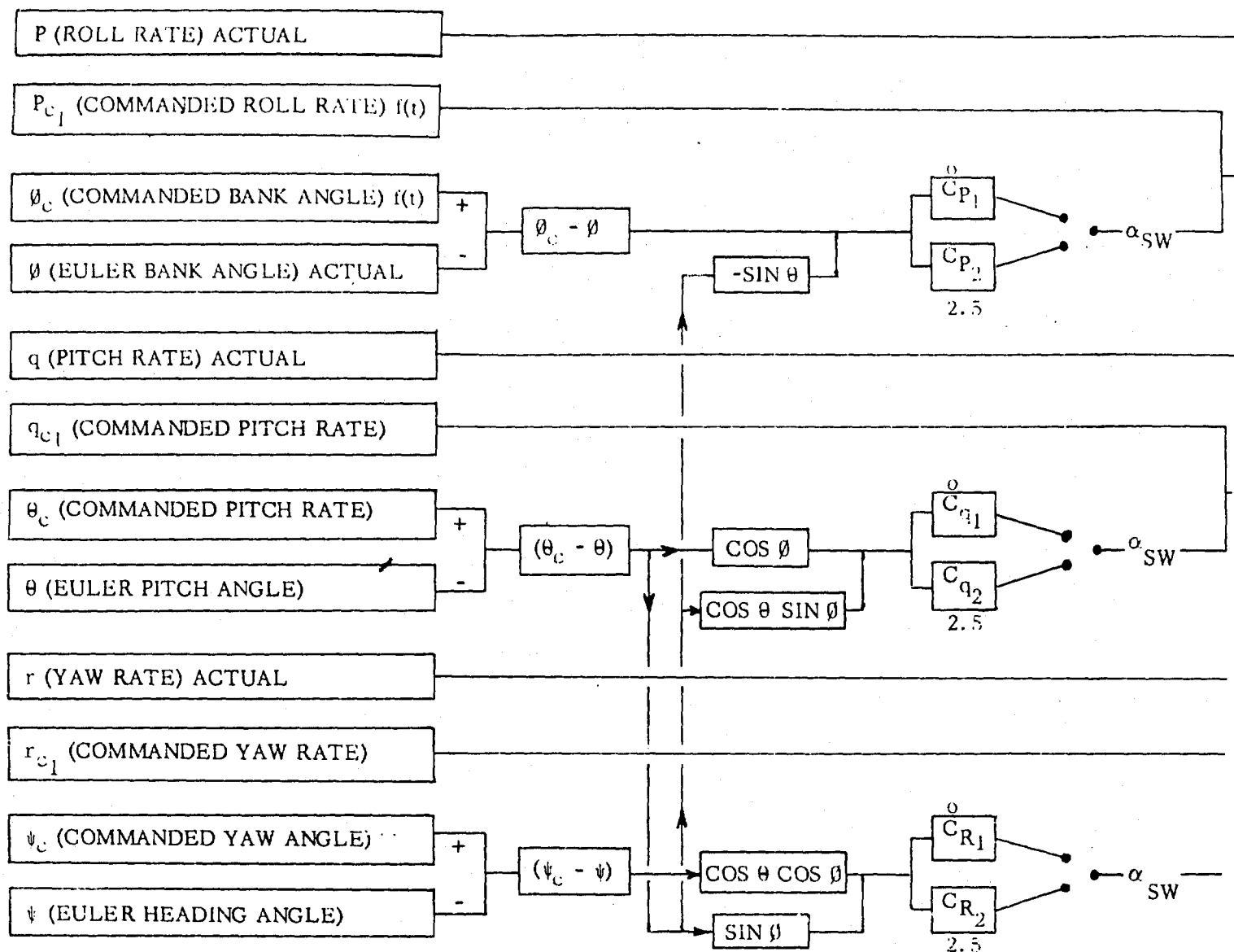
The maneuvering commands are inserted as programmed time histories of either commanded body rates ( $p_c$ ,  $q_c$ ,  $r_c$ ) or command Euler angles ( $\phi_c$ ,  $\theta_c$ ,  $\psi_c$ ), and are assumed triggered by either the separation command and/or the angle of attack switch described below. The large angles associated with the turnaround concept require a resolution of the Euler angle errors into body axis commands, as shown in Figure 40. The azimuth angle error is fed into all three channels, and the pitch angle error into two. For the lifting body, the largest excursion of an Euler angle from straight and level is the initial  $45^\circ$  bank. Thus no resolvers were considered necessary, and the Euler angles ( $\phi$ ,  $\theta$ , and  $\psi$ ) were used in the body-axis channels directly.

The angle errors, when used, are added to the rate errors with a gain of 2.5 deg/deg/sec. This value was selected in Reference 1 and was found to be satisfactory. This gain is noted by CP, CQ, and CR with subscripts of 1 and 2. The 1 denotes before the angle of attack switch and the 2 after the switch is actuated. The limiter sets the maximum commanded angular rates, although this is an input value,  $\pm 15$  degrees per second was generally used. The difference between the commanded angular rates and the actual rates generate the body axis rate errors.

These body axis rate errors are fed into a pure time delay in which on-off switching takes place to actuate the reaction controls. Thresholds in the on-off command of  $\pm 2$  deg/sec were used and proved satisfactory. Each body axis channel as independent reaction controls. The lifting body reaction controls utilized a roll-pitch mixer as indicated in Figure 41. Roll and pitch errors go into the on-off command and if error is greater than the threshold a P and R equal to  $\pm 1$  is sent to the roll-pitch mixer where  $P+R$  and  $P-R$  are resolved. Mixer output goes to another set of on-off commands with a threshold of .5 and if command is  $\pm 2$ , the reaction controls will be actuated as either pure roll, pure pitch, or a combination of roll and pitch.

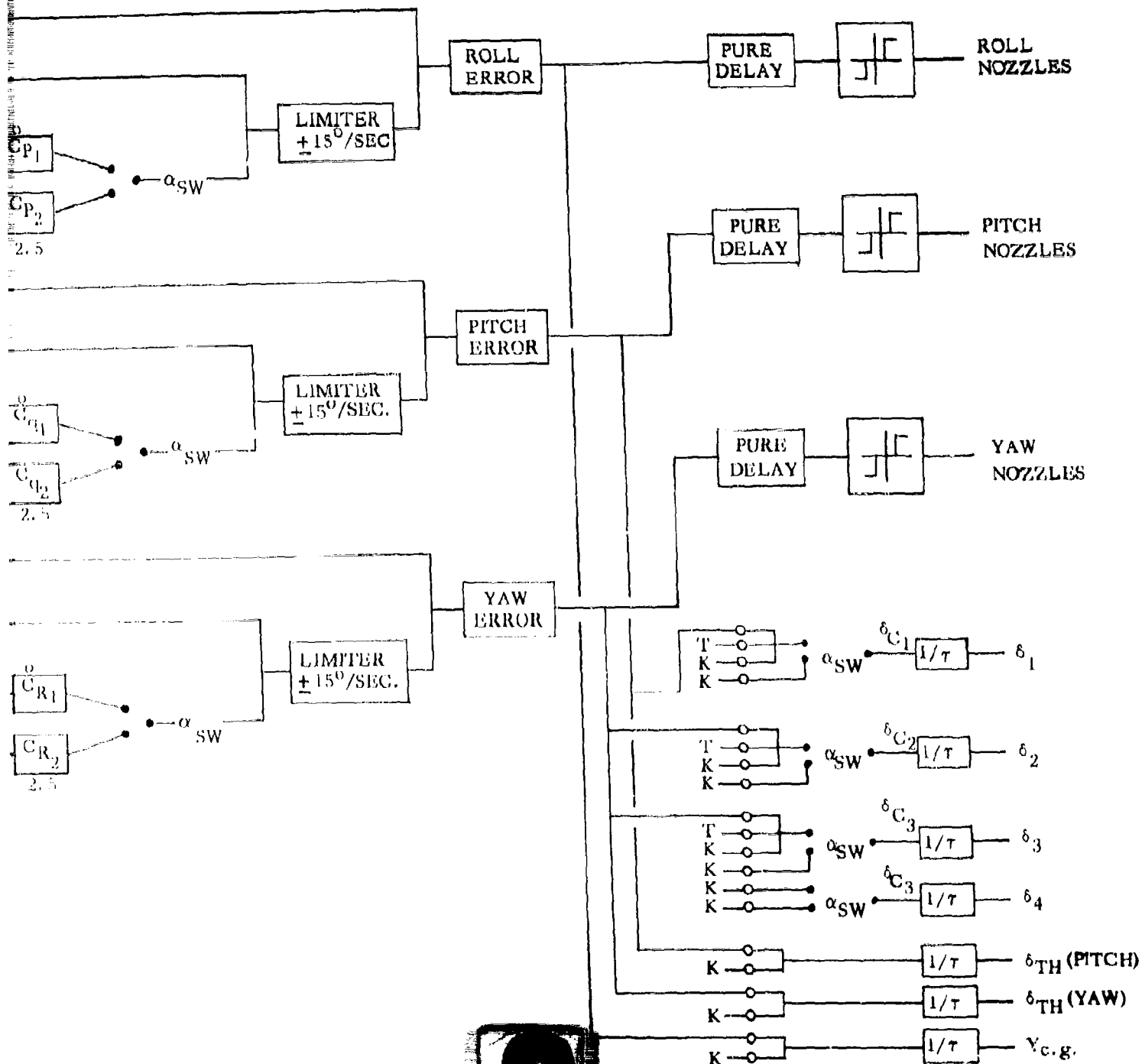
The same body axis rate errors as generated for the reaction controls were also used to drive the aerodynamic surfaces, the thrust gimbals, and the lateral ballast transfer. These were all assumed to be proportional first-order systems. Time





1

Figure 40 - Autopilot Schematic - Tu



1 - Autopilot Schematic - Turnaround Capsule

2

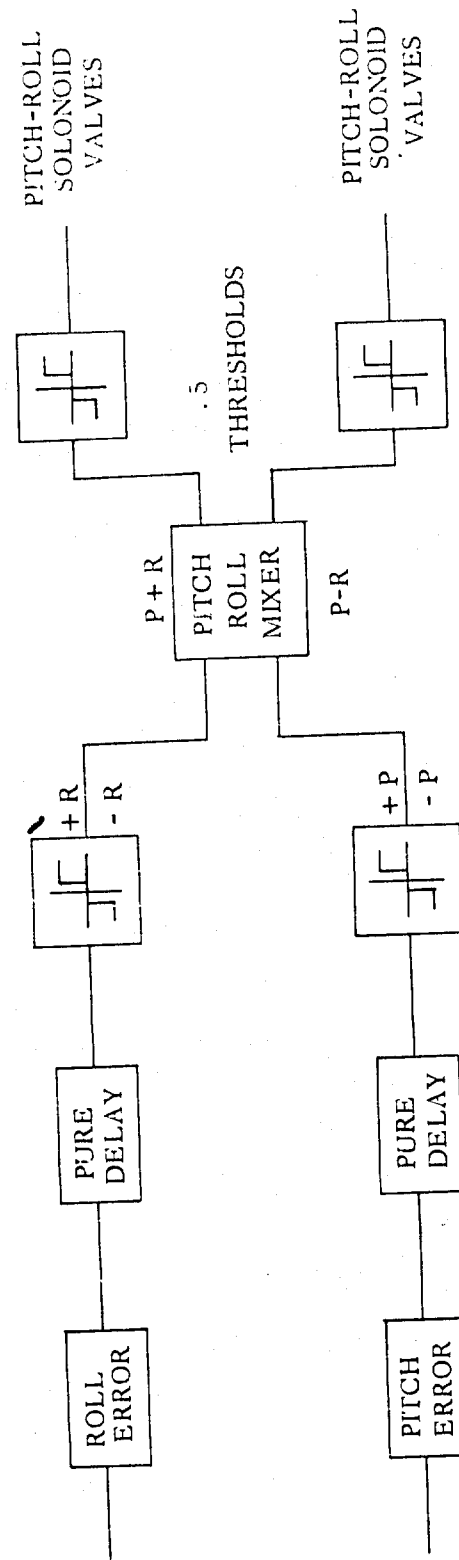


Figure 4: - Pitch Roll Mixer Schematic

constants of .1 second time lag were used for the surface and gimbal actuators, representing responses of hydraulic actuators well within current state-of-the-art. Comparison runs with ideal (no lag) actuators showed no appreciable effect. Program input could cause the flaps to deflect as a function of time or to use the control surfaces as an aerodynamic damping device.

For the turnaround concept it was required to have the flaps retracted on initial separation, and to open after the vehicle had pitched beyond 90 degrees. Thus a one-shot switch was provided, actuated by angle of attack, that opened the flaps to a predetermined position. For the lifting body and the ballistic body the angle of attack switch was not utilized as the flaps were deflected at separation. However, for the pod configuration it was necessary to utilize the switch for actuation of the lower flap because the configuration is buried in the parent vehicle and flap deflection could not take place until sufficient separation was achieved.

The lateral mass transfer system for roll trim was included in the simulation, but was not utilized in the short time histories studied.

4.1.3 **THREE DEGREES OF FREEDOM.** A three degree of freedom trajectory program was utilized for the analysis of separation techniques in the high dynamic pressure regime, on the pad, landing, and for orbital escape. The six degree of freedom program was modified to yield a three degree of freedom program. This program has those same features as discussed in Section 4.1.2 which are applicable to three degrees of freedom. The aerodynamic subroutine was modified to use subsonic and supersonic aerodynamic data.

## 4.2 **AERODYNAMIC HEATING**

4.2.1 **AERODYNAMIC HEATING ANALYSIS PROGRAM.** Aerodynamic heating characteristics were calculated using an IBM 7090 computer program. This program can be used to calculate surface temperature or temperatures interior to the surface as a function of time along any flight trajectory.

The program calculates the heat transfer by convection to the surface and then performs an energy balance at the surface to obtain the surface temperature. The balance is made by convection to the surface, radiation to space, conduction into the surface and storage in the surface material over the calculation time interval.

Convection heat transfer rates are calculated by breaking the configuration to be analyzed down into one or more basic shapes. These shapes are: 1) flat plate; 2) wedge; 3) cone; 4) sphere; and 5) swept cylinder. Eckert's reference enthalpy method for a flat plate is used for 1), 2) and 3). Configurations 2) and 3) can be related to a flat plate. Real gas equilibrium shock layer properties are calculated from curve fits

in the program and used in the reference enthalpy method. Sphere heat transfer rates are calculated using Kemp and Riddell's equation for stagnation point heating. Swept cylinder rates are calculated by modifying sphere rates for two dimensional stagnation line and sweep effects.

Increases in convective heat transfer rates over undisturbed Eckert stagnation values are accounted for by a correction factor which is put into the program as a function of time.

Radiation to space is calculated from the surface temperature and the surface emissivity assuming a zero receiving temperature. Reduction of the view factor to space can be considered by replacing the surface emissivity by an effective surface emissivity. An effective emissivity is defined as the surface emissivity times the view factor.

Conduction into the surface is calculated by a finite difference method which allows for up to 20 segments where each can be a different material. The boundary of the last segment can be adiabatic or diabatic. The diabatic case allows heat transfer to a fluid to be considered. Energy storage of the segments is included. The thermal conductivity and specific heat of each material can be entered as a fourth degree polynomial function of temperature. It is this part of the program which enables insulation thickness, fuel bolloff, structural temperatures, and temperature distributions to be calculated. The first segment temperature is considered the surface temperature.

4.2.2 TRANSITION REYNOLDS NUMBER EFFECTS. Aerodynamic heating rates and the resulting surface temperatures are dependent upon the type of boundary layer existing at the position being investigated. Figure 42 is a schematic of the boundary layer flow over a flat plate at an angle of attack. The forward part of the plate is covered with a laminar boundary layer to the transition line. At the transition line, the shock layer Reynolds number,

$$N_{R_c} = \frac{\rho_s V_s x}{\mu_s}$$

equals by definition the transition Reynolds number value. Downstream from this line, a turbulent boundary layer exists. Figure 43 indicates schematically the difference in temperature levels associated with the two types of boundary layers. The turbulent boundary layer has the higher heat transfer rates and hence the higher surface temperatures.

Now, as the velocity and altitude along a trajectory decrease, the shock layer unit Reynolds number,  $\frac{\rho_s V_s}{\mu_s}$  increases until the Reynolds number at the

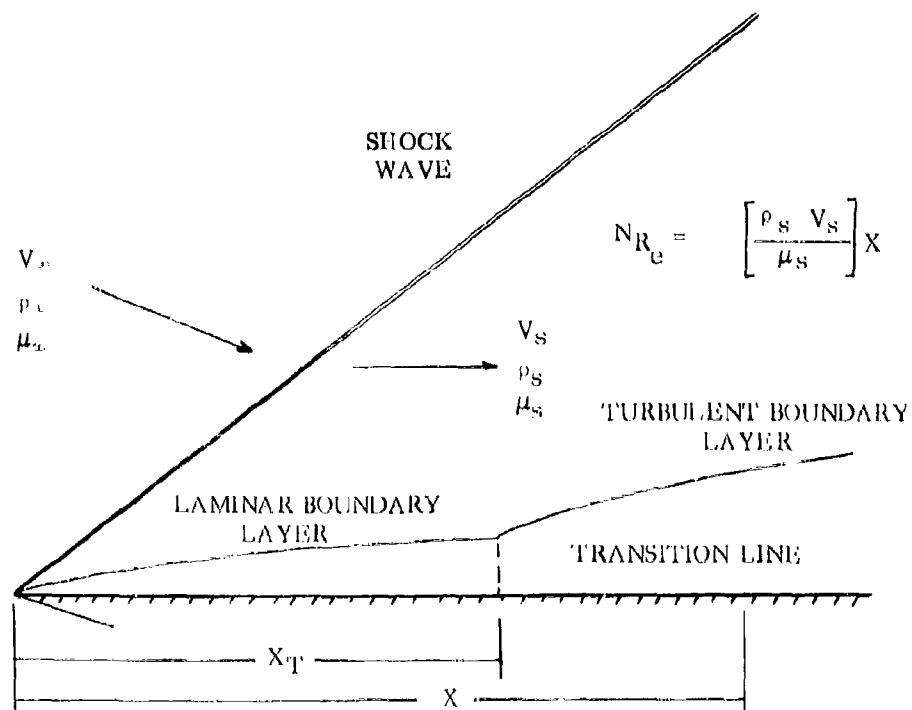


Figure 42 - Boundary Layer Schematic

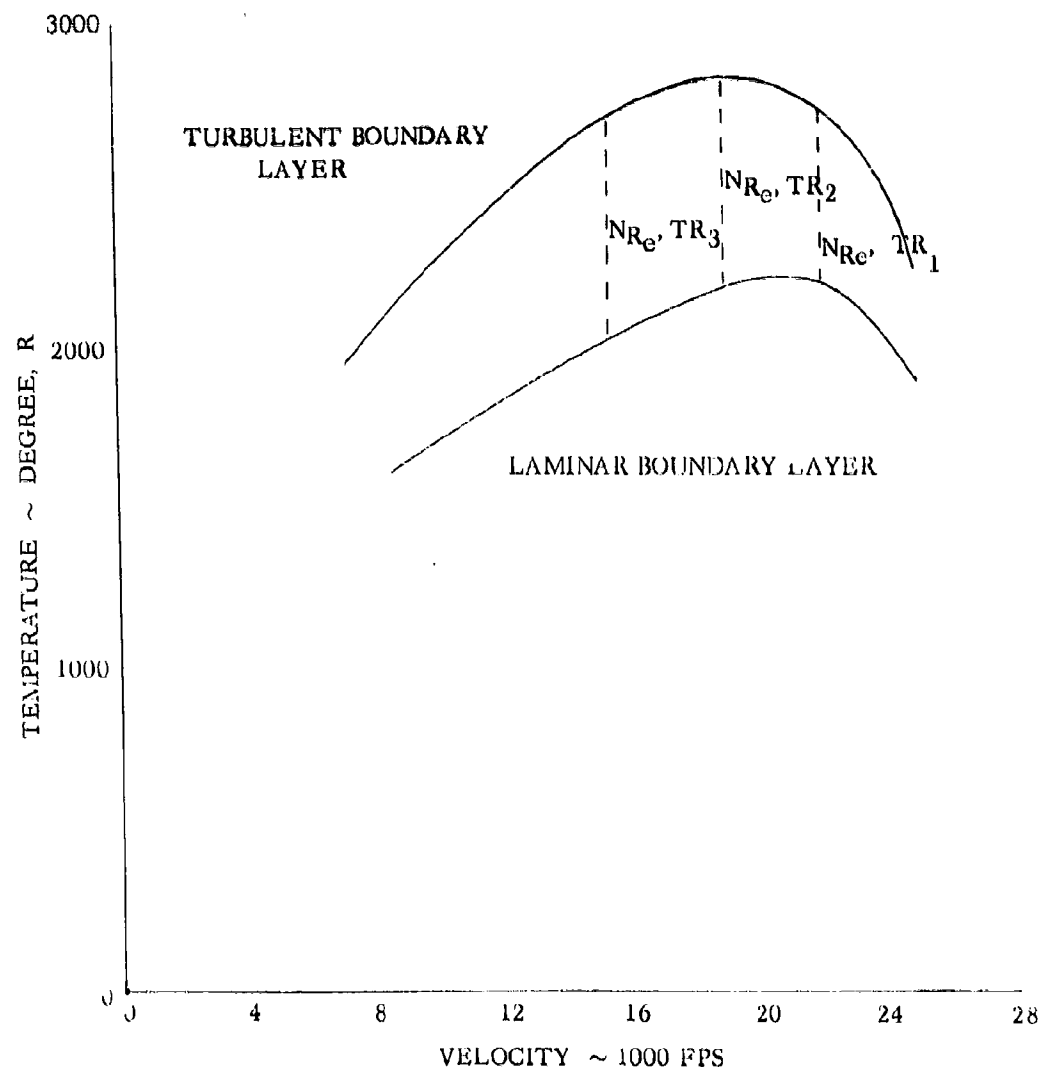


Figure 43 - Effect of Transition Reynolds Number on Temperature

point under investigation can exceed the transition value. Then the point in question experiences turbulent boundary layer flow with the higher heating rates and temperatures. The vertical lines labeled  $N_{R_e}$  TR on Figure 43 indicate the transition to the higher temperatures at three different values of transition Reynolds numbers.

It can be seen from Figure 43 that the value of transition Reynolds number can have an effect on the selection of materials and trajectories. Unfortunately, the definition of the transition Reynolds number for different configurations is not well known.



## SECTION 5

## SEPARATION PROPULSION

An escape capsule requires a propulsion system to supply the force necessary to quickly place the capsule in a safe environment. This section will present the results of a survey of design data and discuss some of the installation aspects of separation propulsion systems for a re-entry escape capsule.

## 5.1 ESCAPE ROCKET DESIGN DATA

5.1.1 SURVEY OF DESIGN DATA. Because of the high reliability and inherent simplicity associated with small solid propellant rockets this type was selected for the separation propulsion system. This selection should not eliminate hypergolic bipropellant liquid escape rockets, with their attendant throttling potential, from future studies.

A review of the major parameters of about fifteen operational, cylindrical case solid propellant rockets was made (References 10 & 11). The range of these parameters, which covers that anticipated for the escape capsule separation rockets, is shown in Table I. These are all fixed nozzle configurations with short burning times and of relatively small total impulse. The range of parameters is comparatively narrow so that a definite trend of parameters with weight or thrust was not evident. However, it was possible to select nominal design values which represent the state of the art. These are shown in Table II. The selected values should apply for some time into the future since a large improvement with time is not to be anticipated in high reliability items of this size.

A useful parameter is total impulse/total weight. Figure 44 shows a plot of this parameter versus total impulse. Points for some of the rockets examined are plotted, all of which have burning times under five seconds. A nominal value of 155 is selected as being appropriate for preliminary design of escape capsule separation rockets.

5.1.2 DESIGN TECHNIQUE. This section gives a preliminary design method for arriving at the escape rocket size and configuration, for use in the escape capsule studies. The parameters used here are those selected for the overall survey described in Section 5.1.1.

Installation problems (discussed in Section 5.3) may require restricting the expansion ratio of the escape rocket nozzles. Reducing the expansion ratio reduces the thrust and specific impulse. For instance, at  $\gamma = 1.20$ , the vacuum specific impulse of 235 lb<sub>F</sub>/lb<sub>M</sub>/second requires an expansion ratio of 7. With an expansion ratio of 3 the specific impulse is reduced to approximately 227 lb<sub>F</sub>/lb<sub>M</sub>/second. These changes are not expected to have a large effect on the overall system. Once a given propellant ratio of specific heats and a given installed expansion ratio are fixed, these numbers can be refined for a specific design.

TABLE 1

## TYPICAL PARAMETER RANGE FOR ESCAPE TYPE SOLID PROPELLANT ROCKETS

ITEM	VALUE	UNITS OR SYMBOL
Total Impulse	1470-58675	Lb <sub>F</sub> - Sec.
Specific Impulse	211-270	Lb <sub>F</sub> /Lb <sub>M</sub> /Sec.
Burning Time	0.27-12.0	Seconds
Thrust, Average	3000-34300	Lb <sub>F</sub>
Chamber Pressure, Max.	780-4000	Lb/In <sup>2</sup>
Expansion Ratio	1-21	ε
Ratio of Specific Heats	1.16-1.25	γ
Inert Parts Fraction	25-53	%
Volumetric Loading Density	60-91.7	%
Total Impulse/Total Weight	84-172	-
Overall Weight	8-281	Lb.
Length	15-107	Inches
Diameter	5-12	Inches

TABLE II  
SELECTED ESCAPE ROCKET CHARACTERISTICS

ITEM	VALUE	UNITS OR SYMBOLS	REMARKS
Propellant Type	-	-	Solid
Temperature Limit	-65 to 200	$^{\circ}\text{F}$	Limit
Total Impulse*	40,000	$\text{Lb}_\text{F} \cdot \text{Sec.}$	For Ballistic Capsule
	25,000	$\text{Lb}_\text{F} \cdot \text{Sec.}$	For lifting body
Nominal Thrust (SL)*	40,000	$\text{Lb}_\text{F}$	For Ballistic Capsule
	25,000	$\text{Lb}_\text{F}$	For Lifting body
Chamber Pressure	1,000	$\text{PSIA}$	Selected Value
Expansion Ratio	7	$\epsilon$	May be reduced for installation.
Ratio of Specific Heats	1.20	$\gamma$	Review for given propellant type.
Specific Impulse (S.L., Delivered)	220	$\text{Lb}_\text{F}/\text{Lb}_\text{M}/\text{Sec.}$	Selected Value
Specific Impulse (S.L., $P_c = 1000$ psia, opt. exp.)	222	$\text{Lb}_\text{F}/\text{Lb}_\text{M}/\text{Sec.}$	$\Delta T \epsilon = 7, \gamma = 1.2$
Specific Impulse (Vacuum)	235	$\text{Lb}_\text{F}/\text{Lb}_\text{M}/\text{Sec.}$	From above value
Total Impulse (SL)	155	$I/W$	For $\epsilon = 7$ .
Total Weight			From above value.
Inert Weight	29.5	%	Nominal state of art selection. See Figure 1.
Total Weight			Follows from item above with $I_{sp} = 220$ .
Volumetric Loading	80	%	$\frac{\text{Propellant Volume}}{\text{Chamber Volume}}$
Max. Burn Rate	5	$\text{In}/\text{Sec.}$	-
Ignitor Type	-	-	Pyrogen
Propellant Density	.063	$\text{Lb}/\text{In}^3$	-
Case Material	-	-	#4130 Steel
* Selected earlier in this study (Reference 4 and 5).			

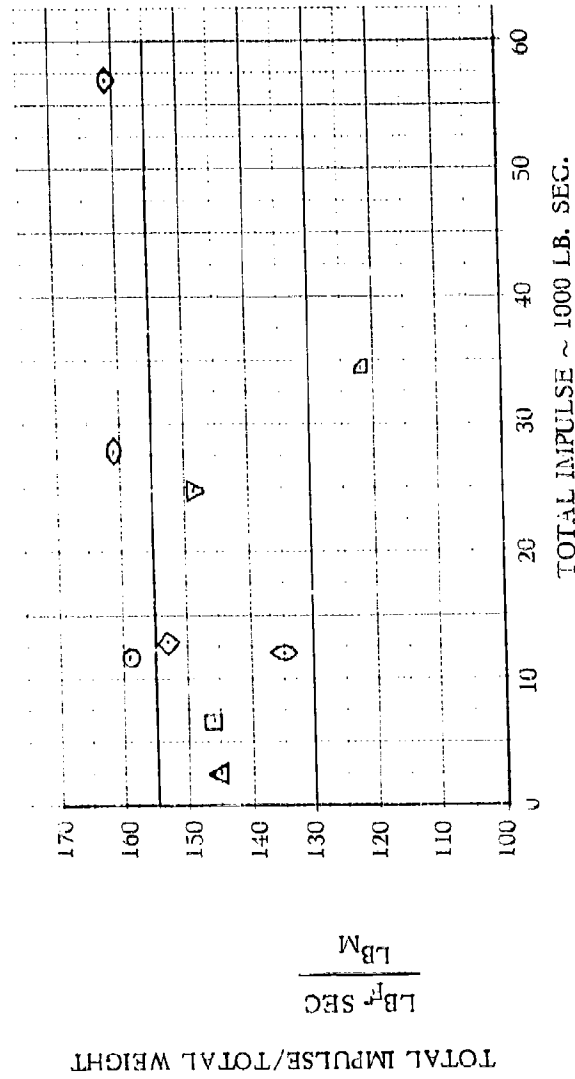


Figure 44 - Solid Rocket Impulse to Weight Characteristics for Several Operational Short Burn Time Configurations

Once the required impulse and burning time are given the rocket can be sized. Take for example a 40,000 pound thrust, 40,000 lb-sec. impulse requirement at sea level. Examine the case where three separate rocket modules make up the requirement, then:

$$F_{SL} = 40,000/3 = 13,300 \text{ lb.}$$

$$\text{Propellant Wt.} = \frac{13,300}{220} = 60 \text{ lb.}$$

$$\text{Total impulse} = 13,300 \text{ lb.}$$

$$\text{Chamber volume} = 1/.80 \times \frac{60}{.063} = 1190 \text{ in}^3$$

Assume a cylindrical chamber with a fineness ratio,  $l/D = 6$ , then

$$D = \sqrt[3]{\frac{4}{6\pi} V} = .596 \sqrt[3]{1190} = \underline{6.3 \text{ in.}}$$

$$\text{Length of cylindrical chamber} = 6 \times 6.3 = \underline{37.8 \text{ in.}}$$

The nozzle is sized as follows:

$$A_t = \frac{F}{C_F \times P_c} = \text{throat area}$$

$$\text{where } F = \text{required thrust} = 13,300 \text{ lb.}$$

$$P_c = \text{chamber pressure} = 1000 \text{ psia}$$

$$C_F = \text{thrust coefficient} = 1.59$$

therefore

$$A_t = \frac{13,300}{1.59 \times 1000} = 8.4 \text{ in}^2$$

$$\text{then } A_t = 3.28 \text{ in.}$$

$$\text{Also } D_{\text{exit}} = D_t \sqrt{\epsilon}$$

$$\text{For an expansion ratio } A_{\text{exit}}/A_{\text{throat}} = \epsilon = 3$$

$$\text{Then } D_e = 3.28 \sqrt{3} = 5.68 \text{ inches.}$$

Preliminary designs for various numbers of rocket modules (from 1 to 5) have been made in the above manner for a 40,000 lb-sec. impulse case. These are shown in Figure 45 where the comparative sizes, and the effects of expansion ratio can be seen.

For preliminary design purposes the nozzle can be straight lined from throat to exit at a  $15^\circ$  angle to the centerline (Figure 45). For the offset nozzles required for the present escape capsule concepts a smooth transition from chamber to throat around the thrust inclination angle must be allowed for.

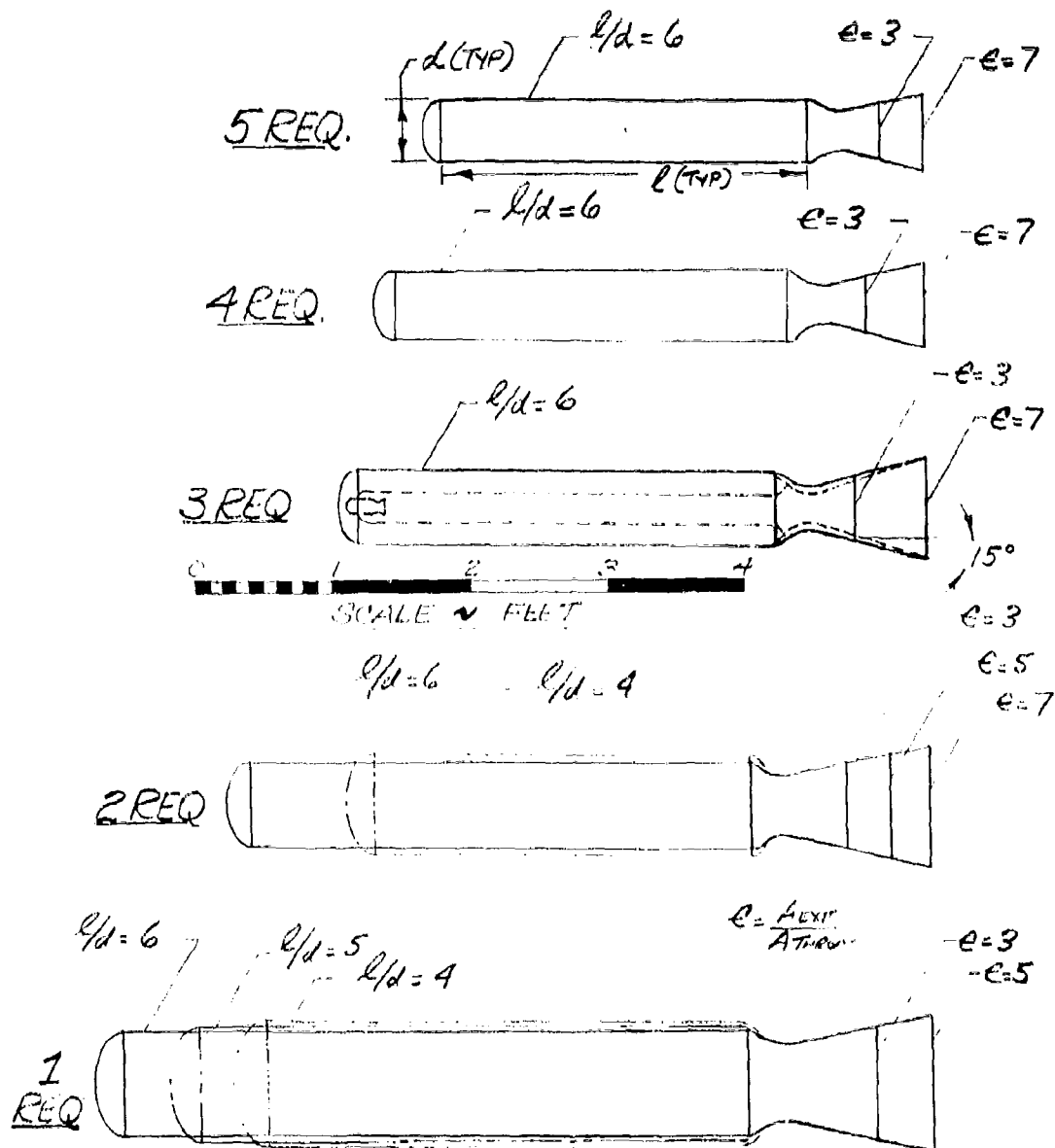


Figure 45 - Comparison of Typical Escape Rocket Size Vs. Number Required ( $F_{TOTAL} = 40 \text{ K\#}$ )

## 5.2 ESCAPE ROCKET REQUIREMENTS

5.2.1 ROCKET SIZE REQUIREMENTS. In all cases the separation rocket thrust must be between that value which provides sufficient separation distance in a brief time and a maximum value determined by human tolerance limits to accelerations.

The rocket size requirements are established by the characteristics at certain critical escape points. For a vehicle which is rocket boosted into orbit and makes a gliding re-entry the following conditions are critical from the standpoint of escape rocket requirements.

- a) On-the-Pad
- b) Maximum Dynamic Pressure
- c) Orbit Escape

5.2.1.1 On-the-Pad. The hazard for on-the-pad escape which places the most severe requirement on the separation propulsion system is the booster explosion hazard. In an explosion the escape capsule must be removed not only from the booster but from the relatively large region in which the explosion overpressures would destroy the capsule. Since there are no relieving aerodynamic forces at this escape condition, human tolerance limits to acceleration dictate maximum allowable escape rocket thrust.

5.2.1.2 Maximum Dynamic Pressure. As in on-the-pad escape the explosion hazard is the most severe hazard at maximum dynamic pressure. The capsule must not only be separated from the primary vehicle but must achieve a safe environment away from the primary vehicle. Escape at this condition is complicated however by the fact that the capsule must overcome large aerodynamic forces in order to achieve separation. The aerodynamic forces at this escape condition determine the minimum escape rocket thrust level. The propulsion system must also have characteristics such that in providing adequate separation it does not place the capsule in an environment at burnout which produces load factors exceeding human tolerance limits.

5.2.1.3 Orbit Escape. There are two requirements on the propulsion system for orbit escape. The capsule must first be separated from the primary flight vehicle and then an impulse is required for de-orbit. Unless an explosive hazard is encountered, such as perhaps a docking collision with a vehicle containing fuel and oxidizer, the departure of the escape capsule from a damaged parent vehicle could be made in relatively leisurely fashion. From a weight standpoint it would be desirable that the separation rockets also serve as the retro-rockets. This would be dependent upon the results of a hazard analysis for a specific vehicle and mission.

5.2.1.4 Selected Rocket Sizes. Two nominal rocket sizes have been selected for the four escape capsule concepts based upon the data presented in Reference 1. These are as follows:

Capsule	Impulse Lb-Sec.	Thrust Lbs.	Burn Time Sec.
Ballistic Body	40,000	40,000	1.0
Lifting Body	25,000	25,000	1.0
Turn-around	25,000	25,000	1.0
Rbd	40,000	40,000	1.0

The detailed thrust-time histories of the two basic escape rocket sizes are presented in Figure 46 and 47. A decreasing thrust with time is used since this follows the trend of the human tolerance limit to acceleration. These thrust characteristics presented in Figures 46 and 47 were the nominal thrust characteristics used in the performance analysis.

**5.2.1.5 Retro-Rocket Characteristics.** It was mentioned above that it is desirable that the separation propulsion system also serve as the retro-rocket system. In view of this, a brief investigation of the retro-rocket capability of the two nominal propulsion sizes listed above has been made. The analysis was made assuming that the total impulse could be obtained from one or up to 5 rocket modules. The selection of the number of modules will be discussed in more detail in Section 5.2.

The potential  $\Delta V$  available for retrofire from each of several modules is shown in Tables III and IV for the two nominal rocket sizes. The values are based on a nominal capsule weight of 2500 lbs. and respective propellant weights of 180 lbs. and 113 lbs. The vacuum specific impulse of 235 Lb<sub>f</sub>/Lb<sub>M</sub>/Sec. is used.

The effect of  $\Delta V$  on re-entry conditions at an altitude of 500,000 ft. is shown in Figure 48. Since the orbit altitude is undefined in the present study it cannot be stated whether the escape rockets would meet the retro-rocket requirement.

**5.2.2 CHOICE OF NUMBER OF ROCKETS.** The previous section has described the conditions necessitating high separation thrust. The performance studies of escape from the maximum heating re-entry point to be discussed in Section 6 indicate that adequate separation performance could be obtained with thrust levels equal to one half the nominal thrust. Based on these considerations, the advantages and disadvantages of breaking the total thrust into as many as five rocket modules were investigated. The final decision as to the number of rockets would be dependent upon the specific vehicle its mission and a thorough reliability analysis of both the vehicle and the separation rockets. The following discussion is meant to serve primarily as a guideline in selecting the number of separation rockets. A maximum of five rockets has been considered although other studies, e.g., Reference 12, have considered larger numbers.



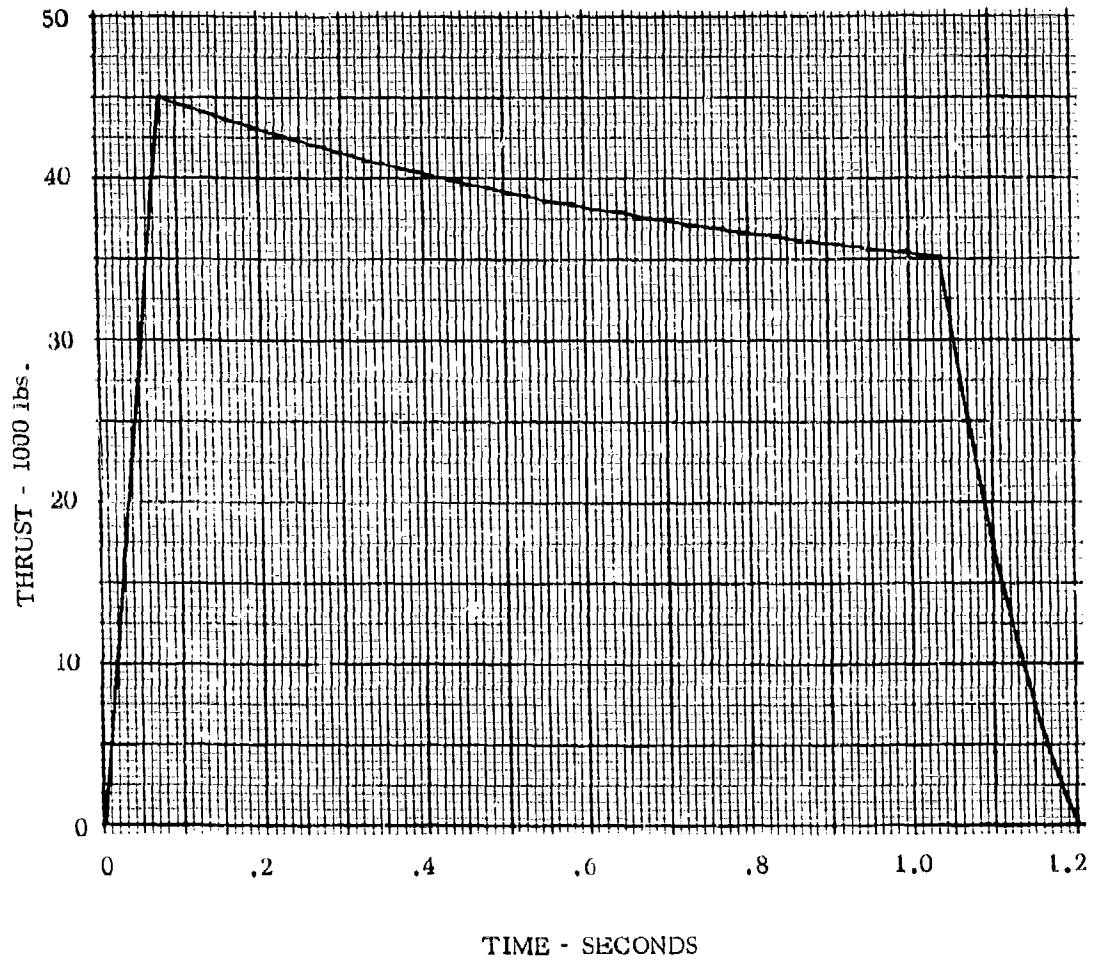


Figure 46 - Escape Rocket Thrust Characteristics - 40,000 Lbs.

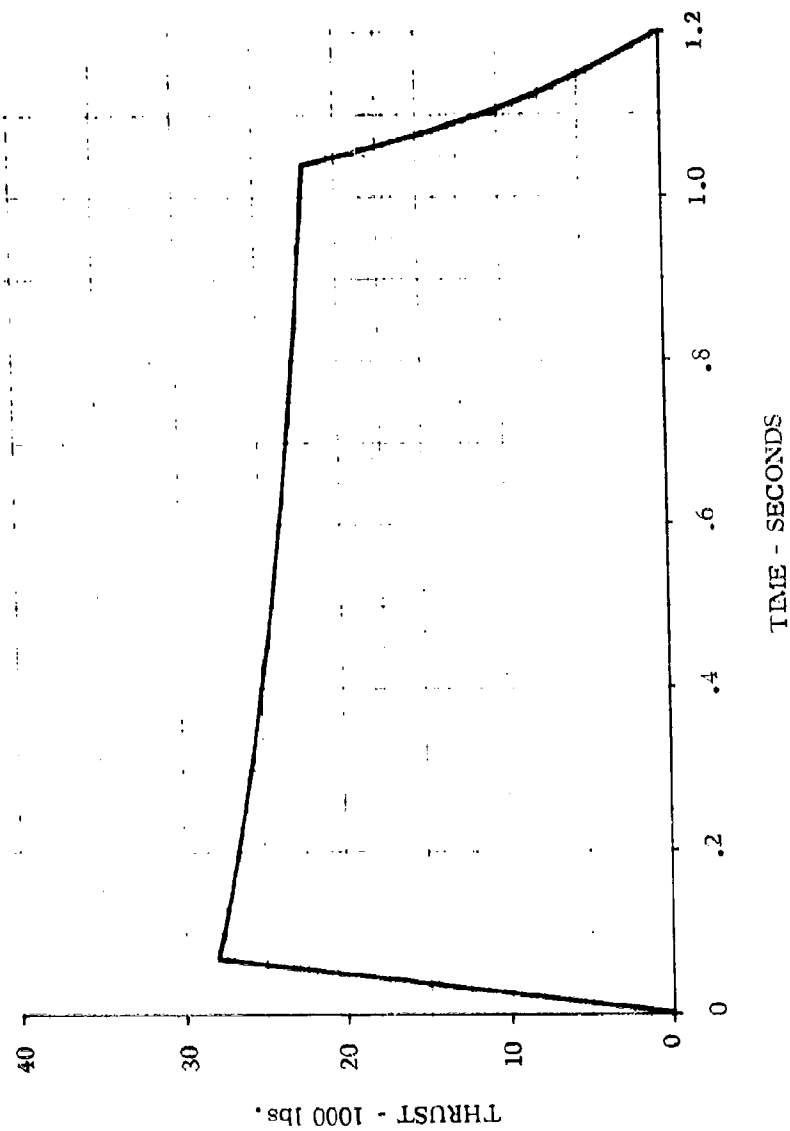


Figure 47 Escape Rocket Thrust Characteristics - 25,000 lbs.

TABLE III  
PROPERTIES OF SEPARATION ROCKET MODULES FOR BALLISTIC CAPSULE

Number of Modules Required	Thrust (each) (Nominal) Lb.	Total Impulse (Each) Lb. - Sec.	$\Delta V$ Retro (Each) Ft. - Sec.	g Max. (Each)
1	40,000	40,000	525*	16.0
2	20,000	20,000	263	8.0
3	13,330	13,330	175	5.33
4	10,000	10,000	131	4.0
5	8,000	8,000	105	3.2
* Also represents total $\Delta V$ available for any group of modules.				

TABLE IV  
PROPERTIES OF SEPARATION ROCKET MODULES FOR LIFTING BODY CAPSULE

Number of Rocket Modules Required	Thrust (Each) (Nominal) Lb.	Total Impulse (Each) Lb. - Sec.	$\Delta V$ Retro (Each) Ft. - Sec.	g Max. (Each)
1	25,000	25,000	332*	10
2	12,500	12,500	165	5
3	8,330	8,330	111	3.3
4	6,250	6,250	81	2.5
5	5,000	5,000	66	2.0
* Also represents total $\Delta V$ available for any group of modules.				

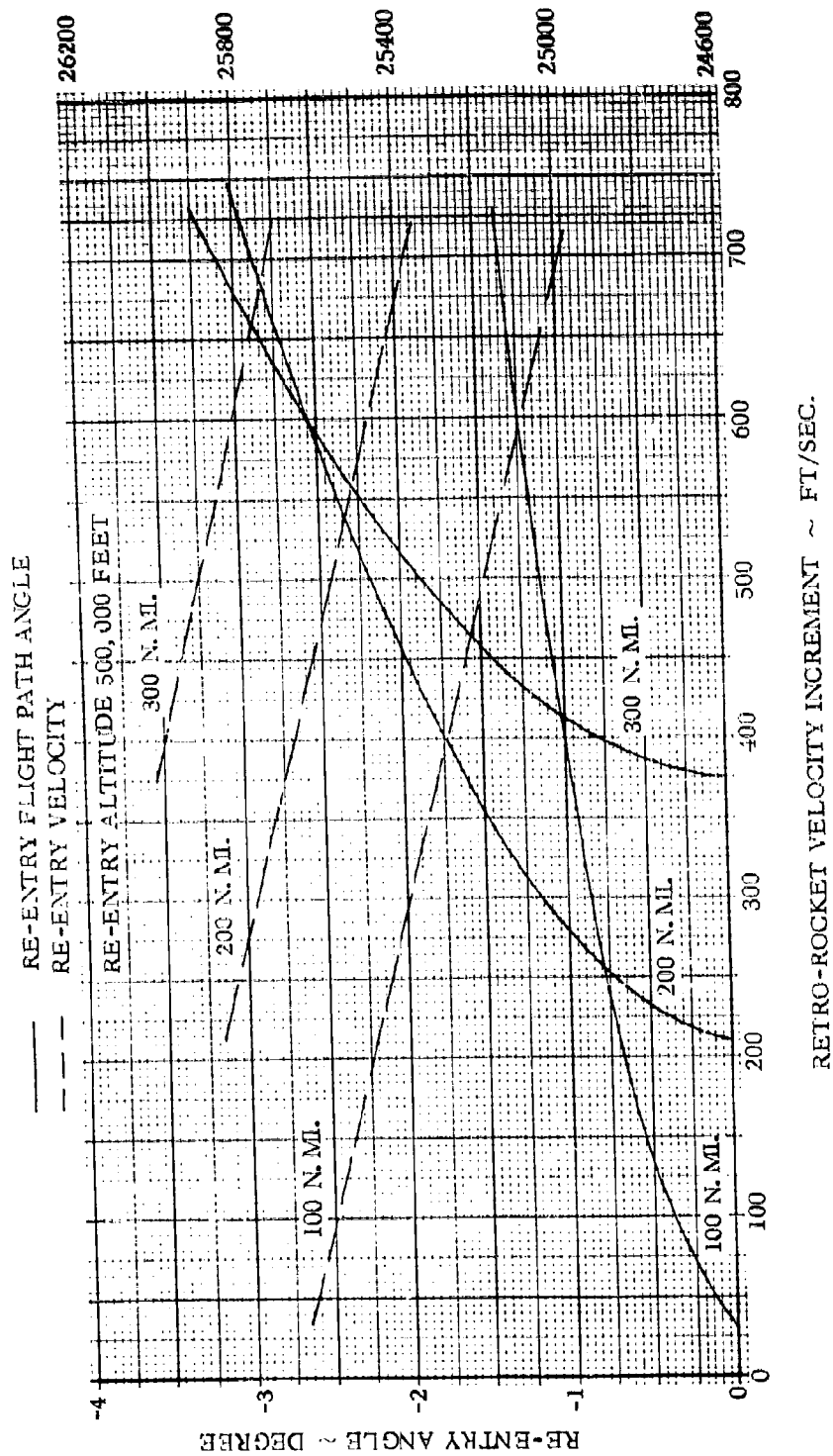


Figure 48 - Effect of Retro-Rocket Velocity Increment on Re-Entry Conditions

**5.2.2.1 One Rocket.** A single rocket is bulky and can be difficult to install from a pilot clearance point of view for small capsules. A single rocket must be installed in the plane of symmetry. Such an installation imposes a structural weight penalty due to the fact that the thrust loads must be transferred outboard to the basic structure. No orbit escape from explosion plus de-orbit retro is possible with a single rocket since only a single impulse can be applied. Only in the case where the vehicle was oriented so that the separation impulse was applied in the desired retro direction could a single rocket meet both requirements. A single rocket does have the advantage of having the highest reliability.

**5.2.2.2 Two Rockets.** Two rockets offer the advantage that they can be installed more easily both structurally and spacewise. Two rockets offer the possibility of half thrust modulation. However, if used in this mode they must have canted nozzles to eliminate thrust moment effects which would incur some thrust penalty. The penalty is more severe with increasing angle as the rockets are moved outboard off the centerline to a more favorable structural attach point and to improve clearance around the pilot and his enclosure. A lower C.G. location also increases the angle and the penalty incurred. There is an additional disadvantage for half thrust operation with a guided separation in that a side load would be imposed upon the guides.

**5.2.2.3 Three Rockets.** Three rockets offer the advantage of thrust modulation capability without imposing sideloads on the guides in a guided separation when used at the 2/3 or 1/3 thrust level. The installation problems of the single rocket are also present for the middle rocket but on a reduced scale. This arrangement also has the possibility as serving as the orbit separation and retro propulsion system.

**5.2.2.4 Four Rockets.** Four rockets offer the advantage of half thrust modulation without a thrust penalty since the nozzles do not have to be canted towards the centerline. For one-quarter thrust modulation a thrust loss would be incurred and the problem of side loads on the guides, if present, would exist. The rockets would be somewhat smaller and thus easier to install. This advantage could be offset somewhat, however, by a slightly more complex structural installation.

**5.2.2.5 Five Rockets.** Five rockets offer a wider range of thrust modulation without a thrust penalty and probably offer the best arrangement for the distribution of thrust between separation and de-orbit for orbit escape. The installation weight penalty would probably be greater due to the fact that there are more thrust loading points.

**5.2.2.6 Conclusions.** As indicated above, the final selection of the number of escape rockets would be dependent upon the specific vehicle, its mission, a weight penalty analysis, and a thorough reliability analysis of both the vehicle and the escape rockets.

Since escape is an emergency operation, an argument for multiple rockets based only on the fact that pilot load factors could be reduced at certain escape conditions is not sufficient. The strongest argument for multiple rockets other than possible installation weight advantages is that a single system would serve for both separation and de-orbit in

the orbit escape condition. Some of the installation problems involved in multiple rockets will be discussed in Section 5.3.

### 5.3 ESCAPE ROCKET INSTALLATION

5.3.1 GENERAL CHARACTERISTICS. The installation of the separation rockets was investigated for each of the four different escape capsule concepts. Installation of the rocket modules ranging from one to five could result in as many as twenty possible combinations. The primary purpose of this study is, however, to uncover the major problems associated with the separation rocket installation and to show typically what such an installation might look like in the various capsule concepts. One typical installation was made for each capsule. While the choice is semi-arbitrary each installation is quite feasible. There are other installations, however, which can be equally as good if not better. The installation methods shown for one capsule can quite probably apply to some of the other capsules. Until such time as more design inputs are available, such as detailed pilot compartment layout, proper capsule size, weight and c.g. location, and structural general arrangement, then the current investigation should suffice to give typical installation requirements for the separation rockets.

Most of the following features apply for rocket installation in all of the capsules:

1. The rocket resultant thrust line must pass through the C.G. in the pitch and yaw planes. If multiple rockets are used, they must have their thrust lines passing through the C.G. in the yaw plane unless fired in symmetrical pairs.
2. The rockets must be thermally protected from the hot environment such that the propellant never exceeds 200°F. This requires insulating the propellant either by increasing the internal insulation or by an external insulation blanket or by retaining the propellant case within the environmentally controlled pilot enclosure. Furthermore, the rocket structural support points must be designed to reduce conduction from the hot truss load carrying structure into the rocket case. Increased internal insulation could be considered here. The nozzle must be insulated and plugged with an insulating diaphragm set to fail at some pre-selected chamber pressure. (An analysis of the heat transfer and insulation requirements for the separation rockets is presented in Section 5.4).
3. The rockets should be mounted so as not to incur dynamic cycling which would increase the propellant temperature to the danger point.
4. The rocket exhaust must be ducted out of the capsule. This infers blow off doors. However, it also creates the problem of exhaust exit holes from the burned out rocket nozzles being exposed to the free stream at re-entry. This requires either closing up the exits, by door or plug or providing enough thermal protection around the rocket case to prevent the heat entering the nozzle from adversely affecting the capsule.

5. There are problems due to the rocket exhaust impinging on the lower flaps. This impingement will induce heating effects and possibly aerodynamic effects. Major impingement will occur at high altitudes due to the fact that the rocket exhaust plumes out. The lower flaps must be designed with this in mind. The heating is reduced by the fact that the burn time is so short.

In order to understand the rocket installation problems, it was necessary to assume a basic structure. For the present study a radiation cooled outer shell supported by a hot truss type structure was assumed. The pilot compartment is an insulated and water cooled environmentally controlled enclosure supported within the hot truss. An initial investigation shows that no untoward problems should be suffered due to the separation rocket thrust loads provided the loads can be introduced into the longitudinal members of the truss without excess eccentricity or offset.

The separation rockets can feasibly be mounted either external to the insulated pilot compartment or inside this compartment. When mounted external to the insulated compartment the main problem is insulating the rocket from the hot truss to which it is attached and also from thermal radiation from the hot environment. If mounted inside the insulated compartment there must be a load carrying connection between the hot truss structure and the rocket. This connection must be insulated to prevent heat being carried to the rocket or the enclosure. It is also required in this case that provisions be included for ducting the rocket exhaust out of the insulated enclosure and also out of the vehicle. The particular capsule installations to be discussed in Section 5.3.2 below have considered the separation rockets mounted external to the insulated pilot compartment.

The rocket support points are envisaged as trunnions attached to the case by bands. These trunnions would have a center pin surrounded by an insulation ring with good compressive stress properties and surrounded by an outer retainer ring attached to the hot structure of the basic capsule.

**5.3.2 INDIVIDUAL CAPSULE INSTALLATIONS.** The following discussion covers the individual capsule installations, which as stated previously are presented as typical examples of possible design approaches.

**5.3.2.1 Ballistic Body Capsule.** The rockets shown in Figure 49 are installed as a pair with nozzles canted outboard and downward so that the thrust line always acts through the C.G. Half thrust modulation is therefore possible. The side force incurred here might present problems in loading on separation guides if used. The structural attach is made to the pressure bulkhead of the capsule as shown. This bulkhead supports the aerodynamic control surfaces and as such should provide a reasonable attach point for the separation rockets.

The rockets are attached as near to the capsule C.G. as possible to reduce pitching moment resulting from C.G. movement during burning. This necessitates lower support brackets of a truss type and longer (and heavier) nozzles. The loss due to canting the nozzles in the yaw plane is about 3% of the desired thrust in the forward direction.

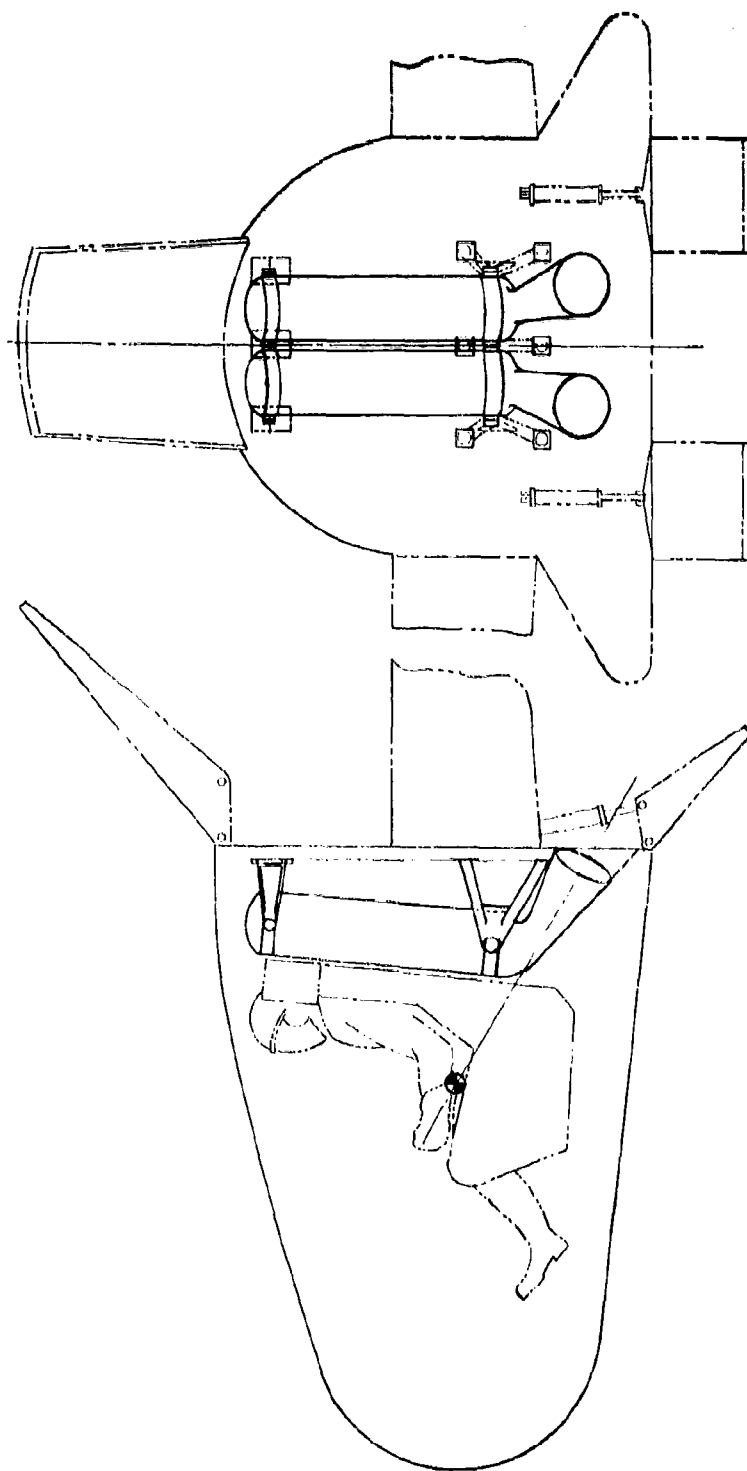


Figure 49 - Ballistic Body Capsule Escape Rocket Installation



Some impingement of exhaust on the edges of the lower flaps is foreseen. The open exhaust exit is in the capsule base and should not be as great a problem at re-entry as on the lifting body and turn around capsules.

5.3.2.2 Lifting Body Capsule. The installation concept shown in Figure 50 has a pair of nominal 12,500 pound thrust rockets installed along the lower truss rails. The rockets are installed outboard to reduce the structural weight penalty due to transferring the thrust loads into the longerons. The thrust vector angle is at  $40^\circ$  to the horizontal in order to minimize the exhaust hole cut out in the capsule under surface, and to reduce the impingement of the exhaust on the lower flaps. No canting of the nozzles is shown in the yaw plane so that no thrust modulation is possible. For half thrust modulation a loss of over half the thrust in the desired direction is incurred by canting the nozzles through the C.G. in the yaw plane. This is due to the large cant angle inherent in the low C.G. location and the outboard location of the escape rockets. Strengthening the floor structure might allow centerline installation of the rocket pair with considerably less cant angle and less consequent thrust losses for thrust modulation but at a weight penalty. Some exhaust impingement will be incurred on the flaps especially in the low ambient pressure regime.

This installation is also applicable to the turnaround configuration discussed in Section 5.3.2.3.

5.3.2.3 Turn-Around Capsule. This installation shown in Figure 51 is very similar to the lifting body installation except that four rockets are installed allowing half thrust modulation. Such an installation would also be applicable to the lifting body. (No cant of nozzles through the C.G. in the yaw plane is required to achieve half thrust modulation.) This allows half thrust and the possibility of the one set of rockets being used for both orbit separation and de-orbit retro. A severe problem is incurred by the open exhaust exit during re-entry, since this is exposed considerably in this configuration due to the turnaround maneuver. The rockets are shown canted down  $30^\circ$ . This could be increased to  $40^\circ$  to reduce the exhaust exit hole size. The heating through the exhaust nozzle could be reduced even more by decreasing the rocket expansion ratio. The penalty in  $I_{sp}$  of going to an expansion ratio of 1 would be in the order to 23% at sea level and 28% in vacuum. There is no problem with rocket exhaust impingement on the flaps with this configuration.

5.3.2.4 Separable Pod Capsule. Four rockets are shown for this installation in Figure 52. Half thrust (symmetrical) modulation is possible without canting the rocket nozzles. The rockets are installed outside the separable pod in an external package. This package recesses into the parent vehicle. The pack is insulated and plugged against the environment of the hot structure parent vehicle. The capsule itself is seen here as an insulated skin stringer shell with floor longerons to take the thrust loads between at least two major frames. This structure is conceptual and surmises attachment of the pod to the parent vehicle at the rear pod bulkhead only. An analysis would have to be made of both pod and parent vehicle carry through structure to confirm or deny the feasibility of this concept. The four rocket package would be ejected prior to re-entry in the same manner as for the Mercury capsule.

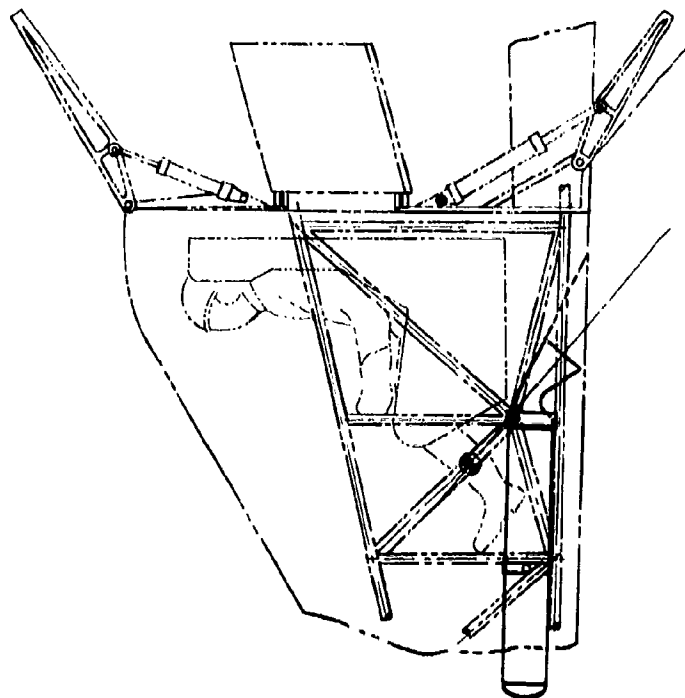
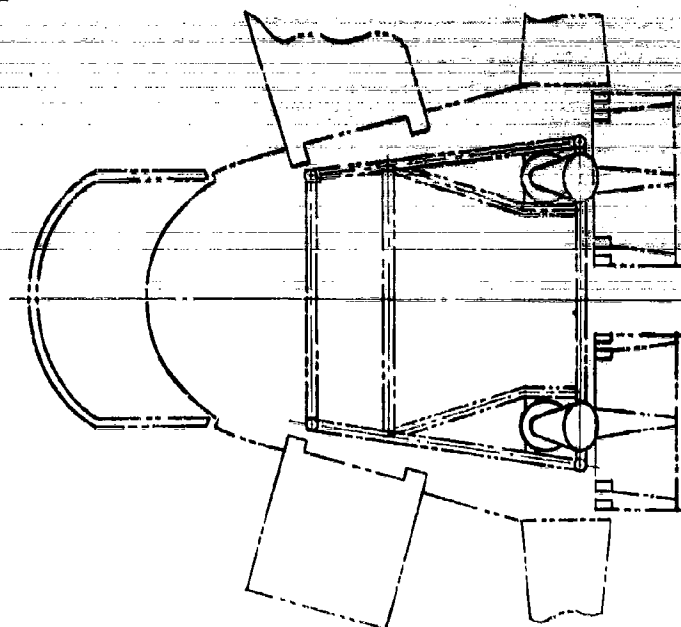


Figure 50 - Lifting Body Capsule Escape Rocket Installation

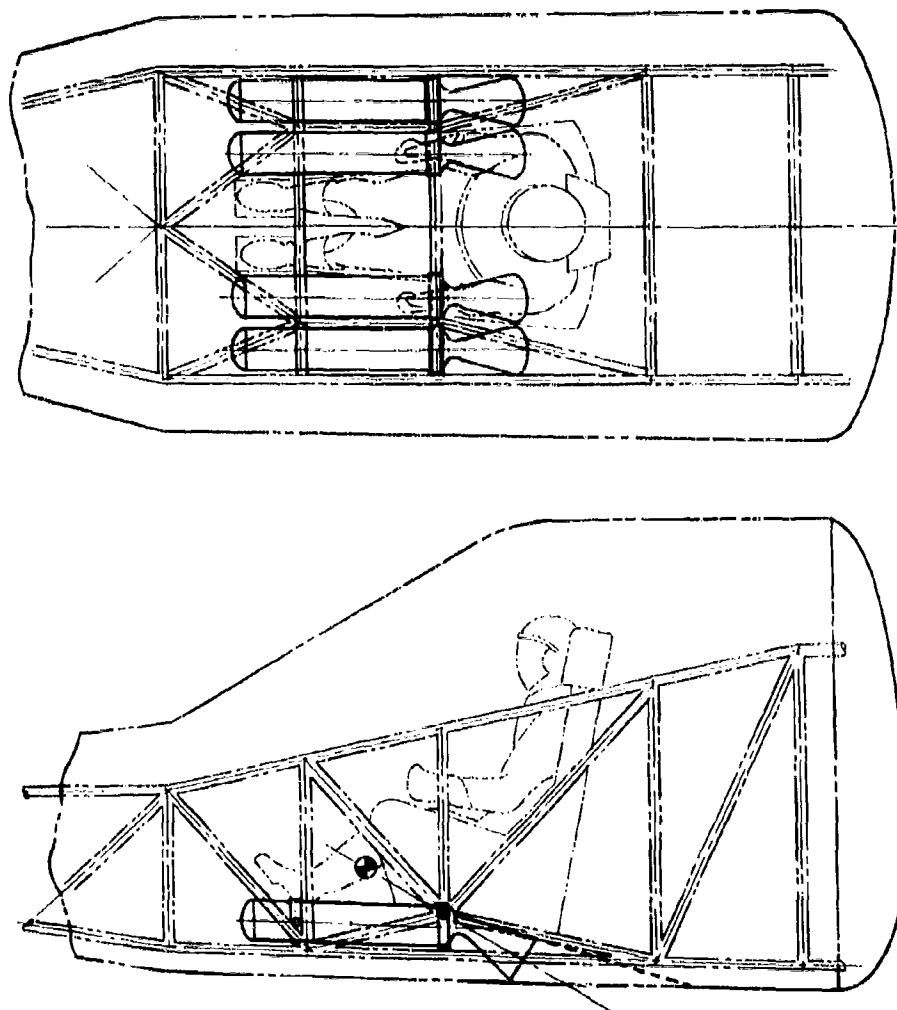


Figure 51 - Turnaround Capsule Escape Rocket Installation

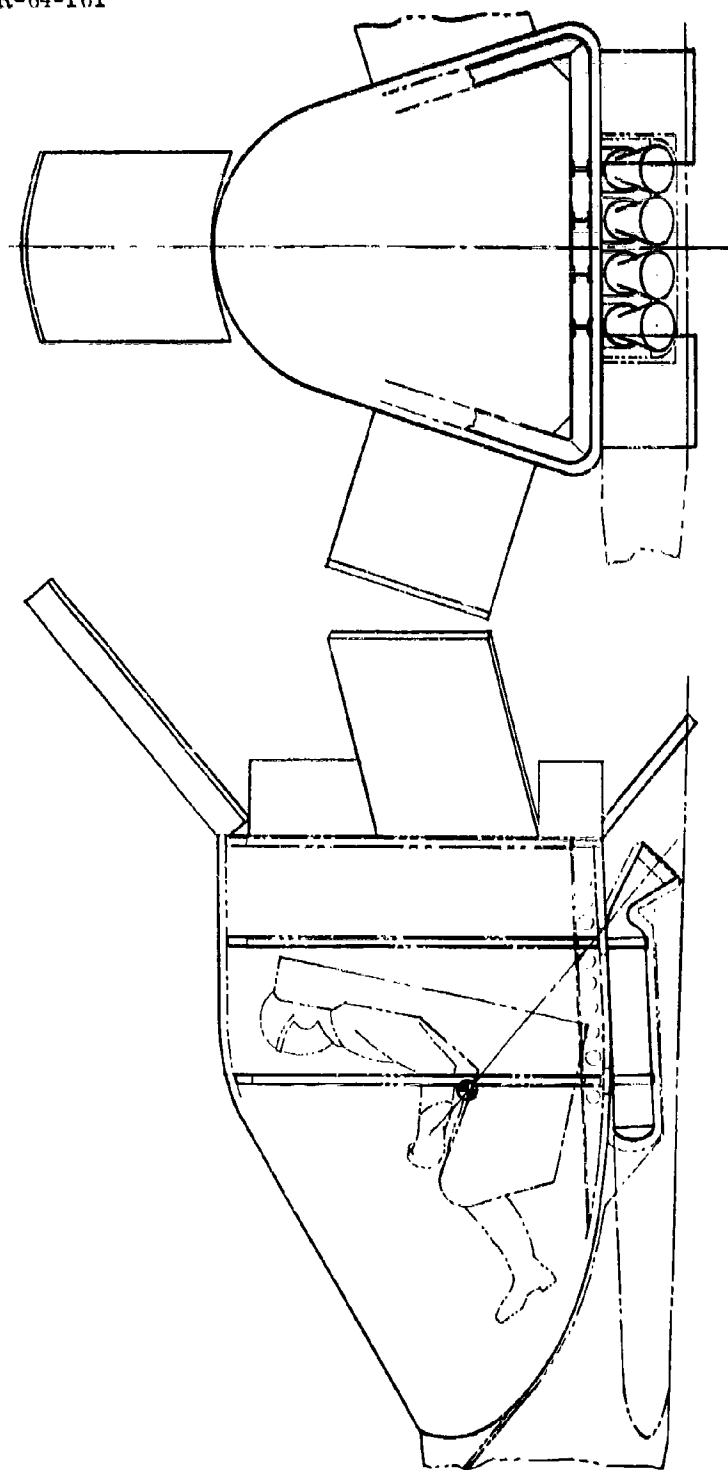


Figure 52 - Separable Pod Escape Rocket Installation

The rocket pack is installed on the capsule centerline, and the C.G. is higher than for the Lifting Body capsule type so that canting of the outboard rockets in the yaw plane could be achieved at small penalty (small angle required) to give a half-quarter-quarter thrust increment breakdown.

This external pack concept would be just as easily adaptable to two, three or five separation rockets depending again on the specific structural clearances required in the parent vehicle.

Some impingement of the exhaust on the lower flaps will occur with this arrangement.

There is no exhaust exit hole cutout in the capsule floor in this concept because of the external package installation. There is, however, a design problem in attaching the external package to the capsule so that the capsule surface, presented to the free stream at re-entry, is not broached by the attachment. When the empty rocket pack is jettisoned a smooth ablating surface should remain on the capsule undersurface. The compressive thrust loads of the rocket pack must be taken by the ablating material and transmitted to the capsule structure.

#### 5.4 ESCAPE ROCKET COOLING REQUIREMENTS

5.4.1 METHODS AND ASSUMPTIONS. The aerodynamic heating characteristics along the primary vehicle re-entry trajectory shown in Figure 3 were determined using the aerodynamic heating computer program described in Section 4.2. The resulting first segment temperature history was used as an input to the thermal conduction portion of the referenced program. This portion of the program was then used to size the insulation to protect the rocket motors.

The separable pod vehicle installation shown in Figure 52 was chosen for the analysis of the rocket motor heating. The temperature history was determined for a point on the lower surface 5 feet aft of the nose. At this point the surface inclination is 10 degrees. A transition Reynolds number of  $2 \times 10^5$  and a surface emissivity of 0.8 were assumed.

A thermodynamic heat transfer model as shown in Figure 53 was chosen for analysis. In the case of the separable pod vehicle, this is a good assumption because the four rocket motors laid side by side approximate a slab. The radiation gap was considered as existing only because of vehicle construction. It was not incorporated as a thermal barrier. The primary vehicle away from the rocket motors was assumed to consist of a 0.25 inch ( $L_1$ ) layer of  $6.0 \text{ lb}_m/\text{ft}^3$  dynaquantz between the cover panel and the hot structure. Radiation heat transfer from the hot structure to the wing upper surface or to the wall of the environmentally controlled capsule maintained the structural temperature

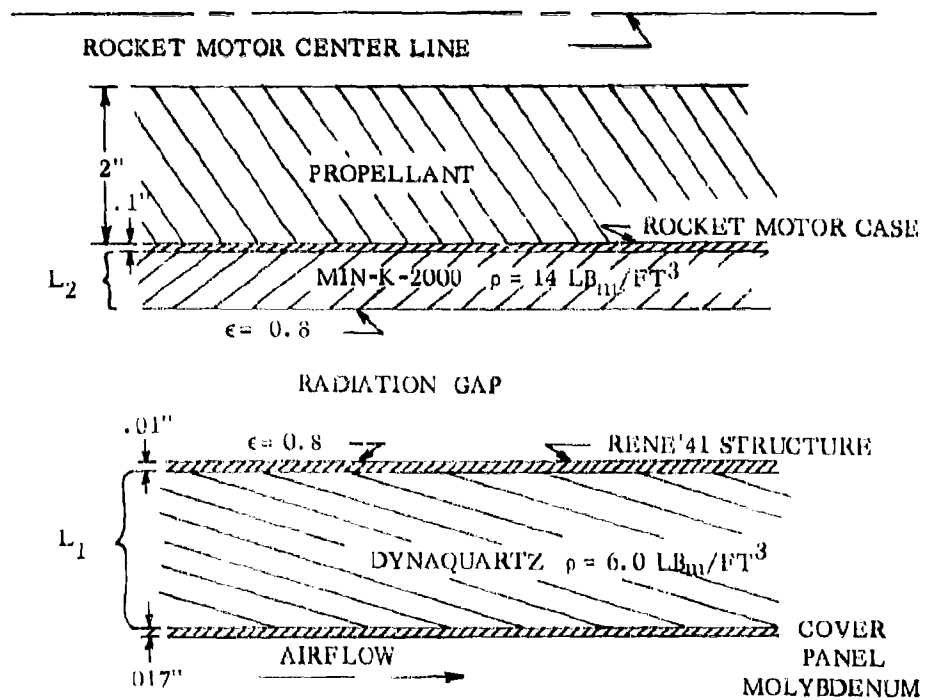


Figure 53 - Thermodynamic Model - Rocket Motor Heating

below 2000R, the design temperature.

Table V summarizes the thermodynamic properties of the materials.

**TABLE V. THERMODYNAMIC PROPERTIES**

Material	Thermal Conductivity, k B/hr ft <sup>2</sup> ° R	Density, lb <sub>m</sub> /ft <sup>3</sup>	Specific Heat, Cp B/lb <sub>m</sub> ° R
Moly	5.65	637	0.075
Dynaquartz	$0.0105 + 0.409(10^{-4})T$ $- 0.235(10^{-7})T^2 + 0.96(10^{-11})T^3$	6.1	0.25
Rene' 41	$3.18 + 0.445(10^{-3})T$	515	0.108
Radiation Gap	$0.1153(10^{-4})T^3$	0.2	0.25
Mink-2000	$0.5(10^{-3}) - 0.5(10^{-6})T$ $+ 0.5(10^{-8})T^2 + 0.15(10^{-11})T^3$	14	0.26
Rocket Motor Case	15.0	485	0.1
Propellant	0.187	102.6	0.326

The radiation heat transfer across the radiation gap was analyzed as heat transfer by conduction. This was necessary because the IBM 7090 heat transfer program does not have provisions for radiation gaps. Therefore, the gap was considered as another segment in the conduction path. To do this, one sets the radiation heat transfer rate equal to a conduction rate from which an effective thermal conductivity can be derived. The equations are:

$$q_r = q_c$$

$$\frac{\epsilon_1 \epsilon_2}{1 - (1 - \epsilon_1)(1 - \epsilon_2)} \sigma (T_1^4 - T_2^4) = k_{\text{eff}} \frac{(T_1 - T_2)}{L}$$

where

$\epsilon_1$  and  $\epsilon_2$  = the radiating surface emissivity

$\sigma$  = Stephan Boltzman constant

$L$  = Distance across gap

Hence,

$$k_{\text{eff}} = L_{\text{eff}} \sigma (T_1 + T_2) (T_1^2 + T_2^2)$$

where

$$\epsilon_{\text{eff}} = \frac{\epsilon_1 \epsilon_2}{1 - (1 - \epsilon_1)(1 - \epsilon_2)}$$

From Reference 13, the above equation for  $k_{\text{eff}}$  can be simplified to:

$$k_{\text{eff}} = 4 L \sigma \epsilon_{\text{eff}} T_{\text{avg}}^3$$

where

$$T_{\text{avg}} = \frac{T_1 + T_2}{2}$$

It was then assumed that the mid-segment temperature calculated by the computer program represented the average temperature between the radiating surfaces. The conductivity of the radiation gap in Table V was calculated assuming  $L$  equalled 3 inches. There was one other point to consider. This was the energy stored in the radiation segment. In radiation heat transfer there would be no energy stored. Therefore, the density and specific heat of the segment were chosen so that the energy stored was less than one (1.0) percent of the energy stored in the rocket motors and the insulation around the motors.

The type of propellant for the rocket motors was not specified. Therefore, the thermodynamic values in Table V are the average of five (5) types taken from Reference 14. The thickness of propellant was based upon a rocket motor diameter of six (6) inches with the void in the propellant segment accounting for the difference in the thickness and the radius of the motor.

**5.4.2 RESULTS.** The analysis was conducted to determine the values of insulation thickness  $L_1$  and  $L_2$  which would keep the rocket motor case temperature below 200°F. The cover panel temperature history associated with the primary flight vehicle



trajectory is shown in Figure 54. The cover panel temperature is not the radiation equilibrium temperature since conduction to the vehicle interior has been reflected in the panel temperature history. This temperature history was used as input to the thermal conduction portion of the aerodynamic heating analysis program and runs were made varying the values of  $L_1$  and  $L_2$ . Final values of  $L_1$  and  $L_2$  were 1.6 inches and 0.45 inches respectively. The structural and rocket motor case temperature histories associated with these insulation thicknesses are also shown in Figure 54. The resulting maximum structural temperature is  $2010^{\circ}\text{R}$  and  $620^{\circ}\text{R}$  for the rocket propellant. Both values are not the exact desired values of  $2000^{\circ}\text{R}$  for the structure and  $660^{\circ}\text{R}$  for the rocket motor case. Further sizing runs were not made because the difference of  $10^{\circ}\text{R}$  in the structural temperature was not considered significant and the  $620^{\circ}\text{R}$  ( $160^{\circ}\text{F}$ ) is the maximum temperature limit of many propellants. However, if  $L_2$  were reduced to 0.3 inches, the structural temperature will decrease and the motor case temperature will rise to approximately  $660^{\circ}\text{R}$  ( $200^{\circ}\text{F}$ ).

The increase in the dynaquantz insulation from 0.25 inches to 1.60 inches will require a modification in the Rene' 41 structure in the area under the rocket motors. An increase in the insulation thickness was required because the rocket motors blocked the radiation heat transfer away from the Rene' 41 structure.

The insulation requirements for the rocket motors of the other escape capsules will be approximately the same. An exception is the ballistic body installation shown in Figure 49 where the rocket motors are located at the rear bulkhead of the capsule. Here the insulation requirements will be considerably less and most important of all, the Rene' 41 structure will not have to be altered in the rocket motor location.

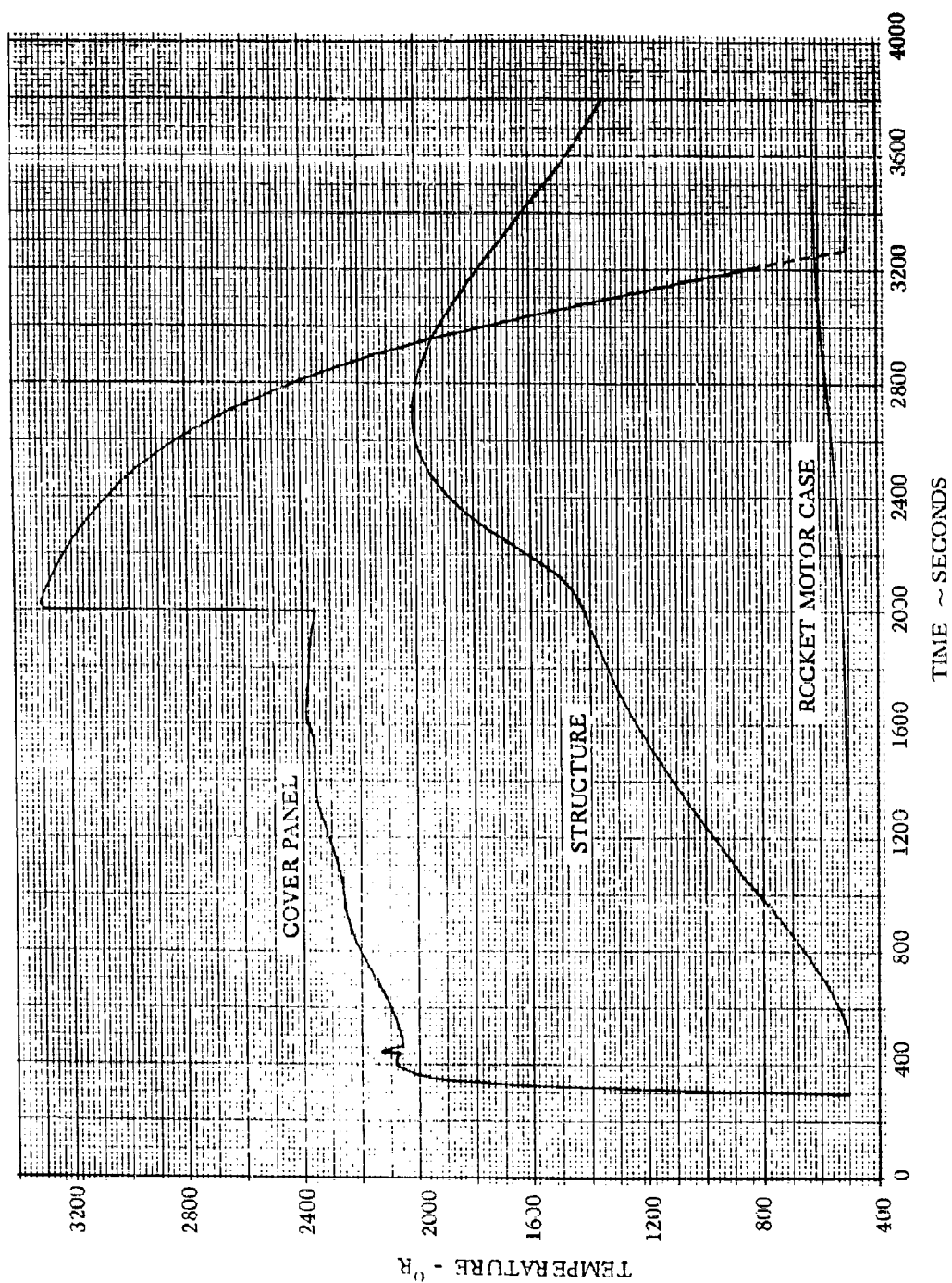


Figure 54 - Temperature Characteristics in Region of Separation Rockets

## SECTION 6

## PERFORMANCE ANALYSIS

The trajectory analysis and aerodynamic heating techniques discussed in Section 4 were used to analyze the separation trajectory characteristics of each of the four escape capsule concepts. The initial investigative phase for each capsule was an analysis of escape performance from the maximum heating point of the primary flight vehicle trajectory. This point has the following conditions which served as the initial conditions for the separation flight dynamics investigation

Velocity	21,913 ft/sec.
Altitude	221,241 ft.
Flight Path Angle	- .14 deg.
Angle of Attack	15.5 deg.
Bank Angle	45.0 deg.

The re-entry escape performance evaluation was divided into two parts. In the first, the separation dynamics during the first 5 to 10 seconds after separation were investigated. In the second phase the long time or complete trajectory characteristics were determined. Aerodynamic heating characteristics were determined for both types of trajectories.

After completion of the analysis of re-entry escape the performance characteristics were evaluated at the following other critical escape points:

Orbit  
On-the-Pad  
Maximum Dynamic Pressure  
Landing

The objective of this phase of the study was the determination of the compatibility of the escape capsule configurations and escape techniques with respect to providing escape throughout the mission profile.

The following initial flight conditions were used for each of the four capsules at these other critical escape areas:

<u>Condition</u>	<u>Flight Path Angle - Deg.</u>	<u>Velocity - fps</u>	<u>Altitude - ft.</u>
On-the-pad	90	0	100
Maximum dynamic pressure	43	1,800	43,000
Orbit	0	25,200	1,000,000
Landing	-2	200	100

At these conditions the effects of the following variables on separation performance were investigated:

- a) Aerodynamic controls
- b) Reaction controls
- c) Thrust inclination angle
- d) Thrust magnitude
- e) Thrust moments
- f) Initial angle of attack
- g) Initial pitch rate

In addition the recovery ceiling characteristics of each of the capsules were determined and compared with the primary flight vehicle recovery ceiling.

## 6.1 BALLISTIC BODY CAPSULE

6.1.1 RE-ENTRY ESCAPE. This investigation phase used the aerodynamic controls rather than the reaction controls. It has been assumed that the vehicle dynamic characteristics obtained with reaction controls as described in Reference 1 are applicable.

6.1.1.1 Separation Dynamics. It was the objective of this phase to determine the separation dynamics as a function of various parameter variations. The analyses in this phase were limited to the first five seconds after escape which was sufficient time to determine the vehicle response characteristics and achieve adequate clearance. The parameters which were investigated are as follows:

- a) Pitch damping
- b) Initial pitch rate
- c) Thrust moments
- d) Thrust damping
- e) Initial sideslip
- f) Initial yaw rate
- g) Initial roll rate
- h) Thrust magnitude
- i) Longitudinal center of gravity position.

The parameter values of the more significant computer runs are listed in Table VI. The results are summarized in Figures 55 through 61.

Figure 55- presents the effect of pitch damping on the angle of attack response as determined from the three degree simulation. Although computed for a zero roll angle, additional studies have indicated that the initial bank angle has a negligible effect on the pitch response so that these results apply equally to the nominal 45 degree bank angle case. Damping was obtained from the upper surface flap and an ideal (no time lag) autopilot was assumed. It is seen that without artificial damping there is essentially no damping which

is typical of vehicles in this flight regime. A gain of .5 deg/(deg/sec) is seen to give satisfactory overshoot characteristics and was selected as the nominal gain for use in the study.

Figure 55 presents the effect of initial pitch rate on the angle of attack response. These and all responses presented in Figures 55 through 61 were determined using the six degree simulation. Initial pitch rate was investigated since it is a measure of separation interference resulting either from aerodynamic interference or separation disconnect disturbances. The sharp rise in angle of attack during the first second is a result of including the moment produced by the thrust. A moment exists since the center of gravity moves during rocket burning and no gimbaling was assumed for these runs. It is seen that the vehicle response is relatively insensitive to initial pitch rate.

Figures 56, 57 and 58 present the effect of thrust moment characteristics on the vehicle response characteristics. The following variations were analyzed and in all cases the nominal aerodynamic damping of .5 deg/(deg/sec) was included.

- a) Thrust moment omitted
- b) Thrust moment included
- c) Thrust gimbaling with autopilot

Thrust moments can exist for almost all escape capsule concepts due to the center of gravity shift as the escape rocket is expended. On the ballistic capsule the thrust vector goes through the empty c.g. which results in a nose up pitching moment initially. This location yields a conservative estimate of the thrust moment effects since a more realistic location would be a position midway between the initial and final centers of gravity.

Figure 56 presents the variation in angle of attack, flap angle and thrust gimbal angle, for the three thrust moment variations which were considered. The case where the thrust moment is omitted is presented for comparison purposes. Including the thrust moment without any thrust gimbaling results in an 8 degree pitchup. The use of an ideal (no time lag) thrust gimbal pitch rate servo with a gain of .1 deg/(deg/sec) decreases the pitchup to about 1 degree.

It can be seen that the most severe flap deflections are required when the thrust moment is included without gimbaling. For this case, a 32 degree deflection angle range is required. The demands on the thrust gimbaling are relatively small being approximately  $\pm 2$  degrees.

Figure 57 presents the load factor and load factor direction characteristics for the thrust moment variations. It is seen that the thrust moment effect is relatively insignificant. These load factor data are essentially the same as those obtained with the other parameter variations in which the nominal thrust level of Figure 46 was used. These load factor characteristics are within human tolerance limits.

Figure 58 presents the separation distance characteristics as a function of the thrust moment variations. In all cases adequate separation distances are achieved. These separation characteristics reflect the change in thrust orientation due to angle of attack changes resulting from thrust moment effects. As with the load factor characteristics presented in Figure 57, these separation characteristics are typical of those obtained for all runs using the nominal thrust characteristics of Figure 46.

Figure 59 presents the effects of initial lateral directional disturbances. As with initial pitch disturbances previously discussed, these may arise from aerodynamic interference, disconnect disturbances or primary vehicle disturbances. In all cases the vehicle response characteristics in the pitch plane were relatively unchanged. The responses shown in Figure 59 were obtained with the nominal pitch damping but with no lateral-directional control. As indicated in Reference 1, there is a need for roll attitude stabilization and roll and yaw damping. These can be obtained with the reaction controls and lateral c.g. shift investigated in Reference 1 or with the addition of control capability to the side and lower flaps. Since the pitch dynamics, which put the most severe demand on the controls, are adequately handled at this flight condition there should be no great problems with an aerodynamic lateral-directional control system.

The effect of thrust level on the load factor and separation distance characteristics is presented in Figure 60. The load factor and separation distances are decreased approximately proportionately. The separation characteristics obtained with the lower thrust level are adequate for separation at this re-entry condition since there is no danger of a large explosion in the primary flight vehicle due to the absence of large amounts of propellant. It would therefore be possible to have two or more smaller rockets. For on the pad and high dynamic pressure escape, all the rockets would be used. At other conditions such as this re-entry condition, some of the rockets would not be used.

Figure 61 presents the effect of varying the longitudinal center of gravity on the angle of attack response and pitch rate characteristics. These center of gravity changes represent changes in capsule stability. The thrust moments have been omitted so the differences are primarily the result of the aerodynamic stability differences. The ballistic body is so stable longitudinally (see Figure 11) that the large c.g. shift considered affects primarily the response time. The corresponding pitch rate characteristics are also shown in Figure 61.

6.1.1.2 Complete Trajectories. Since the ballistic body capsule does not experience

its maximum heating at the maximum heating point of the primary flight vehicle, it was believed to be of interest to determine the trajectories down to a relatively low velocity. Trajectories were computed for three values of wing loading using the two degree of freedom trajectory program. The resulting trajectories are shown in Figure 62. The maximum load factors achieved during these trajectories are as follows:

W/S	Load Factor	Velocity
39.3	8.12	8917 fps
65.5	9.15	9900 fps
91.5	9.28	10,149 fps

6.1.1.3 Aerodynamic Heating. The aerodynamic heating characteristics of selected trajectories were determined using the aerodynamic heating computer program described in Section 4 which computes the thermal radiation equilibrium temperature.

Equilibrium temperatures were obtained at four points on the ballistic body which are critical. These points were as follows:

- a. Nose
- b. Leading Edge
- c. Lower Surface 7.0 ft. aft
- d. Lower Flap 1.0 ft. aft of hinge line

The nose stagnation region was considered as a sphere with a diameter of 3.5 feet. The leading edge has a diameter of .5 ft. and a sweepback of  $73^\circ$ . In analyzing the leading edge and lower surface it was necessary to include the effects of the  $6^\circ$  cant angle on the lower surface. This tends to decrease the effective sweepback angle. The flap was treated as a  $40^\circ$  wedge with respect to the capsule reference centerline.

Figure 63 presents the temperature history of the leading edge of the primary flight vehicle along its maximum heating trajectory. This temperature history differs from the primary flight vehicle temperature history presented in Figure 4 since the configuration when analyzed with the Ballistic body used a 6 degree cant angle on the lower surface. With the other three capsule configurations the leading edge temperature history of Figure 4 is applicable. This minor inconsistency between configurations has no effect on the study results. The peak temperature is seen to be  $3322^\circ\text{R}$  occurring at 1200 seconds after re-entry at the flight conditions previously described. This was the initial point for the re-entry escape analysis.

Figures 64 and 65 present the temperature histories for escape trajectories 6 and 7 respectively at the four positions investigated. For trajectory 6, the leading edge temperature fell from the primary vehicle peak to an approximate value of 2920R in 1.5 seconds corresponding to the decay in angle of attack shown in Figure 56. Along trajectory 7 the leading edge temperature, after a slight dip, rose to a peak of 3357R in 0.5 seconds and then fell to an approximate value of 2910R after 2.0 seconds corresponding to the angle of attack time history shown in Figure 56.

The peak flap temperatures of approximately 3190R shown in Figures 64 and 65 indicates the need of special consideration for a thermal protection system. An ablation material with an ablation temperature greater than the maximum temperature obtained on the undeflected flap during the primary flight vehicle trajectory is a possible solution. The temperatures on the other flaps would be slightly less due to the lower effective angle of incidence.

The sudden jump in temperature of the lower surface was caused by transition to turbulent boundary layer flow. A transition Reynolds number of 300,000 instead of the assumed study value of 200,000 would have resulted in lower temperatures for both trajectories.

Figure 66 indicates the effect of a 3.0 degree yaw angle on the leading edge temperature. The yaw angle increased the leading edge temperature approximately 140°R above the value for trajectory 6. This yaw angle effect has been included to show the effects of possible yaw disturbances on the aerodynamic heating.

Temperature histories for the complete trajectory with a wing loading of 65.5 are shown in Figure 67. Time zero corresponds to the initial escape conditions. The first 5.0 seconds are approximately the same as the temperatures presented in Figure 64. The leading edge temperatures shown in Figure 67 reach secondary peaks which are less than the initial peak. It is seen that for the nose, lower surface and flap, the peak temperatures did not occur at the initial escape point but much further down the trajectory at velocities of the order of 16,000 ft/sec. Due to boundary layer transition the flap temperatures jumped to a value of approximately 5005R. These values would certainly dictate the use of ablation materials on the flaps.

6.1.2 ORBIT ESCAPE. The initial conditions for the ballistic body orbit separation dynamics computer runs are presented in Table VII. Figure 68 presents angle of attack time histories for orbit separation at two thrust levels. Without any thrust moment effects the capsule is oriented within three seconds. Including thrust moment



effects without thrust gimbaling results in a tumbling motion. The pitch rate is decreasing however so that the capsule would achieve its desired altitude in approximately 150 seconds. If thrust gimbaling is used the capsule does not tumble.

The orbit re-entry trajectory characteristics showing the effect of capsule wing loading are presented in Figure 69. The peak load factors are also presented in Figure 69. If the trajectories of Figure 69 are compared with the trajectories from the maximum heating escape point shown in Figure 62 it is seen that orbit re-entry will impose the most severe temperatures.

6.1.3 RECOVERY CEILING. The recovery ceiling characteristics of the ballistic body are presented in Figure 70 showing the effect of wing loading. The recovery ceiling for this capsule is determined by load factor considerations. A load factor limit of 13 g's was used. It can be seen that the ballistic capsule has a greater recovery ceiling capability than the primary flight vehicle.

6.1.4 ON-THE-PAD ESCAPE. The run schedule for on-the-pad escape is presented in Table VIII. Figure 71 presents the angle of attack time history and altitude-range characteristics for this condition. The angle of attack time history presents the effect of thrust moment and thrust gimbaling. The range-altitude characteristics show that with the thrust moments included, unsatisfactory altitude performance is achieved. As expected, reducing the thrust inclination angle increases the altitude. The altitude performance can be made satisfactory with thrust moments if thrust gimbaling is used. The maximum load factor during on-the-pad separation is a result of the escape rocket thrust and is within human tolerance limits.

6.1.5 LANDING ESCAPE. The run schedule for this condition is presented in Table VIII. Figure 72 presents the angle of attack and altitude time history characteristics for the ballistic body separating during the landing approach. It is seen that the reaction controls yield poorer damping characteristics than the aerodynamic controls. Including the thrust moments without control damping introduces oscillations but those do not yield any severe effects either with regard to load factor or altitude. Satisfactory altitude and load factor performance was obtained for all the trajectories.

6.1.6 MAXIMUM DYNAMIC PRESSURE ESCAPE. The run schedule for this escape condition is presented in Table IX.

Figure 73 presents angle of attack, load factor, and load factor direction characteristics for the ballistic body separating at maximum dynamic pressure, both with and without thrust moment effects. In both cases the pitching motion is quickly damped out. The load factor peak occurs at .08 seconds and results from the escape rocket thrust. The load factor decays during rocket burning due to the decreasing thrust. At burnout the load factor decreases and then increases as the resultant force vector rotates from a forward and up direction to an aft and up direction. These load factor characteristics are within human tolerance limits.

Figure 74 presents angle of attack and load factor time histories showing thrust moment effects with and without reaction controls. In both cases fixed aerodynamic controls were assumed. The thrust moment effects introduce large oscillations which the reaction controls can only damp slightly. These oscillations introduce some slight oscillations in the load factor as indicated.

Figure 75 presents the separation distance characteristics at supersonic speeds as a function of time for thrust inclination angles of 40 and 30 degrees. In determining the separation distance it was assumed that the primary vehicle continued along its control flight path at constant velocity.

Figure 76 presents the effect of initial pitch rate on the angle of attack characteristics. These initial rates are a measure of the aerodynamic interference effects. The oscillation resulting from these initial pitch rates is rapidly damped out and the load factor characteristics are within human tolerance limits.

**6.1.7 PERFORMANCE CONCLUSIONS.** The main performance problem associated with the ballistic body capsule is the high temperatures encountered on the flaps in the hypersonic regime. These temperatures require the use of ablation materials. The thrust moment effects result in capsule oscillations but these do not lead to load factors in excess of human tolerance limits. Aerodynamics controls yield good damping characteristics at all conditions. Reaction controls are not as effective at high dynamic pressures but the oscillations do not yield excessive load factors.

TABLE VI  
SUMMARY OF CONDITIONS FOR BALLISTIC BODY RE-ENTRY TRAJECTORY RUNS

Run	Initial Bank Angle Deg.	Trim Angle of Attack Deg	Upper Surface Pitch Damping Deg/ Deg/Sec	Thrust Moment Included	Thrust Gimbel Pitch Damping Deg/ Deg/Sec	Initial Pitch Rate Rad/Sec	Initial Sideslip Deg	Initial Roll Rate Rad/Sec	Initial Yaw Rate Rad/Sec	XCG Ft From Nominal	Thrust Magnitude Ratio to Nominal
1	0.	5.	0.	No	0.	.1	0.	0.	0.	0.	1.
2	0.	5.	.5	No	0.	.1	0.	0.	0.	0.	1.
3	45.	0.	1.	No	0.	.1	0.	0.	0.	0.	1.
4	45.	0.	.5	Yes	0.	.1	0.	0.	0.	0.	1.
5	45.	0.	.5	Yes	0.	-.1	0.	0.	0.	0.	1.
6	45.	0.	.5	No	0.	-.1	0.	0.	0.	0.	1.
7	45.	0.	.5	Yes	.1	-.1	0.	0.	0.	0.	1.
8	45.	0.	.5	No	0.	-.1	3.	0.	0.	0.	1.
9	45	0.	.5	No	0.	-.1	0.	.1	0.	0.	1.
10	45	0.	.5	No	0.	-.1	0.	0.	.1	0.	1.
11	45	0.	.5	No	0.	-.1	0.	0.	0.	0.	.5
12	45	0.	.5	No	0.	-.1	0.	0.	0.	1.05 Aft	1.
13	45	0.	.5	No	0.	-.1	0.	0.	0.	1.05 Fwd	1.

Lower and Side Flaps at 40 Degrees

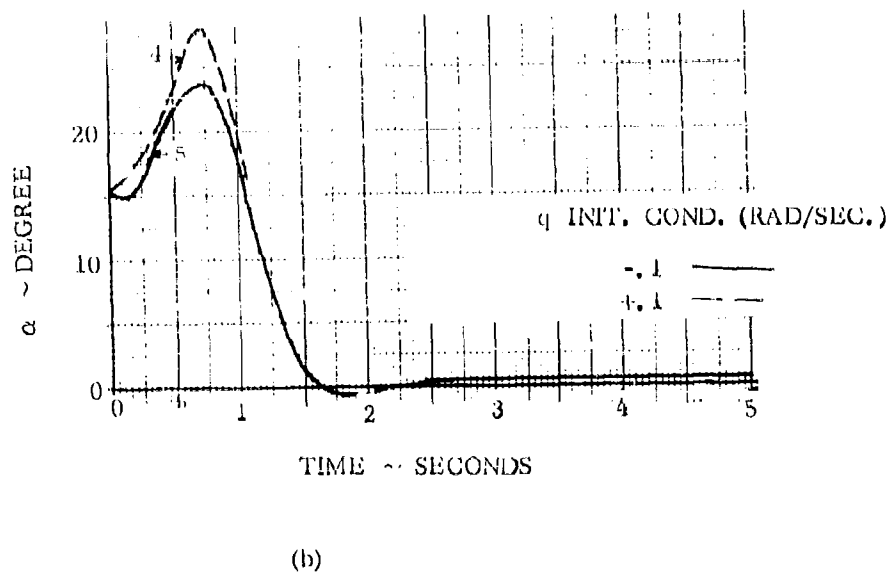
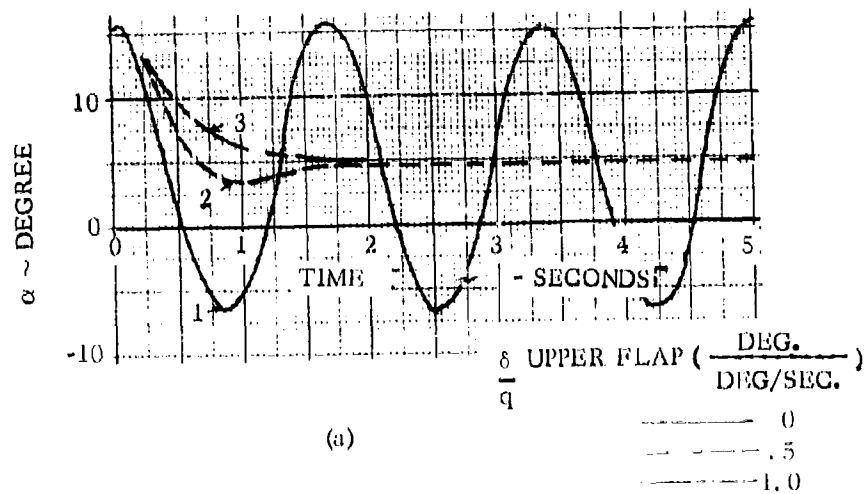


Figure 55 - Ballistic Capsule Angle of Attack Response - Effect of Pitch Damping

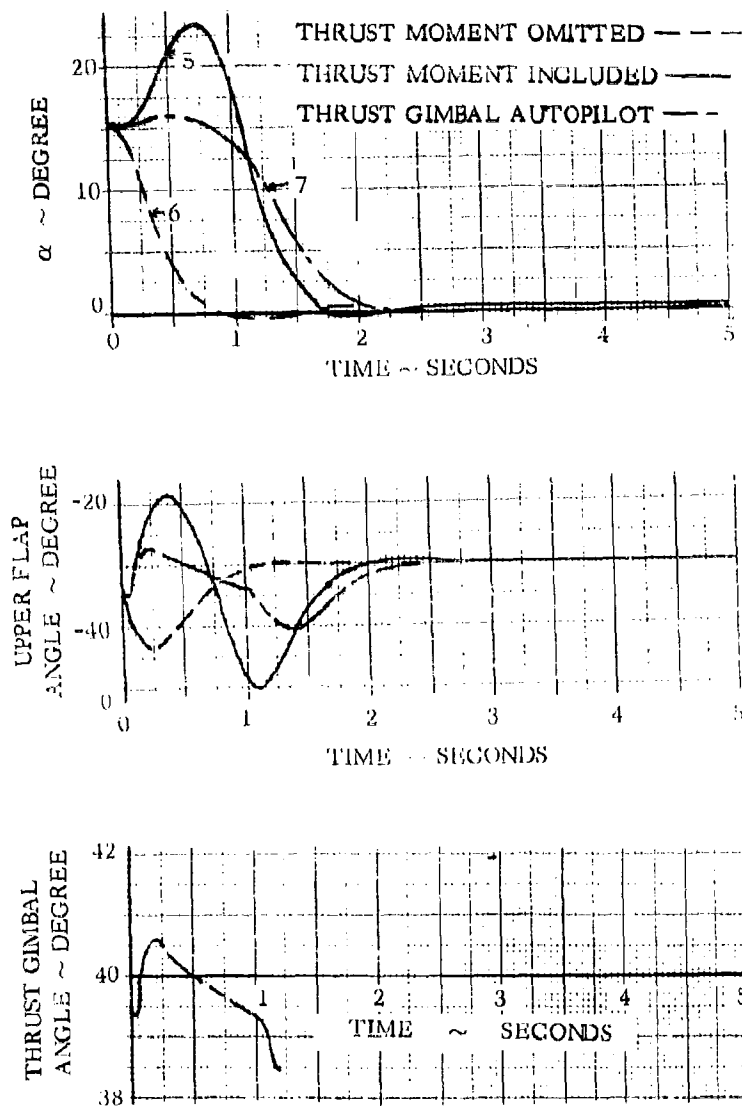


Figure 56 - Ballistic Capsule Dynamic Response - Effect of Thrust Moments

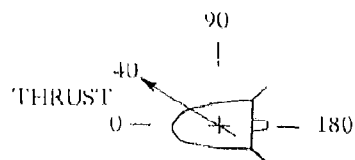
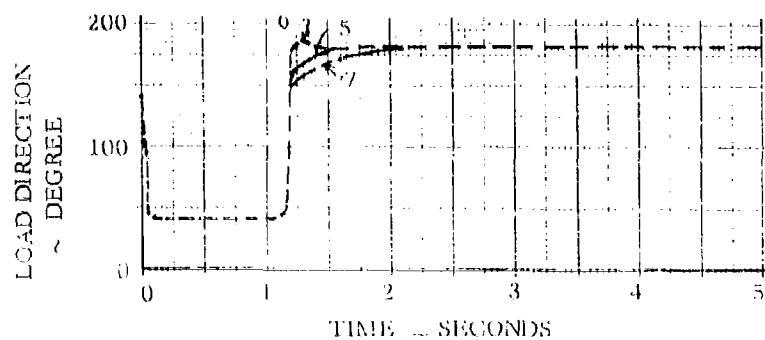
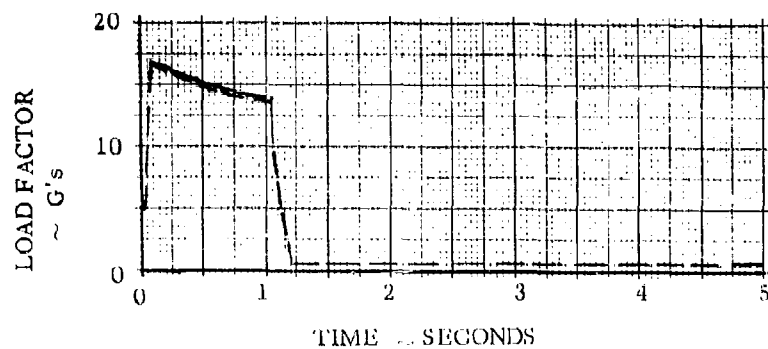


Figure 57 - Ballistic Capsule Load Factor Characteristics - Effect of Thrust Moments

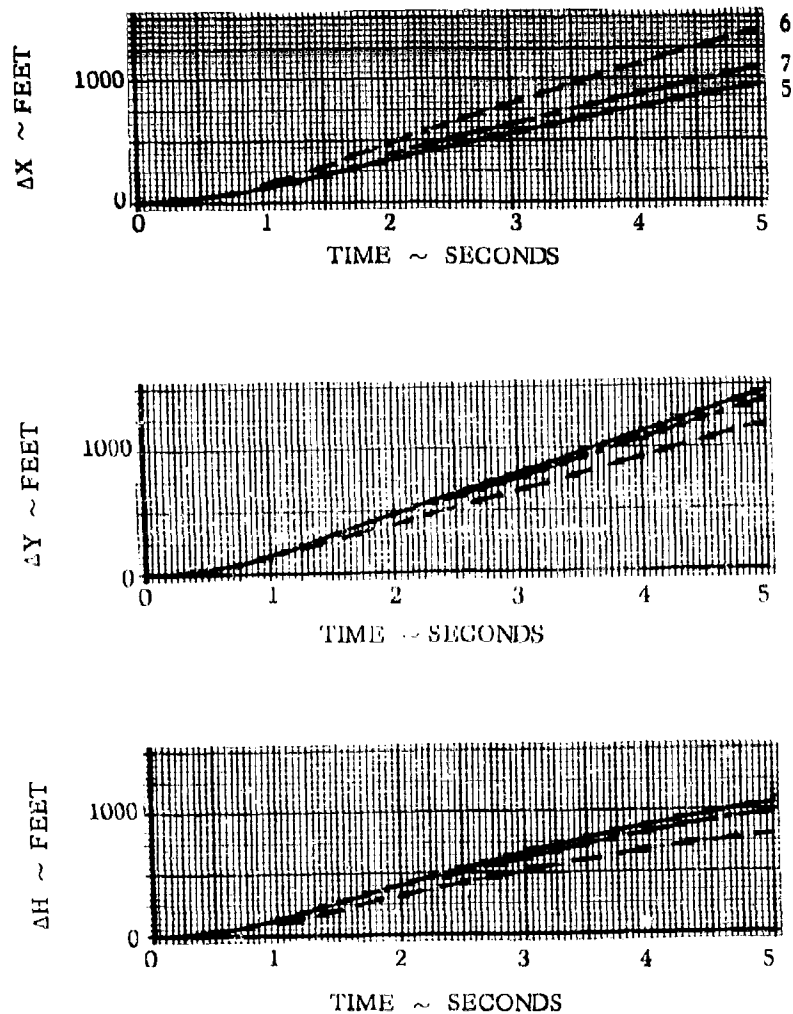


Figure 58 - Ballistic Capsule Separation Characteristics - Effect of Thrust Moments

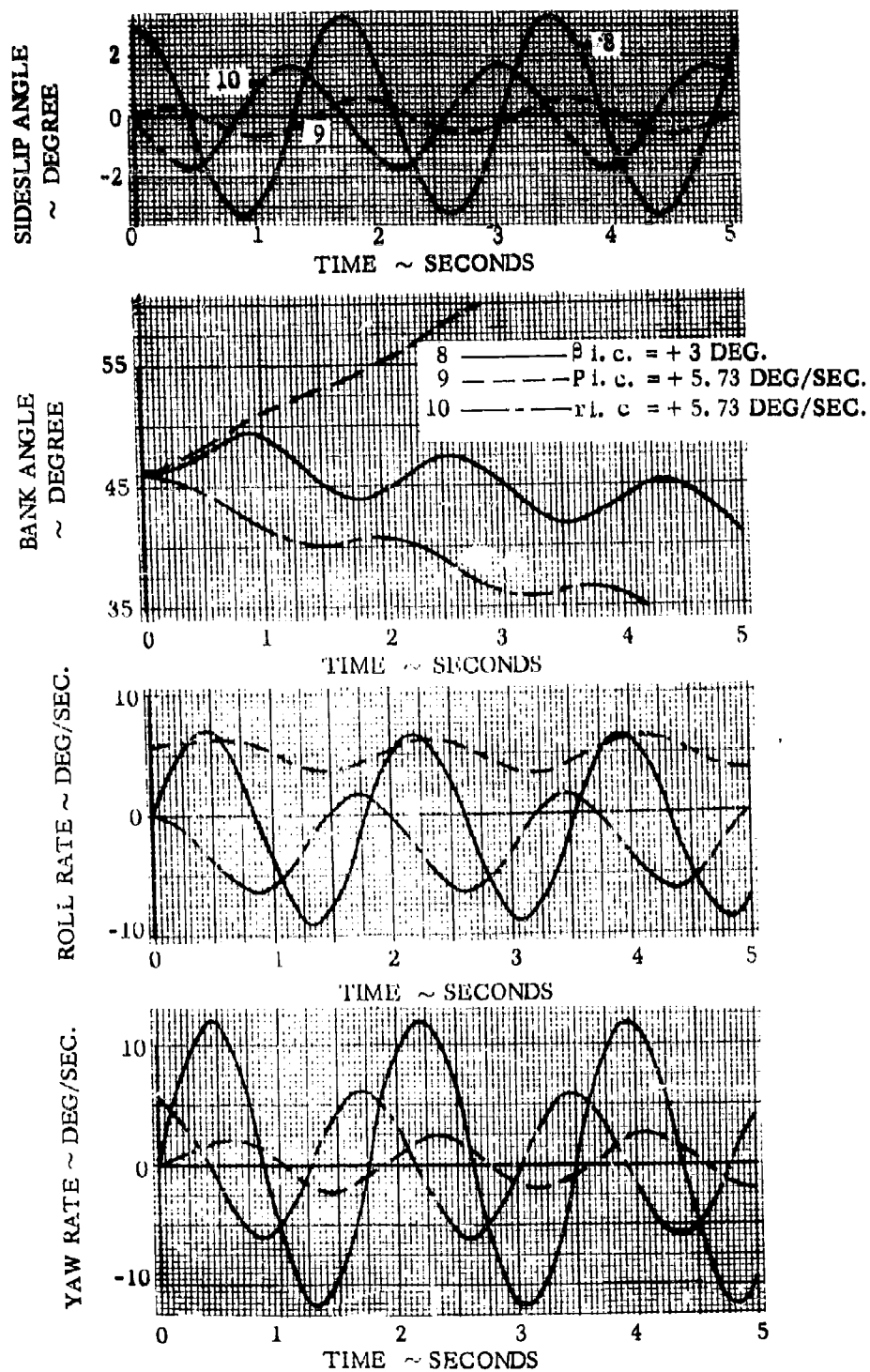


Figure 59 - Ballistic Capsule Dynamic Response - Effect of Lateral - Directional Disturbances



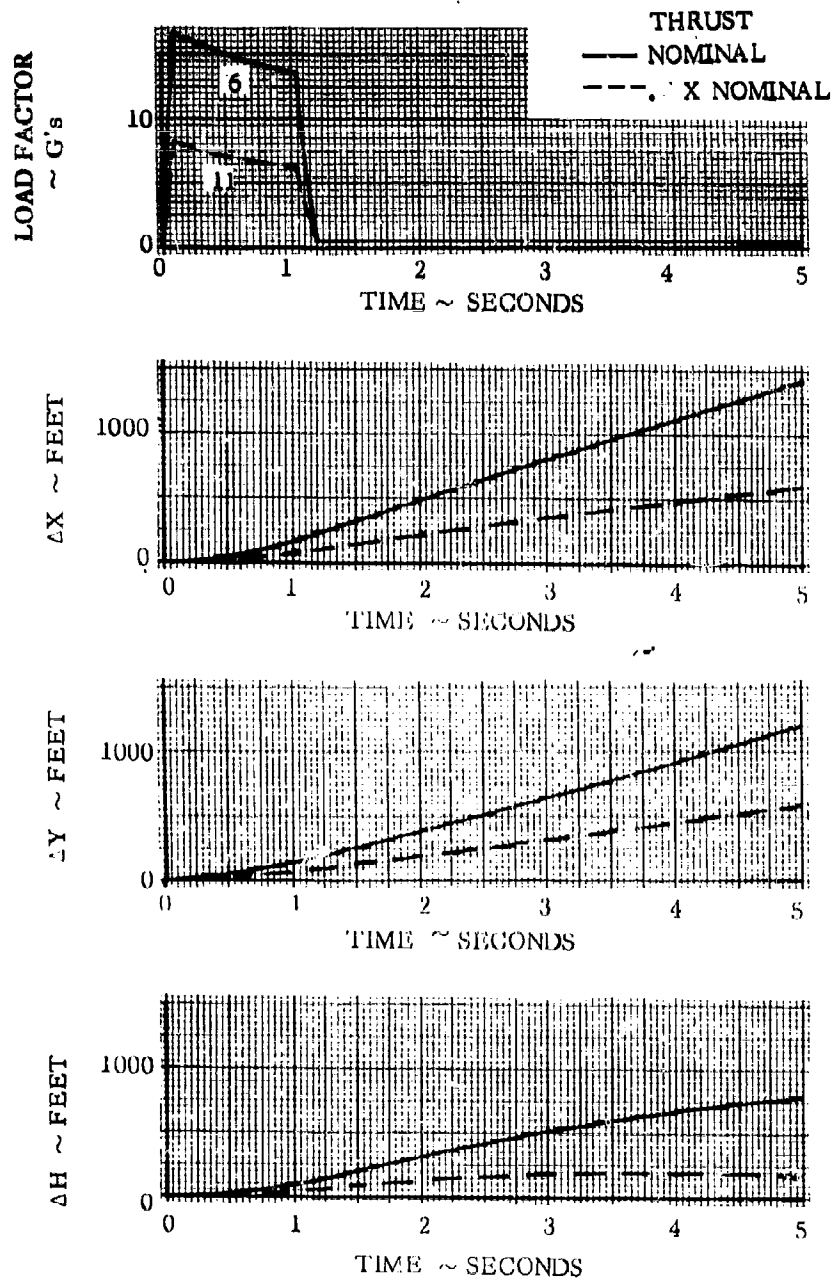


Figure 60 - Ballistic Capsule Load Factor and Separation Characteristics  
Effect of Thrust Level

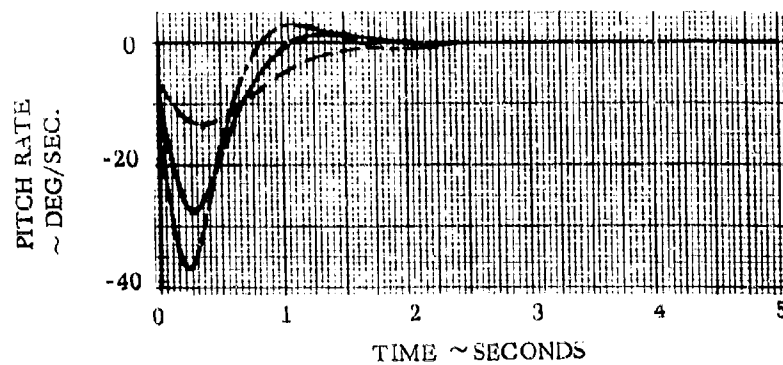
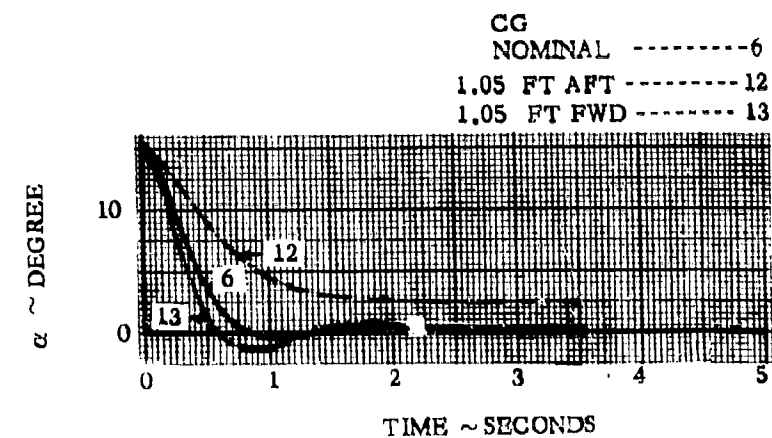


Figure 61 Ballistic Capsule Dynamic Response - Effect of Longitudinal Center of Gravity

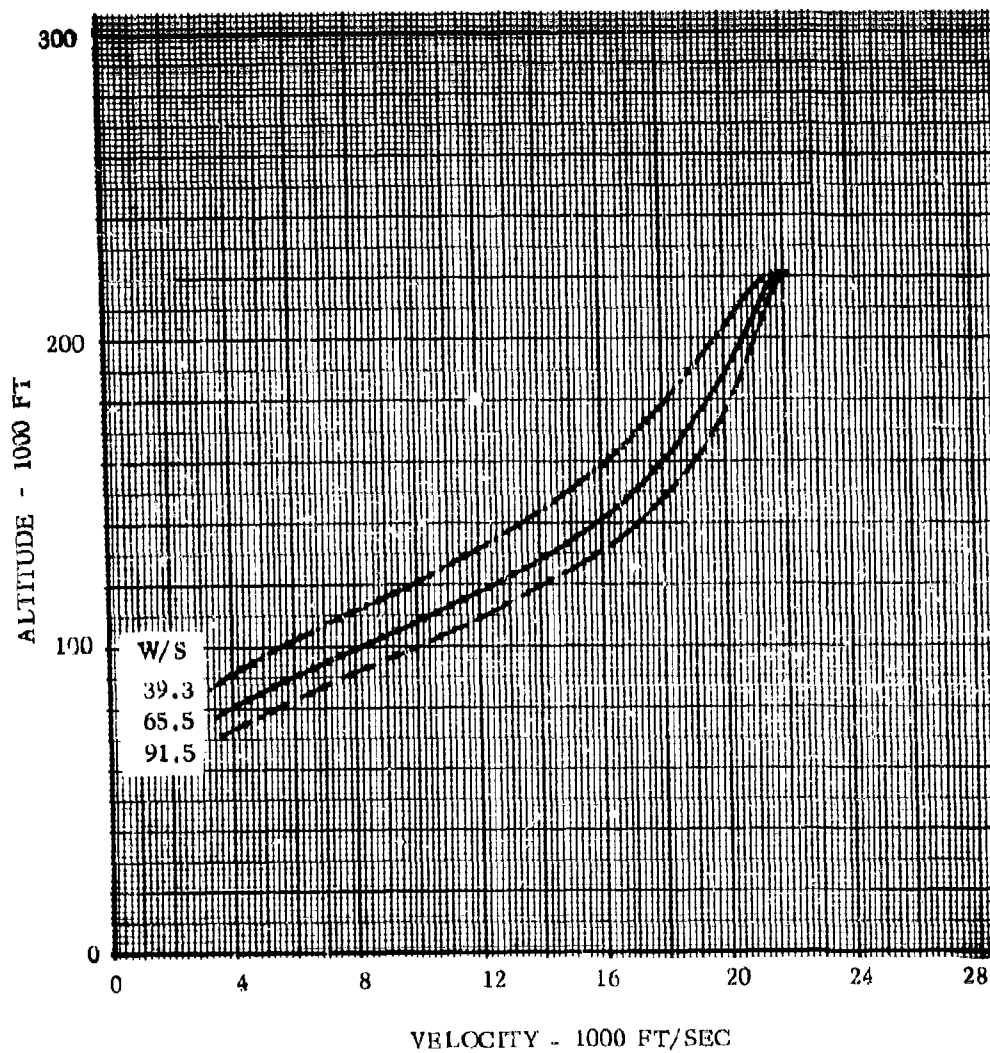


Figure 62 - Effect of Wing Loading on Ballistic Body Escape Trajectories

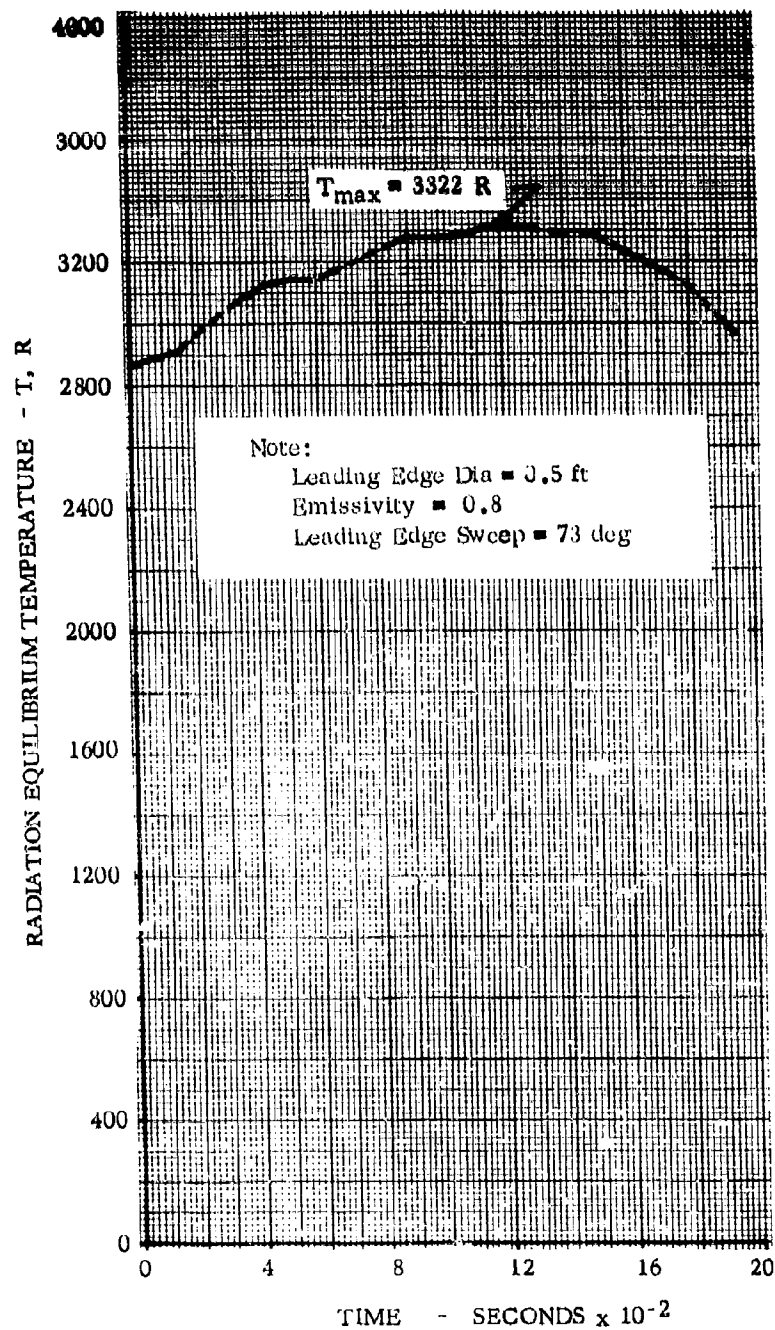


Figure 63 - Primary Flight Vehicle - Temperature History Leading Edge

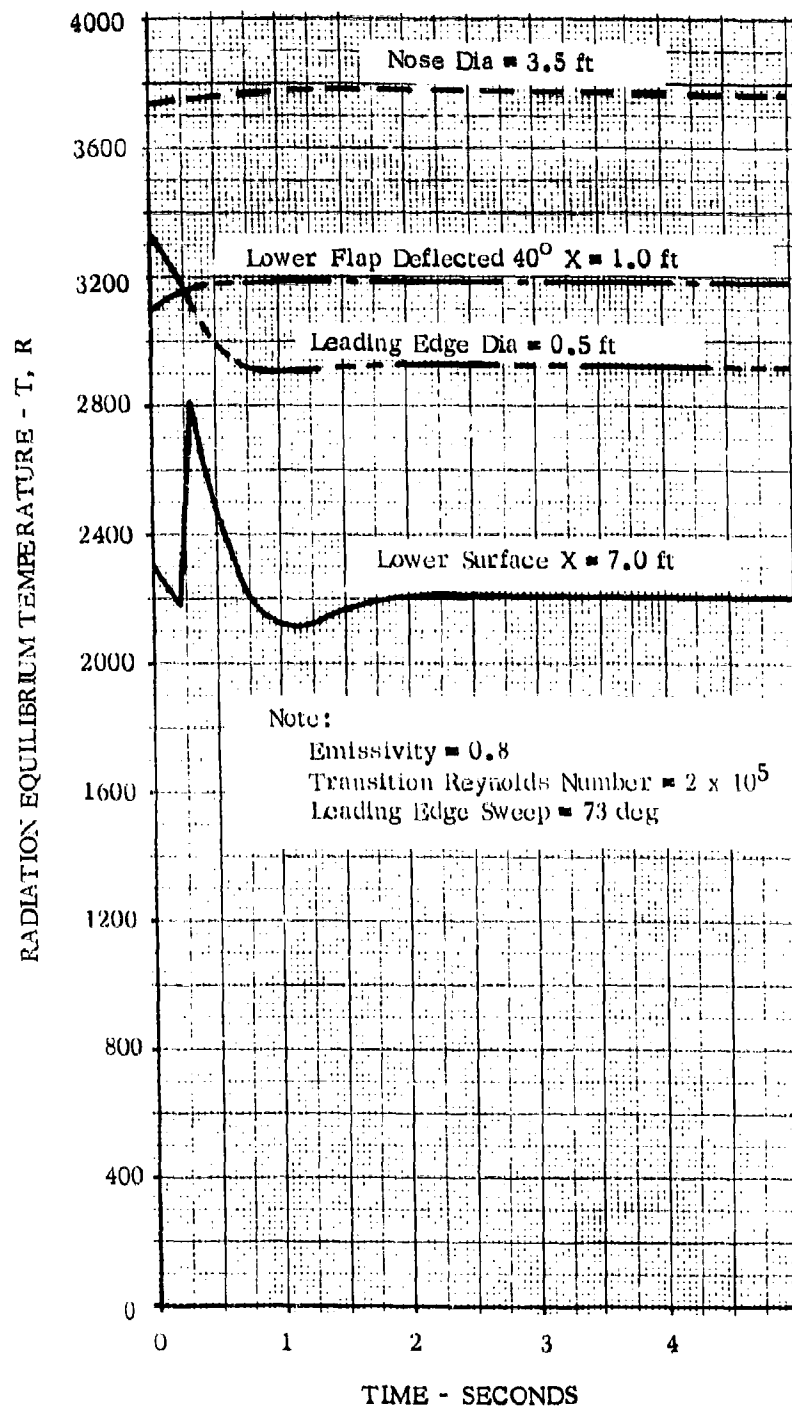


Figure 64 - Ballistic Capsule Separation Temperature History

Run 6

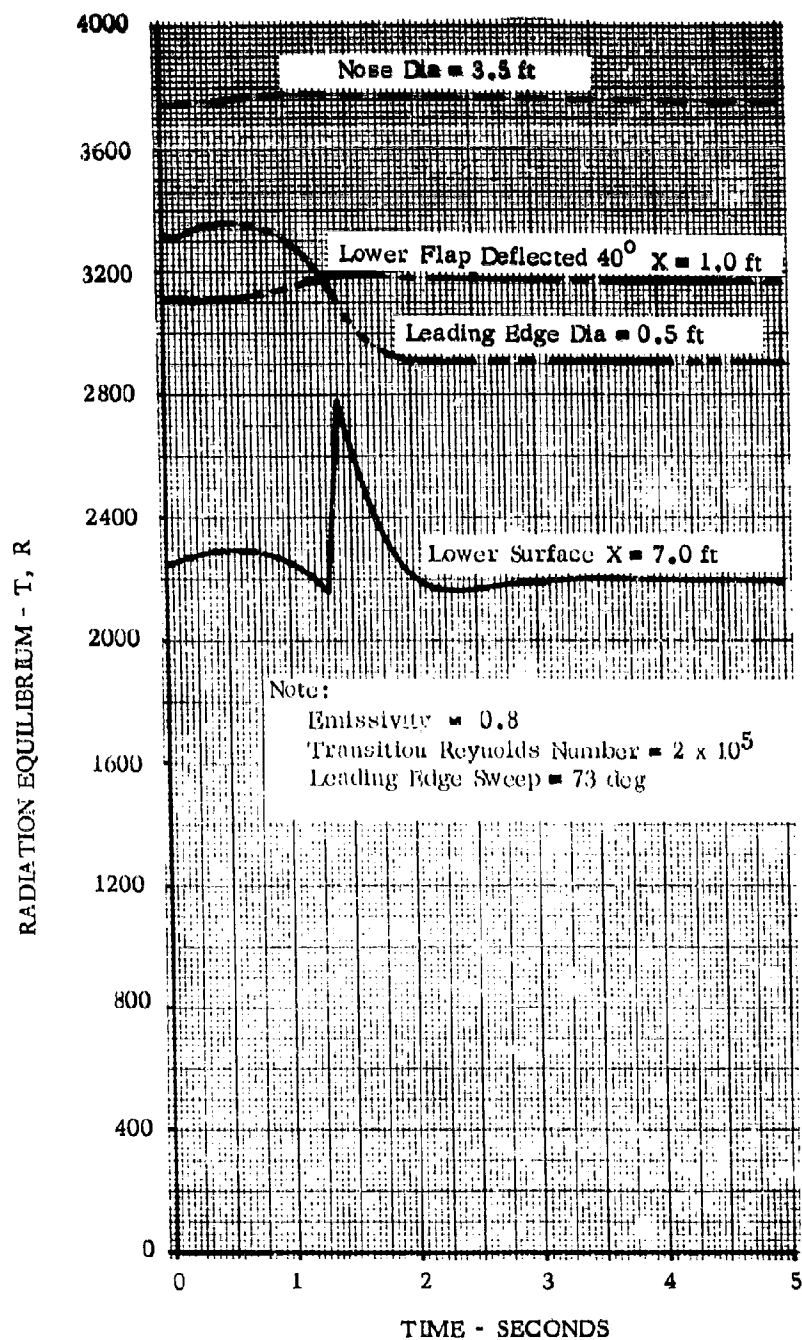


Figure 65 - Ballistic Capsule Separation Temperature History

Run 7

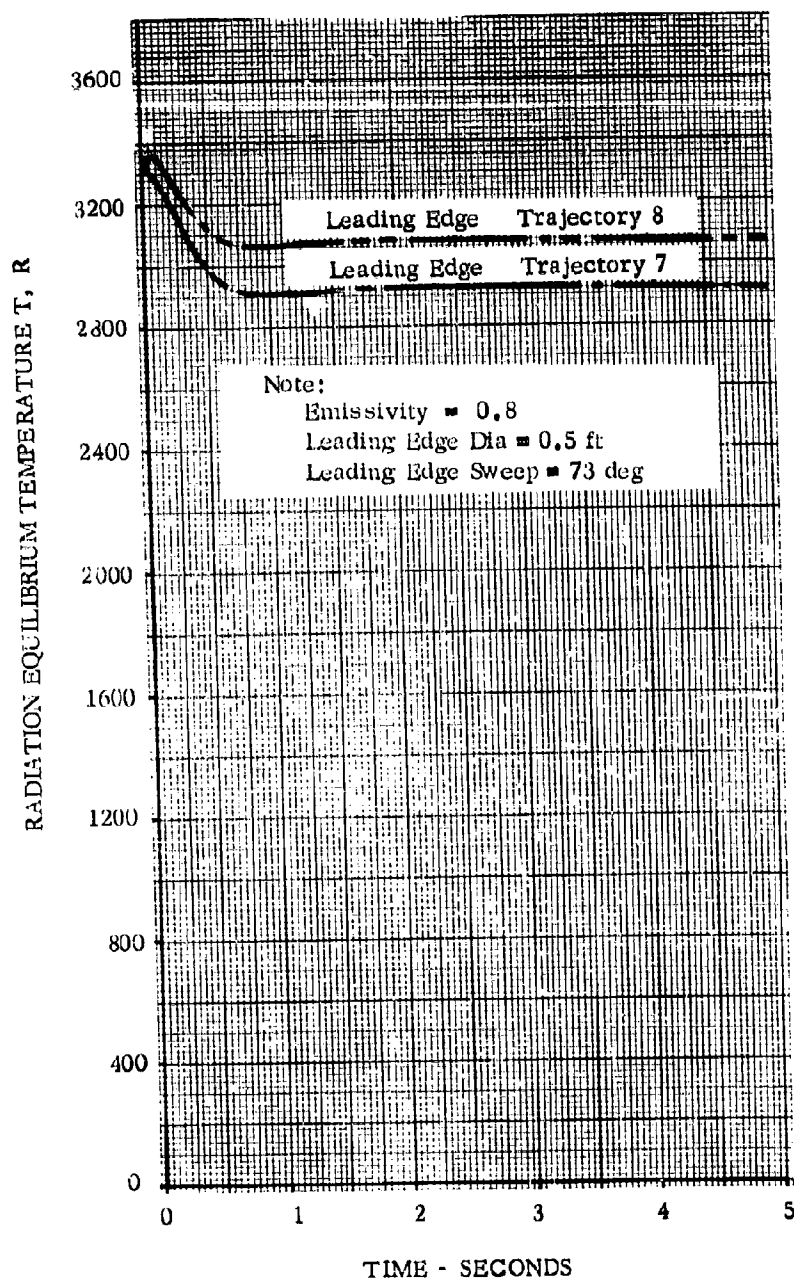


Figure 66 - Ballistic Capsule Separation Temperature History

Run 8

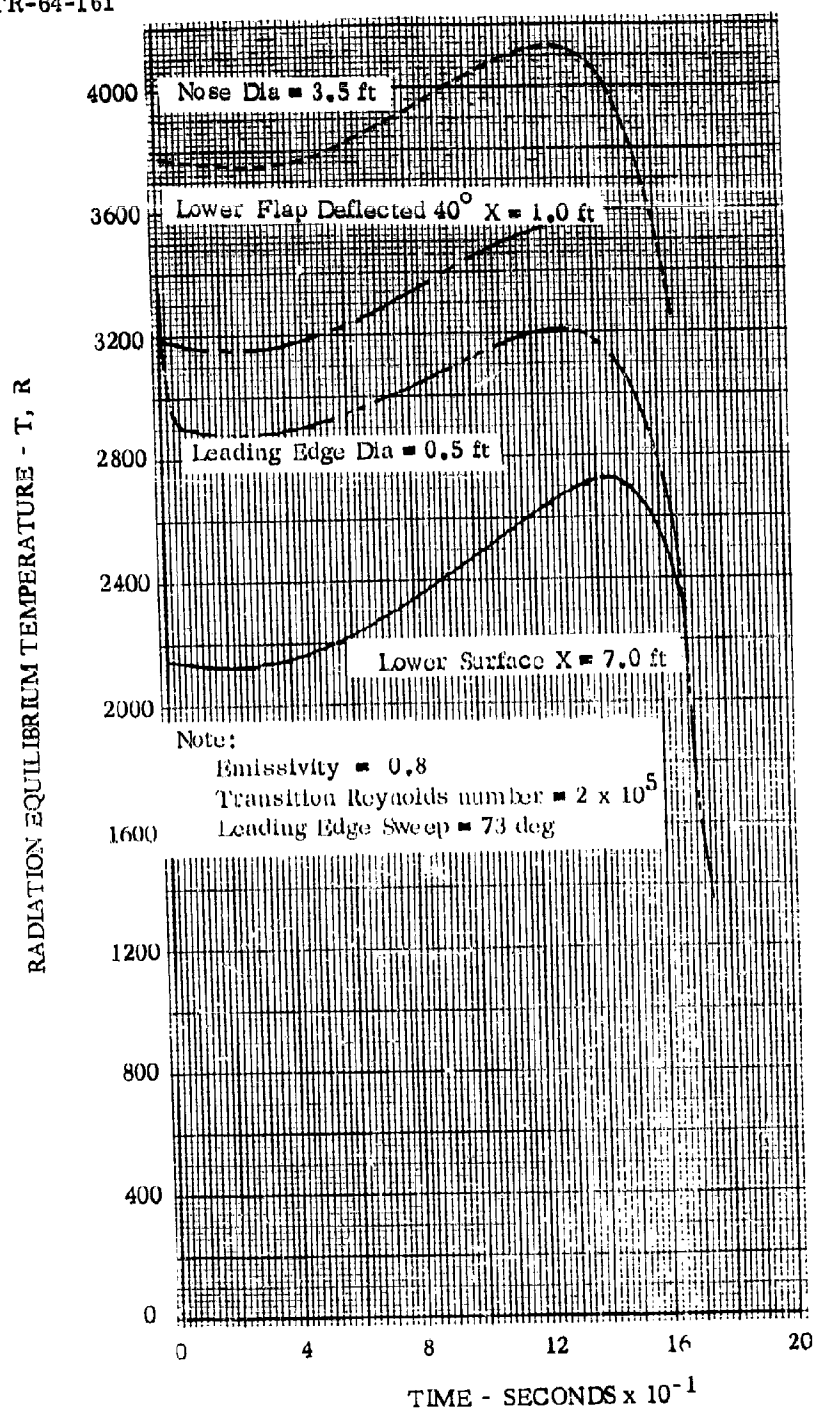


Figure 67 - Ballistic Capsule Temperature History - Complete Trajectory  
Zero Lift



TABLE VII  
SUMMARY OF CONDITIONS FOR BALLISTIC BODY ORBIT TRAJECTORY RUNS

No.	$\theta_i$	$\theta_c$	$\theta_i^\circ$	Reaction	T	$\delta TH$	THM	$\delta TH/q$
1	0	0	1146	IN	40,000	40	OUT	0
2	10							
3	20							
4	10							
5					20,000			
6					10,000	30		
7							IN	
8					40,000	40		
9					10,000			.1
10								
11					40,000			.1

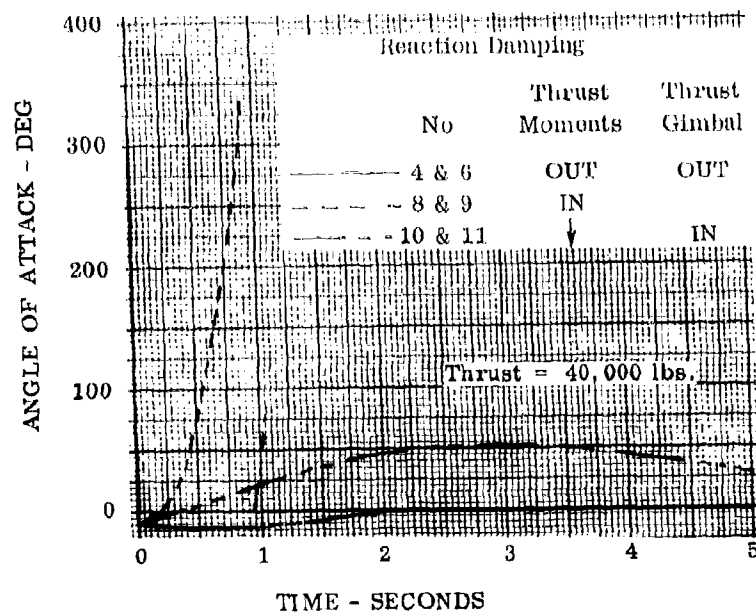
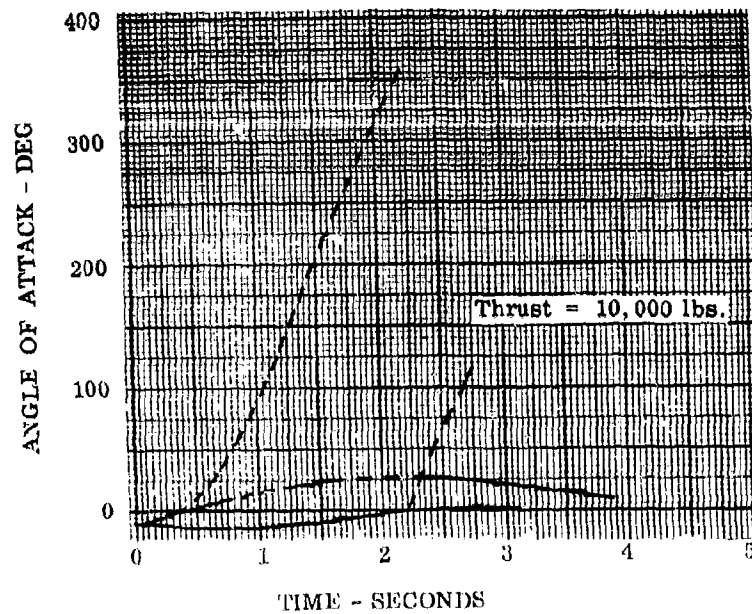


Figure 68 - Ballistic Body - Orbit Escape Trajectory Characteristics

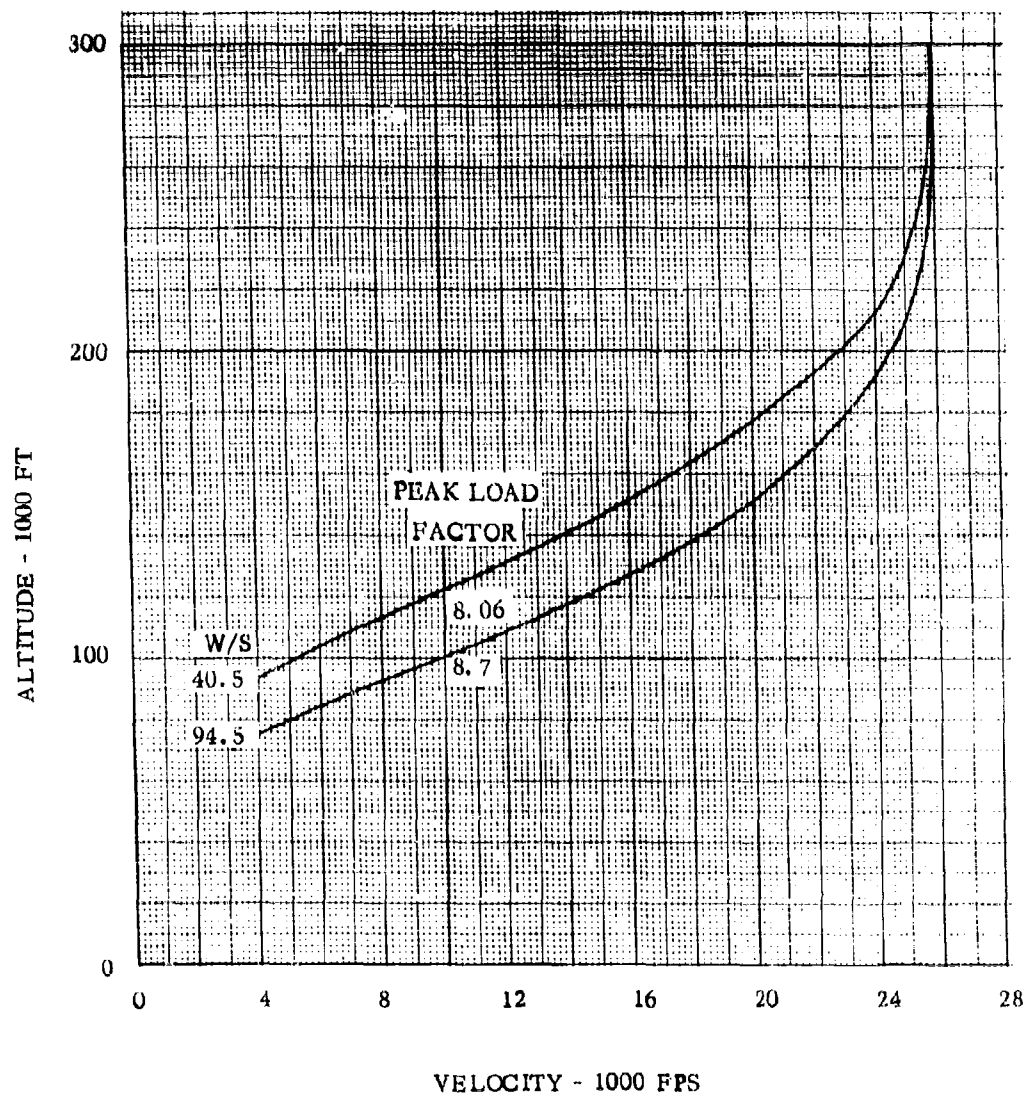


Figure 69 - Ballistic Body Capsule - Orbit Re-entry Trajectories

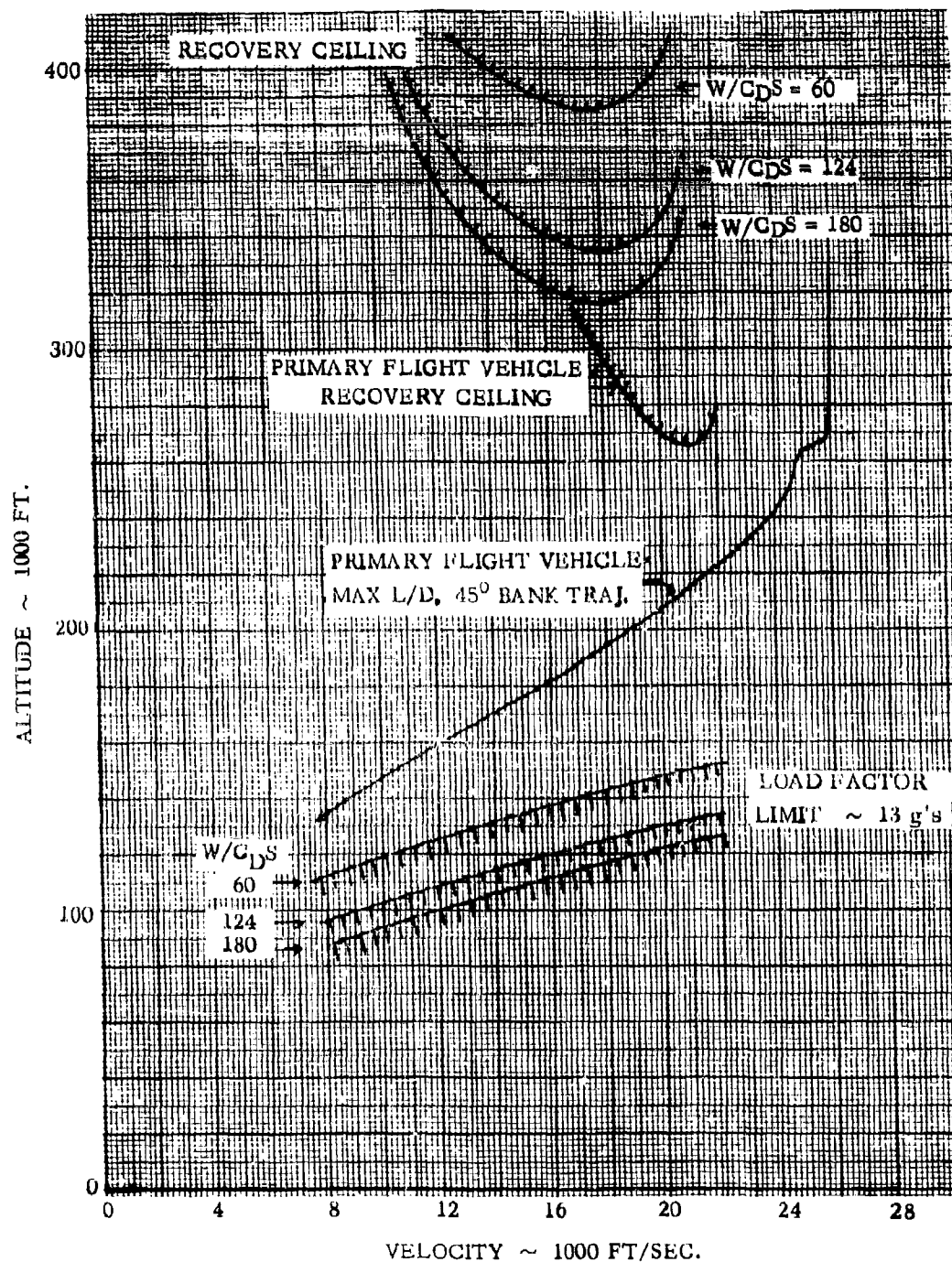


Figure 70 - Ballistic Body - Recovery Ceiling

TABLE VIII  
SUMMARY OF CONDITIONS FOR BALLISTIC BODY SUBSONIC TRAJECTORY RUNS

No.	$\gamma$	$\delta_u$	$\delta_L$	$\alpha_i$	$\theta_i$	$\epsilon_{L/q}$	REACTION	T	$\delta_{TH}$	THM	$\delta_{TH/q}$
86	-2	20	-20	0	0	.5	OUT	40,000	40	OUT	0
87					-11.44						
88											
89						0	IN		30	IN	.1
90							OUT		40	OUT	0
91						.5					
92						0					
93											
94	90			0		.5	IN		30	IN	.1
95						0	OUT		40	OUT	0
96											
97						.5					
98						0					
99											
100						.5					
101						0					
102											

Landing -  $\gamma = -2^\circ$        $V = 200$  FPS      Altitude = 100 FT

On-the-Pad -  $\gamma = 90^\circ$        $V = 0$       Altitude = 100 FT

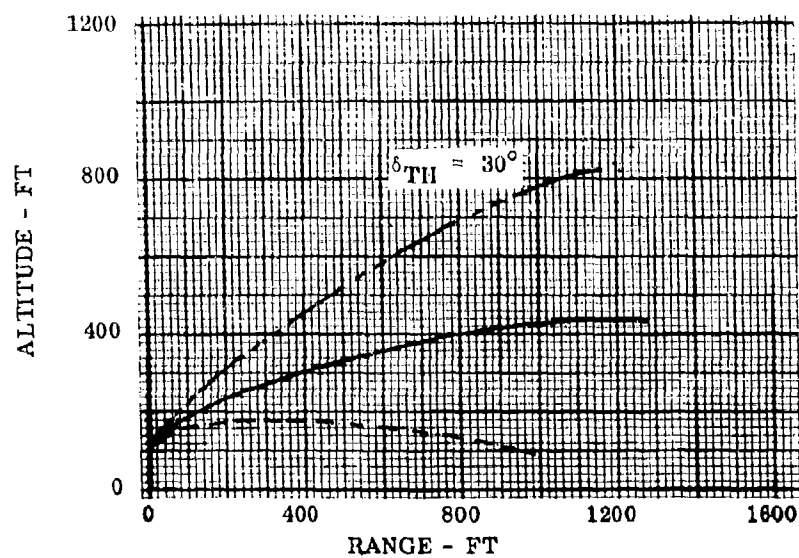
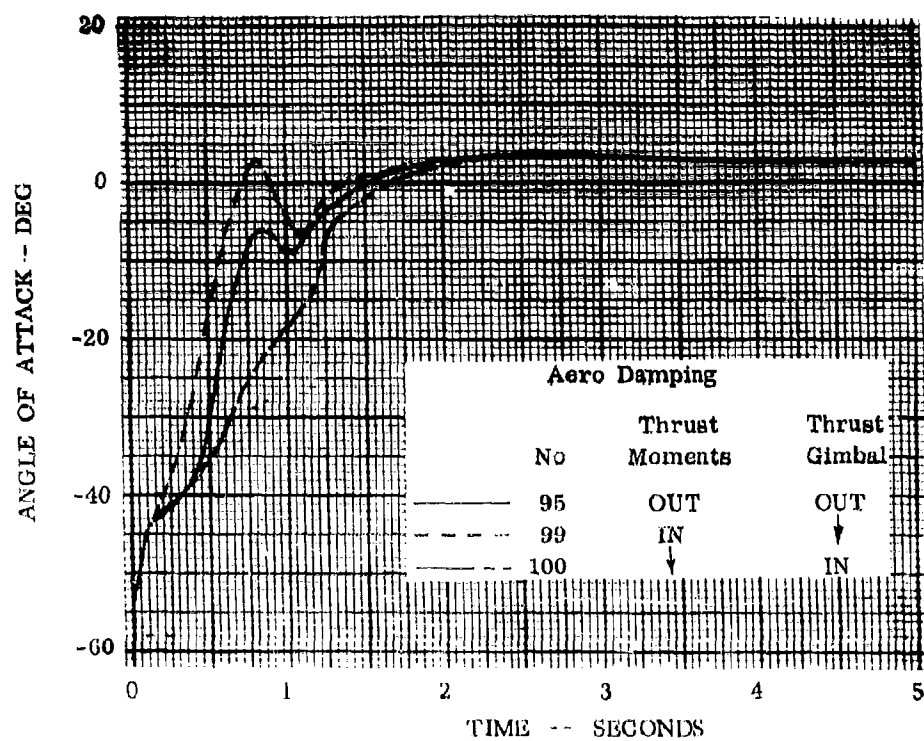
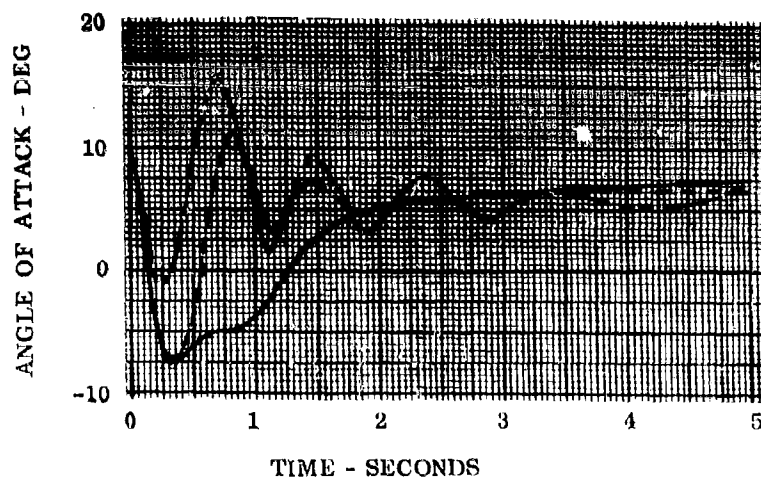


Figure 71-Ballistic Body - On-the-Pad Escape Trajectory Characteristics



	No	Aero Damping	Reaction Damping	Thrust Moments
—	87	IN	OUT	OUT
- - -	89	OUT	IN	↓
- · -	93	↓	OUT	IN

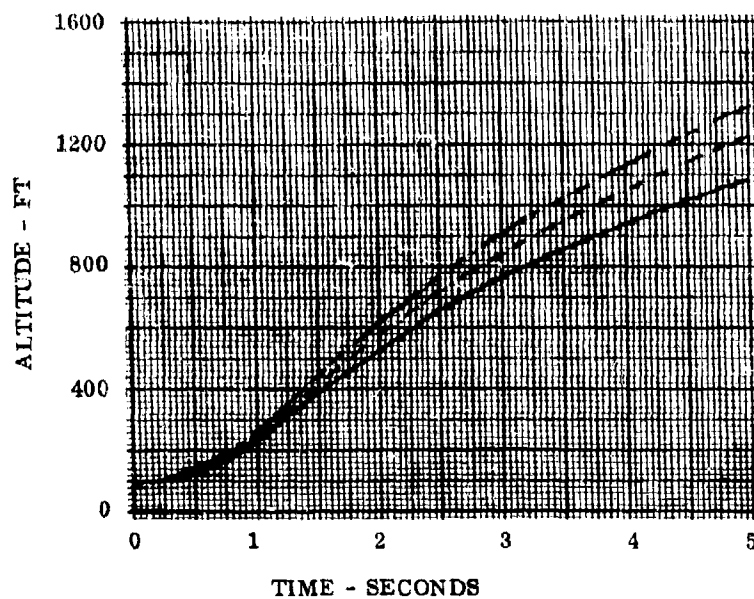


Figure 72-Ballistic Body - Landing Escape  
Trajectory Characteristics

TABLE IX  
SUMMARY OF CONDITIONS FOR BALLISTIC BODY SUPERSONIC TRAJECTORY RUNS

No.	$\xi_u$	$\delta L$	$\alpha_i$	$\theta_i$	$\theta_c$	$\delta L/q$	REACTION	T	$\delta TH$	THM	$\delta TH/q$
1	20	20	3	0	0	.5	OUT	40,000	40	OUT	0
2			0								
3			-3								
4			3								
5			0								
6			3	-5.73	0						
7				-11.46							
8				C							
9											
10											
11											
12											
13					NONE						
14		10									
15		15									
16		25									
17		30									
18		20									
19											
20											
21											
22											
23			-3								
24		25	3								
25											
26											
301				50							
302				100							
303				-50							
304				-100							



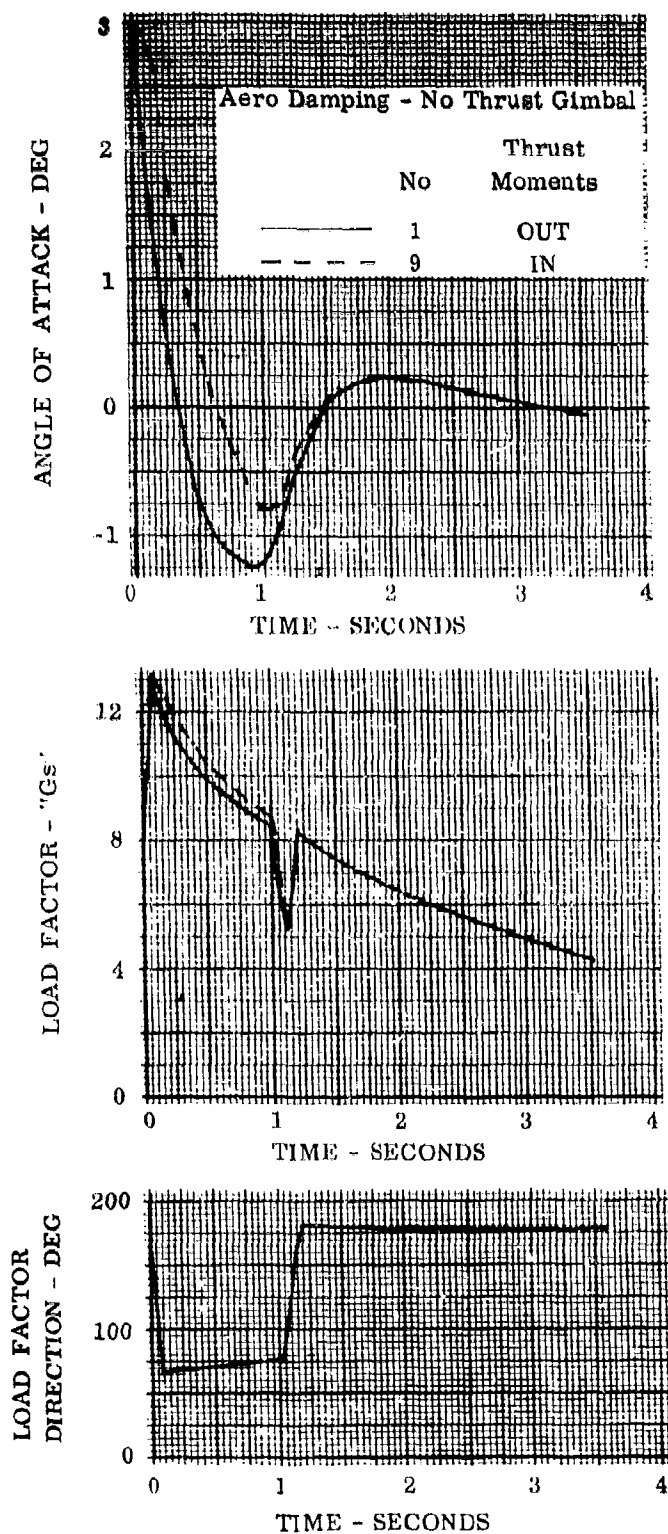


Figure 73-Ballistic Body - Maximum Dynamic Pressure Escape Trajectory Characteristics - Effect of Thrust Moment

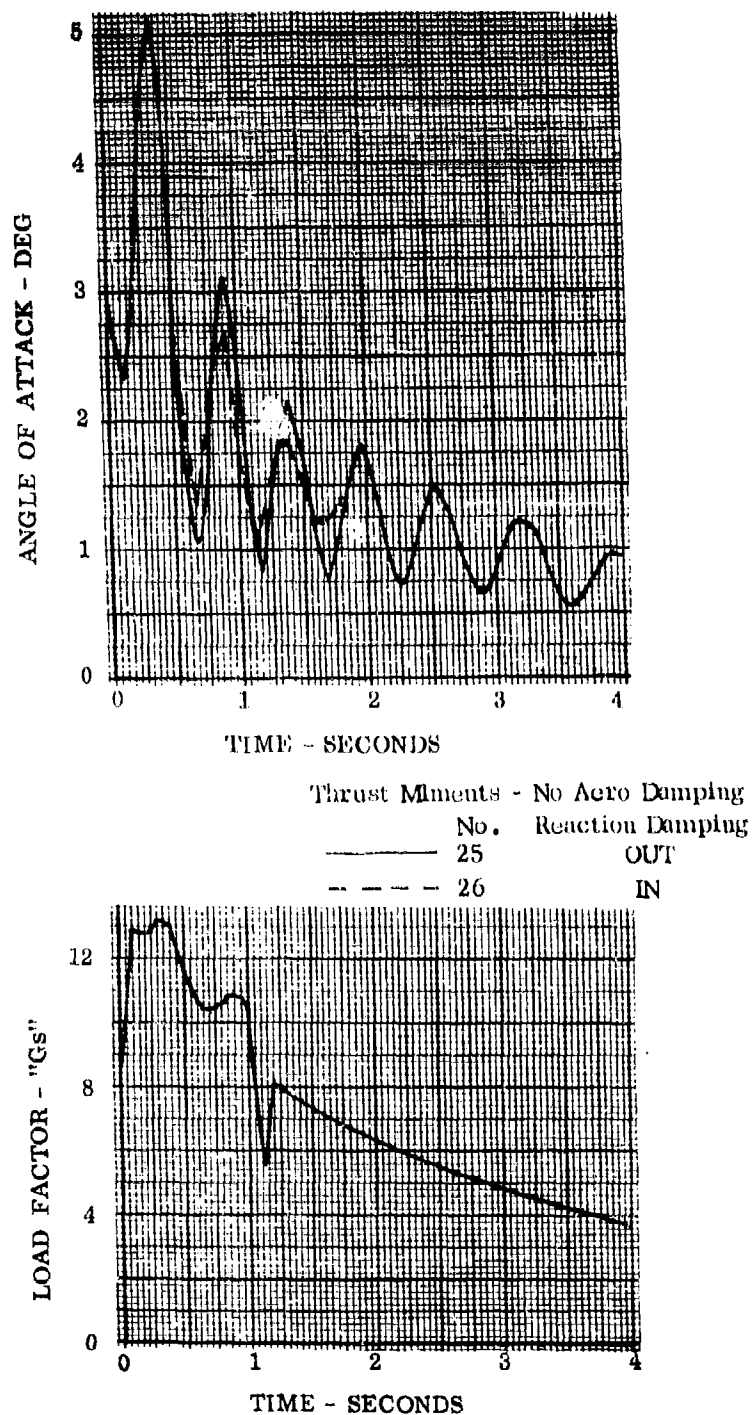


Figure 74 - Ballistic Body - Maximum Dynamic Pressure Escape Trajectory Characteristics - Effect of Reaction Controls

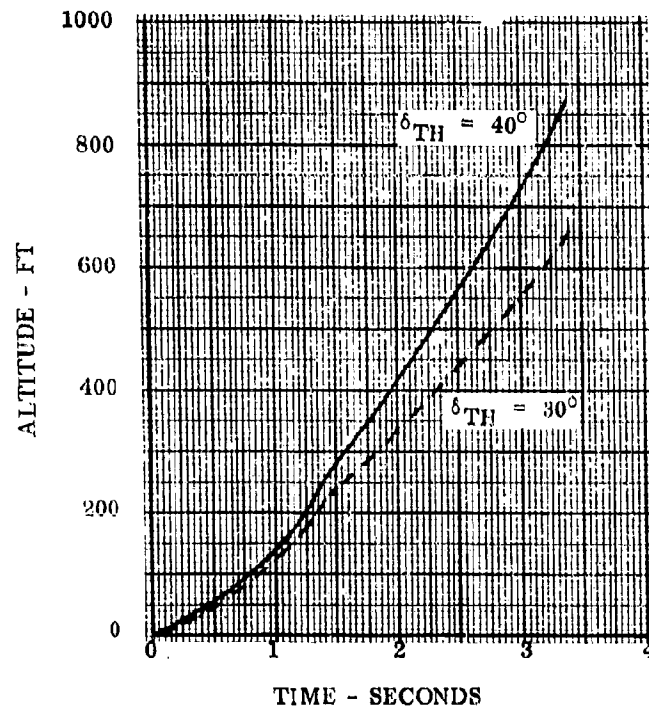


Figure 75 - Ballistic Body - Maximum Dynamic Pressure  
Escape Trajectory Characteristics - Separation  
Distance

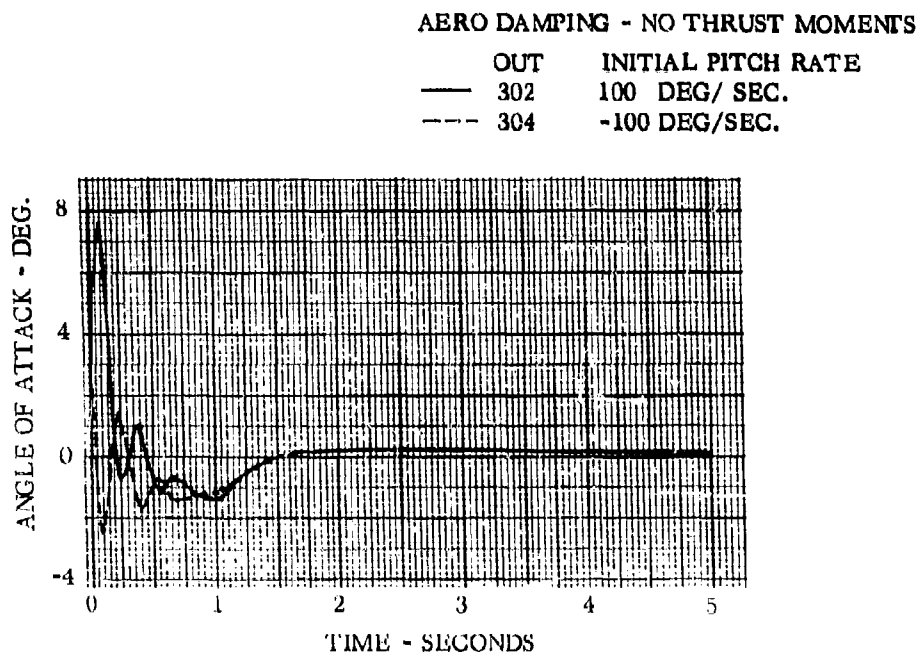


Figure 76 - Ballistic Body - Maximum Dynamic Pressure Escape Trajectory Characteristics - Effect of Initial Pitch Rate

## 6.2 LIFTING BODY CAPSULE

**6.2.1 RE-ENTRY ESCAPE.** As with the ballistic body capsule described above, the re-entry escape performance was calculated in detail for the first five seconds after separation and then the long time trajectory characteristics were investigated.

**6.2.1.1 Separation Dynamics.** This investigative phase considered the use of both aerodynamic and reaction controls. The autopilot described in Section 4.0 was used with a pitch-roll mixer incorporated into the reaction controls. In addition, proportional actuators for the aerodynamic surfaces and rocket gimbals were included, with linear first order time lags.

In performing this phase of the investigation, a basic technique was first determined and then the effect of parameter variations on the basic technique was analyzed. The parameter values used for the more significant computer runs are presented in Table X. The parameters investigated are as follows:

- a. Aerodynamic flap pitch damping
- b. Reaction pitch damping
- c. Thrust moments
- d. Thrust pitch damping
- e. Initial sideslip
- f. Initial roll rate
- g. Initial yaw rate
- h. Thrust magnitude
- i. Longitudinal center of gravity position.

An immediate roll to wings level attitude was incorporated into the separation maneuver for the lifting body. Initially an autopilot command of wings level was used. This maneuver caused too high a roll rate, resulting in pitch roll coupling and diverging values of bank angle, angle of attack, and sideslip. No pitch or yaw damping from the reaction controls was originally used. By adding pitch and yaw damping, and a commanded bank angle time history, stable roll maneuvers were obtained, with roll rates from 5 to 15 deg/sec. A nominal commanded roll rate of 10 deg/sec was used in further simulations.

The directional stability of the lifting body is low and the trajectories did not trim at zero sideslip. A directional gyro was added to the yaw channel, aligned with the initial velocity vector. An on-board knowledge of initial sideslip is thus assumed, and as concluded in Reference 1 must be available throughout the trajectory.

With the addition of the directional gyro, the steady-state sideslip was essentially eliminated. However, unless the azimuth command was coordinated with the roll command, large transient sideslip angles resulted. The azimuth command is required because the initial bank angle and angle of attack result in a body-axis heading of 11 deg. from the initial velocity vector. A linear heading command was found to result in sufficiently small sideslip angles, and more refined coordination was assumed to be unnecessary for this study.

On the first runs using aerodynamic surfaces for damping, the effect of time lag was investigated. An ideal no-lag actuation was compared with a realistic first order time constant of .1 seconds, and the responses were essentially identical. Thus for subsequent trajectories a .1 second actuator lag was used for aerodynamic surfaces or thrust gimbals.

Figure 77 compares reaction damping with aerodynamic damping for a fixed trim angle of attack of 10 degrees. Run 1 has three-axis reaction damping while Run 2 has reaction damping in yaw and roll, and pitch damping from the lower aerodynamic flap. Presented in Figure 77 are angle of attack and lower flap time histories. The responses show either technique is satisfactory at this maximum heating point.

Figure 78 presents the angle of attack, flap deflection and gimbal angle time histories for trajectories with a fixed trim angle of attack of 10 degrees in which thrust moment effects were included. Since the rocket fuel is off the c.g., the c.g. varies during burning. The gimbal point is located so that the thrust vector (without damping) is directed at an intermediate point between the extreme c.g.'s. Comparisons are shown with pitch damping derived from:

- Run 3) lower aero flap
- Run 4) lower aero flap plus thrust gimbal
- Run 5) reaction controls plus thrust gimbal
- Run 6) reaction controls.

Reaction controls are used for roll and yaw damping throughout. The responses show that no major differences are present, and that any of the four techniques are satisfactory.

In addition, comparing Runs 1 and 2 in Figure 77 with Runs 3 and 6 of Figure 78 show the effect of the thrust moments on the trajectories. With the thrust oriented at a nominal c.g., there is no major difference due to the thrust moments. Thrust gimbaling would seem to be required only if there were considerable uncertainty or variation in the c.g.

Run 6 was selected as a separation trajectory with satisfactory response characteristics and Figures 79, 80 and 81 show several response variables from this run. In Figure 79, the angle of attack approaches the trim value of 10 degrees from an initial value of 15.5 degrees, never exceeding the initial value. The bank angle varies smoothly from the initial value to near wings level. The sideslip has a maximum value of 3 degrees during the roll.

Figure 80 presents the load factor and load factor direction characteristics for Run 6. The acceleration has a peak value of 10.8 G's, occurring at .08 seconds and resulting from the rocket thrust. The load factor direction indicates primarily the direction of the thrust during burning, and the direction of the air load after burning.

Figure 81 shows the separation distances from the parent vehicle for Run 6. The computer program estimates the parent vehicle position by simply considering that the initial velocity vector remains constant, in magnitude and direction. Figure 81 shows positive and adequate clearance.

One of the variable parameters is the trim flap settings, resulting in various trim angles of attack. Runs were made varying the trim angle of attack from  $10^{\circ}$  to  $30^{\circ}$ . Figure 82 shows two attempts to stabilize a trajectory with a trim angle of attack of  $30^{\circ}$ . Run 7 uses a commanded roll rate of  $10^{\circ}/\text{sec}$  while Run 16 uses a rate of  $5^{\circ}/\text{sec}$ . The high angle of attack makes the roll coupling problem more difficult. The coordination technique that was adequate for the runs having a trim angle of attack of  $10^{\circ}$  failed for these two. Both Runs 7 and 16 exceed the bank angle scale shown. However, Run 16 did eventually reverse the roll rate, and tended to return to a wings level attitude, while Run 7 diverged in roll and sideslip. These higher trim angles of attack result in higher temperatures. From temperature considerations, it seems that a lower initial trim angle of attack that is gradually increased to a higher value over several minutes would be preferred. This technique is discussed in Section 6.2.1.2. It is not concluded from Figure 82 that stabilization of a higher angle of attack roll is impossible, only more difficult, and in particular requiring more sophisticated coordination of the three axes during the roll.

Figure 83 shows the effect of varying initial conditions of sideslip, roll rate, and yaw rate. Runs 8, 9 and 10 are identical to Run 6, except that in Run 8, the initial sideslip is -3 degrees, in Run 9 the initial roll rate is .1 rad/sec, and in Run 10 the initial yaw rate is .1 rad/sec. All these runs have three axis reaction damping, as well as roll and yaw attitude commands. There are no significant differences in the responses after the first second. The angular rate responses emphasize the off-on

nature of the reaction controls. When the responses tend to converge, only one is shown. These runs show that the satisfactory responses of Run 6 are not sensitive to reasonable variations in asymmetric initial conditions.

Figure 84 shows the effect of reducing the nominal thrust level from 25,000 pounds to 12,000 pounds on load factor and separation distance characteristics. As expected, the load factor and the separation distances are reduced but at this re-entry condition are adequate. On-the-pad and high dynamic pressure escape which will be investigated later in the program will determine the minimum thrust requirements.

Figure 85 shows the effect of varying the longitudinal center of gravity on the responses. Run 12 is essentially a repeat of Run 1, at the nominal c.g. with some slight modifications in the aerodynamic data curve fits. The c.g. for Run 13 is 4.0% of the reference length (15.1 ft.) forward, and that for Run 14 is 2.0% aft. The lower flap was adjusted to maintain the trim angle of attack near 10 degrees. As expected, the angle of attack response for a forward c.g. is faster, and that for the aft c.g. is slower. Differences in the bank angle responses were indistinguishable. Thrust moments were not included for these runs. The effects of thrust moment would be similar to those shown in Figure 78. It is concluded from Figure 85 that satisfactory trajectories are not dependent on reasonable center of gravity shifts if (a) the proper flap setting is used and (b) thrust moments are not large.

Figure 86 presents the effect of thrust angle on separation distance characteristics of the thrust. For Run 12 the thrust vector is 30 degrees above the horizontal body axis, and in Run 15, 40 degrees. The thrust magnitudes in each case were equal to the nominal value presented in Figure 47. As a result Run 12 has more separation from the parent vehicle in the down range direction, and Run 15 more in cross range and altitude. Either response is satisfactory, and thus structural and mechanical disconnect considerations would probably determine the optimum thrust angle.

**6.2.1.2 Complete Trajectories.** The primary problem of the radiation cooled lifting body escape capsule is preventing excessive temperatures during the escape trajectory. The problem can be divided into two parts, 1) controlling temperatures during the first few seconds after escape and 2) controlling temperatures over the entire escape trajectory.

Temperatures are a function of altitude, velocity and angle of attack. Increasing velocity and angle of attack increases temperatures while increasing altitude decreases temperatures. For lifting vehicles in equilibrium flight the decrease in temperature due to increasing trajectory altitude more than offsets the increase in



temperature due to the increase in angle of attack required to achieve the higher altitude. This is not true however for non-equilibrium flight. For the present capsule, escape is initiated at an angle of attack of  $15.5^\circ$ . As discussed in Section 6.2.1.1, if the capsule is separated and trimmed for a high angle of attack, it pitches up to the high angle of attack faster than the altitude increases, leading to excessive temperatures.

There is a maneuver which will prevent the initial pitchup and also achieve the advantage of a high trim angle of attack trajectory. This is a maneuver in which the vehicle separates trimmed for a low angle of attack and then gradually pitches up to a high trim angle of attack.

This maneuver was investigated using the two degree of freedom trajectory program. As a basis of comparison, the trajectories for fixed trim angles of 10, 15 and 30 degrees were determined. Two varying lift trajectories were considered. In the first the angle of attack was increased linearly over a 150 second time period from 10 to 15 degrees. In the second the angle of attack was increased from 15 to 30 degrees over a 150 second time period. The resulting altitude velocity trajectories are shown in Figure 87.

It can be seen from Figure 87 that the constant lift trajectories oscillate with the oscillations becoming more severe as the trim angle is increased. As will be discussed in Section 4.0, these oscillations yield aerodynamic heating problems. Varying the angle of attack from 10 to 15 degrees during the trajectory resulted in a very smooth trajectory. The trajectory in which the angle of attack was varied from 15 to 30 degrees was better than the fixed 30 degree trim angle of attack trajectory, but still exhibited some oscillations. This trajectory could be readily improved by decreasing the rate at which the angle of attack is increased.

The effect of capsule wing loading on these varying lift complete trajectories is presented in Figure 88.

**6.2.1.3 Aerodynamic Heating.** In general, equilibrium temperatures were obtained at four points on the lifting body. These points were as follows:

- a. Leading edge
- b. Lower surface 5.0 ft. aft
- c. Lower surface 12.0 ft. aft
- d. Flap 1.0 ft. aft of hinge line.

The leading edge diameter was 0.5 ft. with a sweep of  $73^\circ$ . A transition Reynolds number of  $2 \times 10^5$  was used in analyzing the lower surface and the flaps. At 5.0 ft. aft on the lower surface the cant angle was  $10.0^\circ$  and at 12.0 ft. aft was  $2.0^\circ$ . The leading edge was analyzed where the cant angle was  $10.0^\circ$  which reduced the effective sweep angle yielding higher leading edge temperatures. Flaps were treated as wedges with a half angle equal to the deflection angle. For the lower surface flap, the vehicle angle of attack was added to the wedge angle to obtain the total flap incidence angle. For the side flaps an effective angle of attack was determined which was then added to the wedge angle to obtain the total flap incidence angle.

Figure 89 compares the leading edge temperature histories for trajectories 3, 4 and 6 from Table 1. These were the trajectories in which aerodynamic control, reaction control and thrust gimbaling were compared. For all these trajectories, the peak leading edge temperature of 3478 R occurs at separation. The variation in temperature between the trajectories is a result of the difference in vehicle response characteristics as shown in Figure 78.

Figure 90 presents the temperature history of the deflected lower flap for trajectory 3. Trajectory 3 is the trajectory in which aerodynamic control is used in pitch and the thrust moment effects are included without thrust gimbaling. The flap temperature is presented for this trajectory since this trajectory places the most severe demands on the flap controls for a trim angle of  $10^\circ$ . There is little variation in flap temperature due to the fact that the flap deflection varied only about 5 degrees from the nominal trim deflection of  $34.5^\circ$  as shown in Figure 78. The flap hinge line is located just aft of the 12 ft. aft point. The flap film coefficient was calculated to be 8.6 times greater than a laminar film coefficient on the vehicle lower surface at the 12.0 ft. aft point just ahead of the flap at 1.2 seconds from separation. Reference 15 would predict a larger increase in film coefficient, however, the experimental data of References 15 and 16 have sufficient scatter that the increase of 8.6 would seem to be a reasonable estimate.

The effects of trim angle of attack on the leading edge and lower surface temperatures at a point 12 ft. aft of the nose are shown in Figure 91. Trajectory 6 represents a trim angle of  $10^\circ$  while trajectory 7 represents a trim angle of  $30^\circ$ . The temperatures for a trim angle of attack of  $30^\circ$  are quite high due to the rapid pitchup shown in Figure 82. For the  $10^\circ$  degree trim angle of attack trajectory the peak leading edge and lower surface temperatures are 3447 R and 2828 R occurring at separation. For the  $30^\circ$  degree trim angle of attack trajectory,

the peak temperatures occur at 1.4 seconds after separation and are 3982 R and 3414 R for the leading edge and lower surface respectively.

Figure 92 presents temperature histories for 4 vehicle locations for trajectory 6 which is referred to as the nominal trajectory. The locations are; leading edge, lower surface - 5 ft. aft, lower surface - 12 ft. aft and lower flap - 1 ft. aft of hinge line. The leading edge temperature was determined for a sweepback of 71.4 degrees. This sweepback was used in order to obtain an estimate of the effects of the slight sideslip present in this trajectory as shown in Figure 79. Comparing the leading edge temperature history of Figure 92 with the temperature history given in Figure 91 for a sweepback of 73 degrees reveals that the small sideslip results in a peak leading edge temperature increase of 31 degrees. Since a primary flight vehicle will be designed to permit sideslips of approximately 3 degrees, this should not be considered a problem area. The peak lower surface temperatures at 5 and 12 feet aft both occur at the initial separation and are 2441 R and 2828 R respectively. The temperature at 12 ft. is higher than at 5 ft. because of the existence of a turbulent boundary layer at 12 ft. Had a transition Reynolds number of  $5 \times 10^5$  been used, the boundary layer would have been laminar at 12 ft. aft and the temperatures less than at 5 ft. aft.

Figure 93 presents leading edge and side flap temperature histories for trajectory 8 in which an initial sideslip angle of 3 degrees was considered. Due to the initial sideslip angle, the leading edge temperature is higher than for trajectory 6. The peak temperature still occurs at separation, however, and is 3507 R. The side flap had a constant deflection of 40 degrees and attained a peak temperature of 3185 R at 24 seconds after separation.

Figure 94 presents the leading edge temperature histories for the constant angle of attack trajectories presented in Figure 87. Increasing the initial trim angle increases the leading edge temperatures. Figure 95 presents the leading edge temperature histories for the two trajectories in which the angle of attack was slowly increased over a 150 second time period. Increasing the angle of attack from 10 degrees to 15 degrees yielded a trajectory in which the peak temperature occurred at separation. The trajectory in which the angle was increased from 15 degrees to 30 degrees also had its peak temperature at separation but still had large temperature oscillations resulting from the trajectory oscillations shown in Figure 87. As discussed in Section 3.4, these oscillations could be decreased by decreasing the pitchup rate.

The effect of wing loading on the complete trajectory leading edge temperature characteristics are presented in Figures 96 and 97 for final trim angles of attack of 15 and 30 degrees respectively. The peak leading edge temperatures are as follows:

W/S	Traj. No.	Trim Angle	T <sub>max</sub> R
28.4	48	15	3275
29.7	105	"	3395
56.6	106	"	3666
28.4	51	30	3431
39.7	107	"	3469
56.6	108	"	3657

6.2.2 ORBIT ESCAPE. The initial conditions for the lifting body orbit separation dynamics runs are presented in Table XI.

Figure 98 presents angle of attack time histories for orbit escape at two thrust levels. Satisfactory performance was obtained in all cases. The thrust moment produces a somewhat greater angle of attack oscillation but it is quickly damped out. Increasing the thrust level decreases the overshoot characteristics. The effect of initial angular rates is negligible.

The orbit re-entry trajectory characteristics presenting the effect of wing loading and trim angle of attack are shown in Figure 99. For a trim angle of attack of 15 degrees the following peak leading edge temperatures were obtained:

W/S	Maximum L.E. Temp <sup>o</sup> R
28.4	3420
41.4	3550
58.8	3640

These temperatures are approximately the same as the maximum leading edge temperatures obtained for escape from the maximum heating point of the primary flight vehicle as presented in Figures 96 and 97.

6.2.3 RECOVERY CEILING. Figure 100 presents the recovery ceiling for the Lifting Body capsule for three values of wing loading. For this configuration the recovery ceiling in the high hypersonic region is determined by temperature limits. The leading edge temperature was used as the base temperature for determining recovery ceiling. From the studies described in Section 6.2.1 a leading edge temperature limit of 3440 R was used. This is unrealistic for the wing loading of 56.6 since the long time trajectory characteristics discussed in Section 6.2.1 indicate that at this wing loading a maximum temperature of 3640 R is reached for escape from the primary flight vehicle

maximum heating point. For this reason, a recovery ceiling based upon this temperature is also shown in Figure 100. The recovery ceiling capability of the lifting body capsule is slightly less than the primary flight vehicle for the low wing loading condition. As the escape capsule wing loading increases the recovery ceiling decreases.

6.2.4 ON-THE-PAD ESCAPE. The run schedule of initial conditions for the performance studies at this flight condition are presented in Table XII. Figure 101 presents the angle of attack time history and altitude range-characteristics for the lifting body separating from the on-the-pad condition. The effects of thrust moments and aerodynamic control damping on the angle of attack characteristics are indicated. Without aerodynamic damping the capsule experiences large oscillations. As expected, decreasing the thrust inclination increases the altitude achieved during separation. The upper curves in Figure 102 show the effect of control system type on separation altitude characteristics. For Run 153 without any controls the altitude is probably below the limits for good parachute recovery. The lower curves in Figure 102 compare the angle of attack characteristics for two nominal flap angle settings. At this subsonic condition a large negative trim angle of attack results. The separation altitude characteristics however were found to be adequate. The maximum load factor for on-the-pad escape results from the escape rocket thrust and is within human tolerance limits.

6.2.5 LANDING ESCAPE. The run schedule for this condition is presented in Table XII. Figure 103 presents the angle of attack and altitude time history characteristics for separation during landing approach. The effects of aerodynamic damping and thrust moment on the angle of attack characteristics are indicated. Aerodynamic damping yields good angle of attack characteristics even when the thrust moment effects are included. The initial decrease in angle of attack is a result of the change in magnitude and direction of the velocity vector due to the rocket thrust. For the landing approach condition, decreasing the thrust inclination angle decreases the altitude although in all cases investigated, sufficient altitude for parachute recovery was obtained.

Figure 104 shows the effect of control system type and flap setting on the angle of attack characteristics. Aerodynamic controls yield excellent damping. The reaction controls show very little effect when compared with the characteristics obtained with no damping. Use of the flap settings used at hypersonic speeds result in a negative trim angle of attack and as a consequence poor separation altitude characteristics. The peak separation altitude achieved was only 130 ft. with escape starting at 100 ft.

As with on-the-pad escape, the maximum load factor results from the escape rocket thrust and is within human tolerance limits.

**6.2.6 MAXIMUM DYNAMIC PRESSURE ESCAPE.** The initial conditions for the escape performance studies at this flight condition are presented in Table XIII. Figure 105 presents the effect of control type on the angle of attack and load factor characteristics. Very good damping is obtained with aerodynamic controls. Large angle of attack oscillations and resulting load factor oscillations occur when reaction controls are used. The load factors however do not exceed human tolerance limits.

Figure 106 presents the effects of flap deflection angle on the angle of attack characteristics. At this flight condition the flap deflections used at hypersonic speeds yield a negative trim angle of attack. Also shown in Figure 103 are the effects of initial pitch rate on the angle of attack characteristics. These high initial pitch rates which are a measure of interference effects have a minor effect on the characteristics. The oscillations which are induced are quickly damped out.

Figure 107 presents angle of attack, load factor and load factor direction characteristics showing the effect of thrust moment. Without damping the capsule experiences large oscillations which result in load factor oscillations. The load factors are still within human tolerance limits however.

**6.2.7 PERFORMANCE CONCLUSIONS.** On the basis of these studies the following conclusions can be made regarding the separate nose lifting body capsule.

1. In order to minimize temperatures the capsule should be separated and trimmed for a lower angle of attack than the 15.5 degrees vehicle angle of attack at the maximum heating condition. After separation the angle of attack should be slowly increased to a high angle of attack.
2. Increasing the capsule wing loading increases the temperature. The temperature limits of the primary flight vehicle are exceeded if the wing loading is greater than approximately 35.
3. Aerodynamic controls yield the best damping characteristics at all atmospheric flight conditions. Despite the relatively poor damping associated with reaction controls at the higher dynamic pressure condition the load factors are still within human tolerance limits.
4. The aerodynamic characteristics of the capsule are such that different flap settings must be used for hypersonic escape and escape at supersonic and subsonic speeds.

TABLE X  
SUMMARY OF CONDITIONS FOR LIFTING BODY RE-ENTRY TRAJECTORY RUNS

RUN	TRIM ANGLE OF ATTACK	LOWER FLAP TRIM ANGLE	LOWER FLAP PITCH DAMPING	THrust ANGLE	THrust GIMBAL PITCH DAMPING	THrust MANEUVER	THrust (NOMINAL)	REACTION DAMPING pitch - p roll - r yaw - y	COMMAND ROLL RATE	INITIAL SIDESLIP	INITIAL ROLL RATE	INITIAL YAW RATE	LONGITUDINAL CENTER OF GRAVITY
	DEG	DEG	DEG DEG/SEC	DEG	DEG DEG/SEC		POUNDS		DEG/SEC	DEG	DEG/SEC	DEG/SEC	
1	10.	34.5	.0	30.	.0	out	25,000	p, r, y	10.	-0.	0	0	NOM
2			.5			↓		r, y					
3			↓		↓	in		↓					
4					.1			↓					
5			.0		↓			p, r, y					
6					0								
7	30.	2.0											
8	10.	34.5								-3	↓	↓	
9										0	5.73	↓	
10						↓				↓	0	5.73	
11						out	12,000					0	
12							25,000						
13													.04 FWD
14													.02 AFT
15	↓	↓		↓					↓				NOM
16	30.	2.0		↓		↓			5.				↓

Side Flaps at 40 Degrees

Upper Flap at 0 Degrees

$\alpha_{\text{TRIM}} = 10^\circ$   
 $T = 25,000 \text{ LBS.}$   
 $\delta_{\text{TH}} = 30^\circ$   
 NO THRUST MOMENTS  
 1 - REACTION CONTROLS  
 2 - AERODYNAMIC CONTROLS

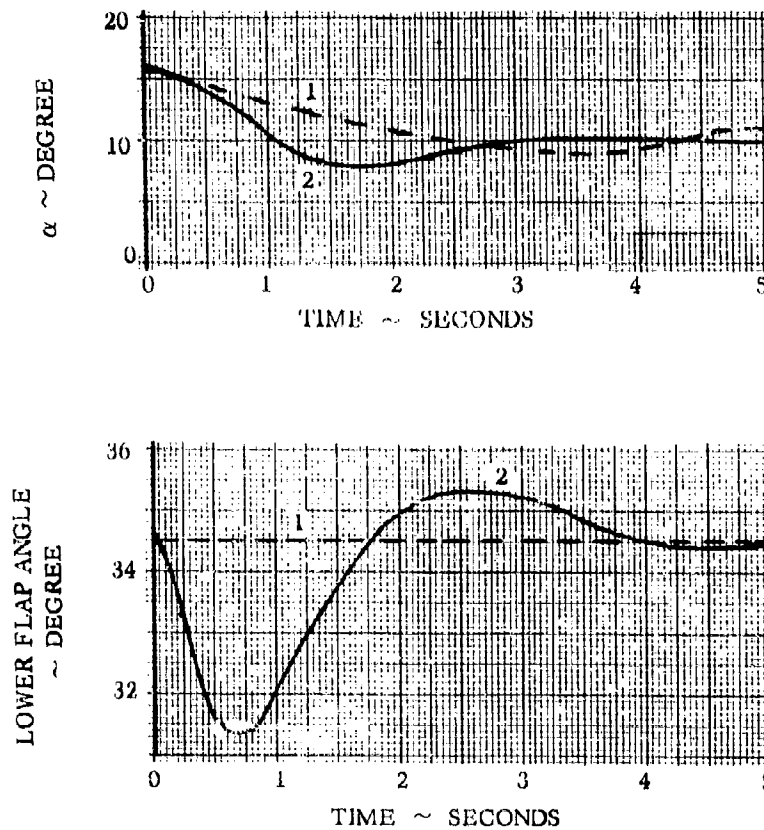


Figure 77 - Lifting Body Dynamic Response - Effect of Aerodynamic and Reaction Control Pitch Damping



$$\alpha_{TRIM} = 10^{\circ}$$

$$T = 25,000 \text{ LBS.}$$

$$\delta_{TH} = 30^{\circ}$$

THRUST MOMENTS INCLUDED

3 - AERO CONTROL - NO GIMBAL

4 - AERO CONTROL - GIMBAL

5 - REACTION CONTROL - GIMBAL

6 - REACTION CONTROL - NO GIMBAL

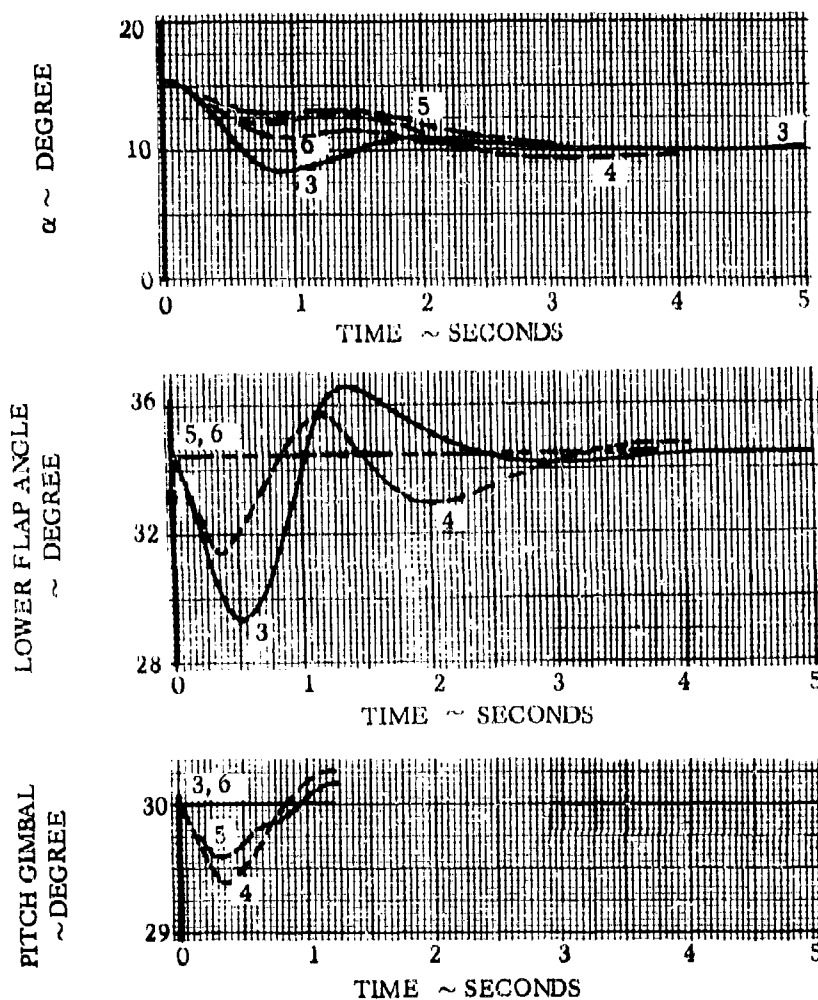


Figure 78 - Lifting Body Dynamic Response - Effect of Aerodynamic, Thrust, Gimbal, and Reaction Pitch Damping

$$\alpha_{\text{TRIM}} = 10^{\circ}$$

$$T = 25,000 \text{ LBS.}$$

$$\delta_{\text{TH}} = 30^{\circ}$$

THRUST MOMENTS INCLUDED  
REACTION CONTROLS  
NO GIMBAL

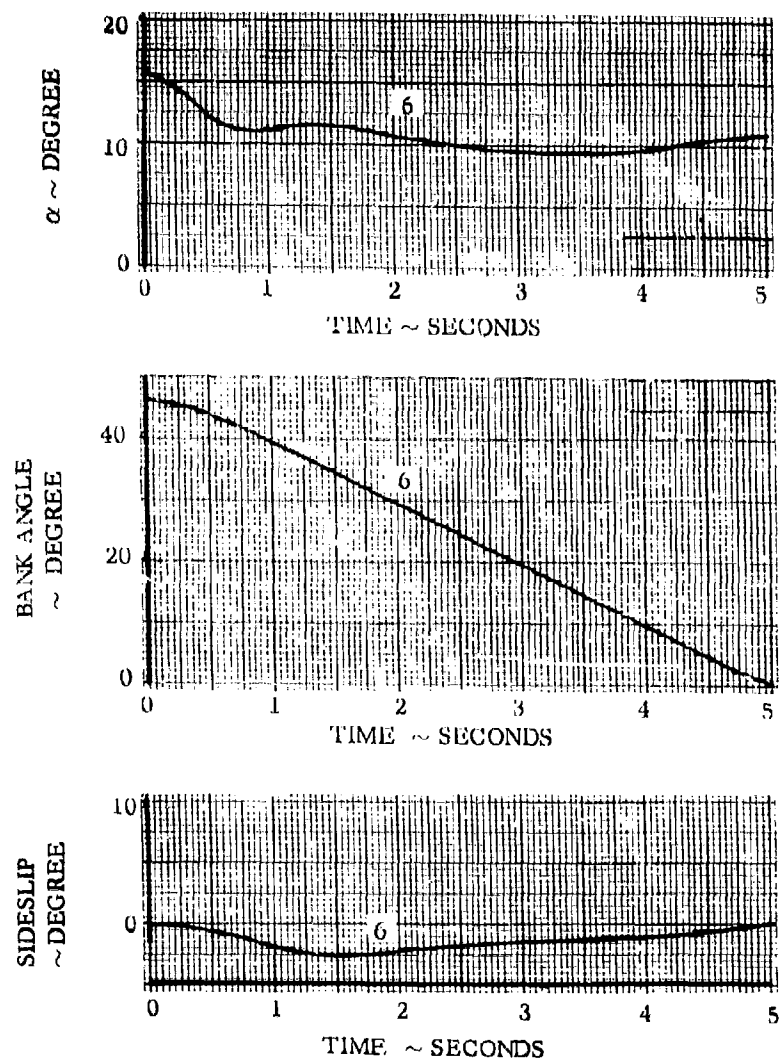


Figure 79 - Lifting Body Motion Characteristics  
Nominal Trajectory

$$\alpha_{\text{TRIM}} = 10^\circ$$

$$T = 25,000 \text{ LBS.}$$

$$\delta_{\text{TH}} = 30^\circ$$

THRUST MOMENTS INCLUDED

REACTION CONTROLS

NO THRUST GIMBAL

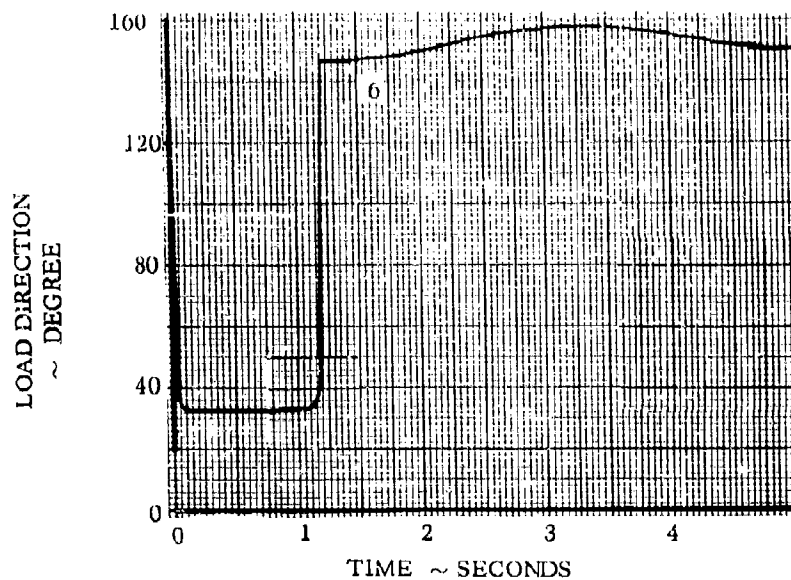
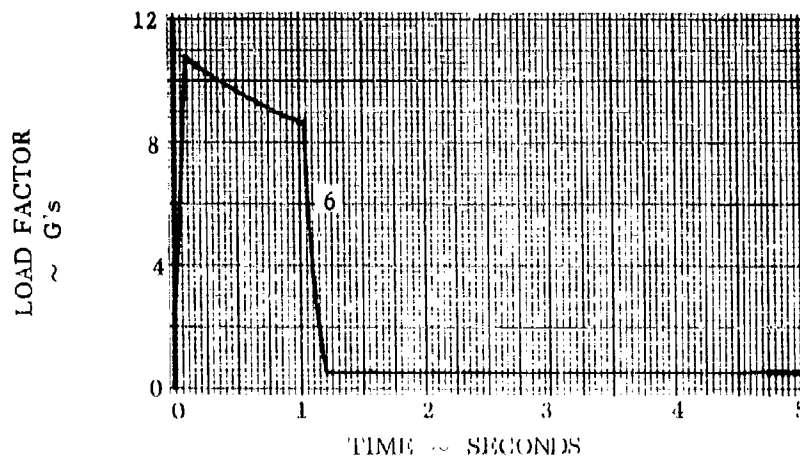


Figure 80 - Lifting Body Load Factor Characteristics Including Thrust Moments - Nominal Trajectory

$\alpha_{\text{TRIM}} = 10^\circ$

$T = 25,000 \text{ LBS.}$

$\delta_{\text{TH}} = 30^\circ$

THRUST MOMENTS INCLUDED

REACTION CONTROLS

NO THRUST GIMBAL

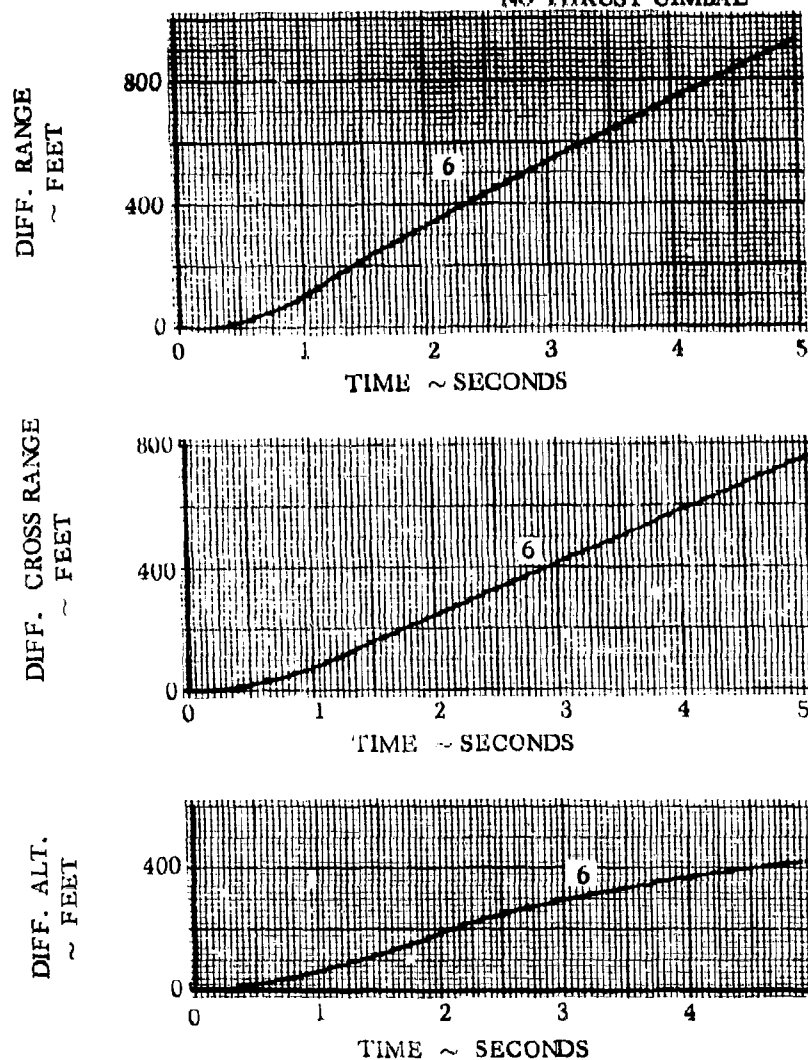


Figure 81 - Lifting Body Separation Characteristics - Nominal Trajectory

$$\alpha_{\text{TRIM}} = 30^\circ$$

$$T = 25,000 \text{ LBS.}$$

$$\delta_{\text{TH}} = 30^\circ$$

THRUST MOMENTS INCLUDED

NO THRUST GIMBAL

7 - 10 DEG/SEC. ROLL RATE

16 - 5 DEG/SEC. ROLL RATE

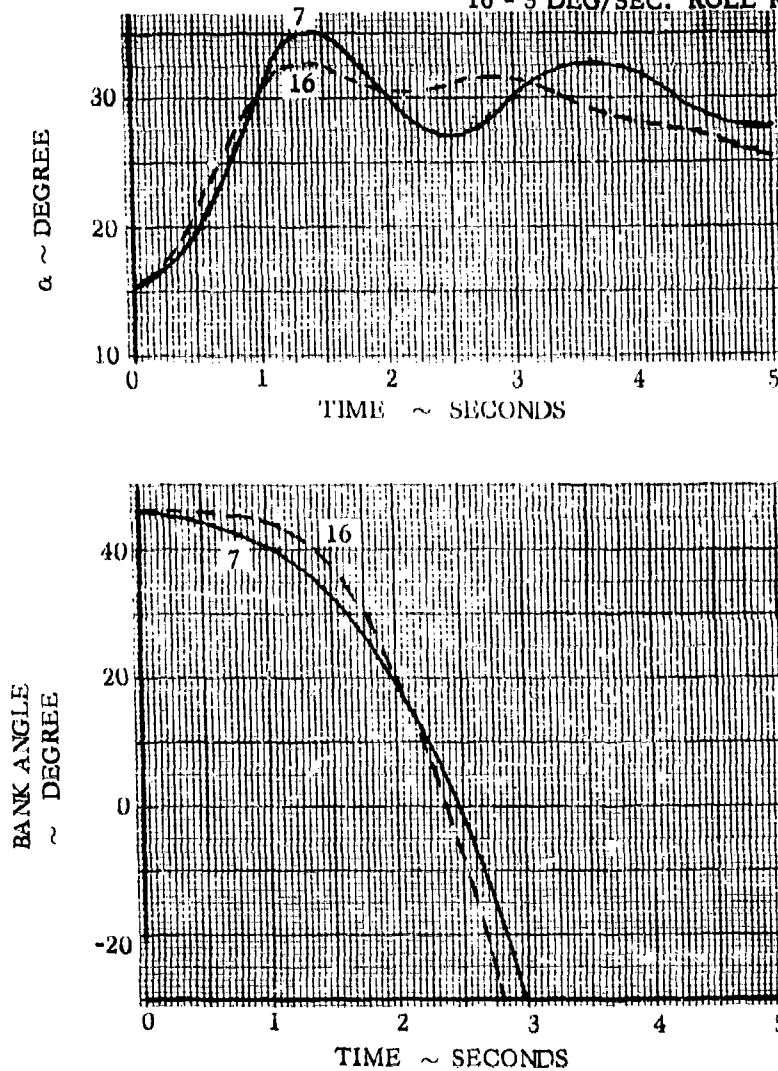


Figure 82 - Lifting Body Dynamic Response - Effects of High Trim Angle of Attack

$\alpha_{TRIM} = 10^\circ$   
 $T = 25,000 \text{ LBS.}$   
 $\delta_{TH} = 30^\circ$

THRUST MOMENTS INCLUDED

8 - INITIAL SIDESLIP =  $3^\circ$   
 9 - INITIAL ROLL =  $5.73 \text{ DEG/SEC.}$   
 10 - INITIAL YAW =  $5.73 \text{ DEG/SEC.}$

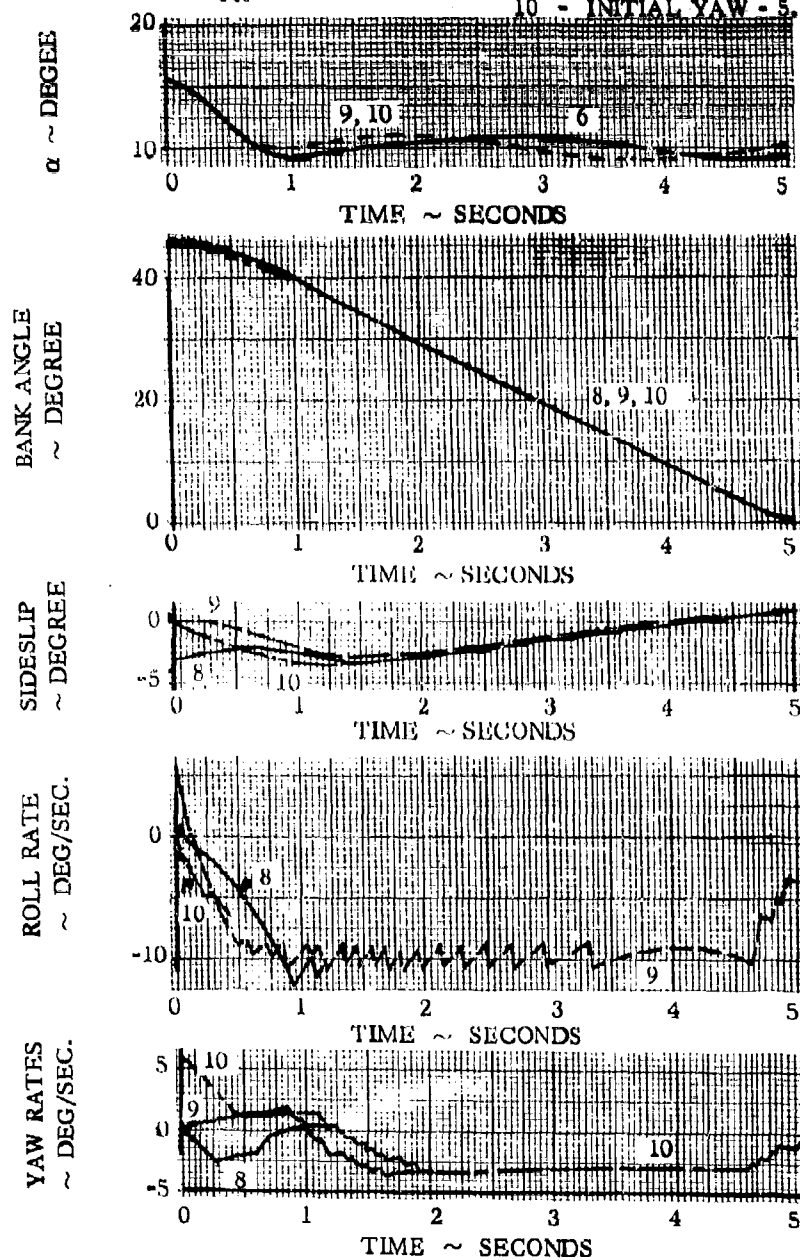


Figure 83 - Lifting Body Dynamic Response - Effect of Lateral - Directional Disturbances

$\alpha_{TRIM} = 10^\circ$   
 $\delta_{TH} = 30^\circ$   
 NO THRUST MOMENTS  
 1 - T = 25,000 LBS.  
 11 - T = 12,000 LBS.

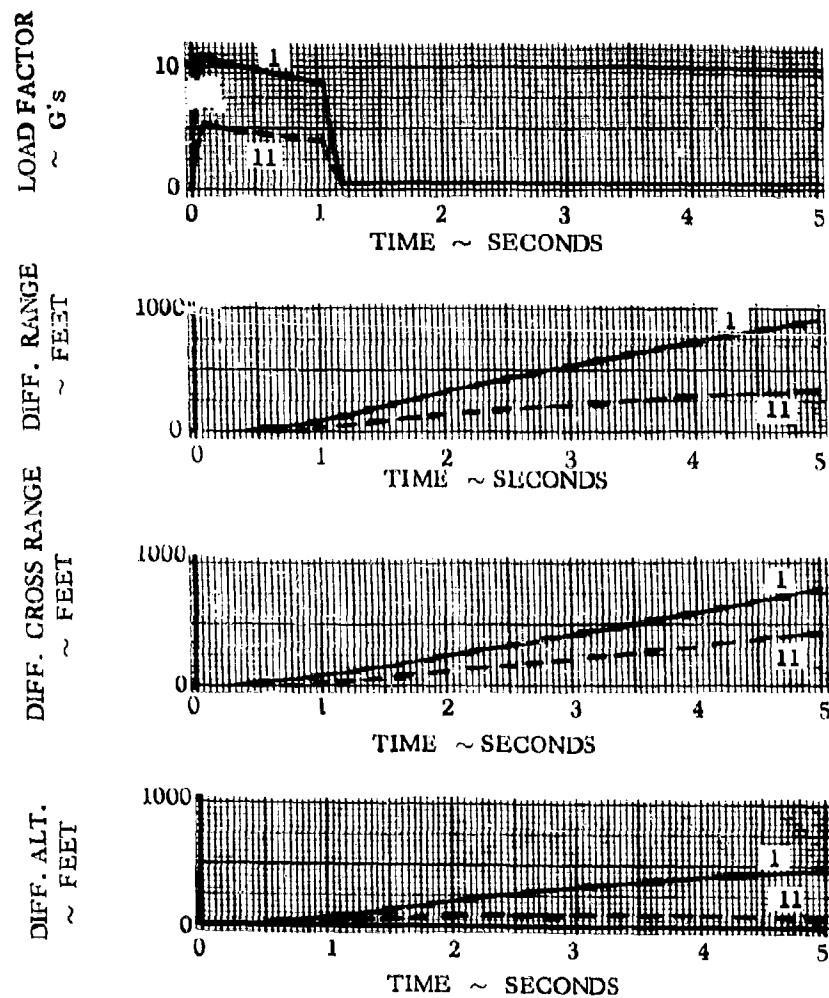


Figure 84 - Lifting Body Load Factor and Separation Characteristics - Effect of Thrust Level

$\alpha_{TRIM} = 10^\circ$   
 $T = 25,000 \text{ LBS}$   
 $\delta_{TH} = 30^\circ$

NO THRUST MOMENTS

13 -  $.04 l_{ref}$  FWD

14 -  $.02 l_{ref}$  AFT

12 - NOMINAL

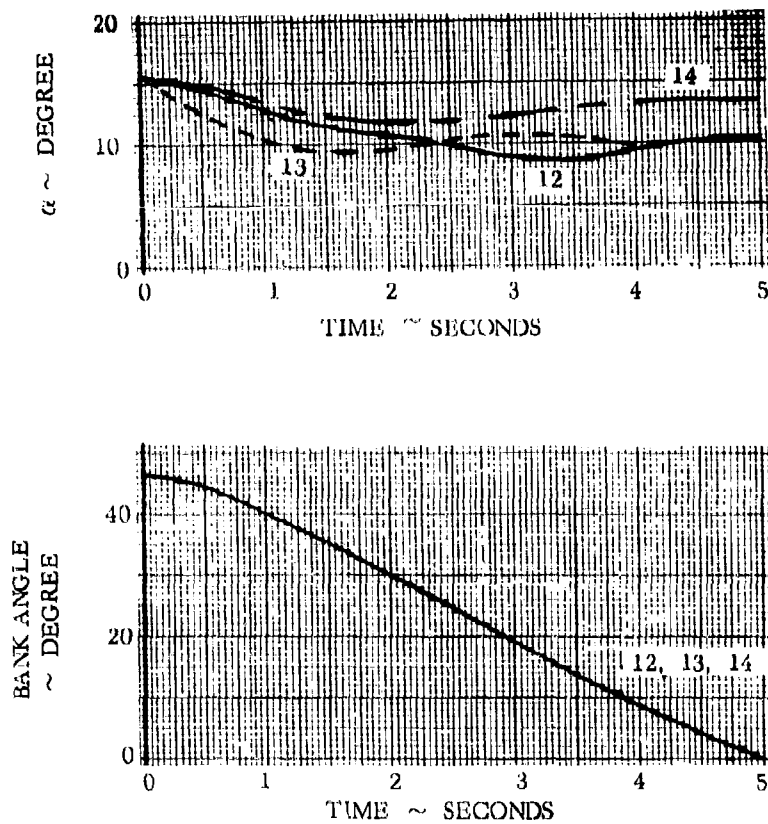


Figure 85 - Lifting Body Dynamic Response - Effect of Longitudinal Center of Gravity



$\alpha_{\text{TRIM}} = 10^\circ$   
 $T = 25,000 \text{ LBS.}$   
 NO THRUST MOMENT  
 $12 - \delta_{\text{TH}} = 30^\circ$   
 $15 - \delta_{\text{TH}} = 40^\circ$

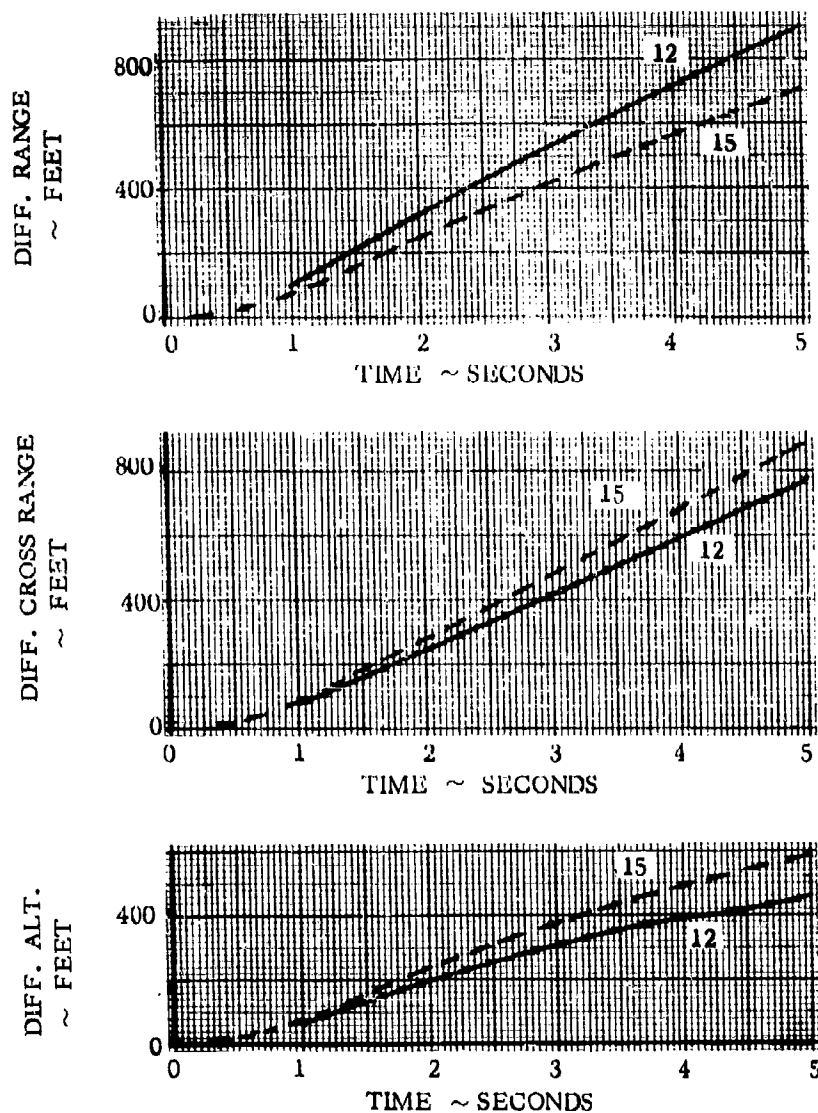


Figure 86 - Lifting Body Separation Characteristics - Effect of Thrust Angle

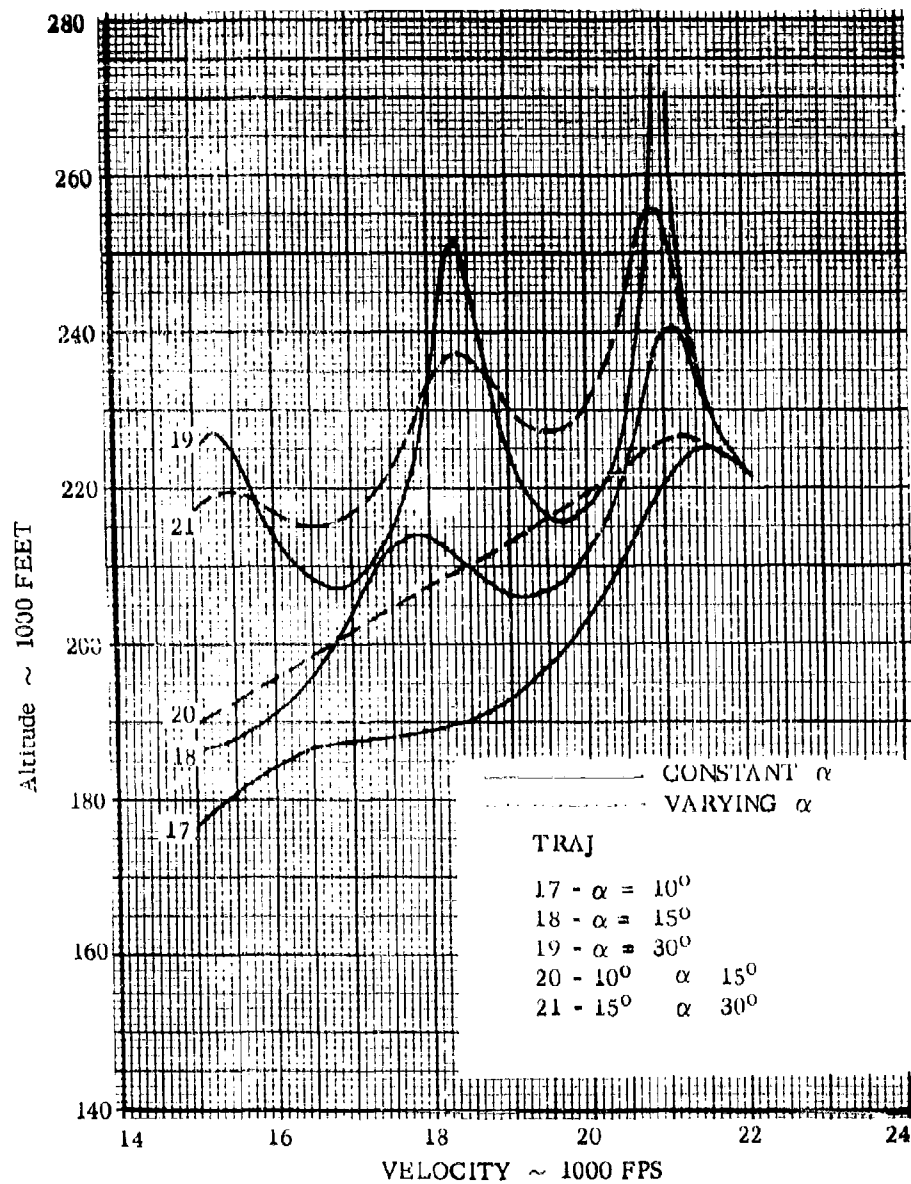


Figure 87 - Lifting Body Trajectories - Effect of Angle of Attack Variation

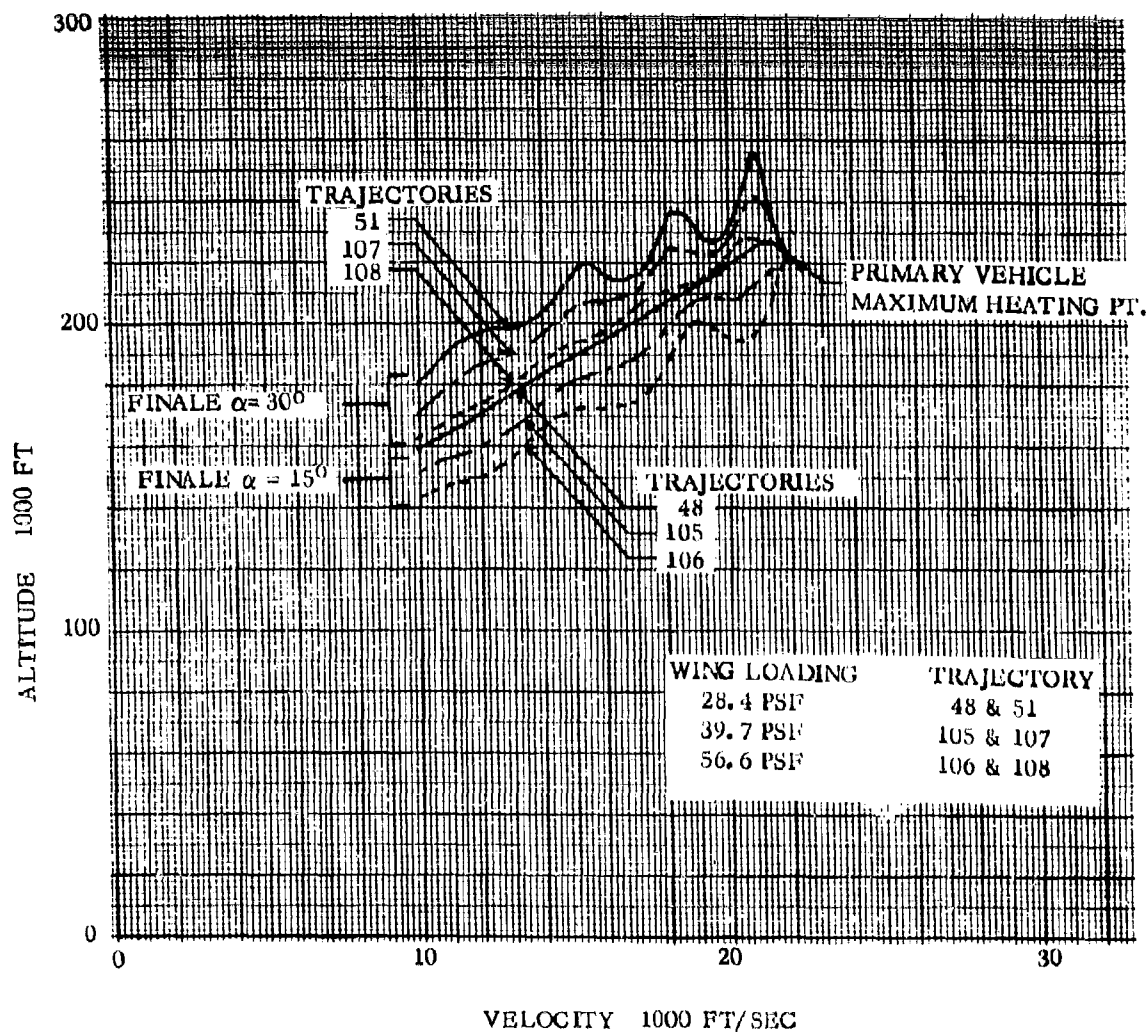


Figure 88 Effect of Wing Loading and Trim Alpha on Lifting Body  
Escape Trajectories

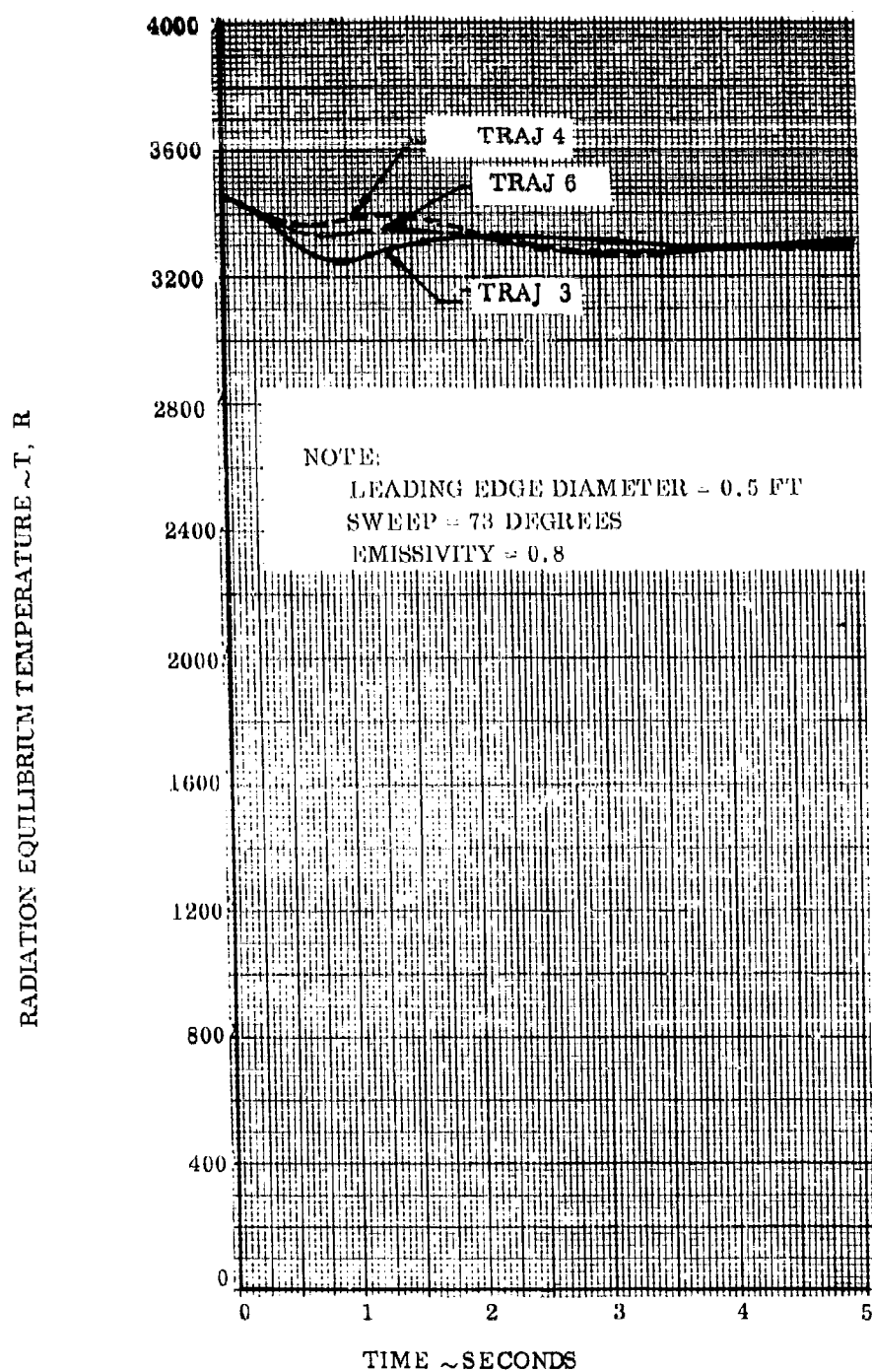


Figure 89. Lifting Body Separation - Leading Edge Temperature Histories - Effect on Aerodynamic Control. Reaction Control and Thrust Gimballing

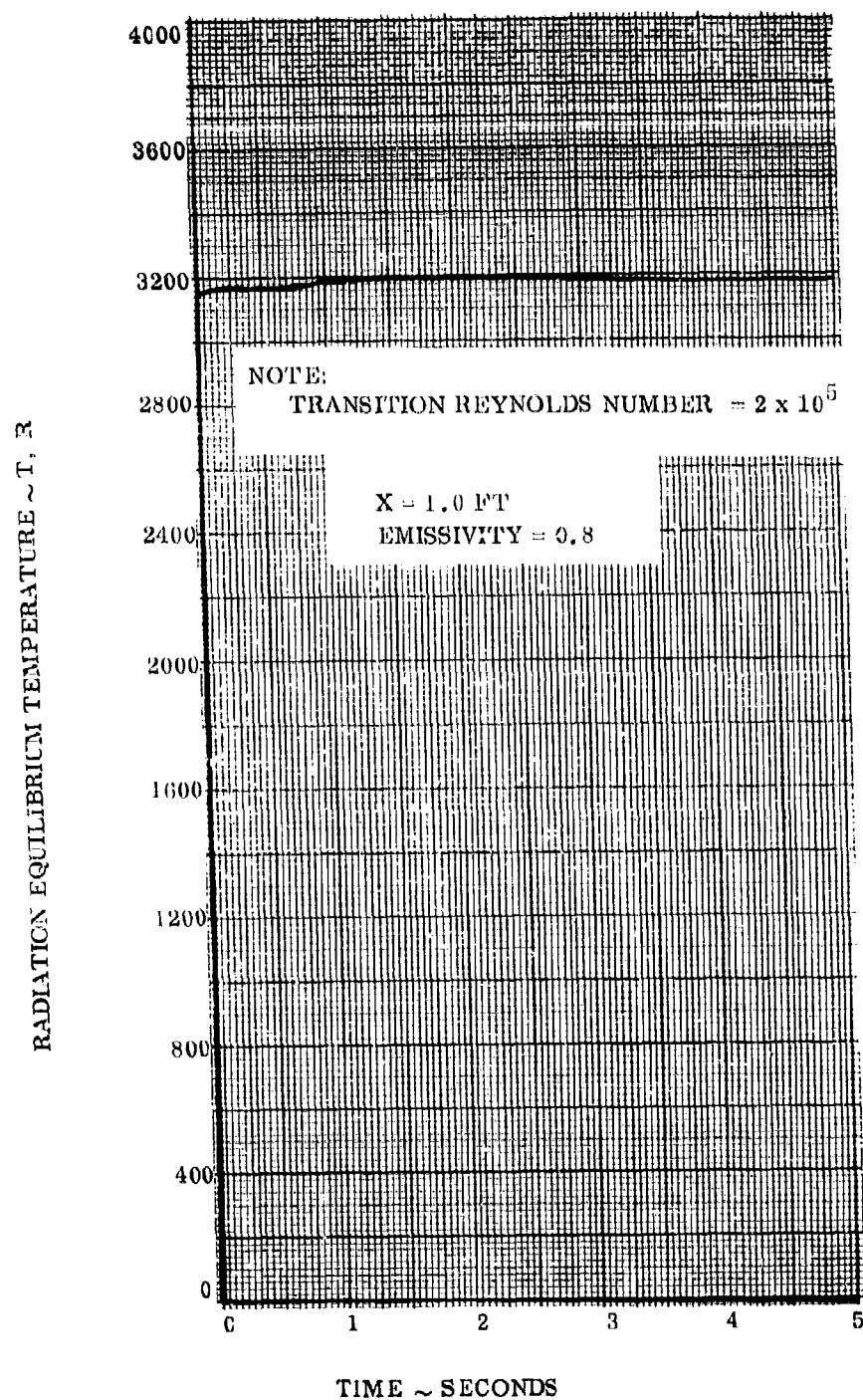


Figure 90. Lifting Body Separation - Lower Flap Temperature History - Trajectory 3

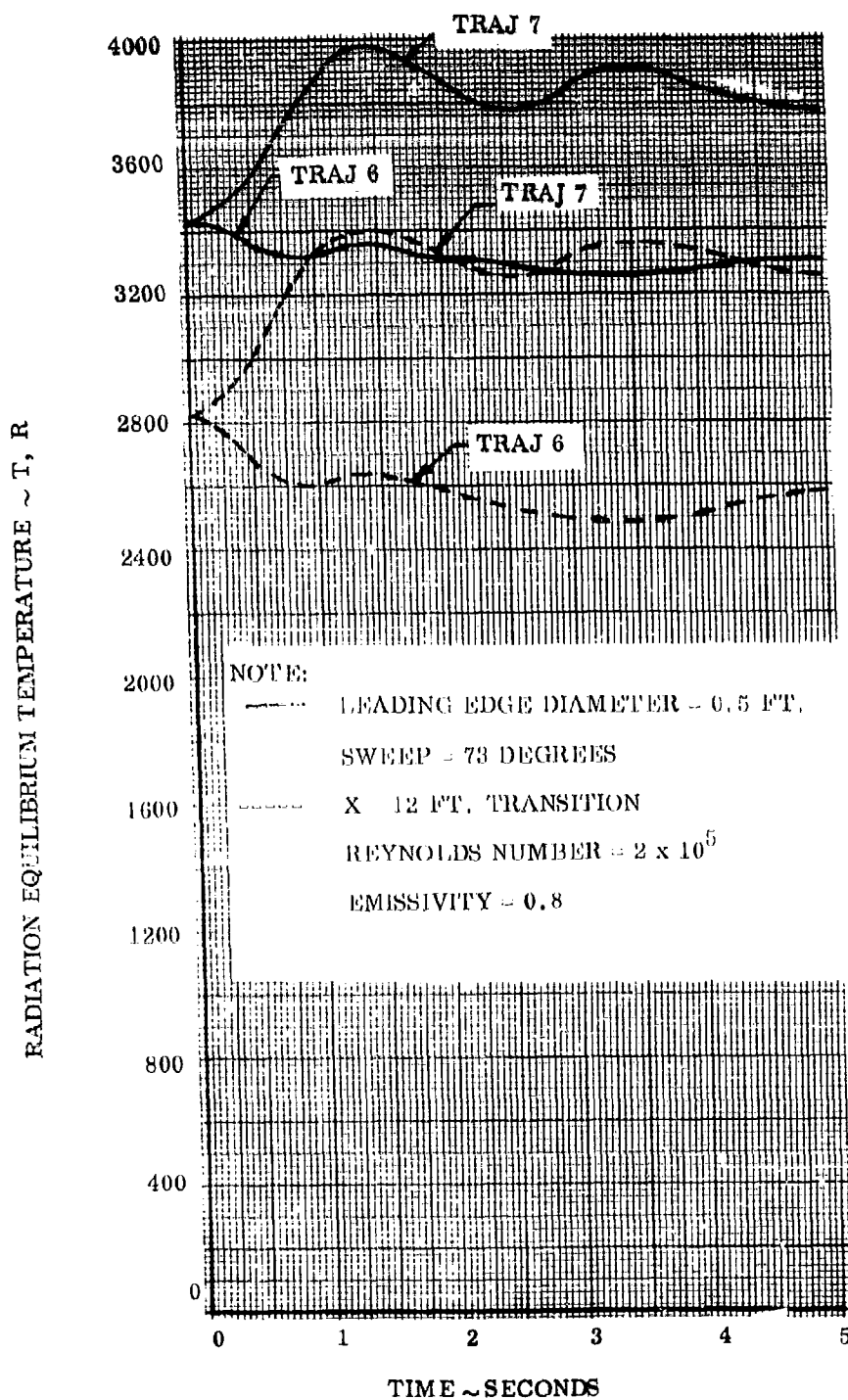


Figure 91. Lifting Body Separation - Leading Edge and Lower Surface Temperature Histories - Effect of Trim Angle

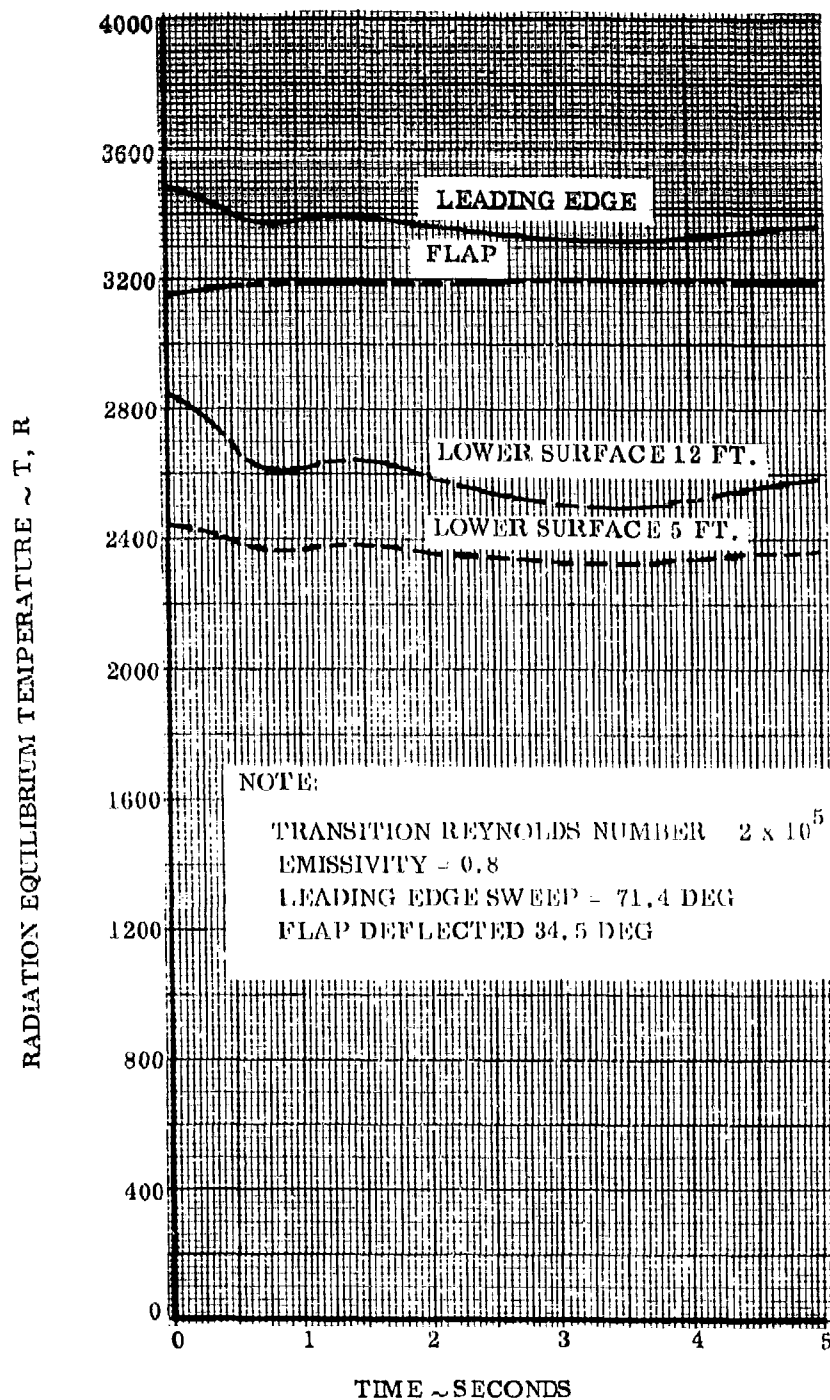


Figure 92. - Lifting Body Separation - Temperature Histories - Nominal Trajectory 6

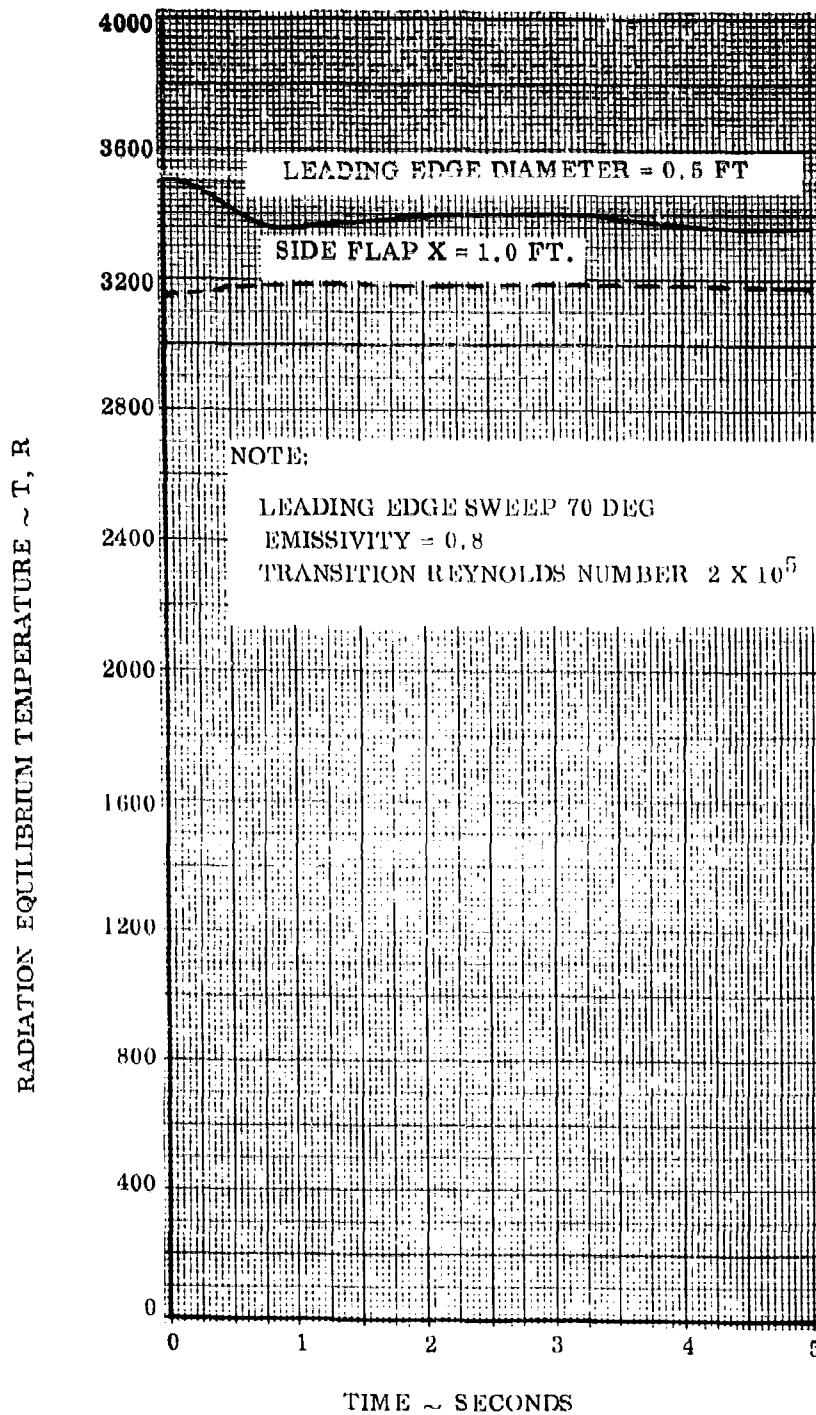


Figure 93. Lifting Body Separation - Leading Edge and Side Edge Flap Temperature Histories - Effect of Initial Sideslip Angle, Trajectory 8



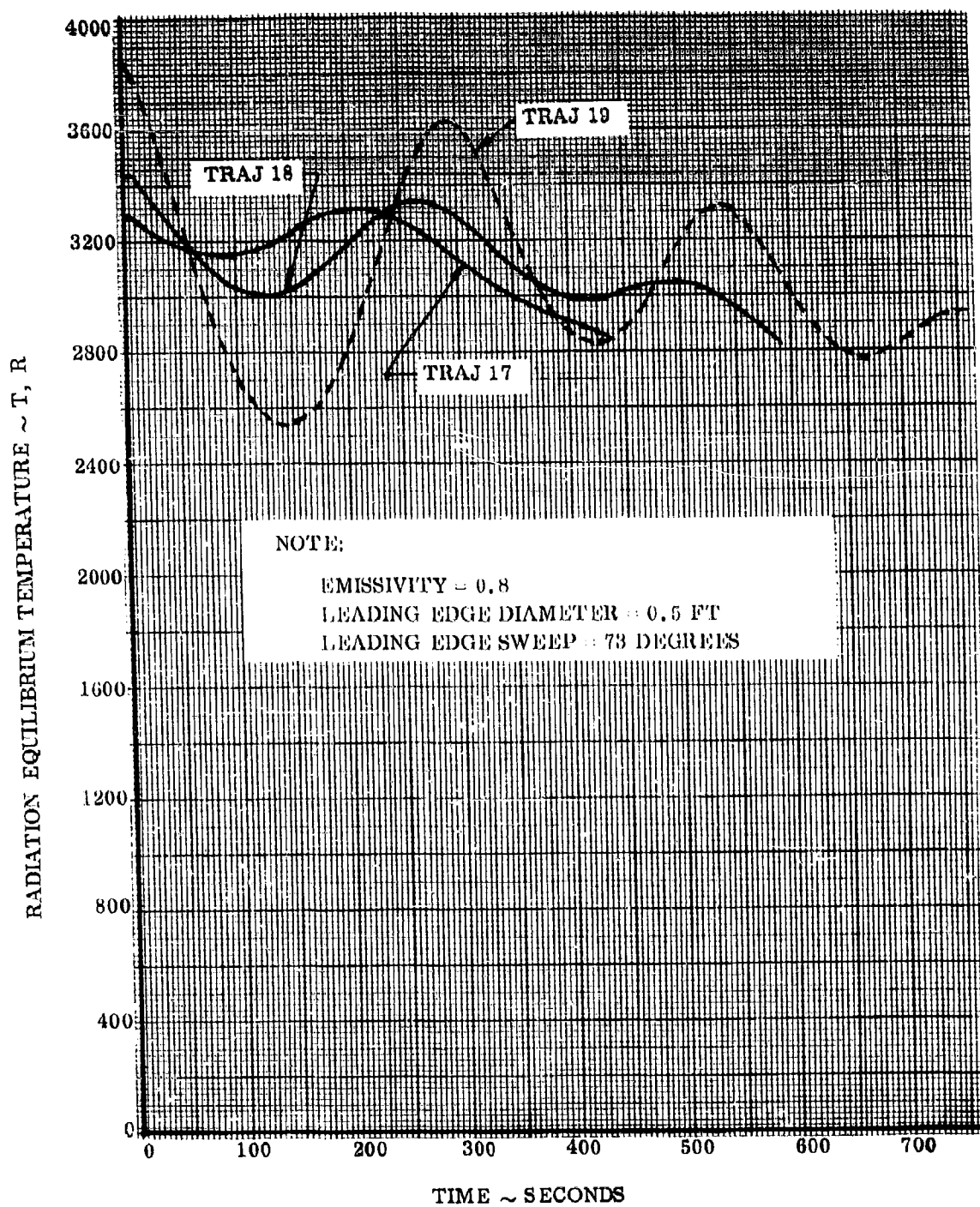


Figure 94. Lifting Body Leading Edge Temperature Histories - Effect of Fixed Angle of Attack

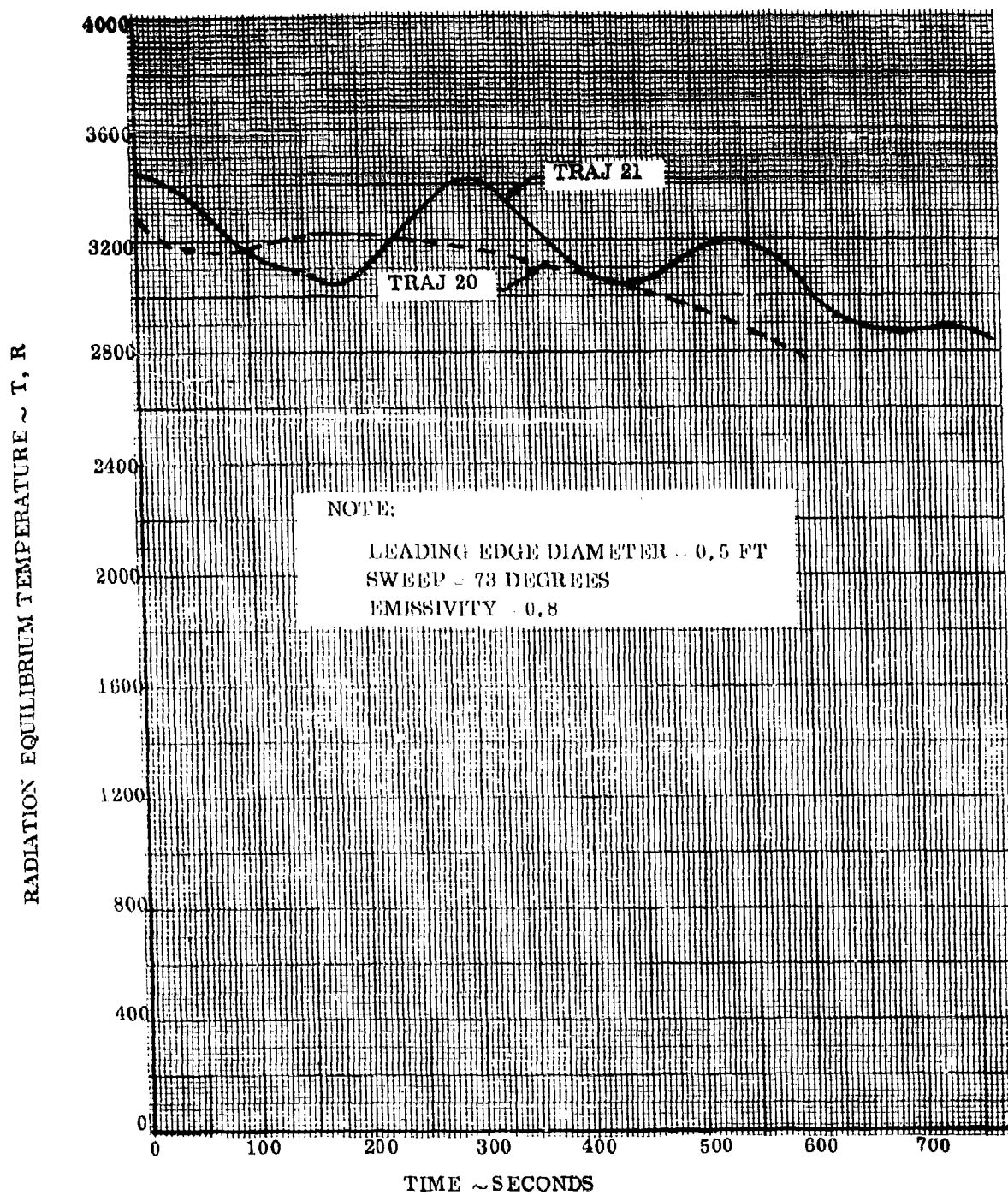


Figure 95. Lifting Body Leading Edge Temperature Histories - Effect of Varying Angle of Attack

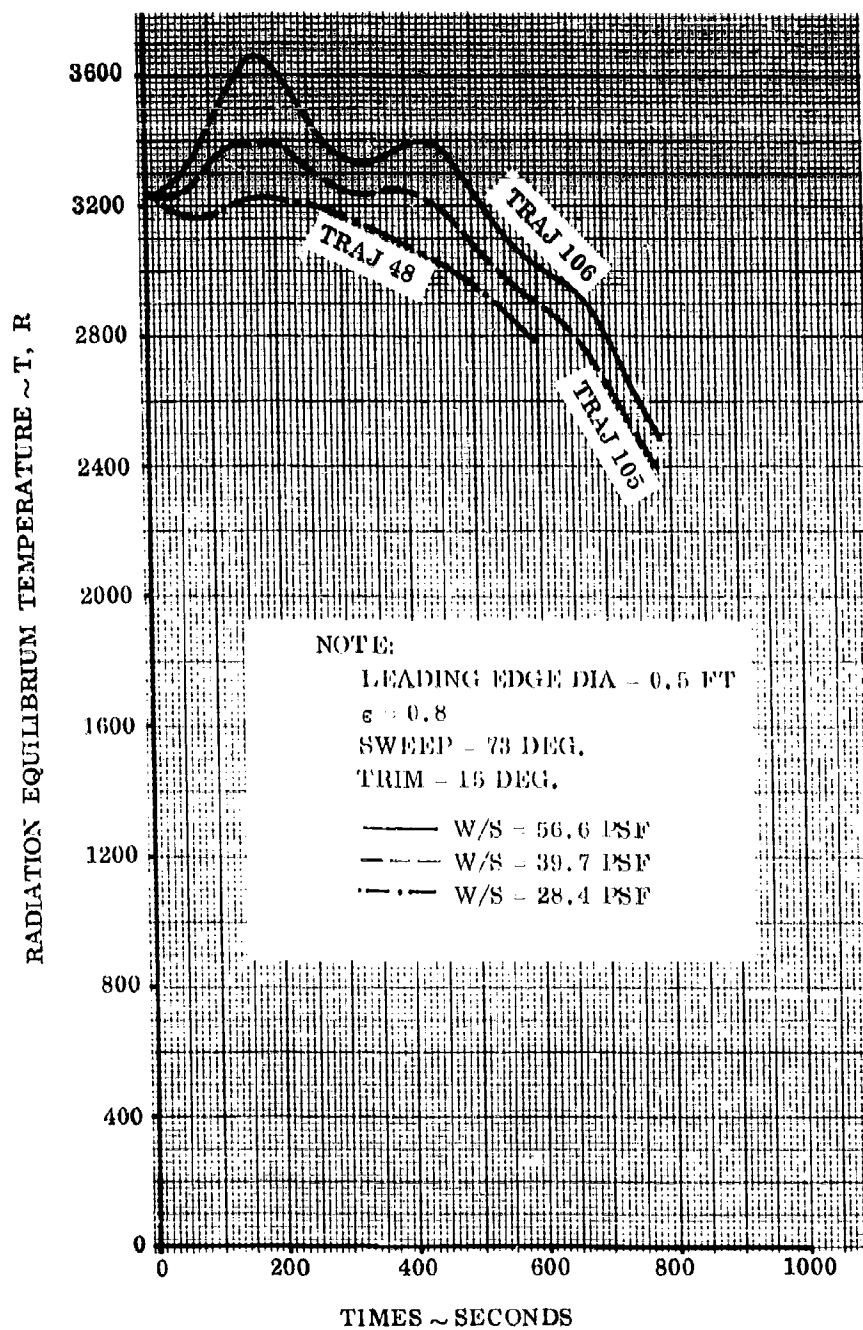


Figure 96 - Lifting Body - Leading Edge Heating - Effect of Wing Loading

Final Trim Alpha = 15°

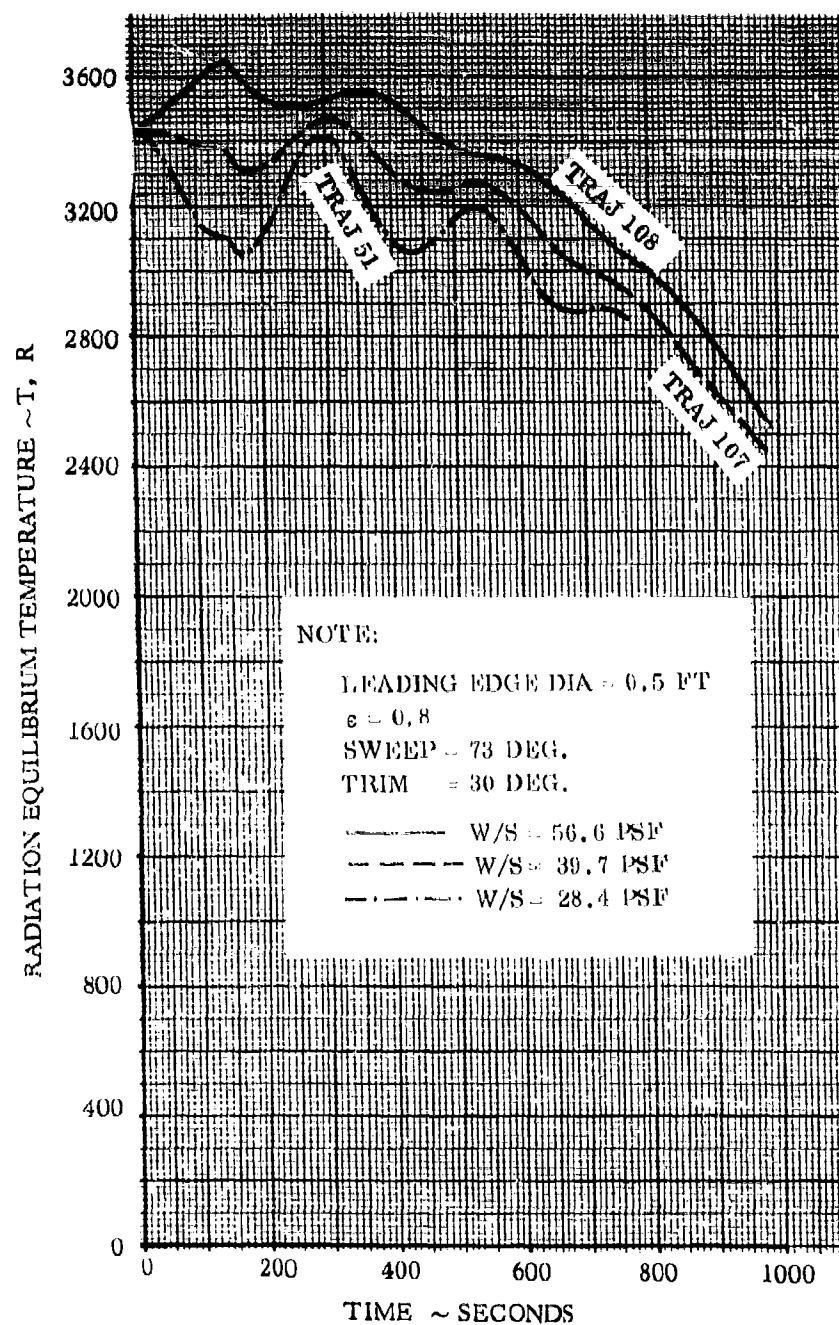


Figure 97 - Lifting Body - Leading Edge Heating - Effect of Wing Loading - Final Trim Alpha = 30°

TABLE XI  
SUMMARY OF INITIAL CONDITIONS FOR LIFTING BODY ORBIT TRAJECTORY RUNS

No.	$\theta_L$	$\theta_C$	$\theta_i$	Reaction	T	$\delta_{TH}$	THM	$\delta_{TH/q}$
1	0	0	-1146	IN	25,000	40	OUT	0
2	↓		0		↓			
3	10		↓		12,000	↓		
4	20		1146		6,000	30	IN	↓
5	10				25,000	40		↓
6					6,000			
7					↓			
8					25,000			
9					6,000			
10					↓			
11					25,000			
12								

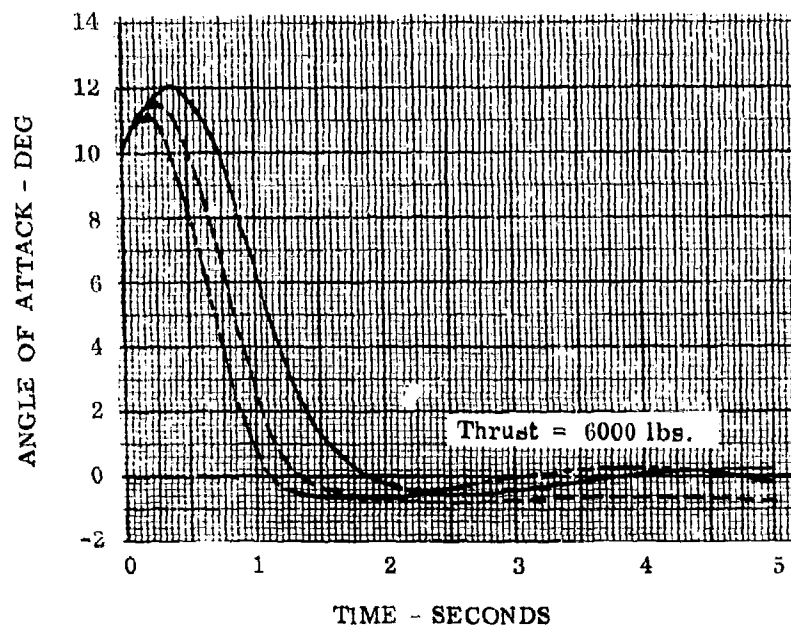
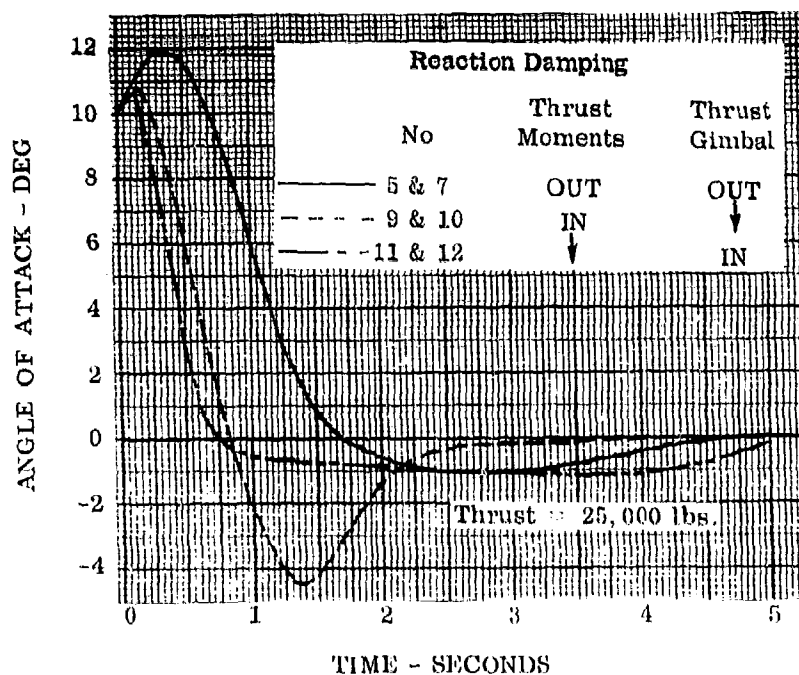


Figure 98 - Lifting Body - Orbit Escape Trajectory Characteristics

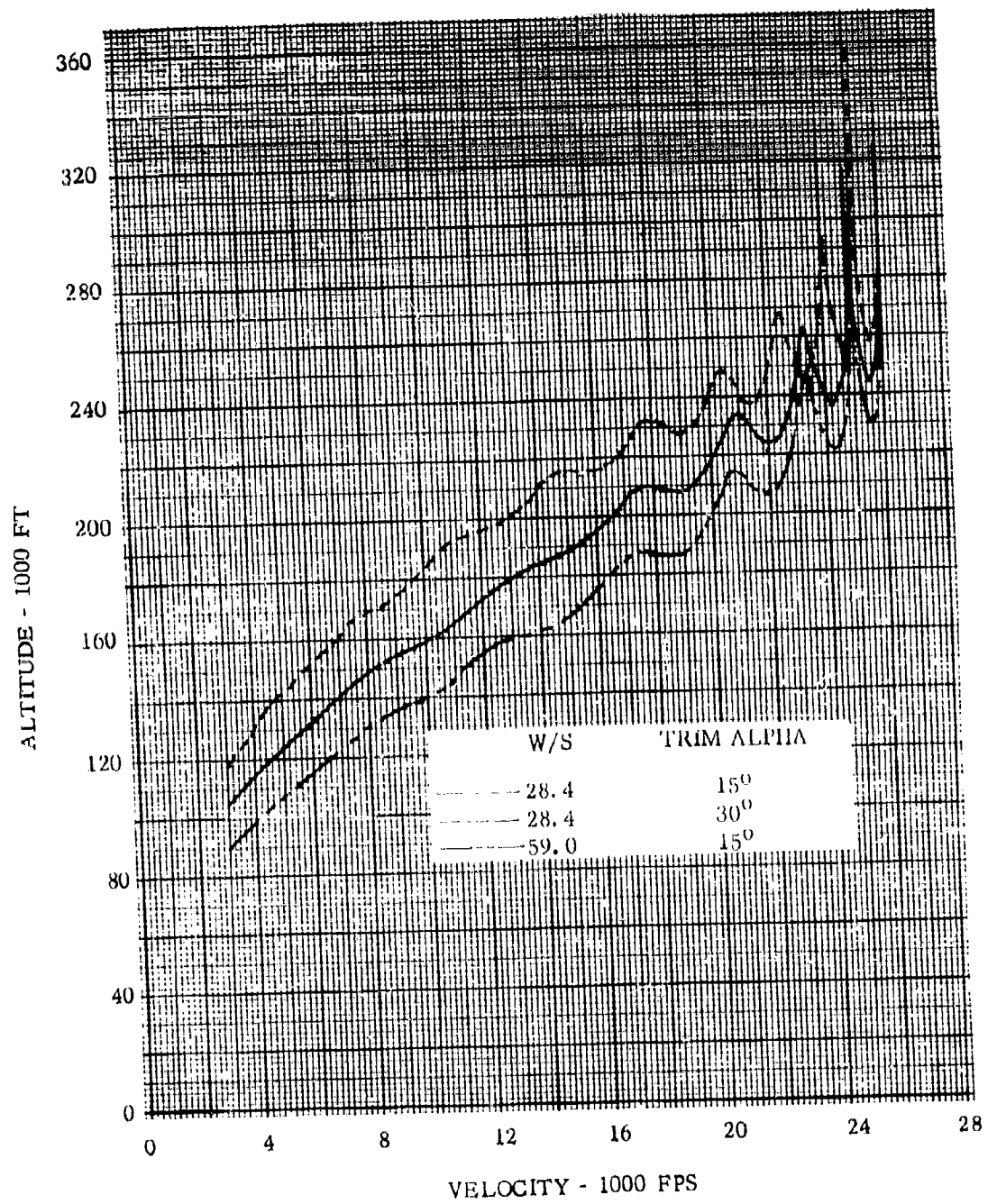


Figure 99 - Lifting Body Capsule - Orbit Re-entry Trajectory

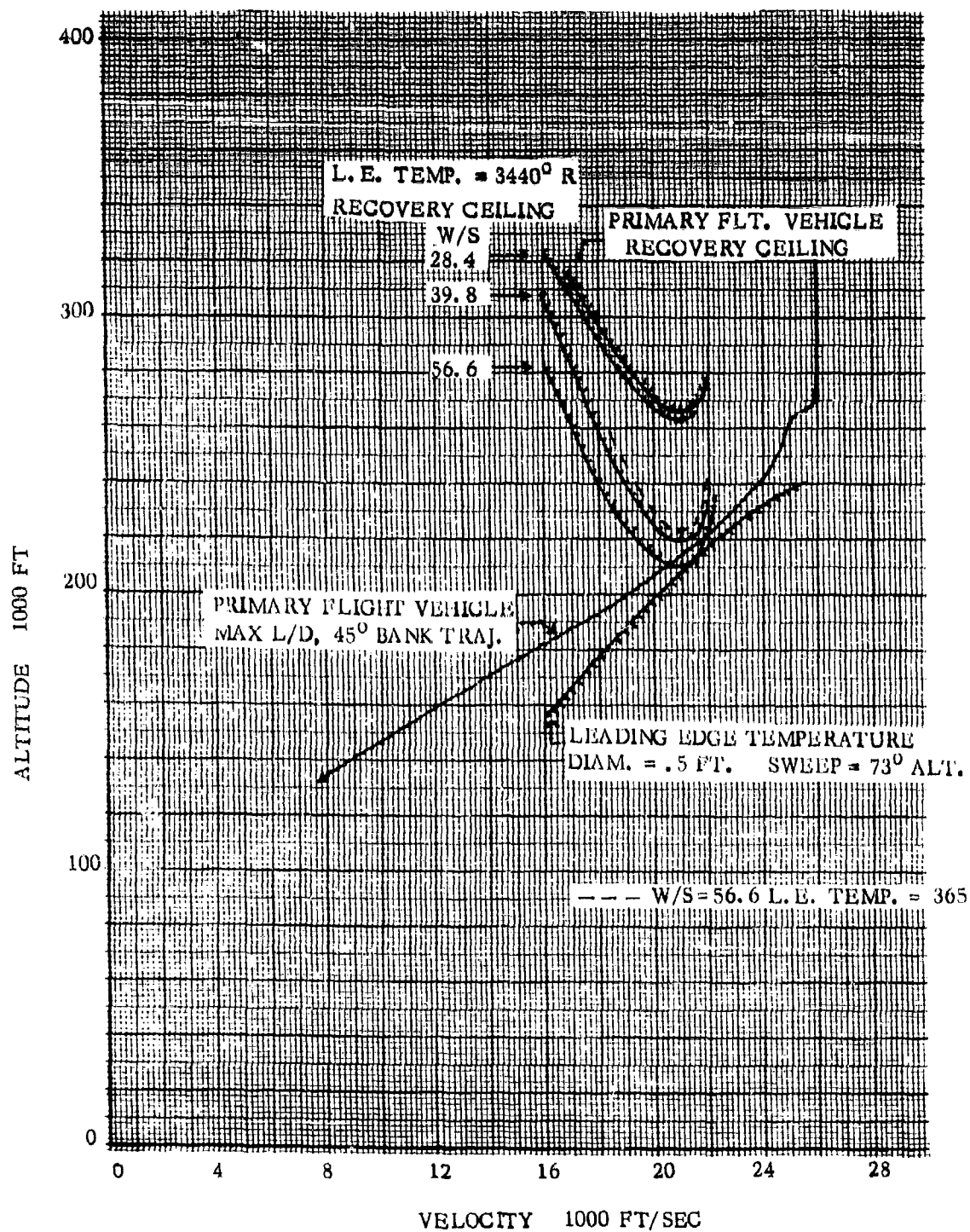


Figure 100 - Lifting Body - Recovery Ceiling



TABLE XII  
SUMMARY OF CONDITIONS FOR LIFTING BODY SUBSONIC TRAJECTORY RUNS

No.	$\gamma$	$\delta_u$	$\delta_L$	$\alpha_i$	$\theta_i$	$\epsilon L/q$	Reaction	T	$\delta_{TH}$	THM	$\delta_{TH}/q$
137	-2	-20	20	10	0	.5	OUT	25,000	40	OUT	0
138					-11.44		IN		30	IN	.1
139						0	OUT		40	OUT	0
140						.5					
141							IN			IN	
142						0	OUT			OUT	
143						.5					
144							IN		30	IN	.1
145						0	OUT		40	OUT	0
146	90			0		.5					
147							IN			IN	
148						0	OUT			OUT	
149						.5					
150							IN			IN	
151						0	OUT			OUT	
152						.5					
153							IN			IN	
154		-30	0				OUT			OUT	
155	-2										
156			34.5			.5					
157	90										

Altitude = 100 FT

V = 200 FPS

Landing -  $\gamma = -2^\circ$ 

Altitude = 100 FT

V = 0

On-the-Pad -  $\gamma = 90^\circ$

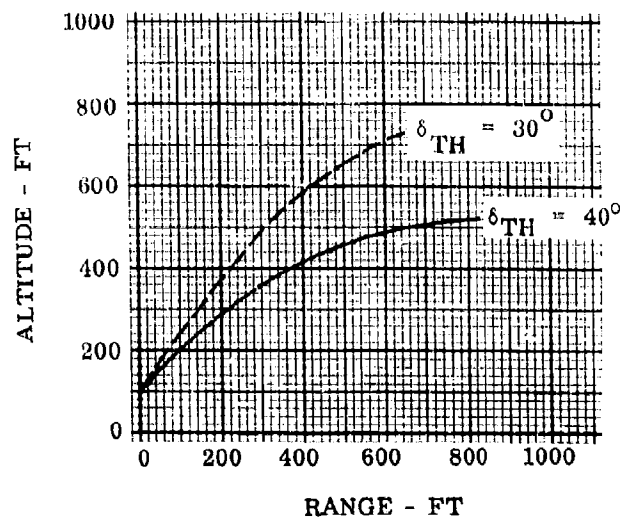
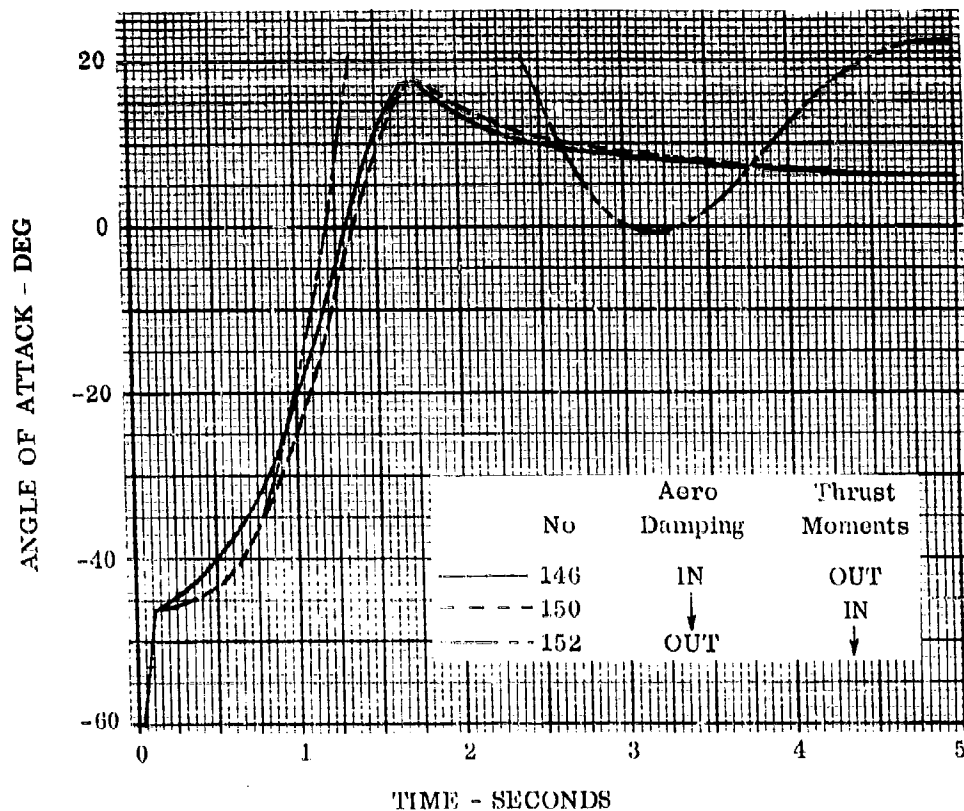


Figure 101- Lifting Body - On-the-Pad Escape Trajectory Characteristics

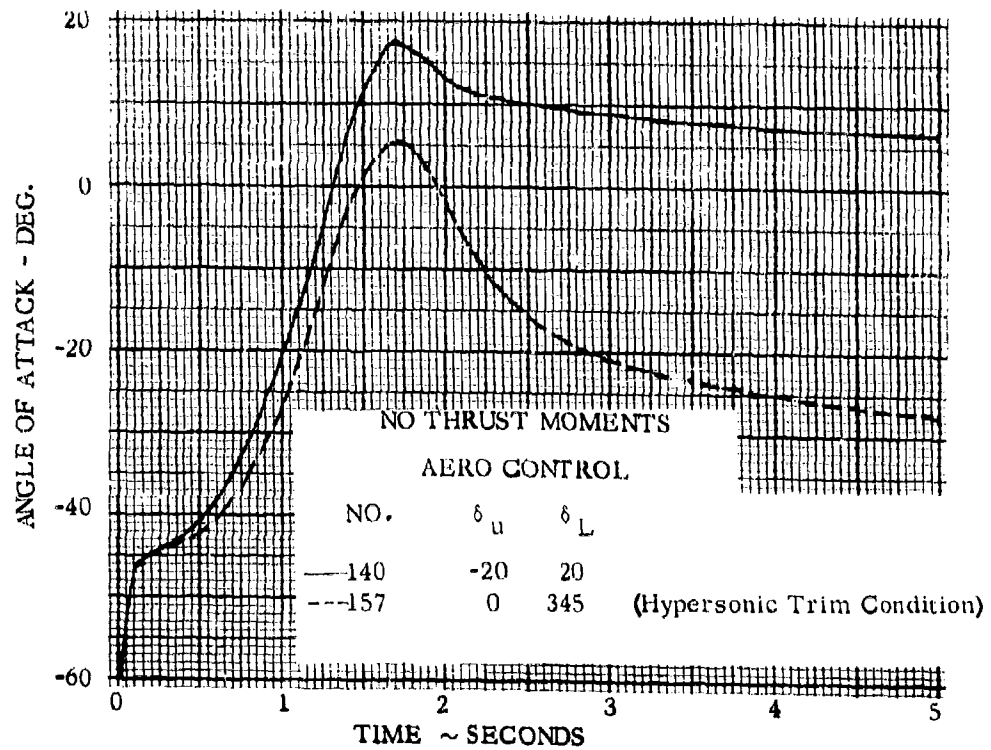
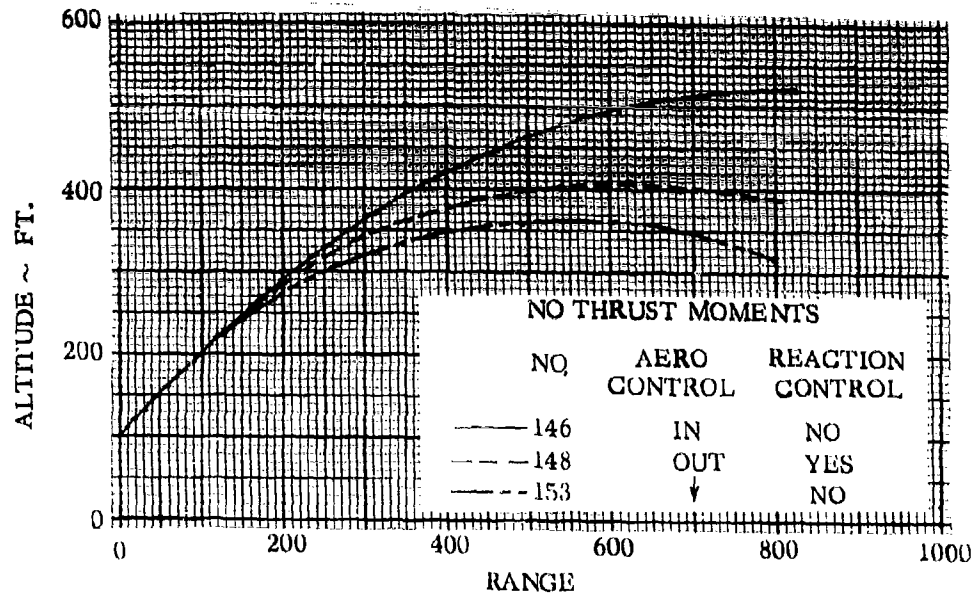


Figure 102 - Lifting Body - On-The Pad Escape Trajectory Characteristics Effect of Control Type and Trim Angle

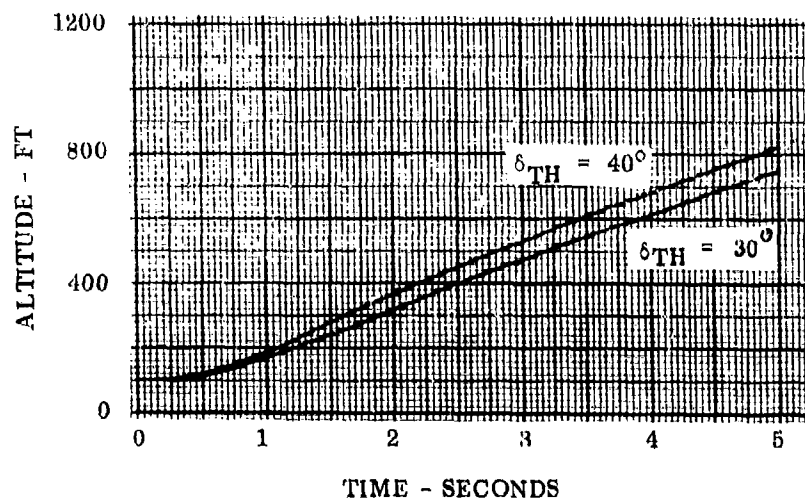
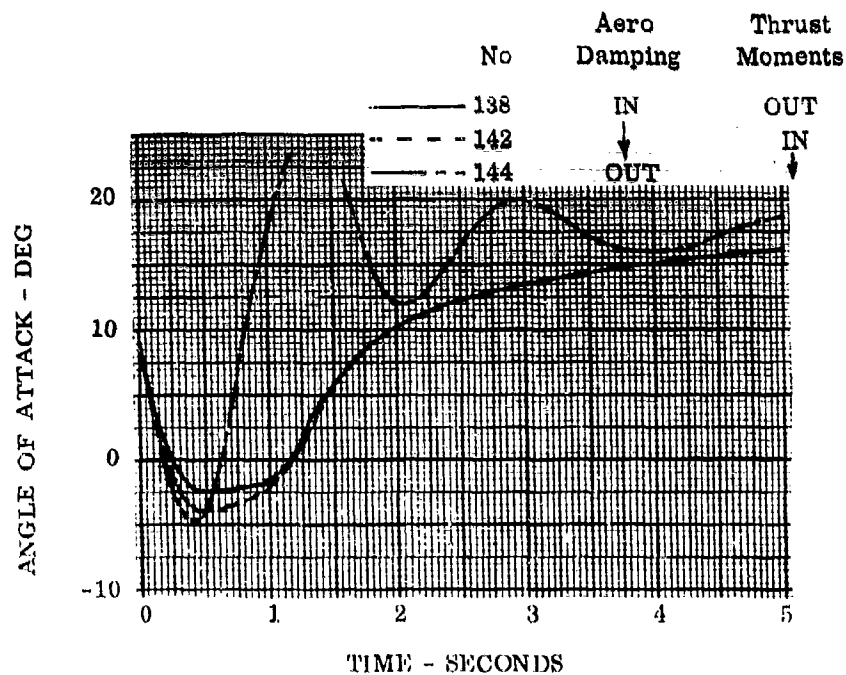


Figure 103 -Lifting Body - Landing Approach Escape Trajectory Characteristics

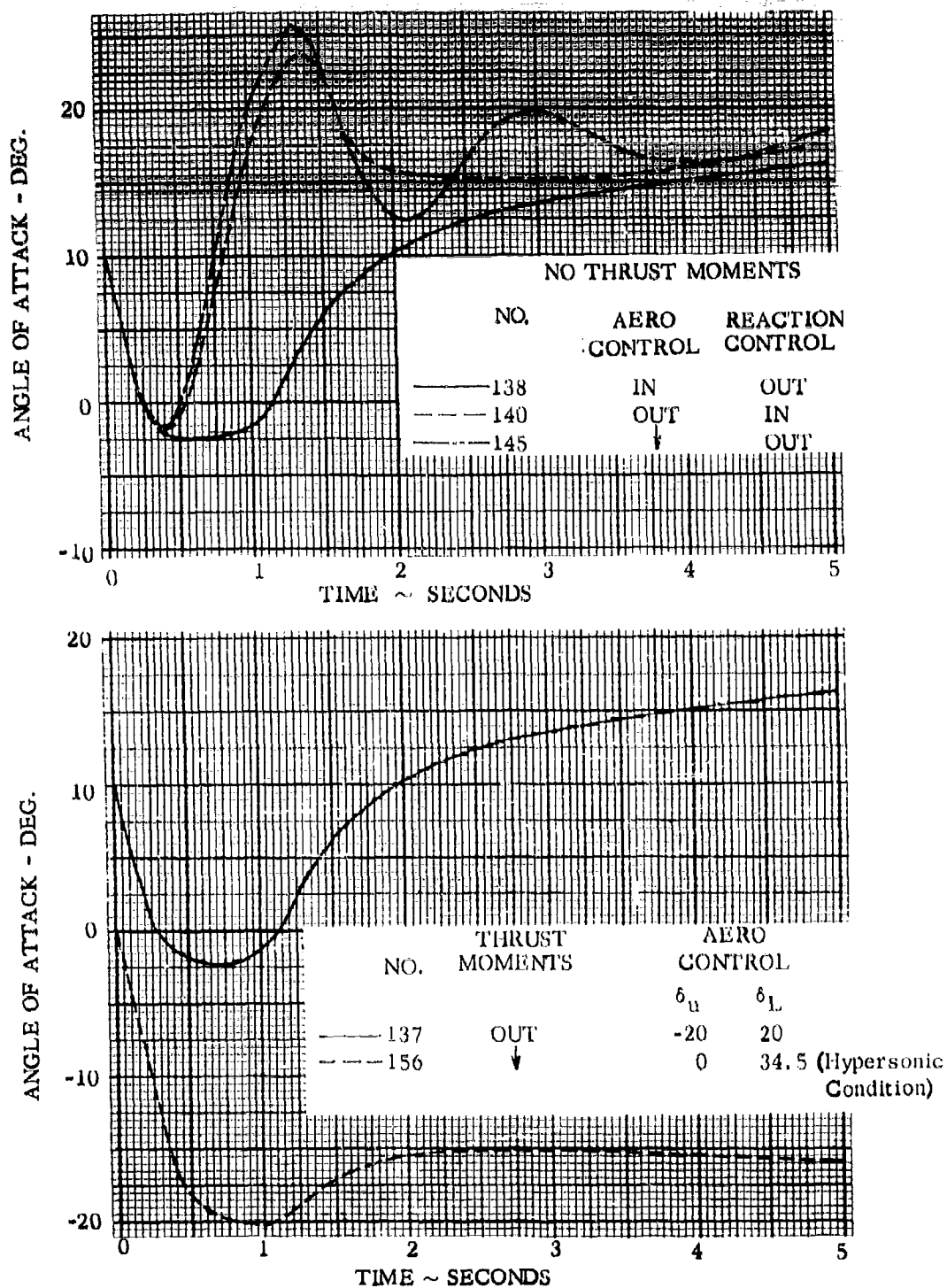


Figure 104 - Lifting Body - Landing Approach Escape Trajectory Effect of Control Type and Trim Angle

TABLE XIII  
SUMMARY OF INITIAL CONDITIONS FOR LIFTING BODY SUPERSONIC TRAJECTORY RUNS

No.	$\delta u$	$\delta L$	$\alpha L$	$\theta_i$	$\delta u/q$	Reaction	Thrust	$\delta TH$	THM	$\delta TH/q$
74	-30	0	-3	0	.5	OUT	25,000	40	OUT	0
75			0	0						
76			-3	-11.46				30	IN	.1
77					0	IN		40	OUT	0
78										
79										
80						OUT				
81					.5					
82					0	IN				
83										
84		34.5								
85	0	0		50	.5	OUT				
201	-30	0		100	0	IN				
202				-50						
203				-100						
204										

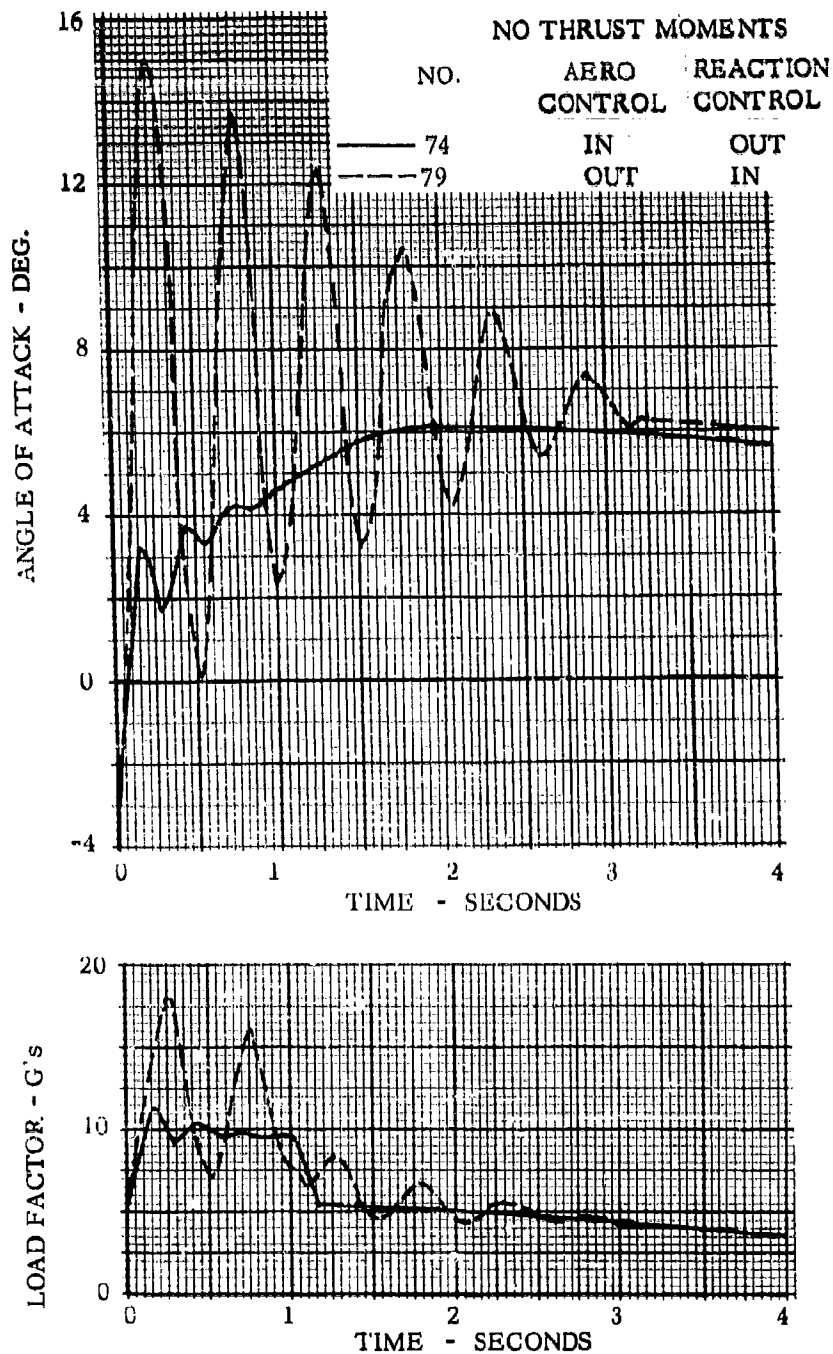


Figure 105- Lifting Body - Maximum Dynamic Pressure Escape Trajectory Characteristics - Effect of Control Type

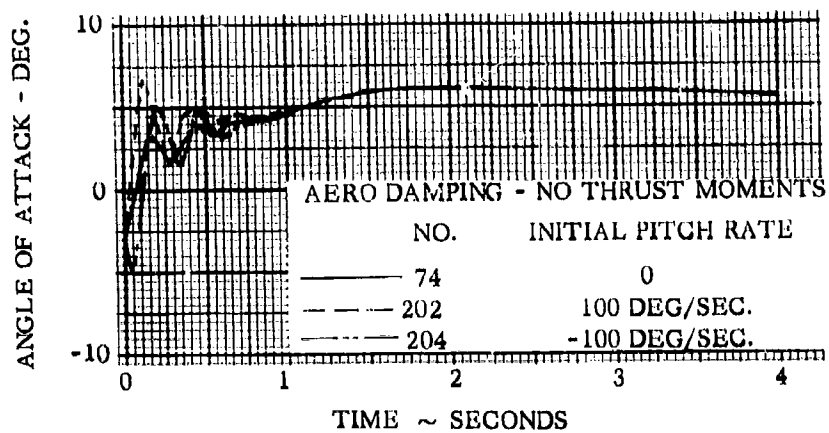
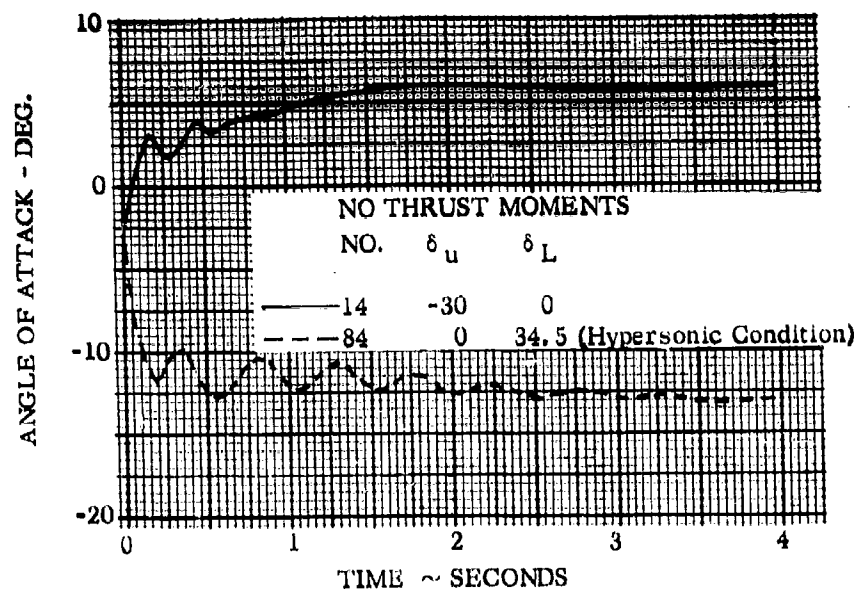


Figure 106 -Lifting Body - Maximum Dynamic Pressure Escape Trajectory Characteristics - Effect of Trim Angle and Initial Pitch Rate



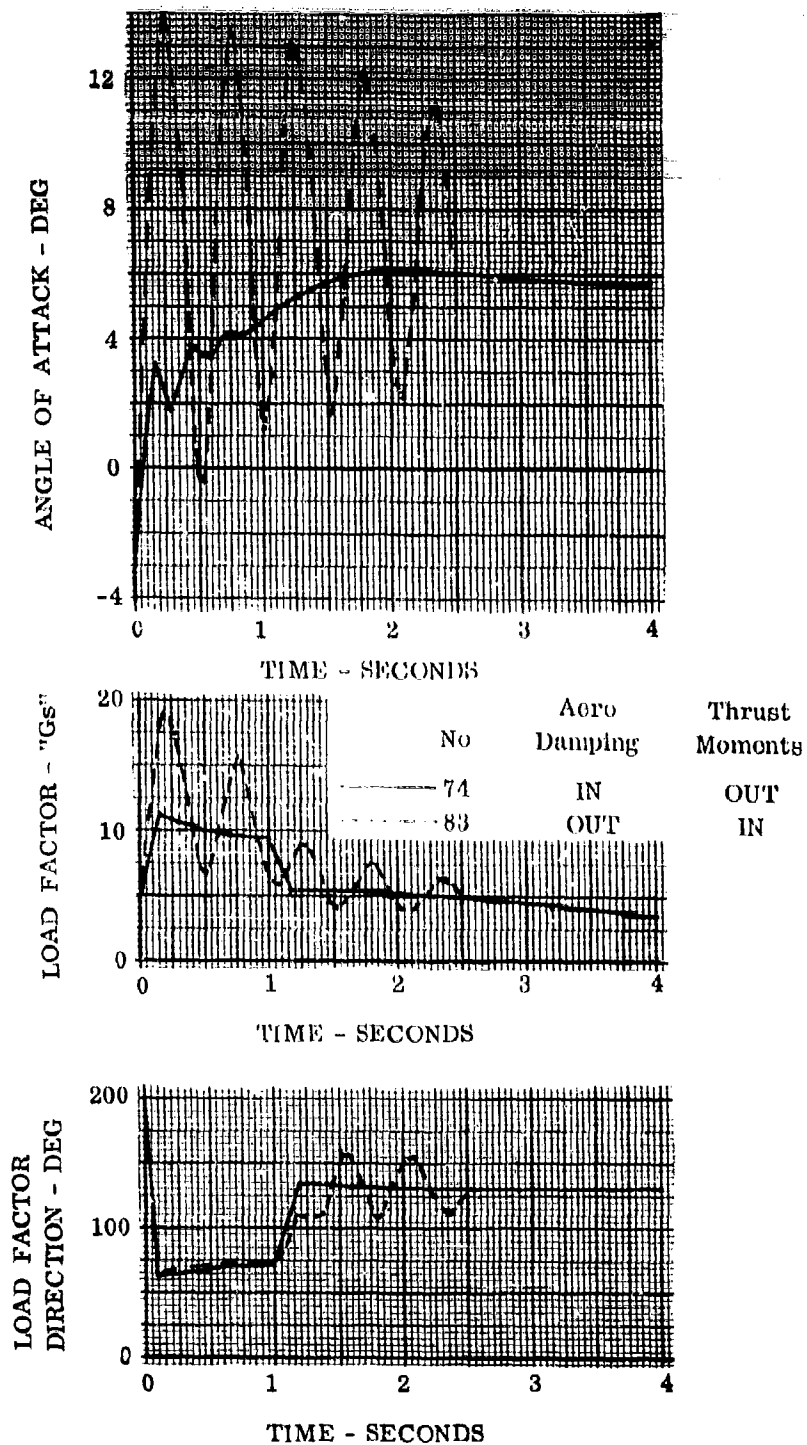


Figure 107 -Lifting Body - Maximum Dynamic Pressure  
Escape Trajectory Characteristics

### 6.3 POD CAPSULE

**6.3.1 RE-ENTRY ESCAPE.** The re-entry escape discussion is divided into separation dynamics (first 10 seconds) and complete trajectories.

**6.3.1.1 Separation Dynamics.** The basic technique selected was that used for the lifting body and described above. A roll to wings level was executed using a commanded roll rate of 15 deg/sec. To prevent pitch roll coupling it was necessary to provide pitch and yaw damping. As with the lifting body, it was necessary to provide an azimuth command to keep small sideslip angles during the roll maneuver. The commanded roll was initiated at the time the lower flaps were deflected.

Since the pod capsule is located in the primary vehicle it is necessary to delay the opening of the lower flaps until the capsule has moved out of the primary vehicle. Investigating the separation distance characteristics of several of the initial runs, which were made with the lower flaps undeflected, indicated that the capsule had sufficient clearance at the point where the angle of attack reached 17 degrees. The parametric investigation described below used 17 degrees as the angle of attack for lower flap deflection. The use of angle of attack as the parameter the  $\alpha$  switch parameter in the autopilot subroutine described in Section 4.0 could be used directly. In actual design a time delay would most likely be used rather than an angle of attack.

In order to account for aerodynamic interference effects, an initial pitch rate of  $-0.1$  rad/sec was used for all the runs as discussed in Section 3.4.

Using the basic technique characteristics listed above the separation dynamics were investigated as a function of the following parameter variations.

- a) Aerodynamic control
- b) Reaction control
- c) Thrust moments
- d) Thrust gimbaling
- e) Initial sideslip
- f) Initial yaw rate
- g) Initial roll rate
- h) Thrust magnitude
- i) Thrust direction
- j) Trim angle of attack.

The parameters for the selected series of runs are shown in Table XIV. The results are summarized in Figures 108 through 115. Run 1 has been selected as the nominal run and Figures 108, 109 and 110 show several response characteristics for this run. The nominal run uses reaction controls and has no thrust moments included. A trim angle of attack of approximately 5.4 degrees was selected.

Figure 108 presents time histories of the angle of attack, sideslip angle and bank angle. The capsule pitches up during the first .5 seconds. This is a result of the delay in deflecting the lower flap. The capsule then has a damped oscillation about the trim angle. The bank angle varies smoothly from the initial 45 degree value to the wings level condition. The sideslip has a maximum value of approximately 2.4 degrees during the roll.

Figure 109 presents the load factor and load factor direction characteristics for the nominal run and Run 2 in which one-half of the nominal thrust was used. Using the nominal thrust, the peak load factor is approximately 16.5 G's, occurring at .08 seconds and resulting primarily from the rocket thrust. Reducing the rocket thrust level by one-half reduces the peak load factor by approximately one-half. The load factor direction shown in Figure 109 indicates primarily the direction of the thrust during burning, and the direction of the air load after burning. The oscillations in the load factor direction result from the angle of attack oscillations shown in Figure 108.

Figure 110 shows the separation distance characteristics from the parent vehicle for Runs 1 and 2. The trajectory analysis computer program estimates the parent vehicle position by simply considering that the initial velocity vector remains constant in magnitude and direction. Figure 110 indicates adequate separation characteristics for both the nominal thrust level of Run 1 and the reduced thrust level of Run 2.

Figure 111 presents the effects of thrust moments on the angle of attack time history characteristics. The thrust moment results from the fact that the separation rocket is located off the c.g. and results in the vehicle c.g. varying during rocket burning. The gimbal point is located so that the thrust vector (without thrust damping) is directed at an intermediate point between the extreme c.g. positions. It can be seen that the thrust moments have a significant effect on the angle of attack response. The vehicle oscillates over an angle of attack range of 45 degrees. The oscillation is damped, however, but would lead to excessive temperatures on the radiation cooled upper surface.

The use of thrust gimbaling as indicated by Run 4 in Figure 111 greatly reduces the oscillations and yields a very satisfactory trajectory. In fact, the use of thrust gimbaling yields a trajectory with smaller oscillations than Run 1, the nominal trajectory. The thrust gimbal angle required in Run 4 is also shown in Figure 12 and is seen to have a peak of 2 degrees.

Figure 112 compares the angle of attack time histories for full reaction control and aerodynamic pitch control. It can be seen that there are no large differences in the angle of attack characteristics. The use of aerodynamic damping provides slightly better damping characteristics than the reaction controls. The aerodynamic damping is provided by the lower flaps. The flap deflection angle for Run 5 is also shown in Figure 112 and is seen to vary from 27 degrees to 50 degrees.

The effects of varying initial conditions of sideslip, roll rate and yaw rate on the vehicle angular response characteristics are presented in Figure 113. The initial conditions are the same as the nominal run, (Run 1) except that in Run 6, the initial sideslip is 3 degrees, in Run 7 the initial roll rate is .1 radians/second and in Run 8 the initial yaw rate is .1 radian/second. These three runs have three axis reaction damping as well as pitch, roll and yaw attitude commands. There are no significant differences in the angle of attack and bank angle time histories. Run 6 with an initial sideslip angle of 3 degrees shows rather poor damping of the sideslip, however the angles are not large. These runs indicate that the response is not sensitive to reasonable variations in asymmetric initial conditions.

The effects of thrust angle on the separation distance characteristics are indicated in Figure 114. For Run 1, the nominal run, the thrust deflection angle was 40 degrees above the horizontal body axis and in Run 9, 30 degrees. The thrust magnitudes in each case were equal to the nominal value given in Figure 46. As a result, Run 1 has more separation from the parent vehicle in cross-range and altitude, and Run 9 more in the down range direction. Either response is satisfactory, and thus structural and mechanical disconnect considerations would probably determine the optimum thrust angle.

Figure 115 shows the effect of trim angle of attack and center of gravity position on the angle of attack time histories. It is seen that increasing the trim angle decreases the magnitude of the pitch oscillations for trim angles up to the initial angle of attack.

Varying the longitudinal center of gravity by 5% of the reference length in both the forward and aft directions has a negligible effect on the magnitude of the pitch oscillations, affecting mainly the frequency of the oscillations.

**6.3.1.2 Complete Trajectories.** The peak temperatures experienced by an escape capsule may not necessarily occur at the maximum heating point of the primary flight vehicle. For this reason complete escape trajectories were determined from the primary vehicle maximum heating point.

Figure 116 presents altitude-velocity trajectories for the pod capsule showing the effects of trim angle of attack and wing loading. Increasing the trim angle of attack results in higher altitude trajectories. Increasing the wing loading decreases the altitude leading to more severe temperatures.

**6.3.1.3 Aerodynamic Heating.** Equilibrium temperatures were calculated at five points on the pod vehicle. These points were as follows:

- a. Nose - diameter 2.5 ft.
- b. Lower surface - 2.0 ft.
- c. Lower surface - 4.0 ft.
- d. Upper surface - 2.0 ft.
- e. Lower flap - 1.0 ft. aft of hinge line.

A transition Reynolds number of  $2 \times 10^5$  was assumed for the lower surface and flap calculations. The lower surface was inclined 10.0 degrees at the 2.0 foot location and 0.0 degrees at the 4.0 foot location. This angle was added to the pod angle of attack to obtain the surface inclination angle to the flow. The flap was considered as a wedge with a half angle equal to the deflection angle. The vehicle angle of attack was added to the deflection angle to obtain the flap incidence angle. A boundary layer flow distance of 1.0 feet was assumed.

A swept cylinder analysis was applied to the upper surface at the 2.0 foot location. The upper surface was inclined 30 degrees to the pod centerline and had a diameter of 3.4 feet.

Figures 117 and 118 present the temperature histories for Run 1. The peak nose temperature was 3935 R at 1.2 seconds after separation. The peak temperature of 3195 R on the flap also occurred at 1.2 seconds. An upper surface peak temperature of 2825 R occurred at 1.6 seconds after separation. Lower surface temperatures at 2.0 feet and 4.0 feet both peaked at the same time of 0.6 seconds. The 2.0 foot point was at a higher temperature than the 4.0 foot point; 2800 R as compared to 2365 R. The temperature oscillations are a result of the angle of attack oscillations shown in Figure 108. Temperature fluctuations of the lower surface and the upper surface are

180 degrees out of phase because as the lower surface flow inclination was increased the upper surface inclination was decreased. An increase in flow inclination results in higher temperatures.

Temperature histories for trajectory 11 having a trim angle of attack of 14 degrees are presented on Figure 119. Again the 2.0 foot location on the lower surface has temperatures greater than the 4.0 foot location. The peak temperature was 2810 R at 0.6 seconds after separation at the 2.0 foot location; 10° R higher than the results in Figure 118. An upper surface peak temperature of 2365 R at 1.4 seconds was realized. This was 460° R lower than the results on Figure 117. This is as expected, since increasing the vehicle angle of attack decreases the angle of inclination of the upper surface. For the pod capsule, which is assumed to have ablation material on the lower surface and be radiation cooled on the upper surface, the upper surface is the critical heating point. For this reason, a high trim angle of attack would be desirable for escape trajectories in the hypersonic regime.

The temperature characteristics corresponding to the angle of attack of 30 degrees complete trajectories presented in Figure 116 are shown in Figure 120. The lower surface attains relatively high temperatures but these are within the state of the art of ablation materials. The upper surface temperatures are relatively low, being approximately 500 degrees lower than the temperatures on the upper surface during primary vehicle flight. For this reason, a slightly lower trim angle of attack could be used.

6.3.2 ORBIT ESCAPE. The initial conditions for the orbit escape performance studies are presented in Table XV.

Figure 121 presents angle of attack time history characteristics for separation in orbit. The data in Figure 121 shows the effects of thrust moments and thrust gimbaling. Without thrust gimbaling the capsule pitches to a very high angle of attack. This is not severe however since the reaction controls would bring the capsule to the desired low angle of attack position in less than one minute.

The complete orbit re-entry trajectories for wing loadings of 55 and 91.5 psf are presented in Figure 122 for a trim angle of attack of 30 degrees. The peak upper surface temperature 2.0 feet aft and lower surface temperature 4.0 feet aft are as follows:

Wing Loading	Position	Peak Temperature
55 psf	lower	3340°R
	upper	1500°R
91.5 psf	lower	3750°R
	upper	1550°R

These peak temperatures are approximately the same as those attained for the complete trajectories from the primary flight vehicle maximum heating point as presented in Figure 117.

**6.3.3 RECOVERY CEILING.** The recovery ceiling characteristics determined for the pod capsule configuration are presented in Figure 123. These trajectories were determined for an angle of attack of 30 degrees. The recovery ceiling in the hypersonic regime was determined by temperature limits. It was assumed that the temperature limit was the peak lower surface temperature 4.0 feet aft of the nose obtained on the escape trajectory from the primary vehicle maximum heating point. These temperature characteristics were presented in Figure 120. Also shown in Figure 123 is the recovery ceiling capability if a peak lower surface temperature of 3800°R is used. If higher lower surface temperatures are allowed and the recovery ceiling were based on the upper surface temperatures much higher recovery ceilings would be obtained. The recovery ceiling of the primary flight vehicle is shown on Figure 123 for comparison.

**6.3.4 ON-THE-PAD ESCAPE.** The run schedule for this escape condition is presented in Table XVI. Figure 124 presents the effects of thrust moment and control system on the angle of attack characteristics and the effect of thrust angle on the separation distance characteristics. The use of aerodynamic damping rapidly eliminates the pitch oscillations.

Figure 125 shows the effect of control system type on the angle of attack characteristics without thrust moment effects. The reaction controls yield poor damping but in all cases the load factor characteristics are within human tolerance limits. Also shown in Figure 125 is the effect of thrust moment on the separation distance characteristics using various types of damping. The only acceptable altitude characteristics are obtained with the use of thrust gimbaling.

**6.3.5 LANDING ESCAPE.** The parameter variations for the performance investigation at this escape condition are presented in Table XVI. Figure 126 presents the

angle of attack characteristics showing the effect of control system type. Good damping characteristics are obtained with the aerodynamic controls. The reaction controls have very little effect.

Figure 127 shows the effect of thrust moments on the angle of attack characteristics with aerodynamic damping. Also shown in Figure 127 are the effects of thrust inclination angle on the separation altitude. Adequate altitude and separation characteristics were obtained in all cases investigated. The maximum load factor results from the rocket thrust and is within human tolerance limits.

**6.3.6 MAXIMUM DYNAMIC PRESSURE ESCAPE.** The initial conditions for the performance runs at these conditions are presented in Table XVII.

Figure 128 presents the angle of attack load factor and load factor direction characteristics showing the effect of trim angle of attack and initial pitch rate using aerodynamic damping. Increasing the initial pitch rate increases the magnitude of the oscillation but the load factor remains within human tolerance limits.

The upper curves in Figure 129 show the effect of aerodynamic controls on the angle of attack characteristics with thrust moments. The aerodynamic controls yield good damping. The lower curves compare aerodynamic and reaction controls with no thrust moments. For this configuration the differences are not too great.

**6.3.7 PERFORMANCE CONCLUSIONS.** On the basis of the performance investigation of the pod capsule the following conclusions can be made:

1. Allowable temperature characteristics can be obtained if a moderate trim angle of attack is used, e.g.  $20^{\circ}$  to  $30^{\circ}$ .
2. Either reaction controls or aerodynamic controls can be used in the atmosphere. Although the damping is not as good with reaction controls at the higher dynamic pressures the resulting oscillations do not lead to excessive load factors.
3. Different flap settings are required in the hypersonic regime than at the lower Mach numbers.



TABLE XIV  
SUMMARY OF CONDITIONS FOR POD CAPSULE RE-ENTRY TRAJECTORY RUNS

RUN	TRIM $\alpha$ DEG	COMMAND ROLL RATE DEG/SEC	INITIAL SIDESLIP DEG	INITIAL ROLL RATE DEG/SEC	INITIAL YAW RATE DEG/SEC	PITCH DAMPING DEG/SEC	REACTION DAMPING pitch - p roll - r yaw - y	THRUST (NOMINAL) POUNDS	THRUST ANGLE DEG	THRUST MOMENT	THRUST GIMBAL PITCH DAMPING DEG/SEC	LONGITUDINAL CENTER OF GRAVITY
1	5.4	-15.	0.	0.	0.	0.	p, r, y	40,000	40	out	0.	NOM
2								20,000		↓		
3								40,000		in	↓	
4						↓				↓	.1	
5			↓			.5	r, y			out	0	
6			3	↓		0.	p, r, y					
7			0.	5.73	↓							
8				0	5.73				↓			
9	↓				10.				30			
10	9								40			
11	14											.05 fwd
12	5.4	↓								↓		.05 aft
13	↓											

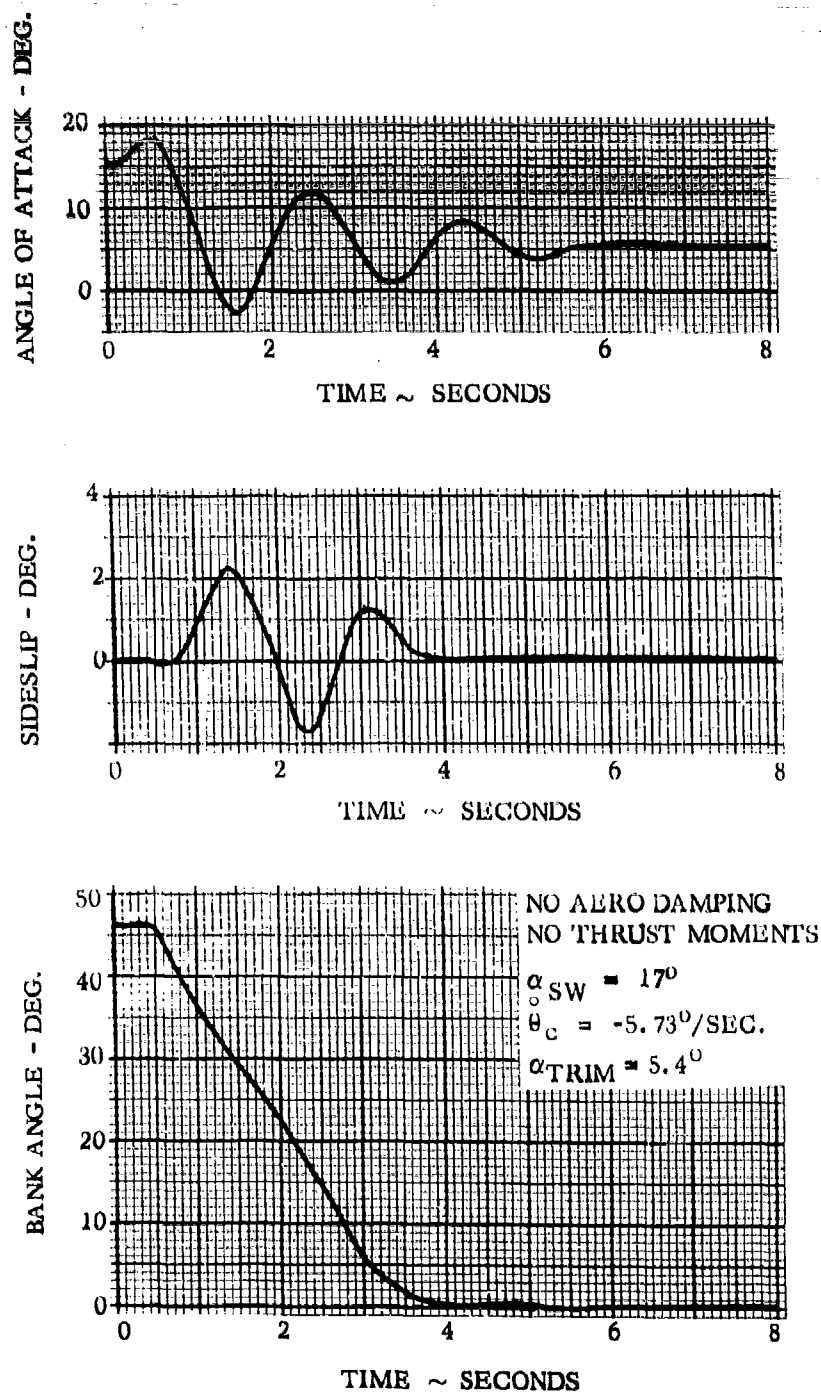


Figure 108 - Pod Capsule Dynamic Response - Nominal Trajectory

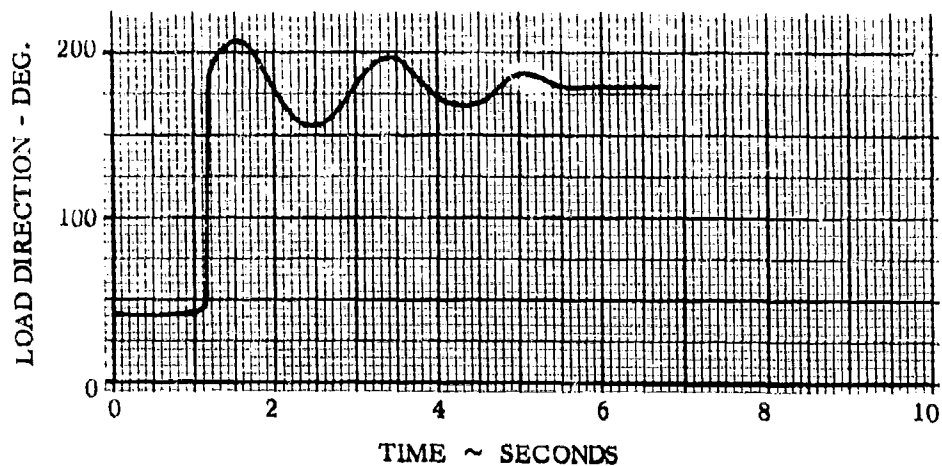
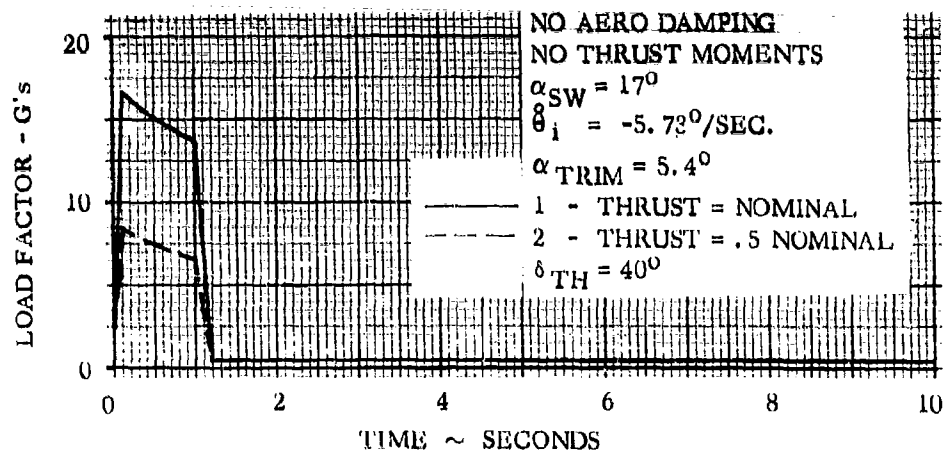


Figure 109 - Pod Capsule Load Factor Characteristics - Effect of Thrust Level

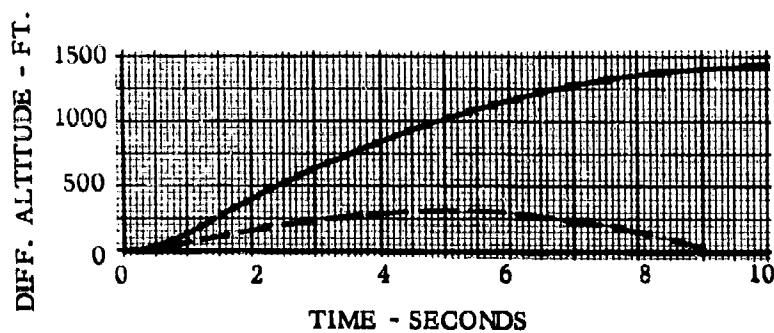
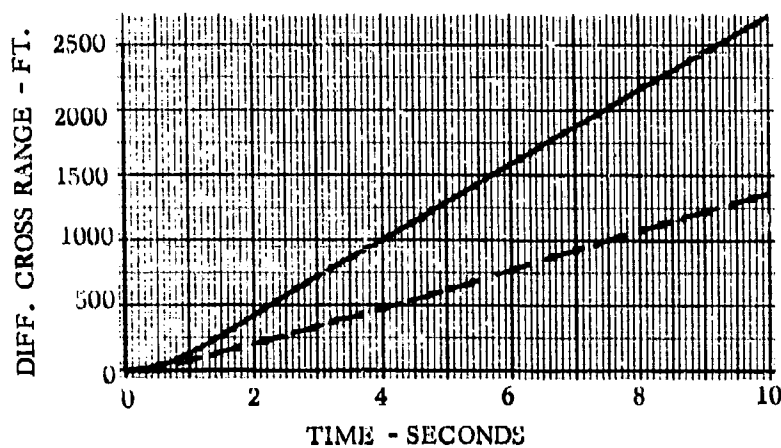
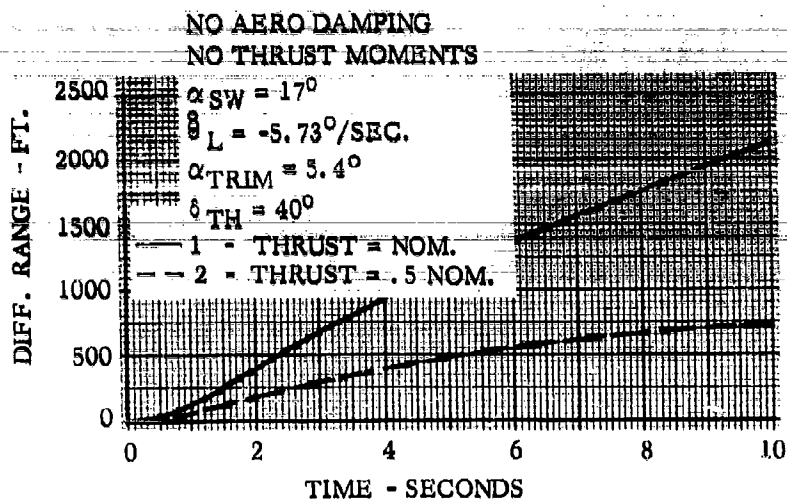
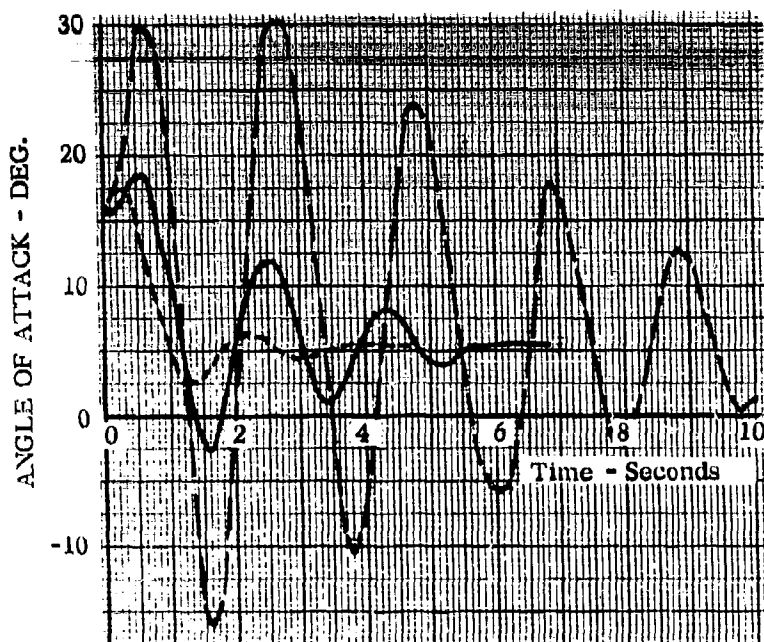


Figure 110 - Pod Capsule Separation Characteristics - Effect of Thrust Level



NO AERO DAMPING

$$\alpha_{SW} = 17^\circ$$

$$\theta_i = -5.73^\circ/\text{SEC.}$$

$$\alpha_{\text{TRIM}} = 5.4^\circ$$

$$\delta_{TH} = 40^\circ$$

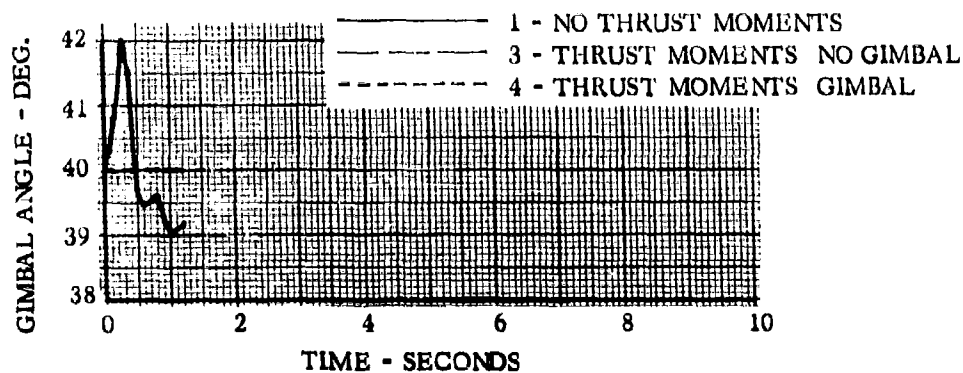
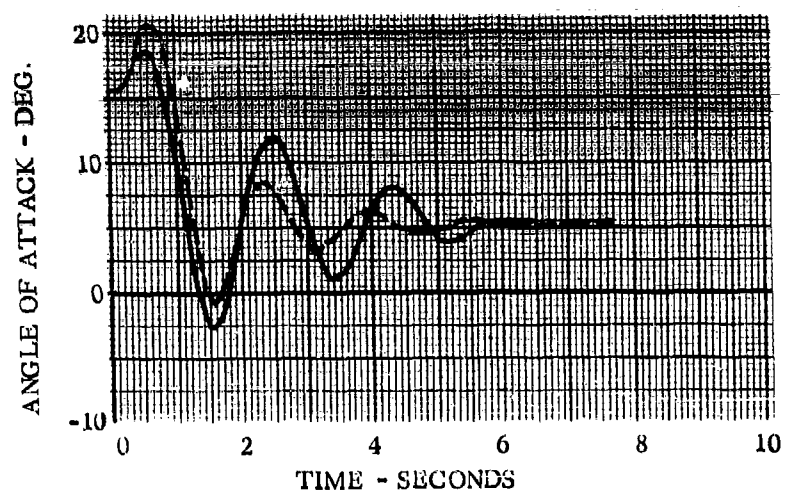


Figure 111 - Pod Capsule Dynamic Response - Effect of Thrust Moment and Thrust Gimbal



NO THRUST MOMENTS

$$\alpha_{SW} = 17^{\circ}$$

$$\dot{\theta}_1 = -5.73^{\circ}/\text{SEC.}$$

— 1 - NO AERO DAMPING

- - - 5 - AERO DAMPING - NO PITCH REACTION

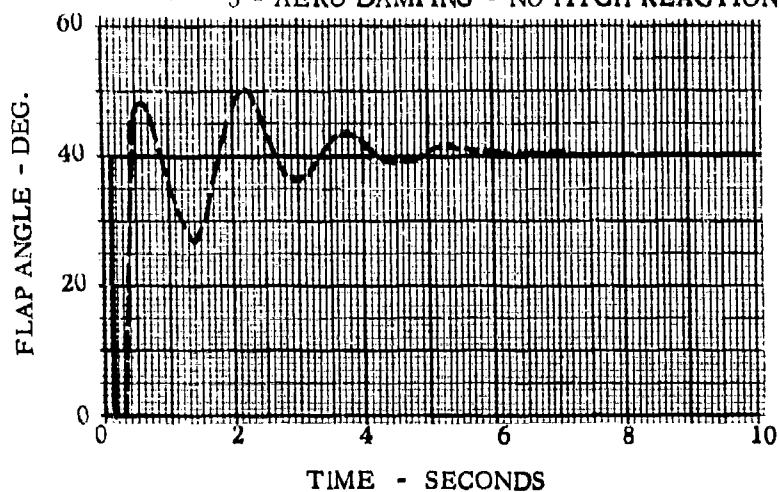


Figure 112 - Pod Capsule Dynamic Response Effect of Aerodynamic Damping

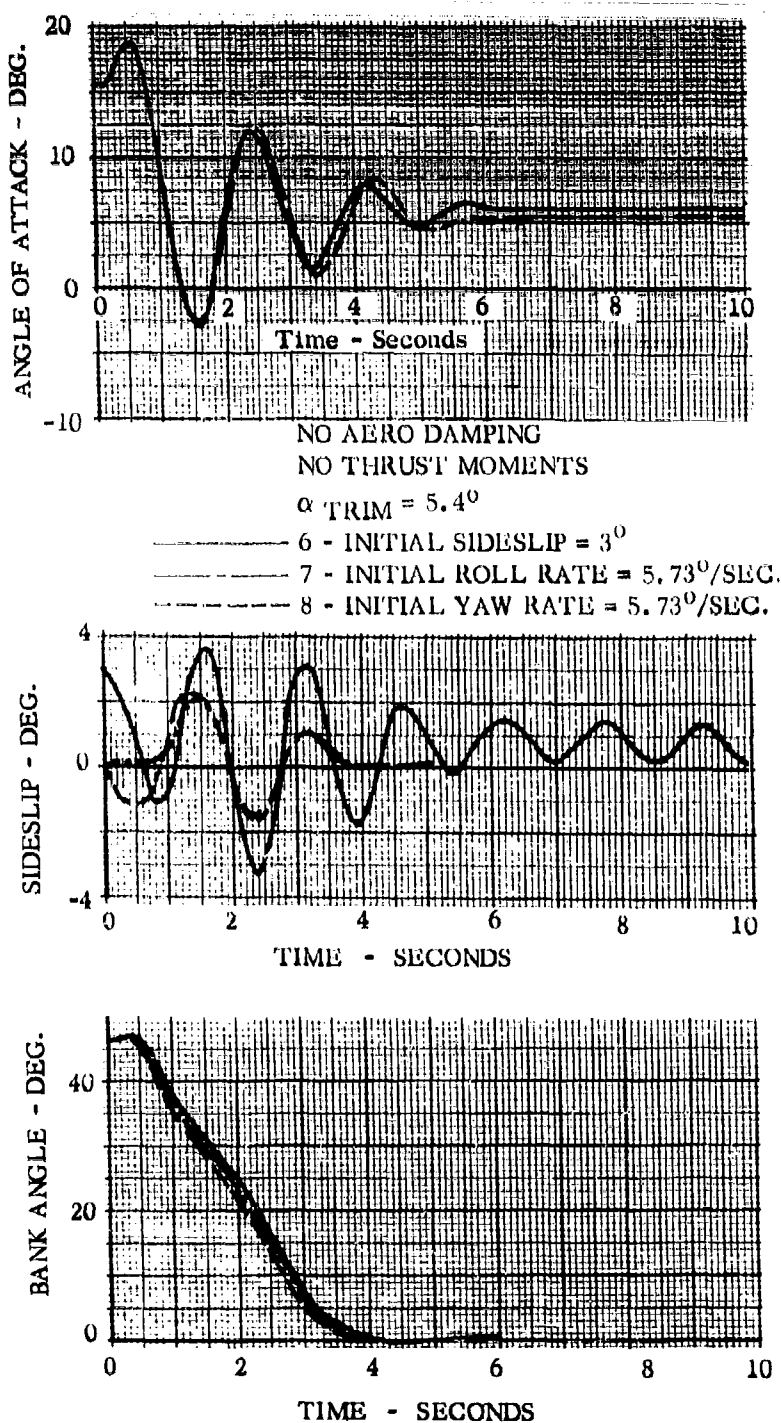


Figure 113 - Pod Capsule Dynamic Response - Effect of Lateral - Directional Disturbances

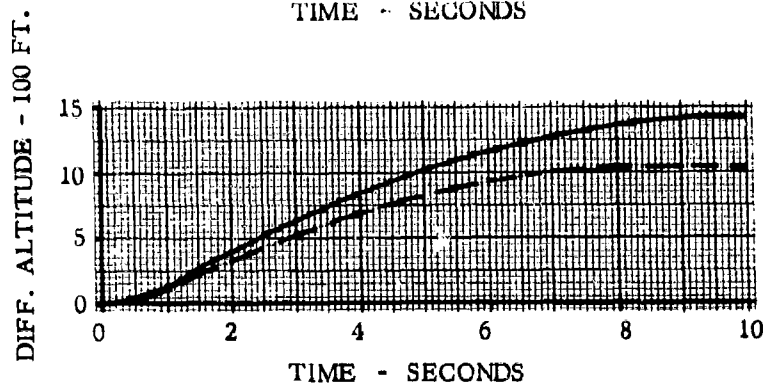
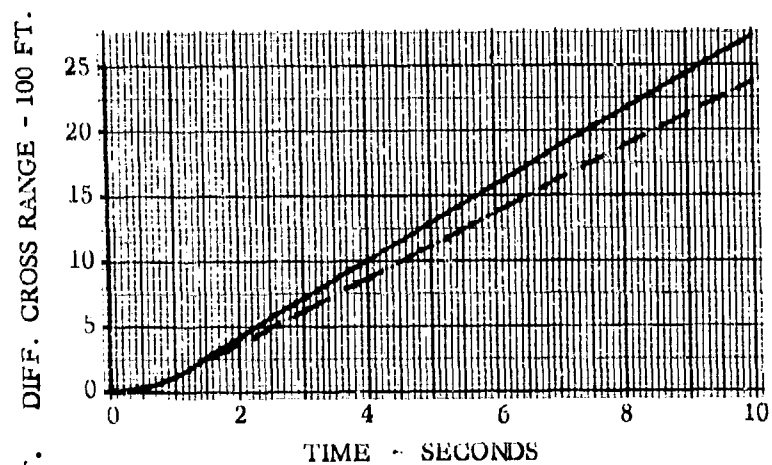
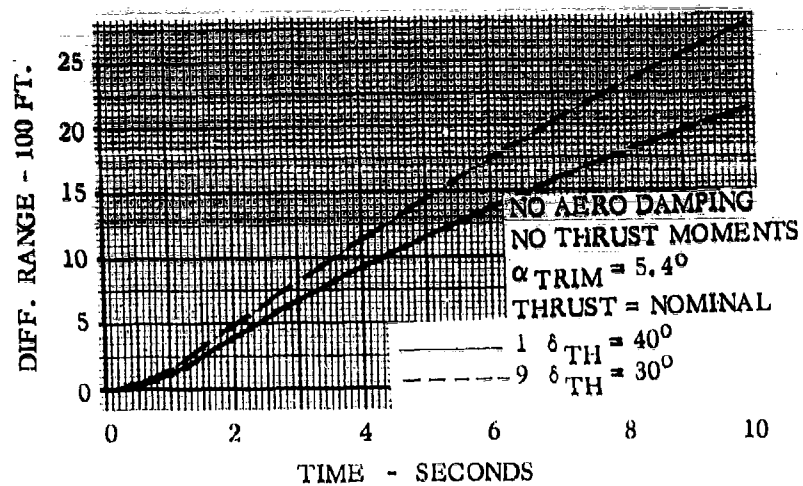


Figure 114 - Pod Capsule Separation Characteristics - Effect of Thrust Angle



NO AERO DAMPING  
 NO THRUST MOMENTS  
 $\delta_{SW} = 17^\circ$   
 $\theta_1^\circ = -5.73^\circ/\text{Sec.}$   
 NOMINAL C. G.

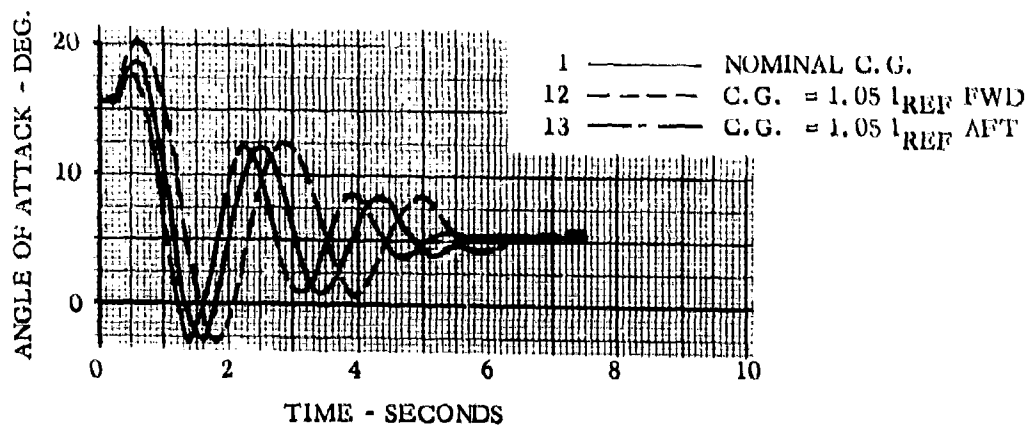
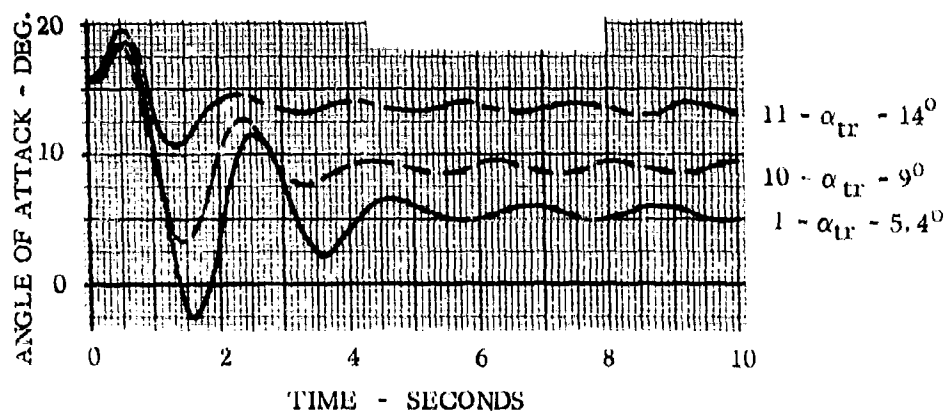


Figure 115 - Pod Capsule Dynamic Response - Effect of Trim Angle of Attack and Center of Gravity Location

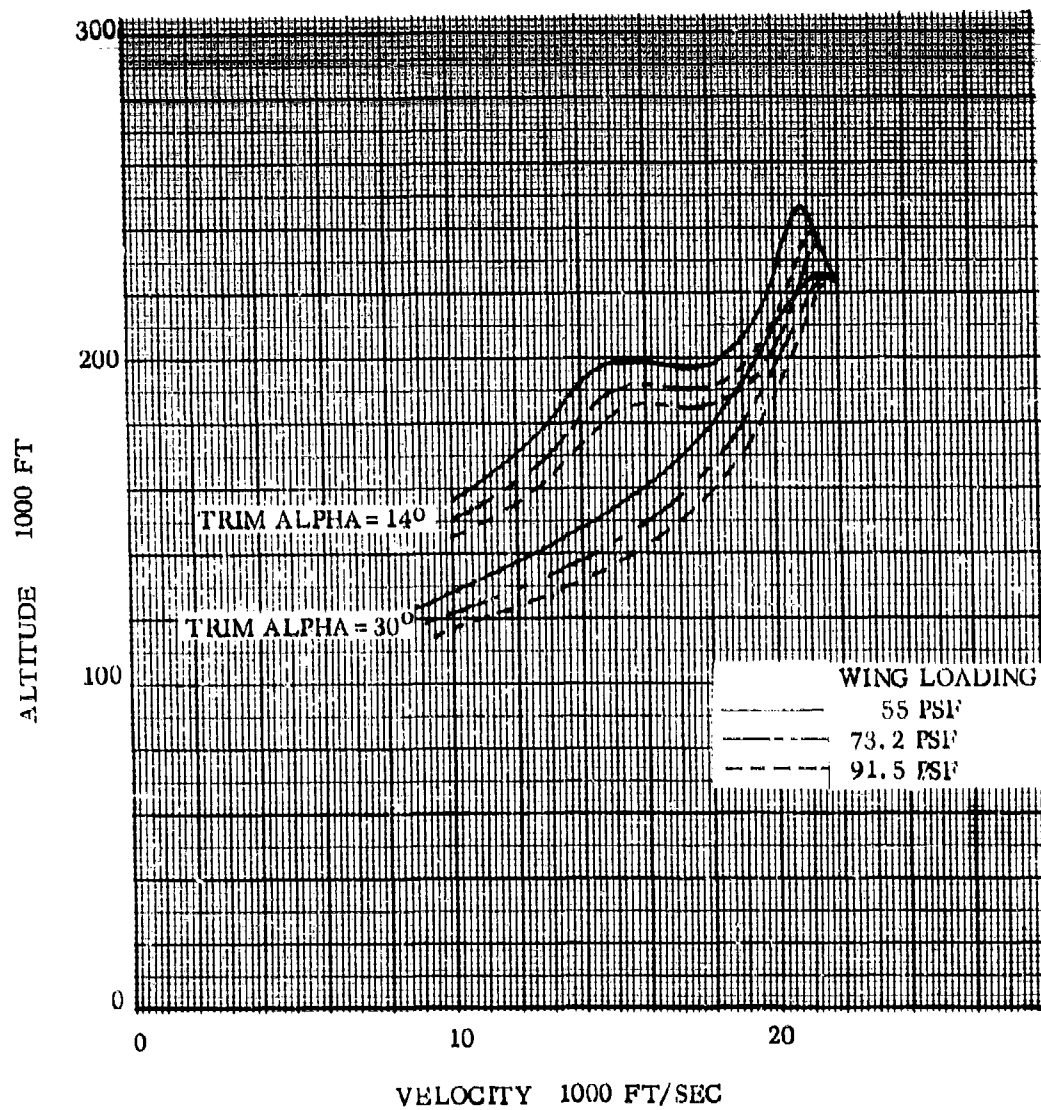


Figure 116 Effect of Wing Loading and Trim Alpha on Pod Capsule  
Escape Trajectories

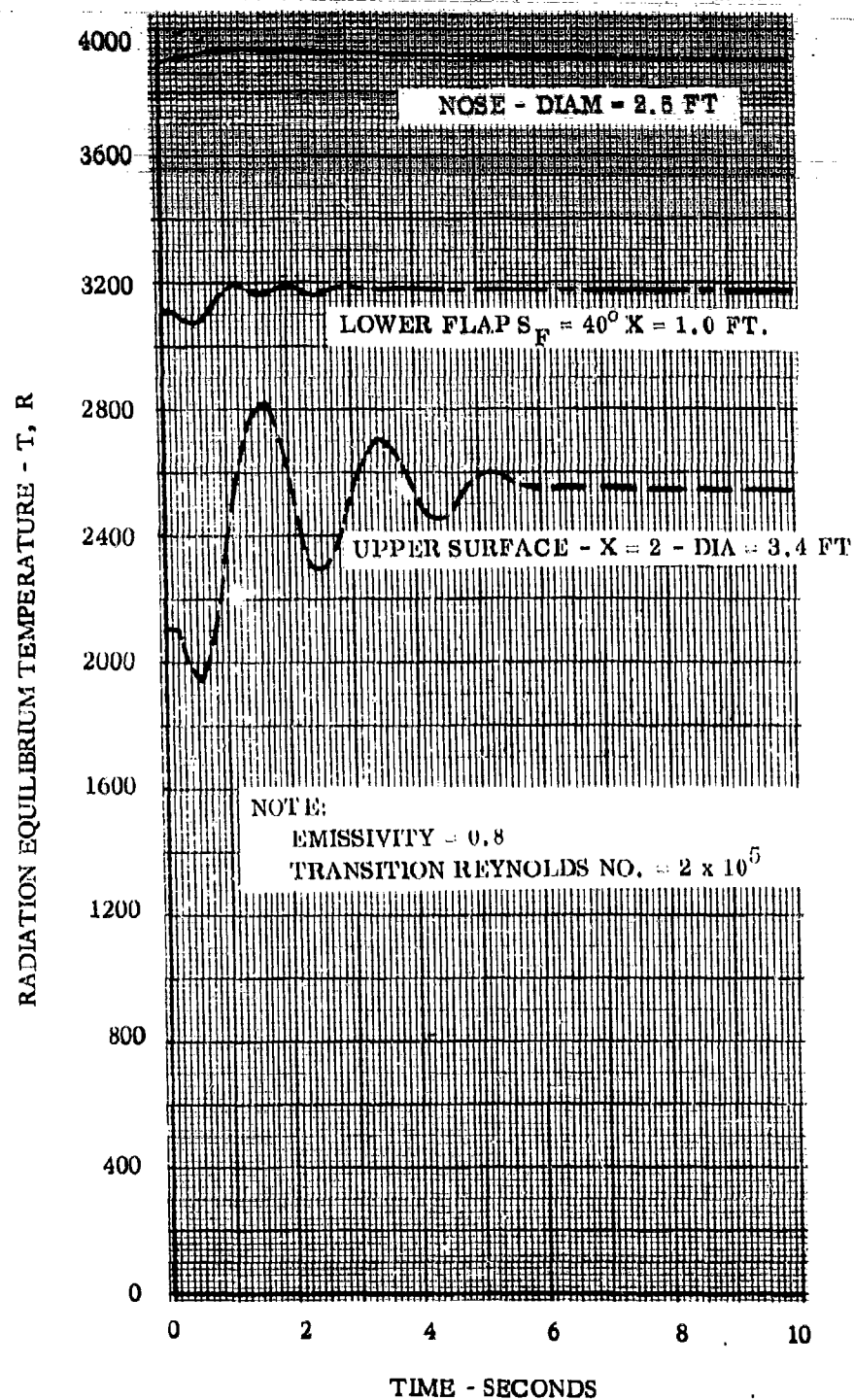


Figure 117 Pod Capsule Temperature Histories - Nominal Run, Nose, Lower Flap and Upper Surface

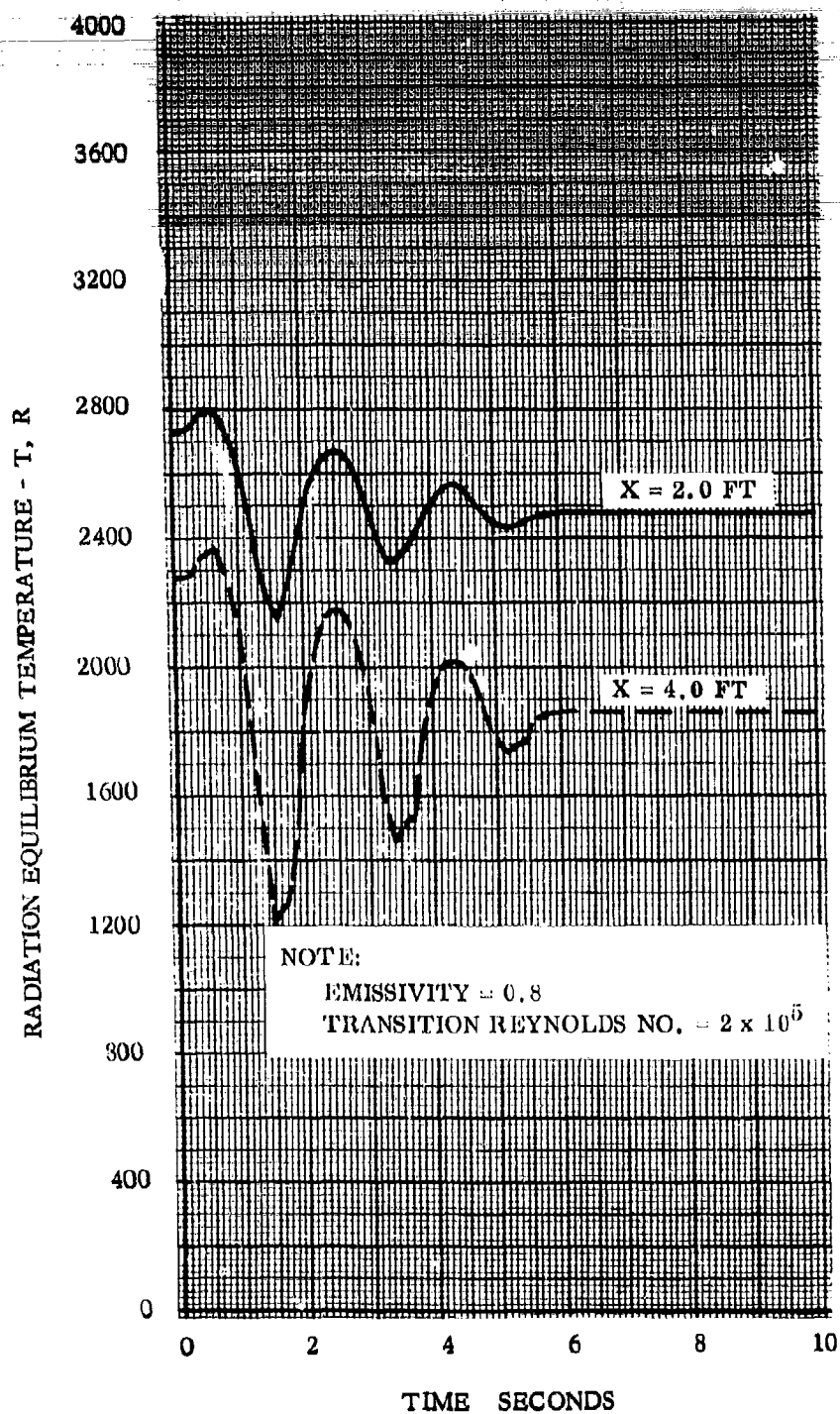


Figure 118 Rod Capsule Temperature Histories - Nominal Run  
 Lower Surface

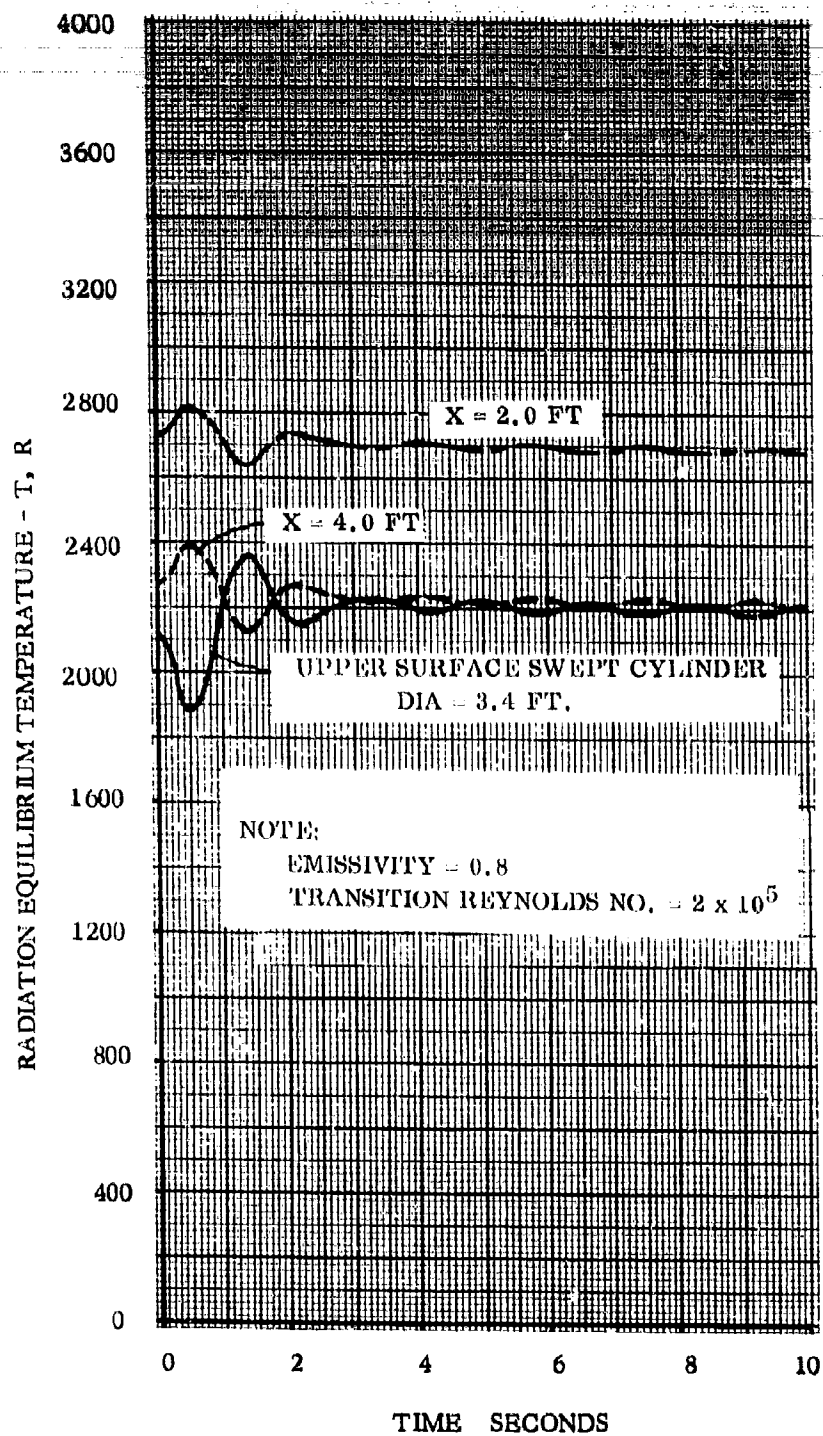


Figure 119 Rod Capsule Temperature Histories - Run 11  
Upper and Lower Surface

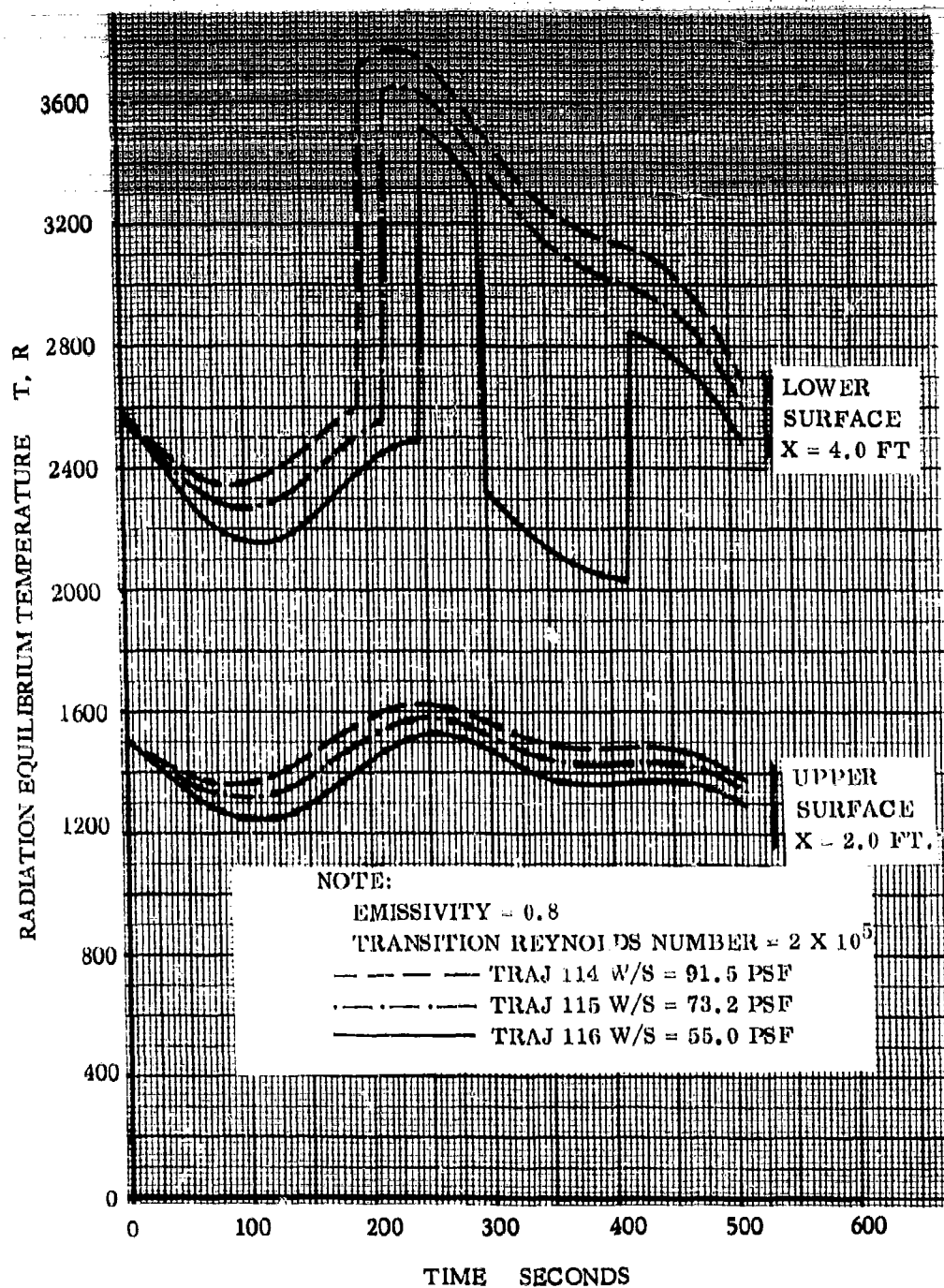
Figure 120 Pod Capsule - Effect of Wing Loading - Trim Alpha =  $14^\circ$

TABLE XV  
SUMMARY OF INITIAL CONDITIONS FOR POD CAPSULE ORBIT TRAJECTORY RUNS

No.	$\theta_i$	$\theta_c$	$\theta_i$	Reaction	T	$\delta TH$	THM	$\delta TH/q$
1	0	0	-11.46	IN	40,000	40	OUT	0
2	10		0					
3	20				20,000			
4	10		11.46		12,000	30	IN	.1
5					40,000	40		
6					12,000			
7					40,000			
8					12,000			
9					40,000			
10								
11								
12								

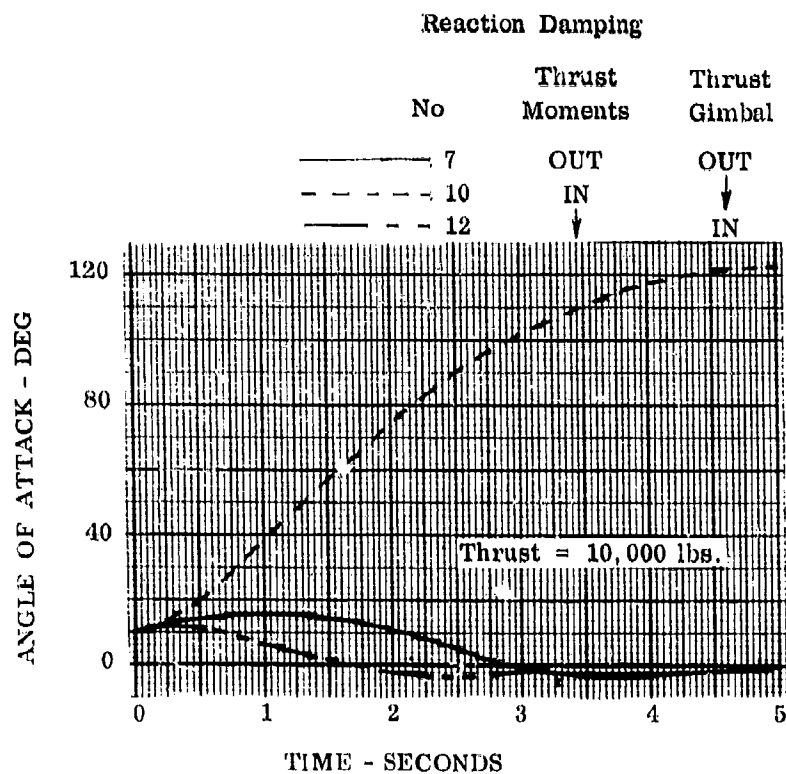


Figure 121 Pod Capsule - Orbit Escape Trajectory Characteristics



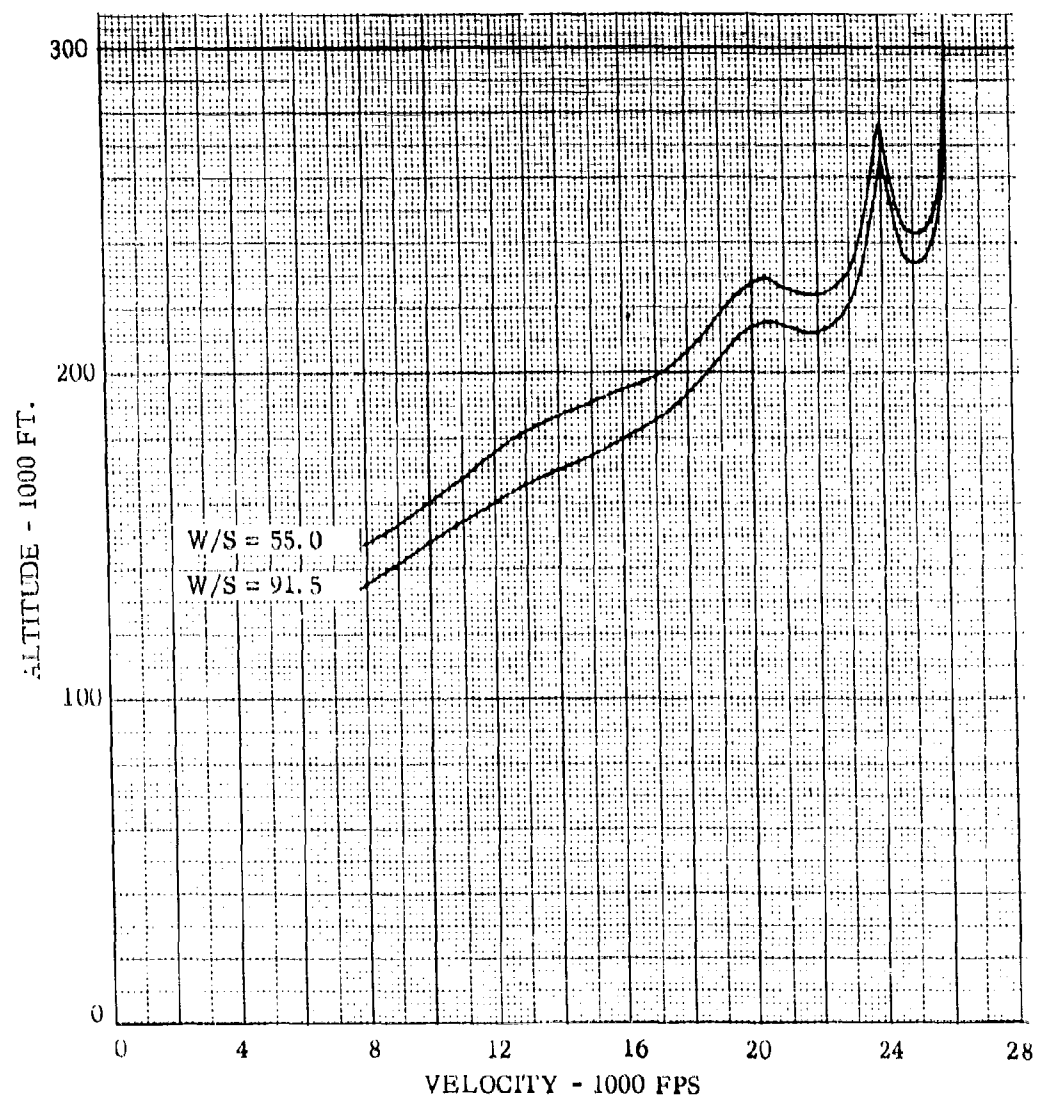


Figure 122 - Pod Capsule - Orbit Re-entry Trajectories

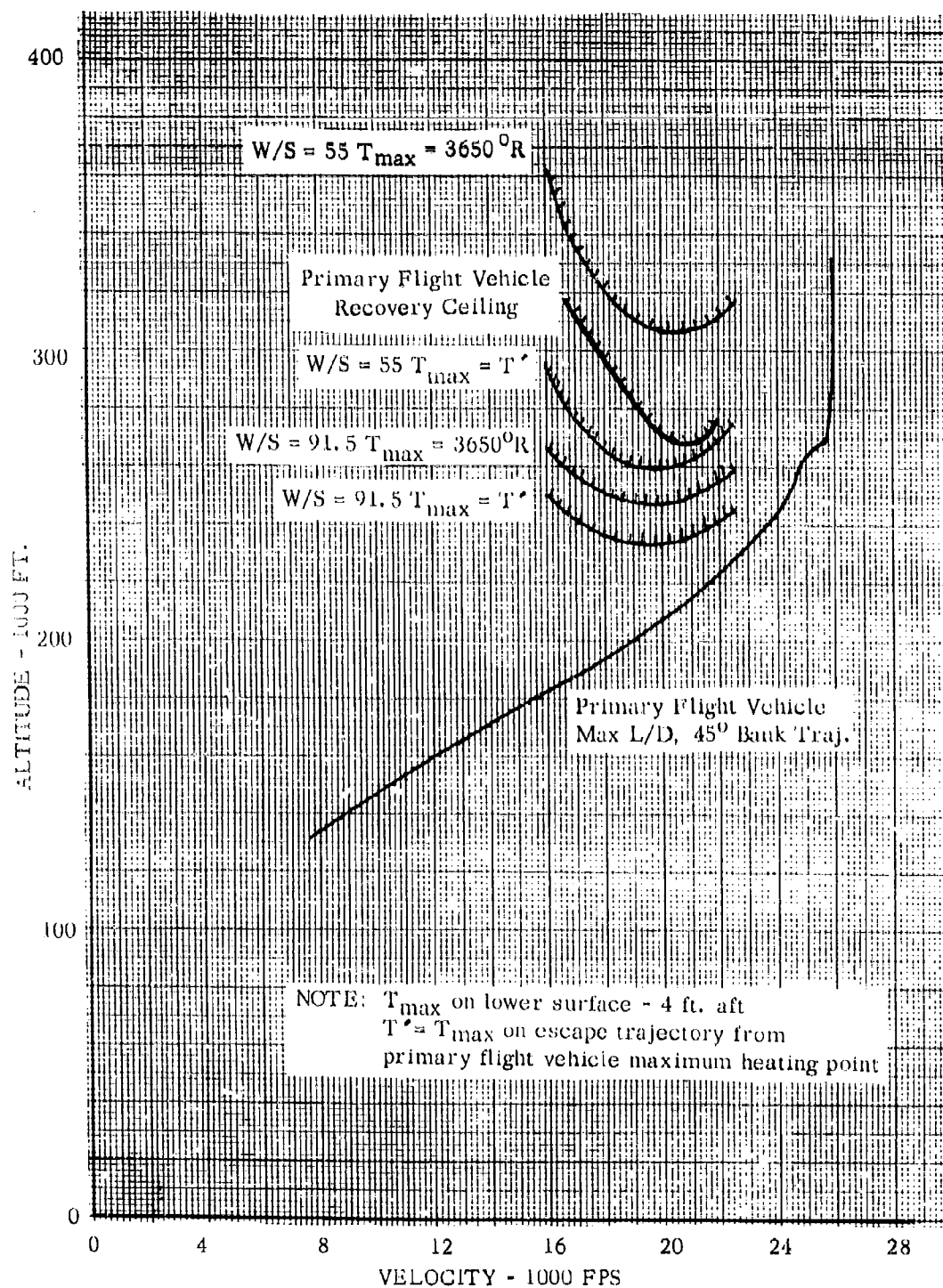


Figure 123 - Pod Capsule - Recovery Ceiling

TABLE XVI  
SUMMARY OF CONDITIONS FOR POD CAPSULE SUBSONIC TRAJECTORY RUNS

No.	$\gamma$	$\delta u$	$\delta L$	$\alpha_i$	$L/q$	Reaction	T	$\delta TH$	THM	$\delta TH/q$
1	-2	20	-20	10	.5	OUT	40,000	40	OUT	0
2								30		
3					0	IN		40	IN	.1
4										
5					.5	OUT				0
6					0					
7										
8										
9	90							30	OUT	
10				0	.5			40		
11					0	IN			IN	
12										
13					.5	OUT				.1
14					0					0
15										
16										
17									OUT	

Landing -  $\gamma = -2^\circ$        $V = 200$  FPS      Altitude = 100 FT       $\alpha_{sw} = \pm 13^\circ$   
 On-the-Pad -  $\gamma = 90^\circ$        $V = 0$       Altitude = 100 FT       $\alpha_{sw} = \pm 3.5^\circ$

With the exception of Run 2, initial flap deflection angles were  $0^\circ$ . On Run 2 the upper surface was deflected  $20^\circ$  prior to release.

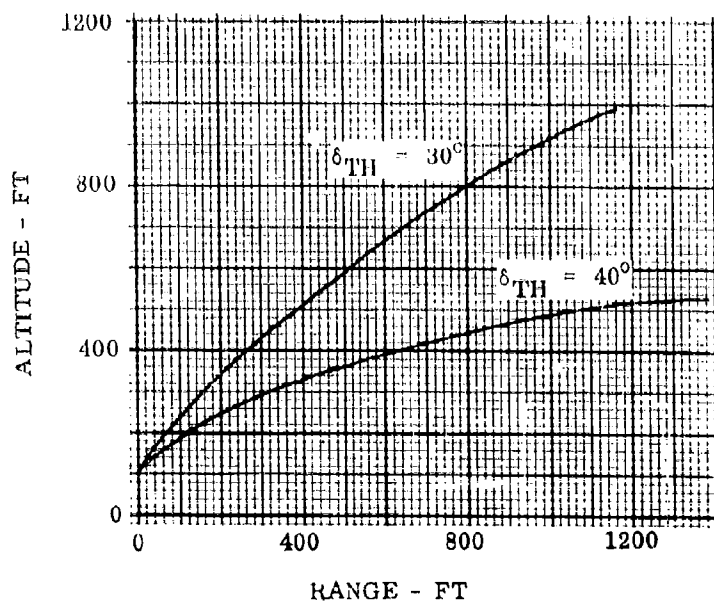
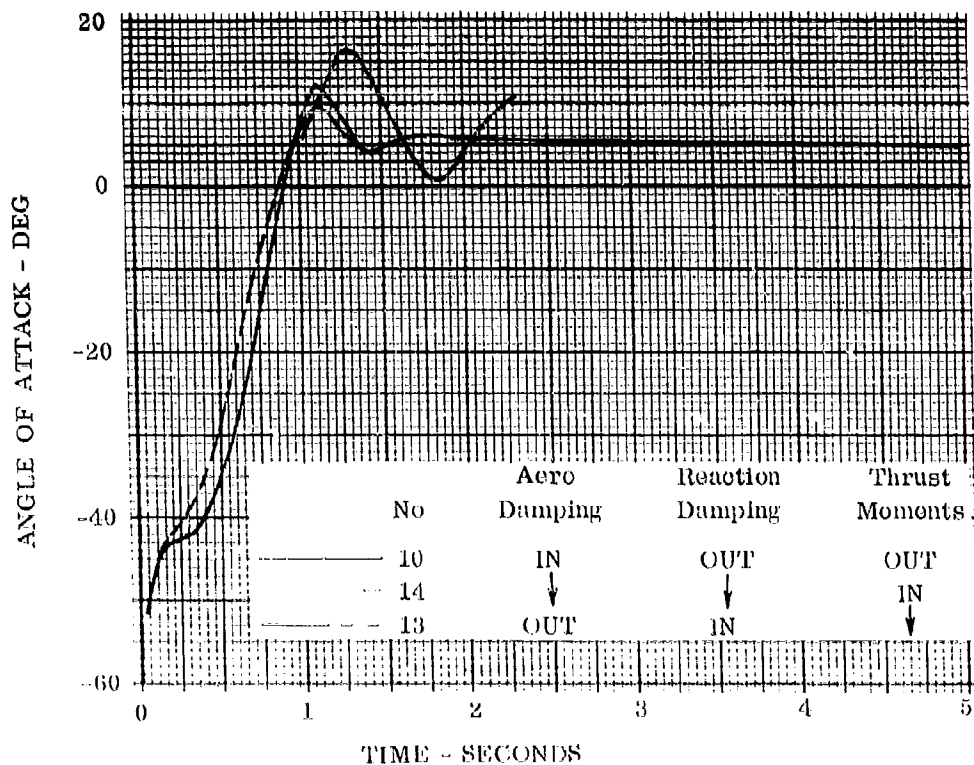


Figure 124-Pod Capsule - On-the-Pad Escape Trajectory Characteristics

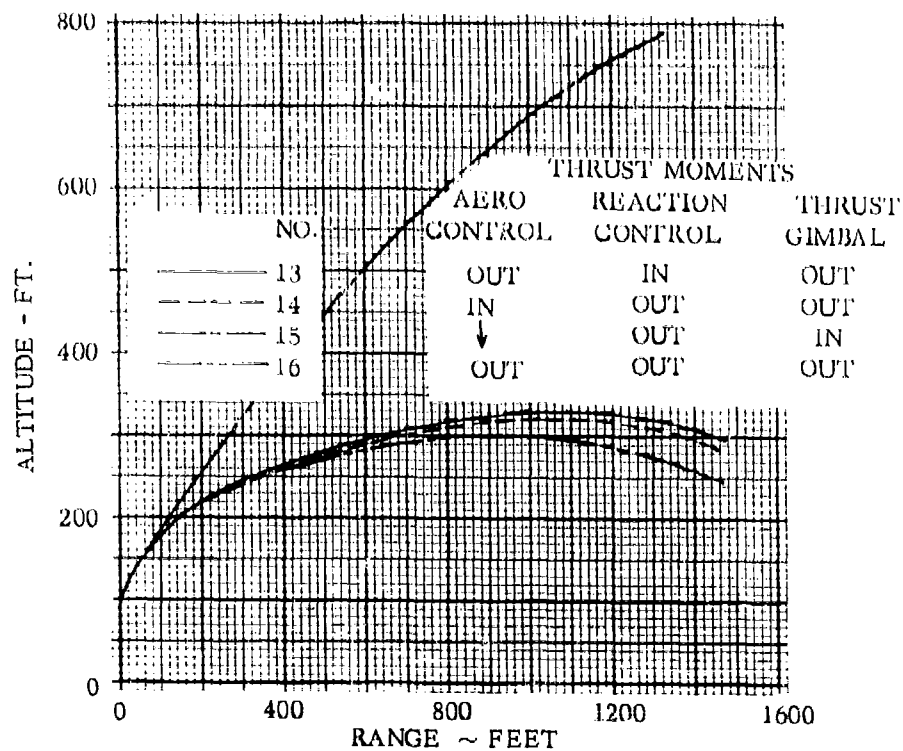
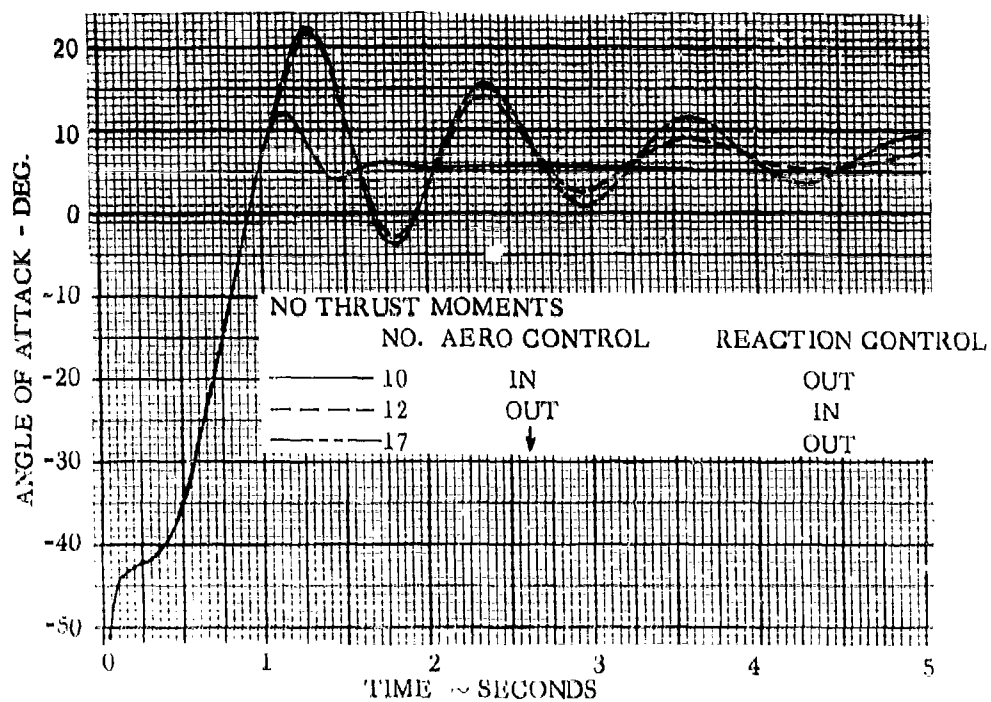


Figure 125 - Pod Capsule - On-The-Pad Escape Trajectory Characteristics Effect of Control Type and Thrust Moments

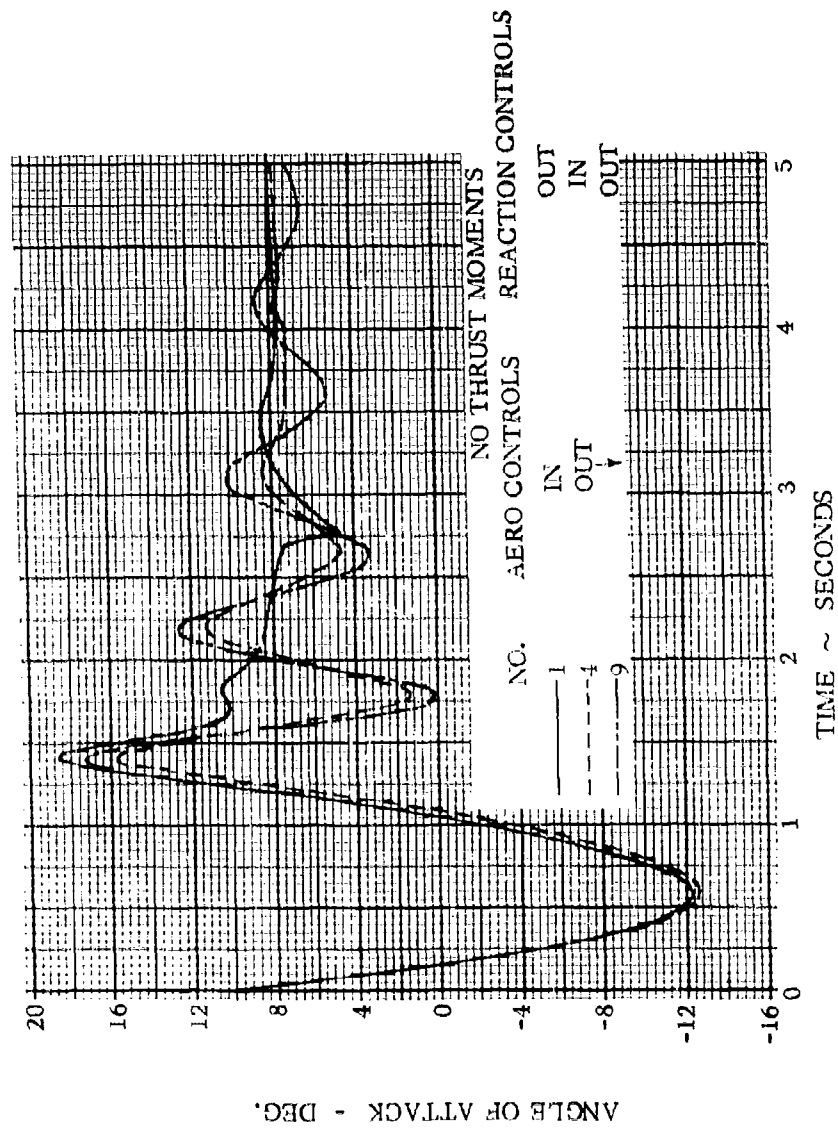


Figure 126 - Pod Capsule - Landing Approach Escape Trajectory Characteristics - Effect of Control Type

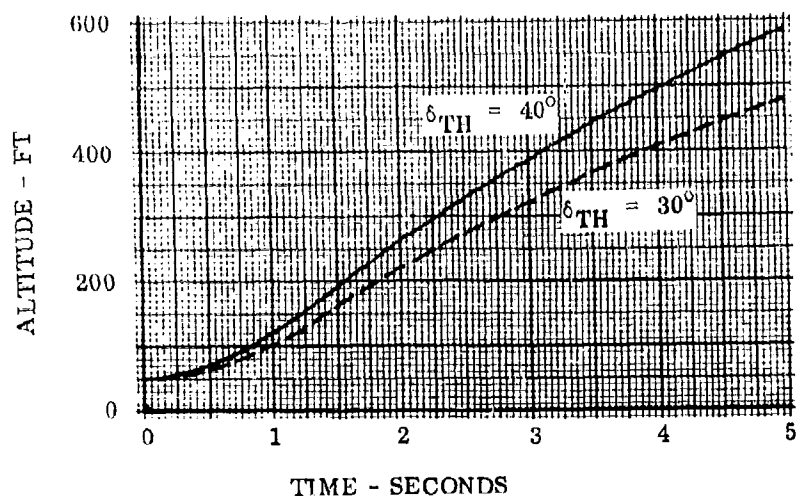
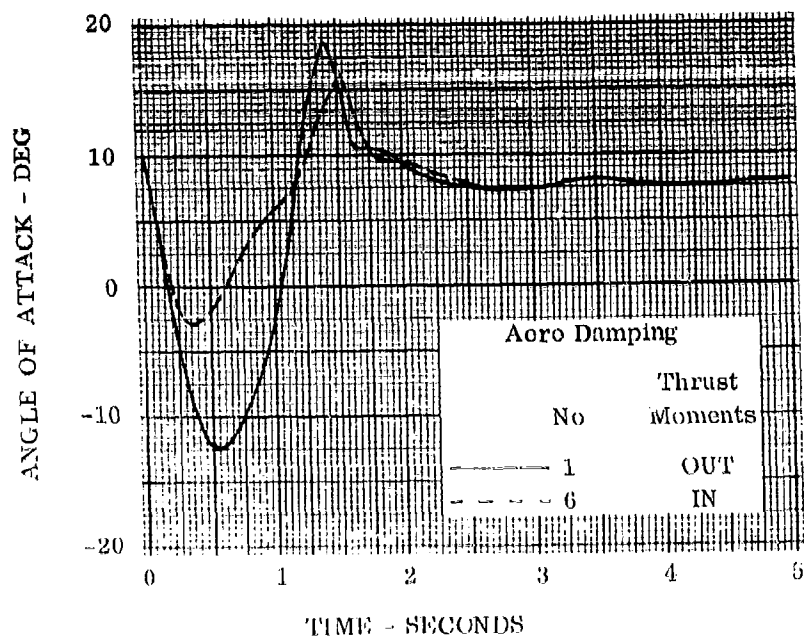


Figure 127 - Pod Capsule - Landing Approach Escape Trajectory Characteristics

TABLE XVII  
SUMMARY OF INITIAL CONDITIONS FOR POD CAPSULE SUPERSONIC TRAJECTORY RUNS

No.	$\delta_L$	$\delta_u$	$\alpha_i$	$\theta_i$	$\delta L/q$	Reaction	Thrust	$\delta TH$	THM	$\delta TH/q$
1	20	-20	3	10	.5	OUT	40,000	40	OUT	0
2				25						
3				40						
4		-40		10				30		
5				25				40		
6				40						
7		-20		0						
8			-3							
9										
10										
11										
12										
13										
14										
15										

$\alpha_{SW} = 3.5^\circ$



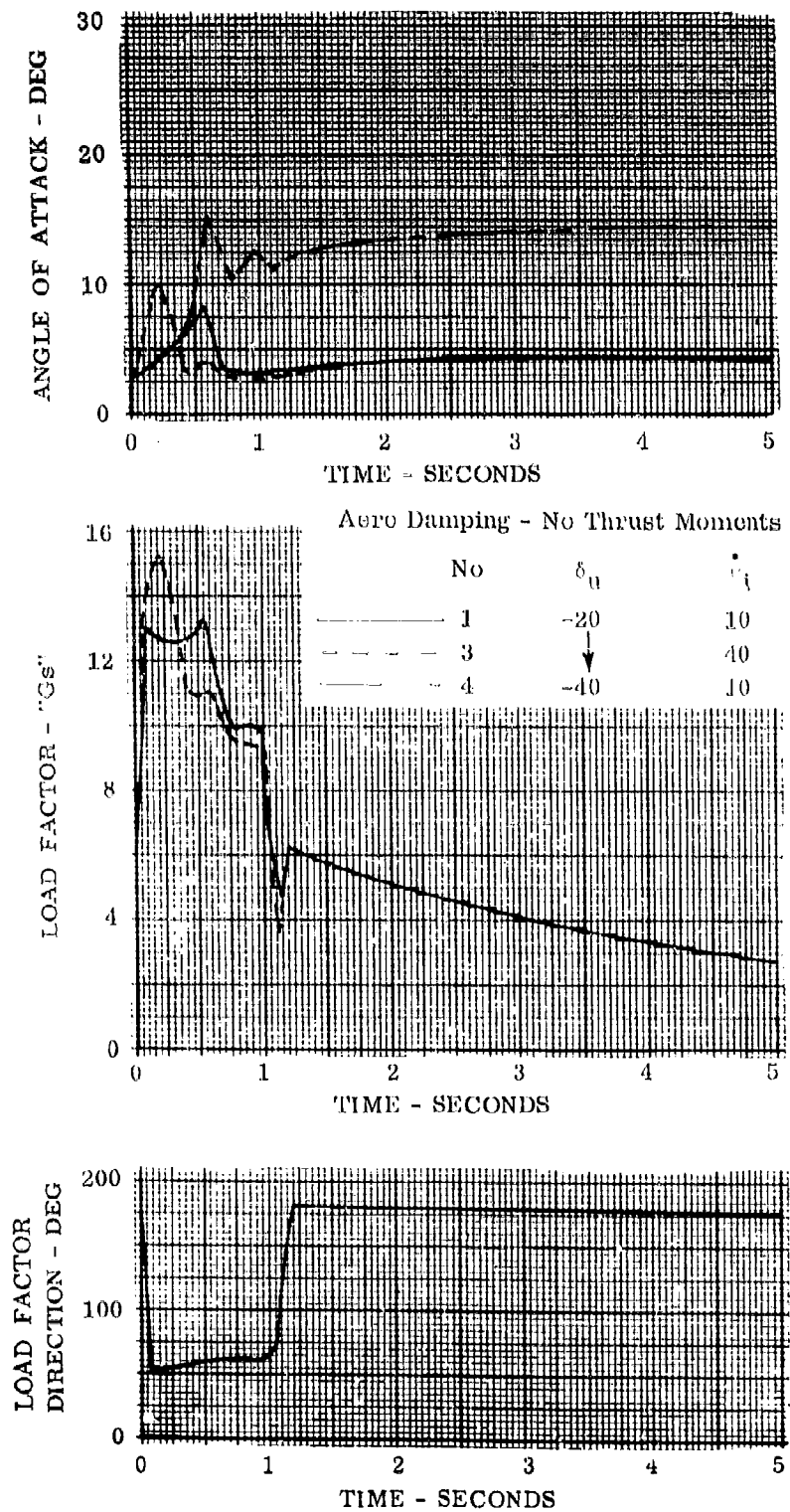


Figure 128 -Pod Capsule - Maximum Dynamic Pressure  
 Escape Trajectory Characteristics

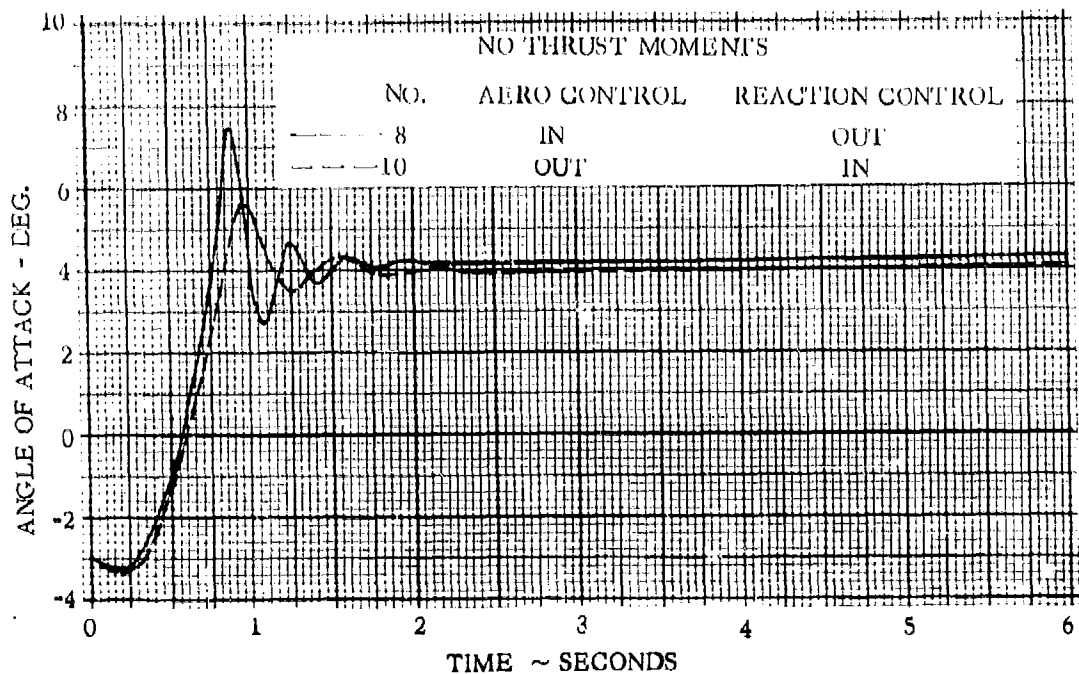
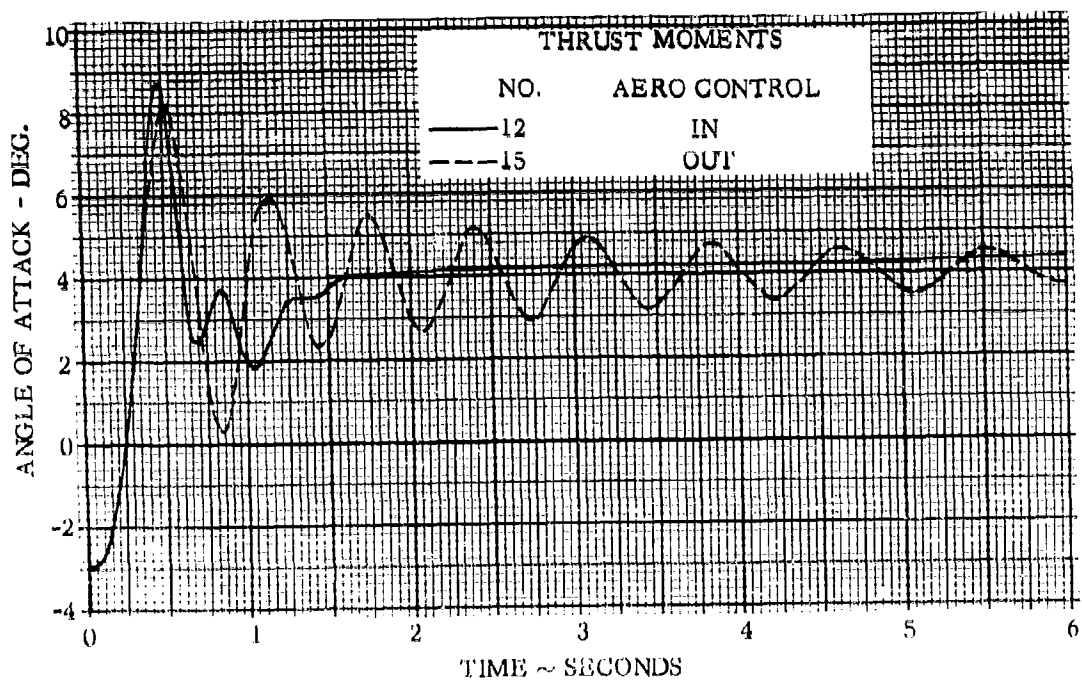


Figure 129 - Pod Capsule - Maximum Dynamic Pressure Escape Trajectory Characteristics - Effect of Control Type and Thrust Moments

#### 6.4 TURNAROUND CAPSULE

6.4.1 RE-ENTRY ESCAPE. The performance at this flight condition will be discussed under separation dynamics and complete trajectories.

6.4.1.1 Separation Dynamics. The analysis was limited to the first twelve seconds after separation, which was sufficient to determine the response characteristics, and achieve adequate clearance. The initial phase consisted of determining a basic technique while the final phase consisted of investigating the effect of various parameter variations using the basic technique.

It was decided to perform the turnaround maneuver in the pitch plane. This would expose the lower surface to the high aerodynamic heating and loads encountered during turnaround and would be more in line with the heating and loading distributions on the primary flight vehicle.

The initial runs were made with a zero bank angle initial condition in order to investigate the pitch plane motion. It was found that the vehicle could be turned around by aerodynamic forces if the center of gravity was located such that the vehicle was unstable in the initial separation orientation and stable with the heat shield forward. It was found that the vehicle pitch characteristics were extremely sensitive to the center of gravity location (stability characteristics). A nominal center of gravity as shown in Figure 9 was selected for the study. As indicated in Section 3.1 it was necessary to delay the opening of the flap controls until the vehicle had pitched beyond ninety degrees angle of attack (conventional angle of attack measured to the smaller nose). The angle of attack of initial flap opening is designated  $\alpha$  switch.

After these initial studies of the pitch plane characteristics the performance was investigated with the initial condition of a 45 degree bank angle. It was desired during the separation maneuver to roll the vehicle to a zero degree bank angle. The technique selected was one in which the roll command was initiated at the same time as the flaps were extended,  $\alpha$  switch. Another technique would be to delay the roll orientation maneuver until the pitch maneuver was completed. In order to keep the sideslip low it was necessary to include a linear heading command which was coordinated with the roll command, as with the lifting body.

Table XVIII presents a summary of conditions for the more significant trajectories which were analyzed. Figures 130, 131 and 132 present trajectory characteristics for Run 1 of Table XVIII which was selected as a nominal run. The nominal run uses reaction controls and has no aerodynamic damping or thrust moments. A

commanded pitch rate of -10 degrees per second was used. The flaps were deflected when the angle of attack reached  $80^{\circ}$  ( $\alpha$  switch) and at this time a commanded roll rate of 15 degrees per second was introduced. Figure 130 presents time histories of angle of attack, sideslip angle and bank angle. The angle of attack definition for all the trajectories to be presented is indicated in Figure 130. The angle of attack overshoots the zero trim angle by about 10 degrees but is quickly damped out. The peak sideslip angle which is a result of coupling between motions is less than 2.5 degrees. This could be lowered by a more refined autopilot but was not believed to be necessary for this study. The vehicle reaches a maximum bank angle of 115 degrees and then decays to zero degrees. The high bank angle is a result of the turnaround maneuver. For example, an unbanked vehicle performing a  $180^{\circ}$  turnaround maneuver in the pitch plane would end up at a  $180^{\circ}$  bank angle.

Figure 131 presents the load factor and load factor direction characteristics of the nominal run. The acceleration has a peak value of 11 g's, occurring at .08 seconds and resulting from the rocket thrust. The load factor at a 90 degree angle of attack is approximately 2.3 which is within the structural load factor limits. The load factor direction results from the combination of rocket thrust and aerodynamic loads. The large changes in direction can be attributed to the turnaround motion of the capsule.

Figure 132 presents the separation distance characteristics for the nominal run. The computer program estimates the parent vehicle position by simply considering that the initial velocity vector remains constant, in magnitude and direction. Figure 131 shows positive and adequate clearance.

Using Run 1 as a basis, the effects of the following parameters on the separation trajectory characteristics were investigated:

- a) Aerodynamic damping
- b) Thrust moments
- c) Thrust gimbaling
- d) Pitch rate command
- e) Initial sideslip
- f) Initial roll rate
- g) Initial yaw rate
- h) Initial pitch rate
- i) Thrust magnitude
- j) Longitudinal center of gravity position.

The effects of varying the angle at which the flaps are opened and the commanded roll is initiated are presented in Figure 133. This figure presents time histories of the angle of attack, sideslip angle and bank angle for  $\alpha_{\text{switch}}$  values of 80 degrees, and 68 degrees. Reducing  $\alpha_{\text{switch}}$  to 68 degrees increases the time to reach the zero trim angle and decreases the overshoot somewhat. The effects on sideslip and bank angle are negligible.

The effects of varying initial conditions of sideslip, roll rate and yaw rate are shown in Figure 134. The three runs shown in Figure 134 all have three axis reaction damping and pitch, roll, and yaw attitude commands. It is seen that there are no significant effects due to these reasonable variations in asymmetric initial conditions.

Figure 135 compares the angular time histories obtained with reaction controls and aerodynamic controls. Run 1 has three axis reaction damping while Run 6 has reaction damping in yaw and roll and pitch damping from the lower flap. For both runs the flaps remained undeflected until an angle of attack of 80 degrees was achieved. Each run had a commanded pitch rate of -10 degrees per second. This command was bypassed for Run 6 until the flaps were deflected thus a faster turnaround maneuver was accomplished using aerodynamic controls for pitch control. It is seen from Figure 135 that the type of control has an insignificant effect on the pitch overshoot. The bank angle time history varies somewhat corresponding to the variation in angle of attack time history. Figure 135 also indicates the lower flap angular time history for Runs 1 and 6.

The effects of commanded pitch rate and thrust moment characteristics on the angle of attack time histories are presented in Figure 136. Varying the commanded pitch rate from 0 to -10 degrees per second has a negligible effect on the angle of attack. As expected, increasing the commanded angular rate decreases the turnaround time.

Since the rocket is located off the c.g., the c.g. varies during burning. The gimbal point is located so that the thrust vector (without damping) is directed at an intermediate point between the extreme c.g.'s. The effects of including this thrust moment with and without gimbaling are shown in Figure 136. It is seen that there is a relatively insignificant effect of thrust moments. The main effect is a slight change in turnaround time.

Figure 137 shows the effect of varying the longitudinal center of gravity on the capsule responses. The effects of center of gravity positions 1.5% of the reference length forward and aft of the nominal c.g. were investigated. Forward and aft are

measured with respect to the heat shield. The characteristics for Run 1 with the nominal c.g. are also shown in Figure 137. It can be seen from Figure 137 that the capsule is extremely sensitive to center of gravity position. Moving the c.g. forward towards the heat shield increases the capsule instability at the initiation of separation resulting in a severe turnaround maneuver with a 45 degree overshoot. This severe pitch maneuver couples with the motion in the other planes to produce an erratic roll history and a large sideslip angle. Moving the c.g. aft as shown by Run 12 increases the capsule stability at the initiation of separation such that the capsule never reaches the flap initiation angle of 80 degrees and trims at an angle of attack of approximately 115 degrees. These rather significant effects of c.g. location could be lessened by increasing the size of the reaction jets. This of course would increase the weight penalty of the control system.

Figure 138 shows the effect of thrust level, thrust deflection angle and rocket burning time on the angle of attack and bank angle time histories. It can be seen from Figure 138 that these variations change the time histories somewhat but have no adverse effects in terms of trajectory oscillations or overshoots.

Figure 139 shows the effect of the thrust variations presented in Figure 138 on the load factor and separation distance characteristics. Reducing the nominal thrust level from 25,000 pounds to 12,000 pounds reduces the initial load factor by approximately .5 and still provides adequate separation characteristics. Decreasing the thrust deflection angle from 40 degrees to 30 degrees increases the longitudinal range separation and decreases the cross-range and altitude separation. The separation distance is still adequate however.

Increasing the rocket burning time to 2.0 seconds increases the separation distance.

6.4.1.2 Complete Trajectories. Complete trajectories for the turnaround capsule from the maximum heating point of the primary flight vehicle are presented in Figure 140 for three values of wing loading. The maximum load factors obtained during these trajectories are as follows:

W/S	Load Factor	Velocity
32.6	7.26	8198
40.6	7.64	8629
73.2	8.54	9260

6.4.1.3 Aerodynamic Heating. Surface temperature characteristics were determined using the aerodynamic heating techniques presented in Section 4.0. The heat shield was analyzed in two sections. In the side view, the lower corner of the heat shield has a diameter of 0.8 feet and the heat shield diameter at the center line is 9.05 feet. Temperature histories were calculated at both locations after the vehicle had rotated to the 90 degree angle of attack position.

A swept cylinder was assumed for the lower surface. This was necessary because of shock detachment at the high angles of attack. The proper cylinder diameter was chosen by matching the swept cylinder temperature history to the lower surface flat plate temperature history up to shock detachment. A check on the peak temperature was made using the delta wing at high angle of attack theory of Bertram from Ref. 17. The thermal lag of the surface was obtained by using the unmodified aerodynamic heating program assuming a cover panel, insulation, and structure.

The flaps were assumed to be wedges with a boundary layer run of 1.0 foot.

Figure 141 gives the temperature histories of the two points on the heat shield for the nominal run after an angle of attack of 90 degrees. The dashed line represents the shift in stagnation point with the vehicle rotation. The corner temperature was approximately  $4980^{\circ}\text{R}$  for 0.2 seconds and then the heat shield face was approximately  $3330^{\circ}\text{R}$  for the remaining time. Thermal lag will suppress the corner temperature.

The results of the lower surface temperature history studies are shown on Figure 142. The temperature histories were calculated using swept cylinder theory. The 4.0 foot point temperatures are lower than the 12.0 foot point because the boundary layer was laminar while at the 12.0 foot point it was turbulent. The peak temperatures at 4.0 feet and 12.0 feet were  $3380^{\circ}\text{R}$  at 1.7 seconds and  $4315^{\circ}\text{R}$  at 1.8 seconds, respectively. These occurred when the surfaces were at 90 degrees to the flow; the vehicle angles of attack were 100 degrees and 88 degrees respectively, due to the inclination of the surfaces with respect to the body center line. The results of a check on the swept cylinder assumption at the 4.0 foot location using the theory reported by Bertram in Ref. 17 are indicated in Figure 142. It gave a temperature of  $3360^{\circ}\text{R}$ ;  $20^{\circ}\text{R}$  less than the swept cylinder assumption. Location 4.0 was also used to show the thermal lag of the surface temperature due to the presence of a finite structure behind the surface. The dashed curve shows a peak temperature of  $2945^{\circ}\text{R}$ , at 2.4 seconds. The peak surface temperature was reduced  $435^{\circ}\text{R}$  and delayed 0.7 seconds by including the thermal lag due to the structure and insulation behind the surface. A check of the structural temperature at the 4.0 foot point indicated a temperature rise of approximately 30 degrees.

Figure 143 presents the temperature histories of the flaps for the nominal run and run 6 which had aerodynamic damping. In both cases the peak temperature was approximately  $3160^{\circ}\text{R}$ .

Figure 144 presents the heat shield face temperature history for the complete escape trajectory shown in Figure 140 with a wing loading of  $40.6\text{ psf}$ . The peak temperature of  $3365^{\circ}\text{R}$  occurred during initial separation.

**6.4.2 ORBIT ESCAPE.** The initial conditions for the turnaround capsule orbit separation dynamics runs are listed in Table XIX. Figure 145 presents the angle of attack time history characteristics for orbit separation. In all cases the capsule pitches around to the desired zero angle of attack condition in approximately six seconds.

The orbit re-entry trajectories for wing loading values of  $32.6$  and  $73.5\text{ psf}$  are presented in Figure 146. The peak load factors are also presented in Figure 146. Comparing the orbit re-entry trajectories of Figure 146 with the complete escape trajectories from the maximum heating point given in Figure 140 shows that orbit re-entry will impose the most severe temperatures.

**6.4.3 RECOVERY CEILING.** The recovery ceiling characteristics of the turnaround capsule are presented in Figure 147, showing the effect of capsule wing loading. The recovery ceiling characteristics are based on a load factor limit of  $13\text{ g's}$ . The recovery ceiling of the primary flight vehicle is also shown in Figure 147. The turnaround escape capsule is seen to have a greater recovery ceiling capability than the primary flight vehicle.

**6.4.4 SUPERSONIC AND SUBSONIC ESCAPE.** Figure 148 presents the angle of attack and load factor characteristics for the turnaround capsule at the maximum dynamic pressure condition. These data were calculated using the hypersonic aerodynamic characteristics presented in Section 3. A brief investigation of the supersonic aerodynamic characteristics revealed that using these data would increase the time to perform the turnaround maneuver resulting in longer periods of time at the high load factors associated with angles of attack near  $90^{\circ}$ . Since the hypersonic aerodynamic characteristics were already curve fitted for use in the trajectory program, the trajectory was determined using these data. Since the capsule is unstable with the "sharp" nose forward, it pitches around yielding load factors in excess of human tolerance limits.



Figure 149 presents the angle of attack and altitude time history characteristics for the turnaround capsule at subsonic speeds. Data for both on-the-pad and landing approach are presented in Figure 149. In both instances the vehicle turns around by pitching down (with respect to "sharp" nose). The resulting pitching motion is poorly damped and the vehicle turns completely around. During landing approach this pitching motion results in insufficient altitude for parachute recovery.

6.4.5 PERFORMANCE CONCLUSIONS. The following conclusions are reached on the basis of the performance studies described above for the turnaround capsule:

1. Satisfactory turnaround trajectories can be achieved at the re-entry escape point and in orbit by means of a pitch maneuver.
2. Reaction controls are adequate for orbit and re-entry escape and the effects of thrust moments are negligible.
3. The lower surface experiences a transient temperature rise during the re-entry turnaround maneuver which is possibly tolerable due to the short time involved.
4. At maximum dynamic pressure the turnaround capsule experiences load factors exceeding human tolerance limits during the turnaround maneuver.
5. The turnaround maneuver which occurs at subsonic speeds makes recovery difficult especially during landing approach where insufficient altitude is achieved.
6. During the turnaround maneuver at the re-entry escape condition the load factors are less than the primary flight vehicle design load factor.

TABLE XVIII

## SUMMARY OF CONDITIONS FOR TURNAROUND CAPSULE RE-ENTRY TRAJECTORY RUNS

RUN	OL SWITH	COMMAND PITCH RATE	COMMAND ROLL RATE	INITIAL SIDESLIP	INITIAL ROLL RATE	INITIAL YAW RATE	REAR PITCH DAMPING	REAR PITCH DAMPING	REAR PITCH DAMPING	THRUST	THRUST RUGGLE	THRUST MOMENT	THRUST LINEAL	LONGITUDINAL CENTER OF GRAVITY	ROCKET BURN TIME
	DEG	DEG/SEC	DEG/SEC	DEG	DEG/SEC	DEG/SEC	DEG/SEC	DEG/SEC	DEG/SEC	FOUNDS	DEG		DEG		seconds
1	80	-10	15	0	0	0	0	0	0	25,000	40	Out	0	NOM	1.
2	68				5.73										
3	80				0	5.73									
4						0									
5				3		0									
6				0		0									
7		0													
8		-5													
9		-10													
10															
11															
12															
13															
14															
15															
															2.

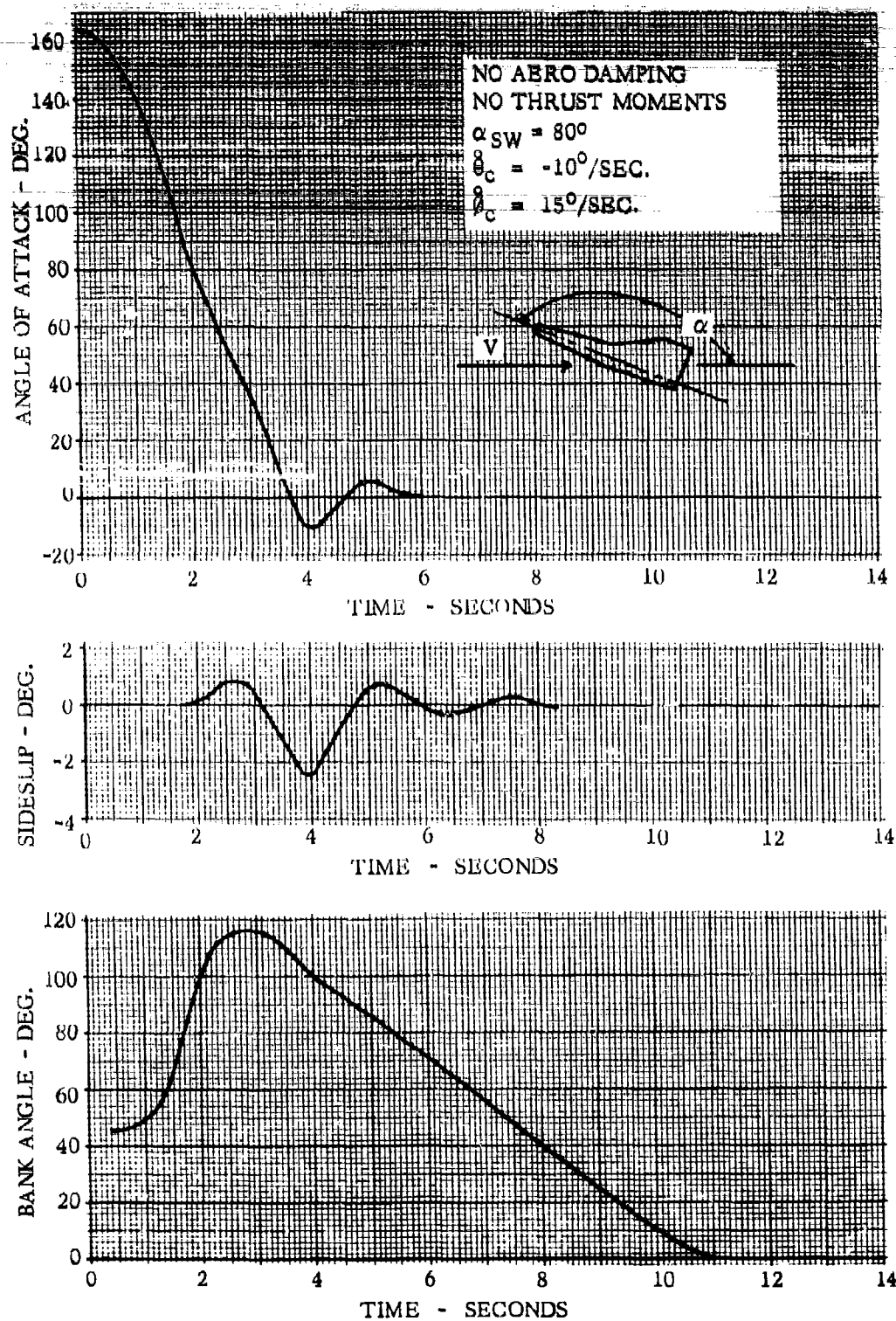


Figure 130 - Turnaround Capsule Dynamic Response - Nominal Trajectory

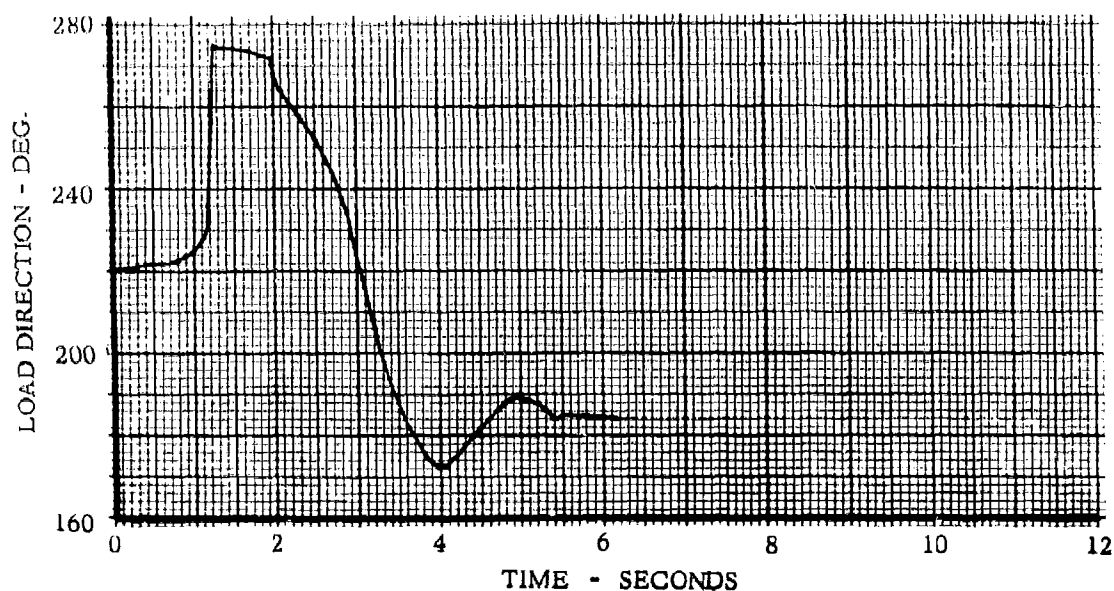
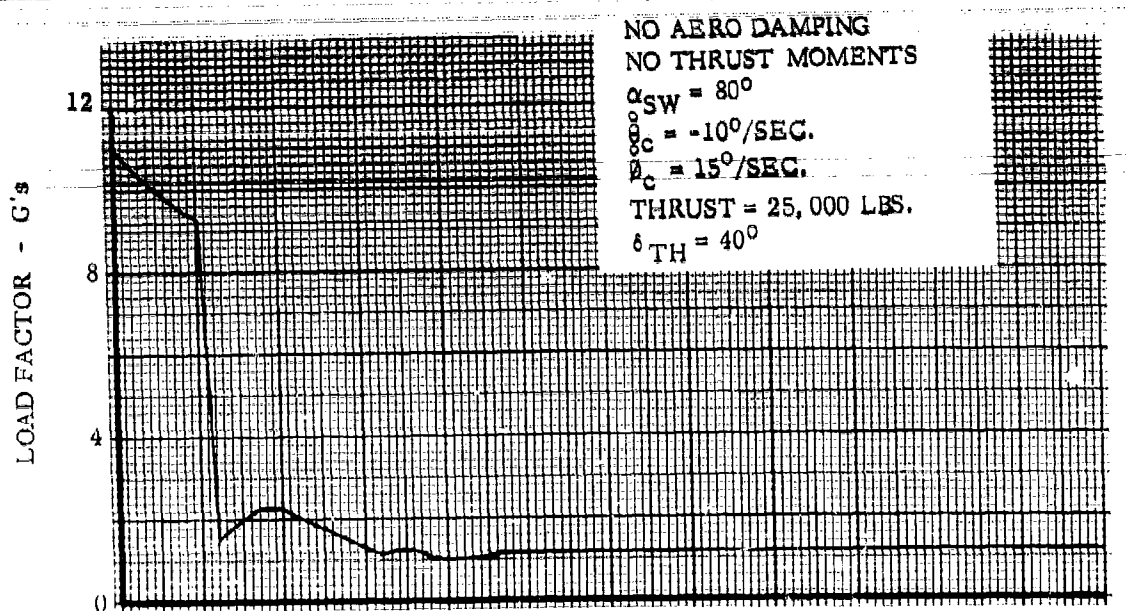


Figure 131 - Turnaround Capsule Load Factor Characteristics - Nominal Trajectory

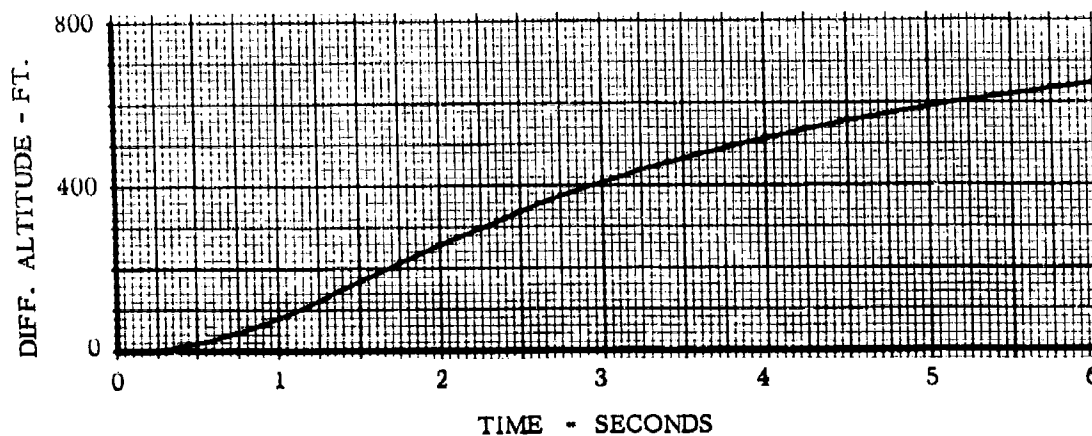
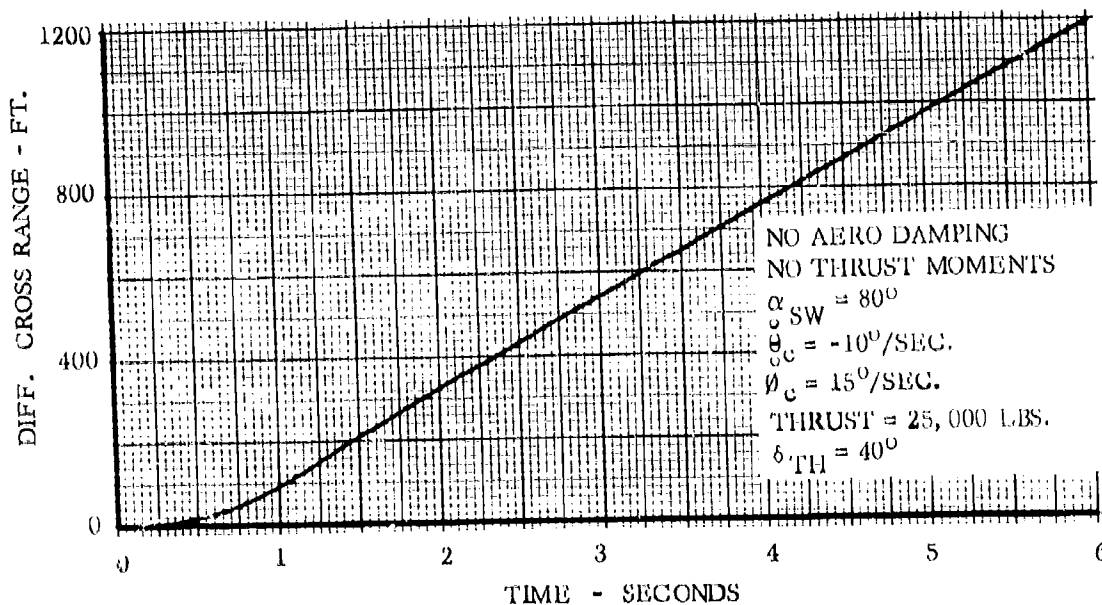
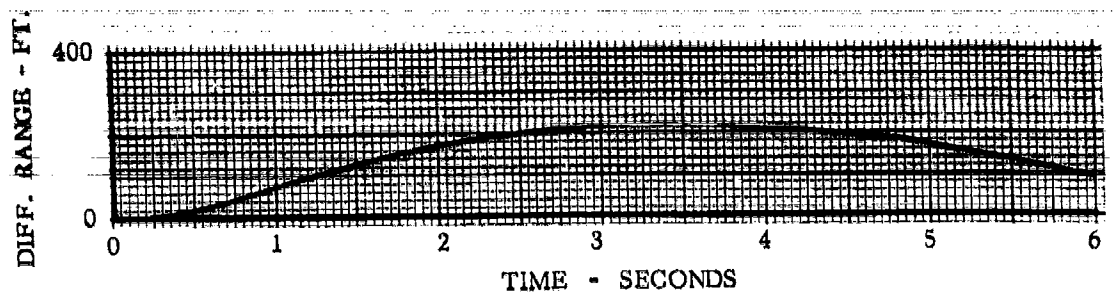


Figure 132 - Turnaround Capsule Separation Characteristics - Nominal Trajectory

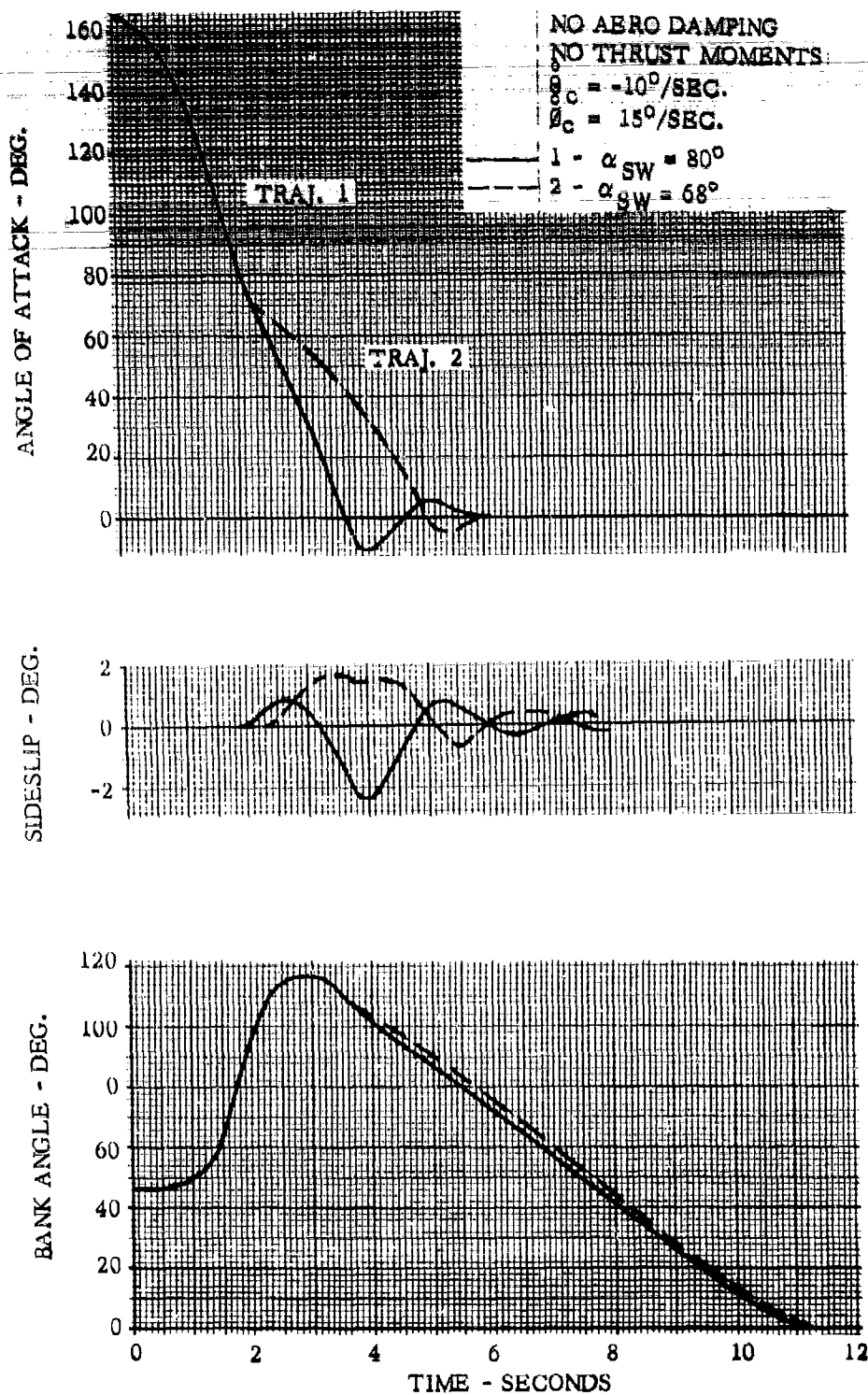
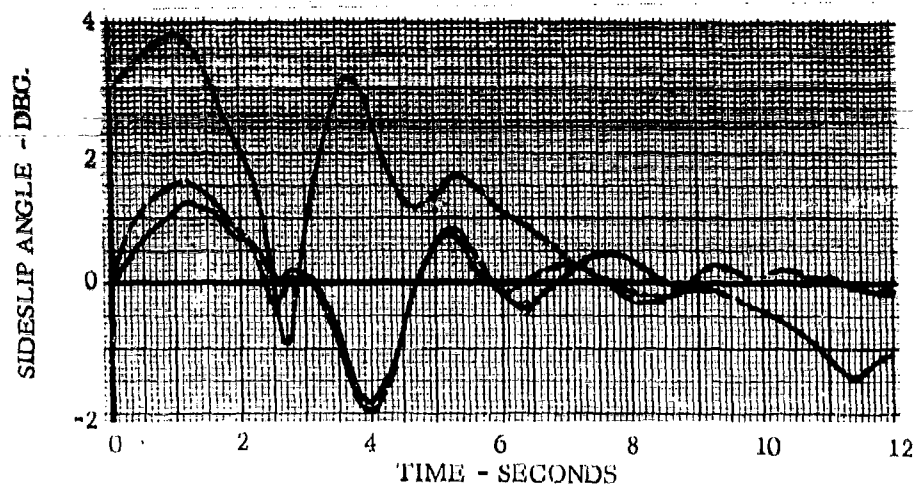


Figure 133 - Turnaround Capsule Dynamic Response - Effect of Flap Deflection Point



NO AERO DAMPING  
NO THRUST MOMENTS

$\alpha_{SW} = 80^\circ$

$\dot{\theta}_C = -10^\circ/\text{SEC.}$

$\dot{\phi}_C = 15^\circ/\text{SEC.}$

- 3 - INITIAL ROLL RATE  $\approx 5.73^\circ/\text{SEC.}$
- - - 4 - INITIAL YAW RATE  $\approx 5.73^\circ/\text{SEC.}$
- · - 5 - INITIAL SIDESLIP  $\approx 3^\circ$

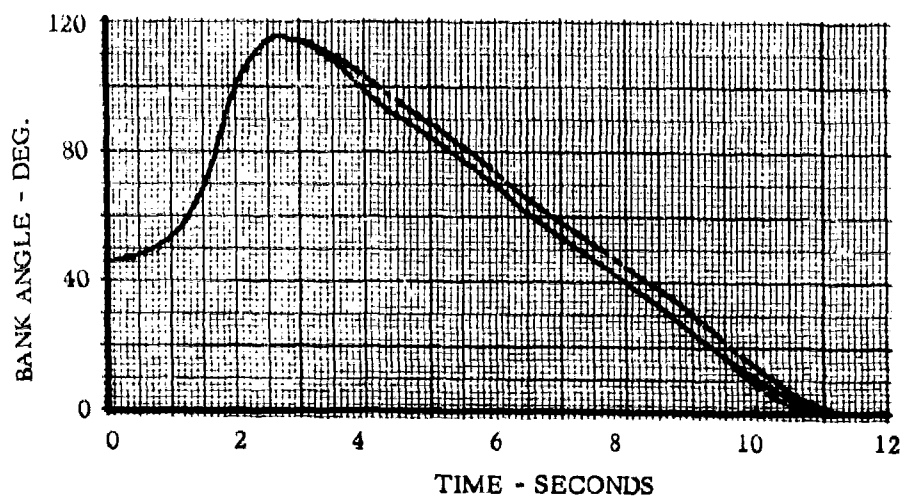


Figure 134 - Turnaround Capsule Dynamic Response - Effect Of Lateral - Directional Disturbances

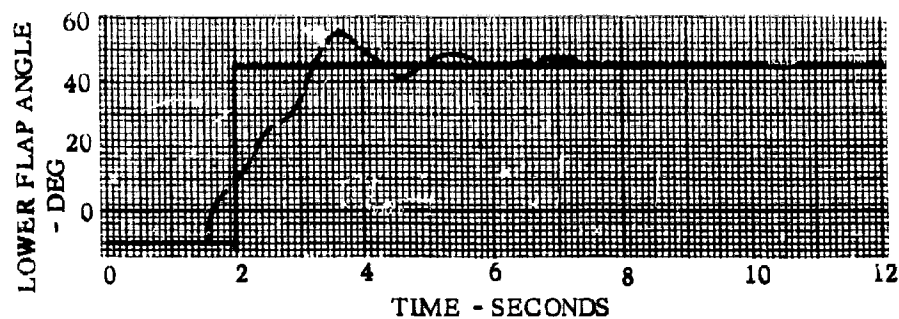
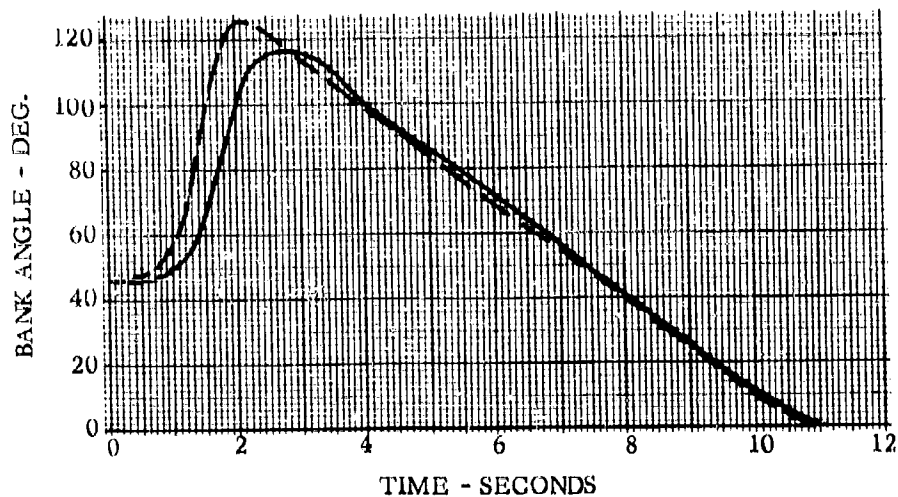
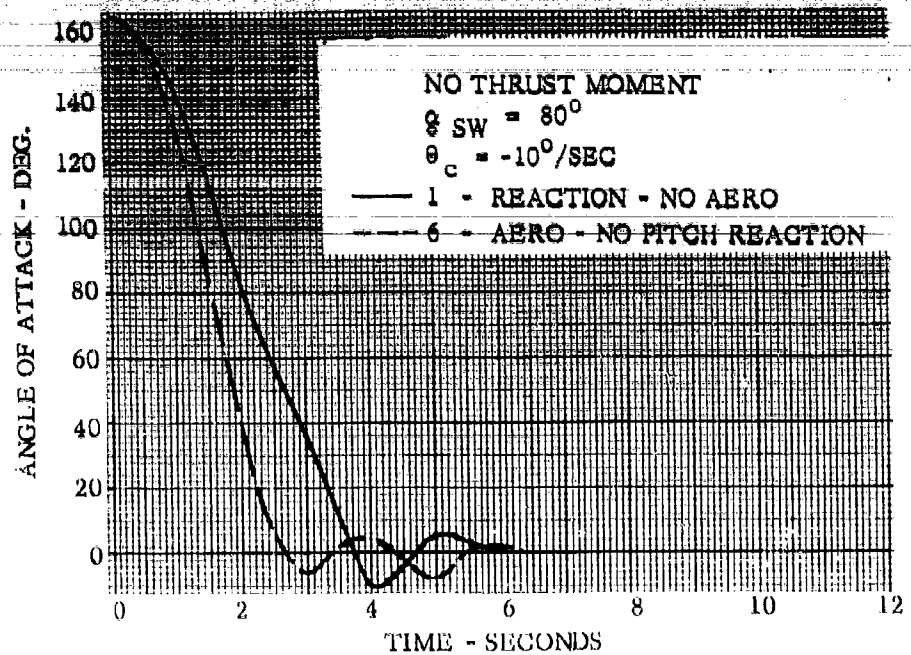


Figure 135 - Turnaround Capsule Dynamic Response - Effect of Aerodynamic and Reaction Control Pitch Damping



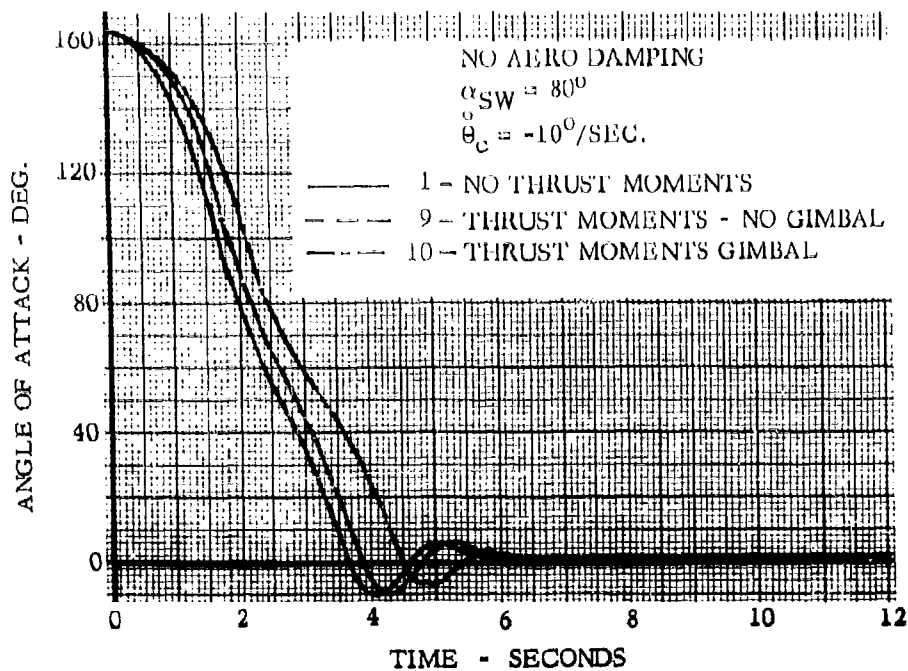
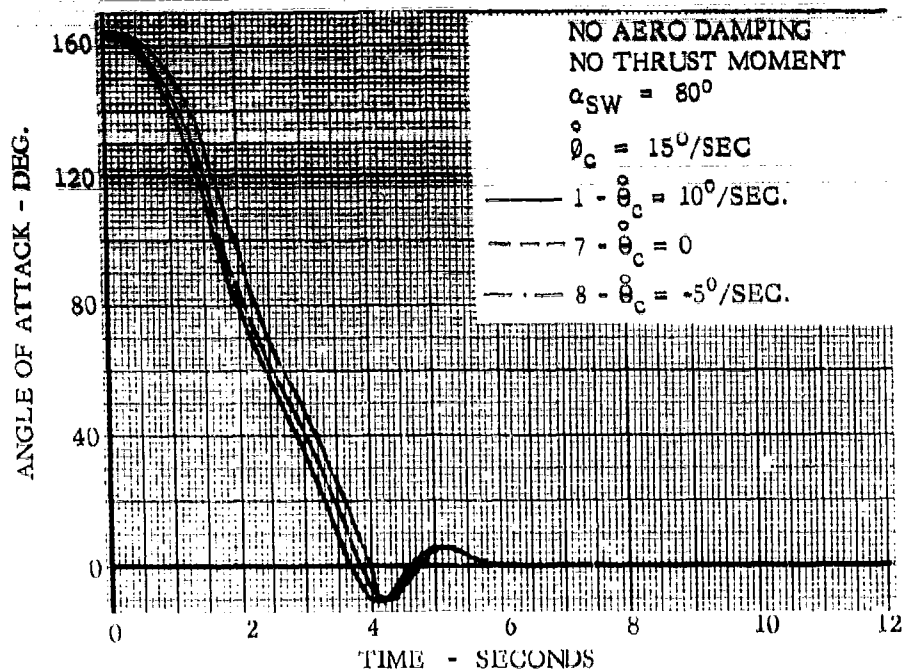


Figure 136 - Turnaround Capsule Dynamic Response - Effect of Command Pitch Rate and Thrust Moments

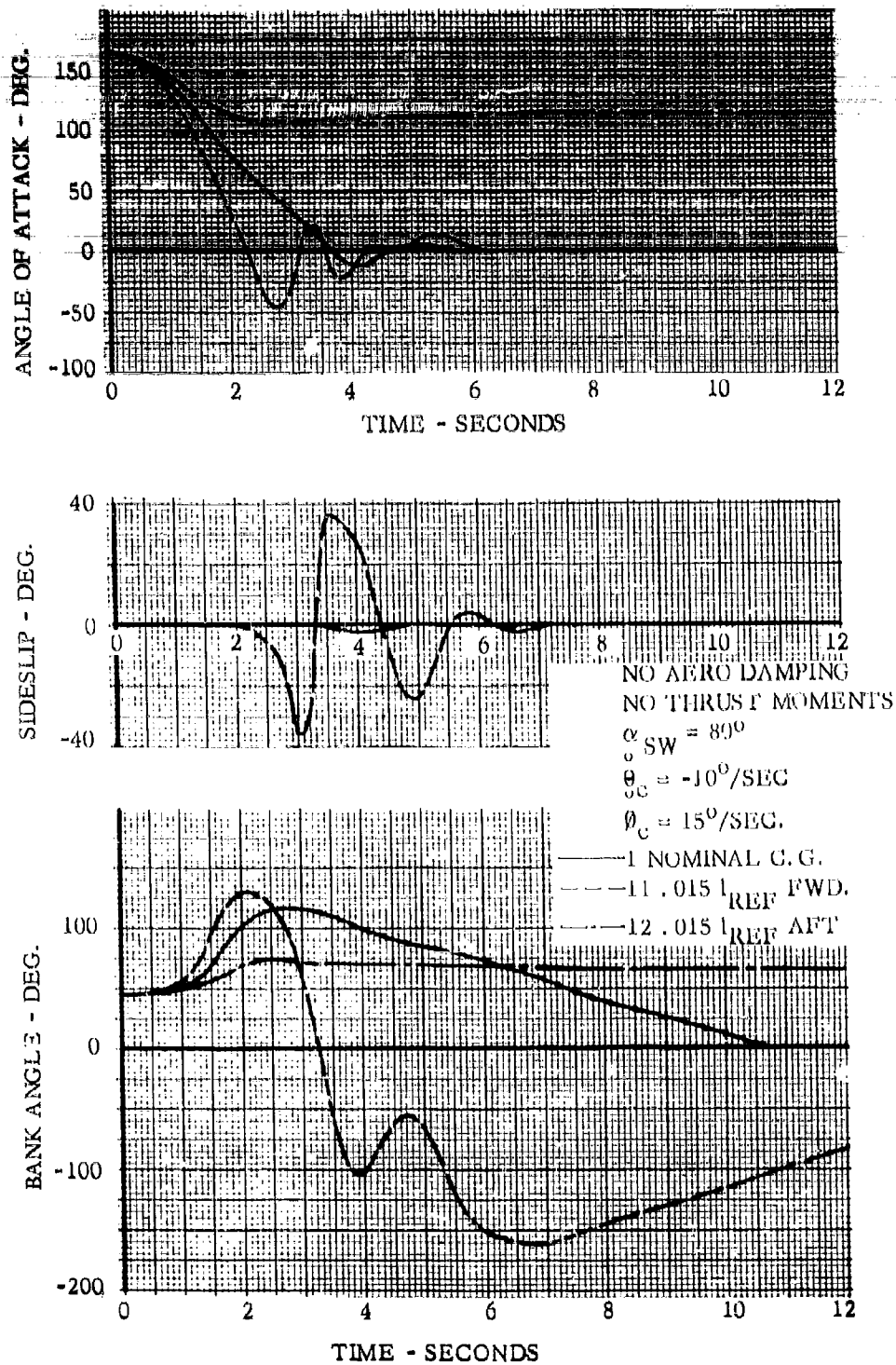


Figure 137 - Turnaround Capsule Dynamic Response - Effect of Longitudinal Center of Gravity

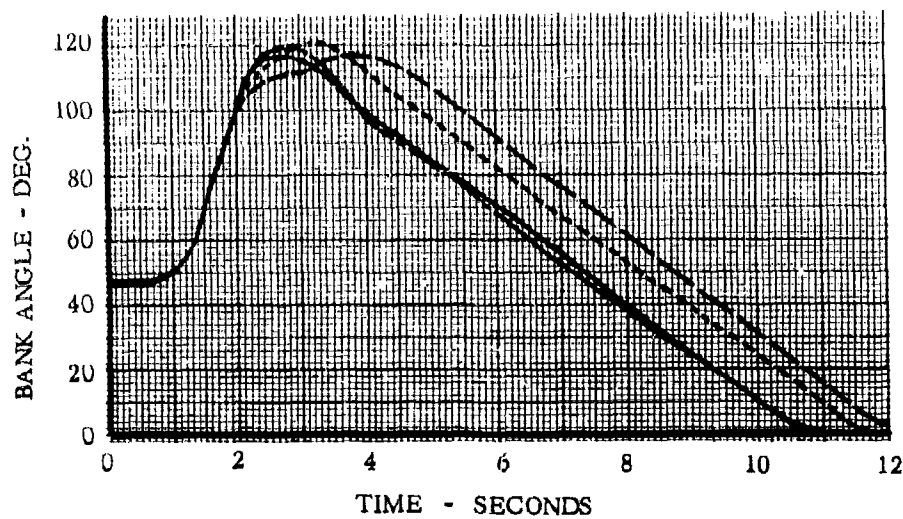
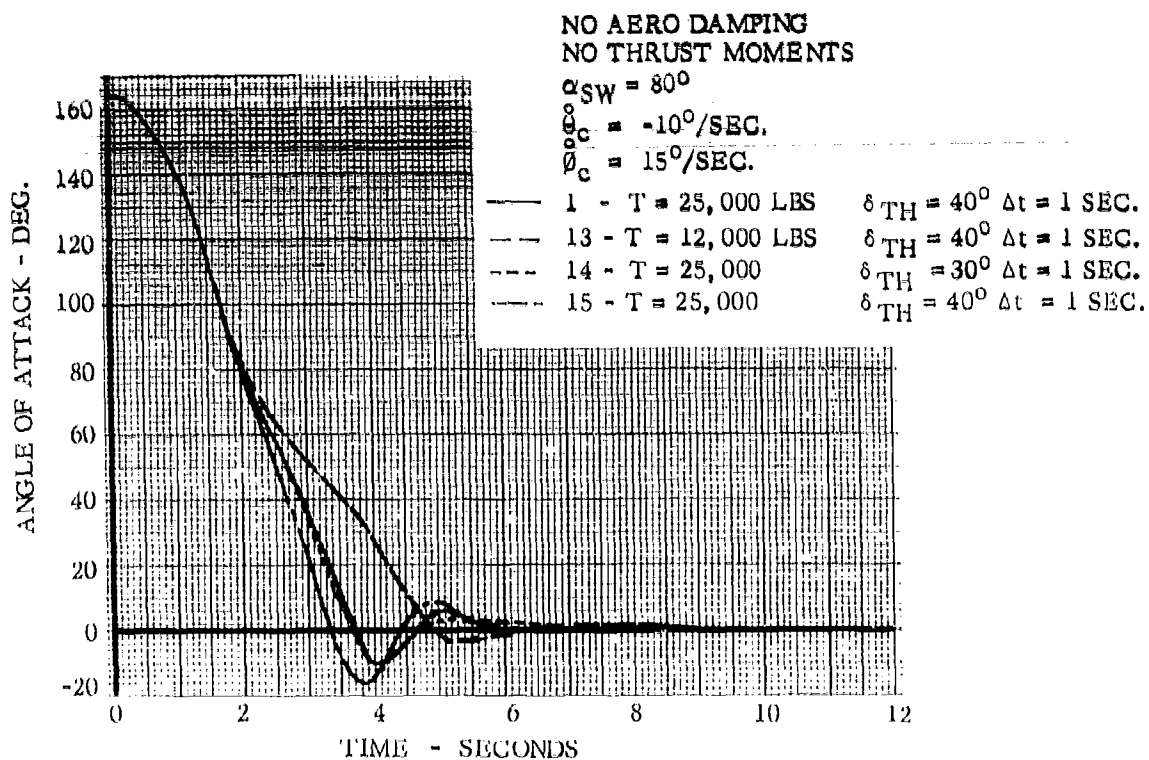


Figure 138 - Turnaround Capsule Dynamic Response - Effect of Thrust Level, Thrust Angle and Burning Time

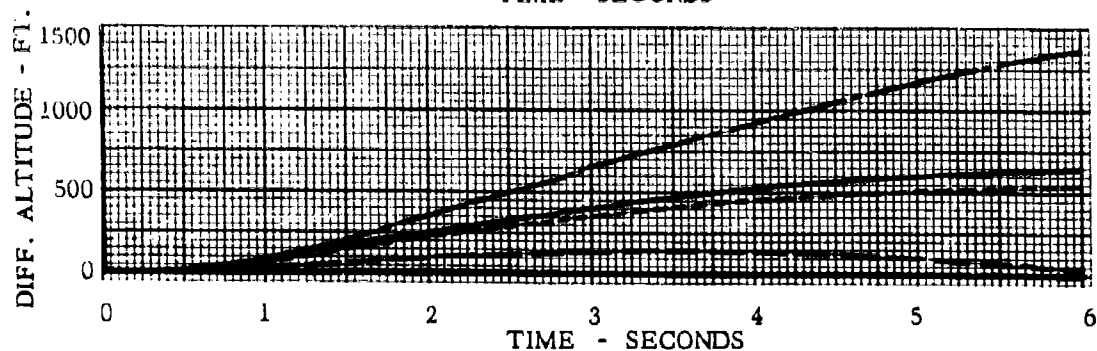
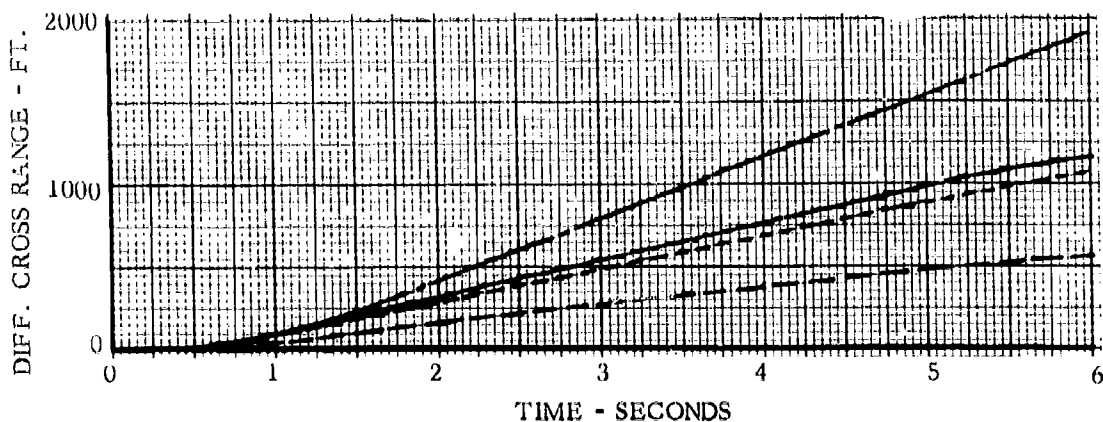
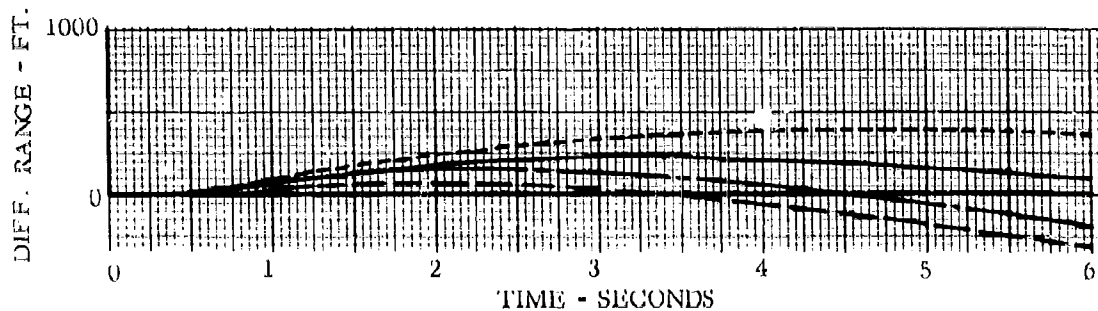
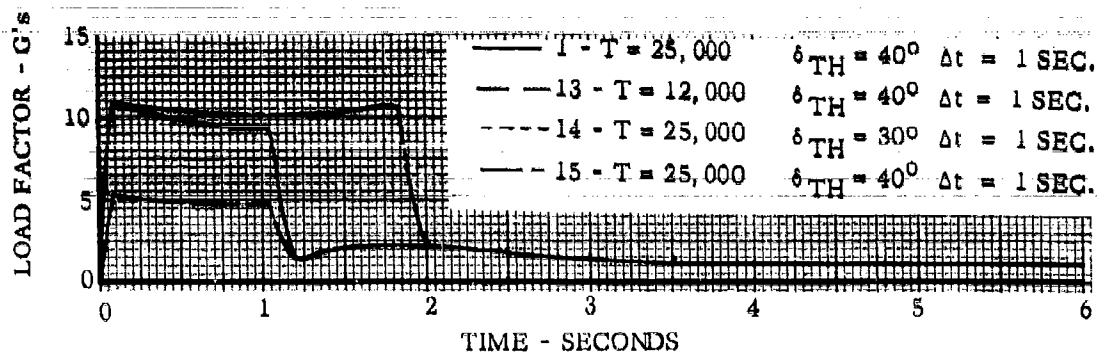


Figure 139 - Turnaround Capsule Load Factor and Separation Characteristics - Effect of Thrust Level, Thrust Angle and Burning Time

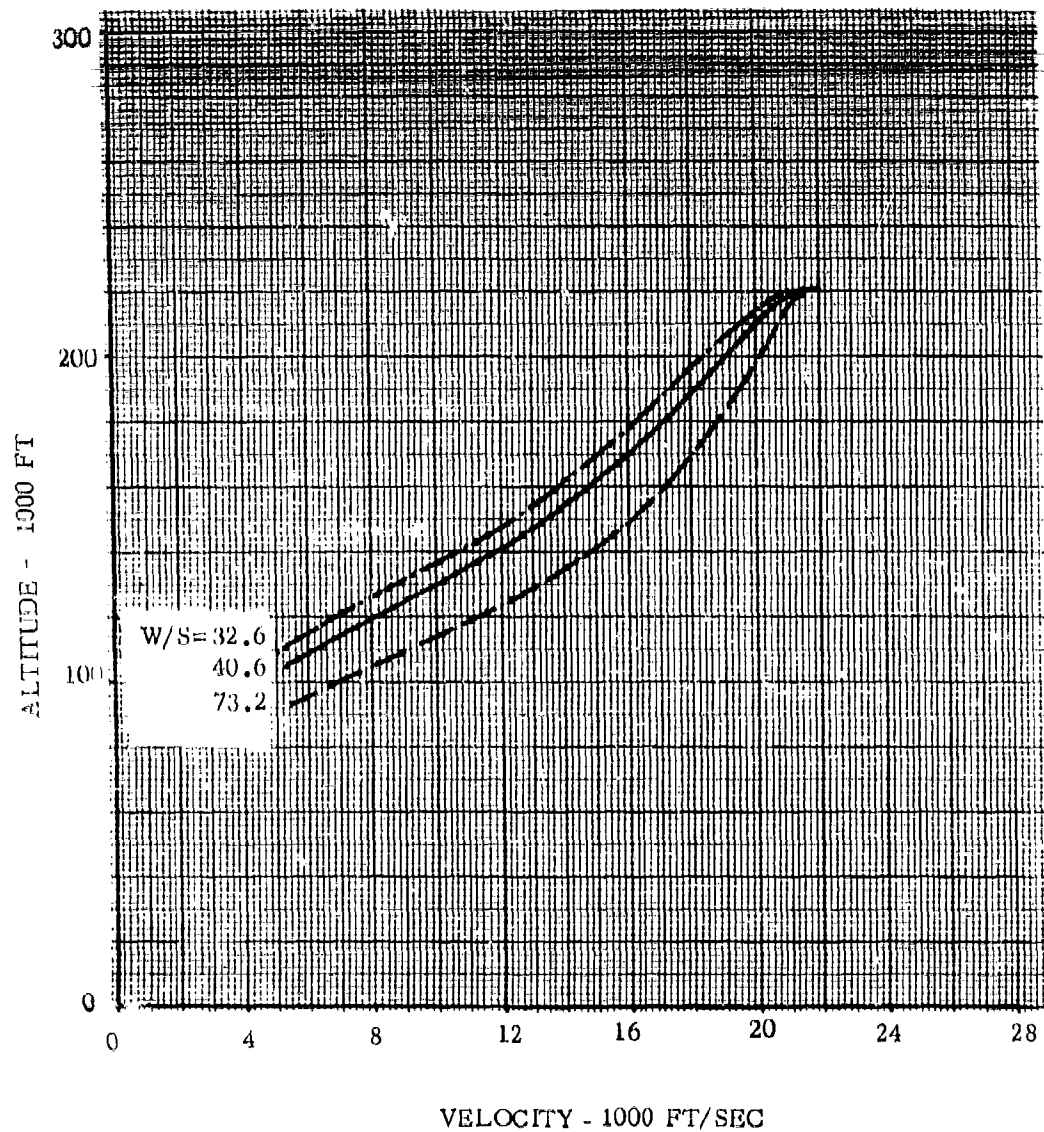


Figure 140- Effect of Wing Loading on Turnaround Capsule Escape Trajectories

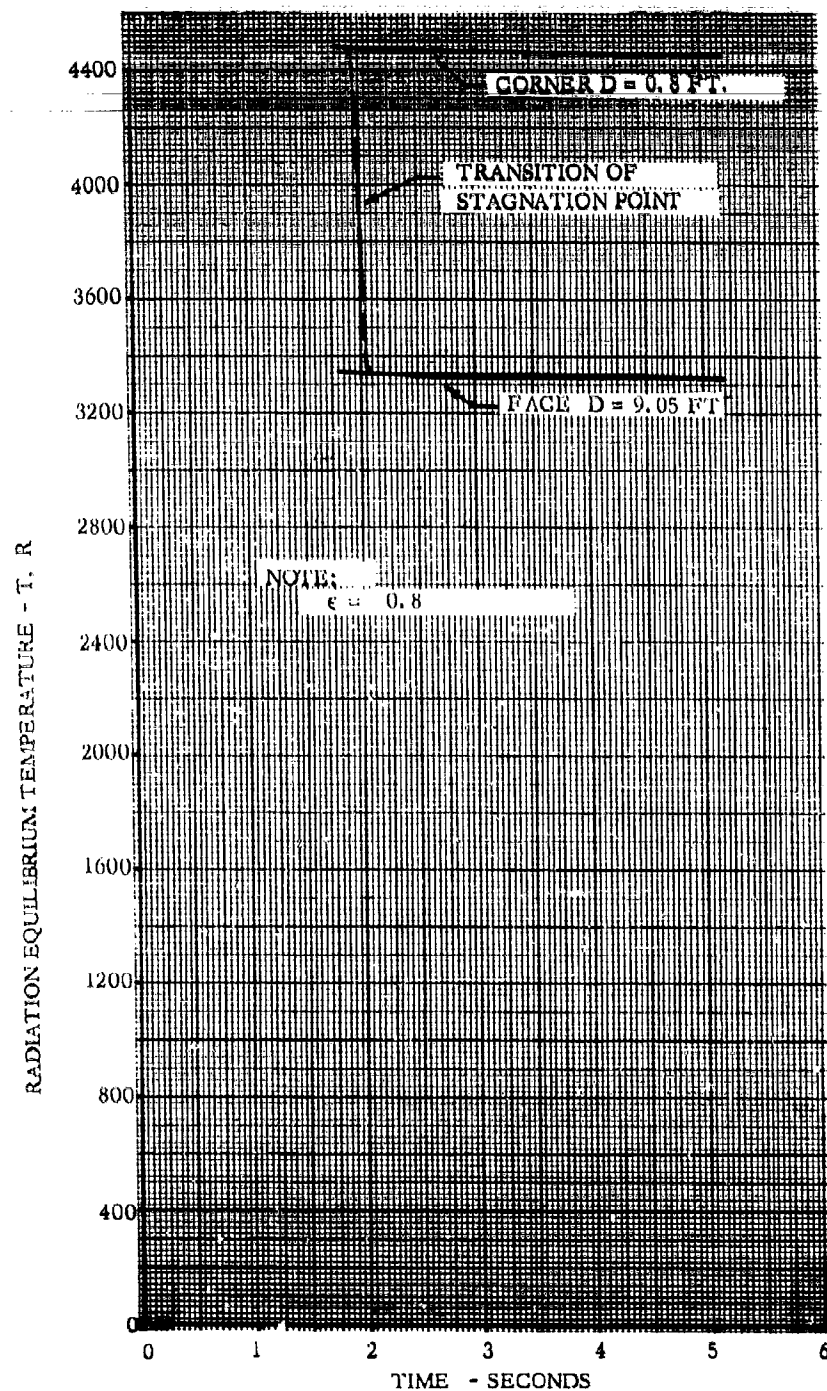


Figure 141 - Heat Shield Temperature History - Run 1 - Turnaround Capsule

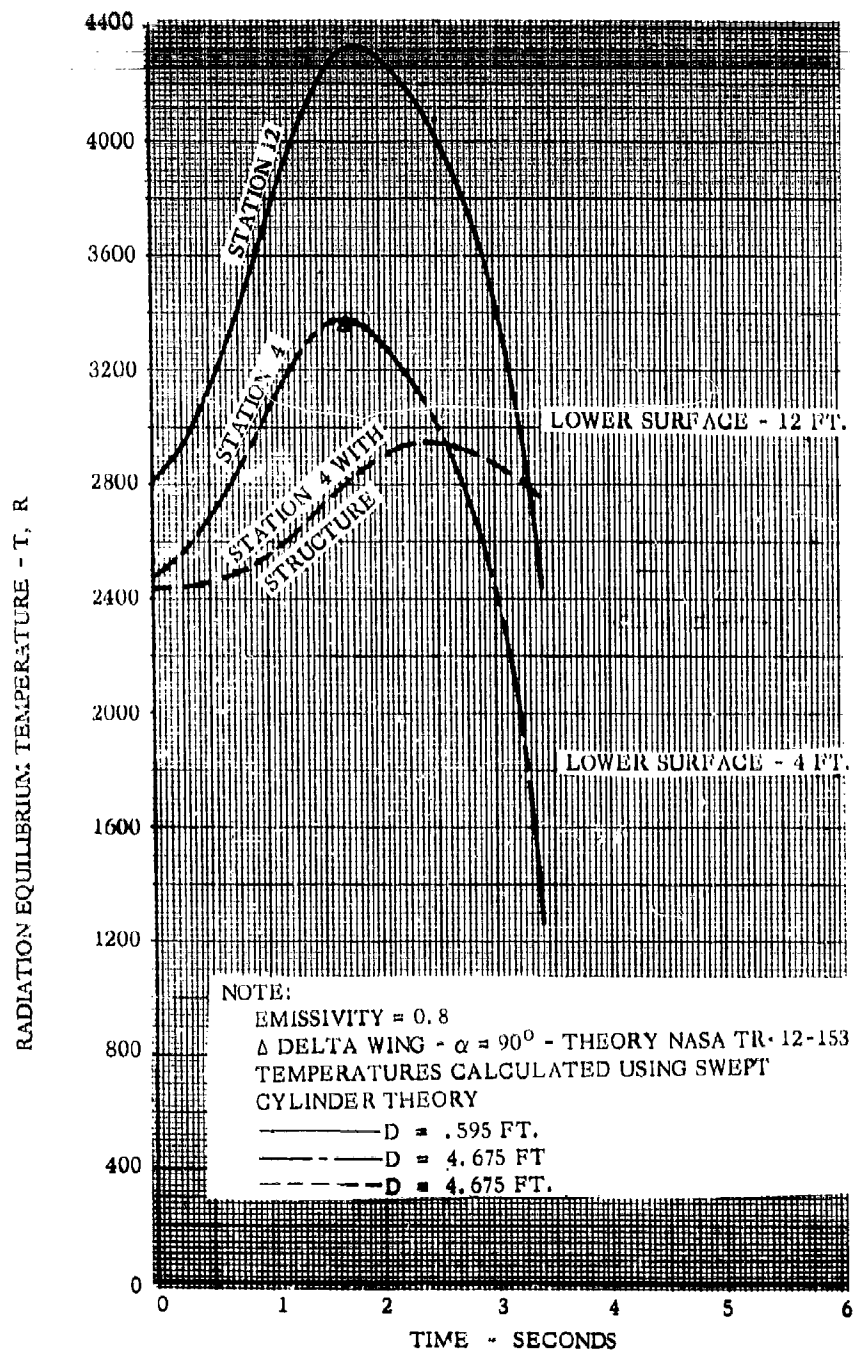


Figure 142 - Lower Surface Temperature Histories - Run 2 -  
Turnaround Capsule

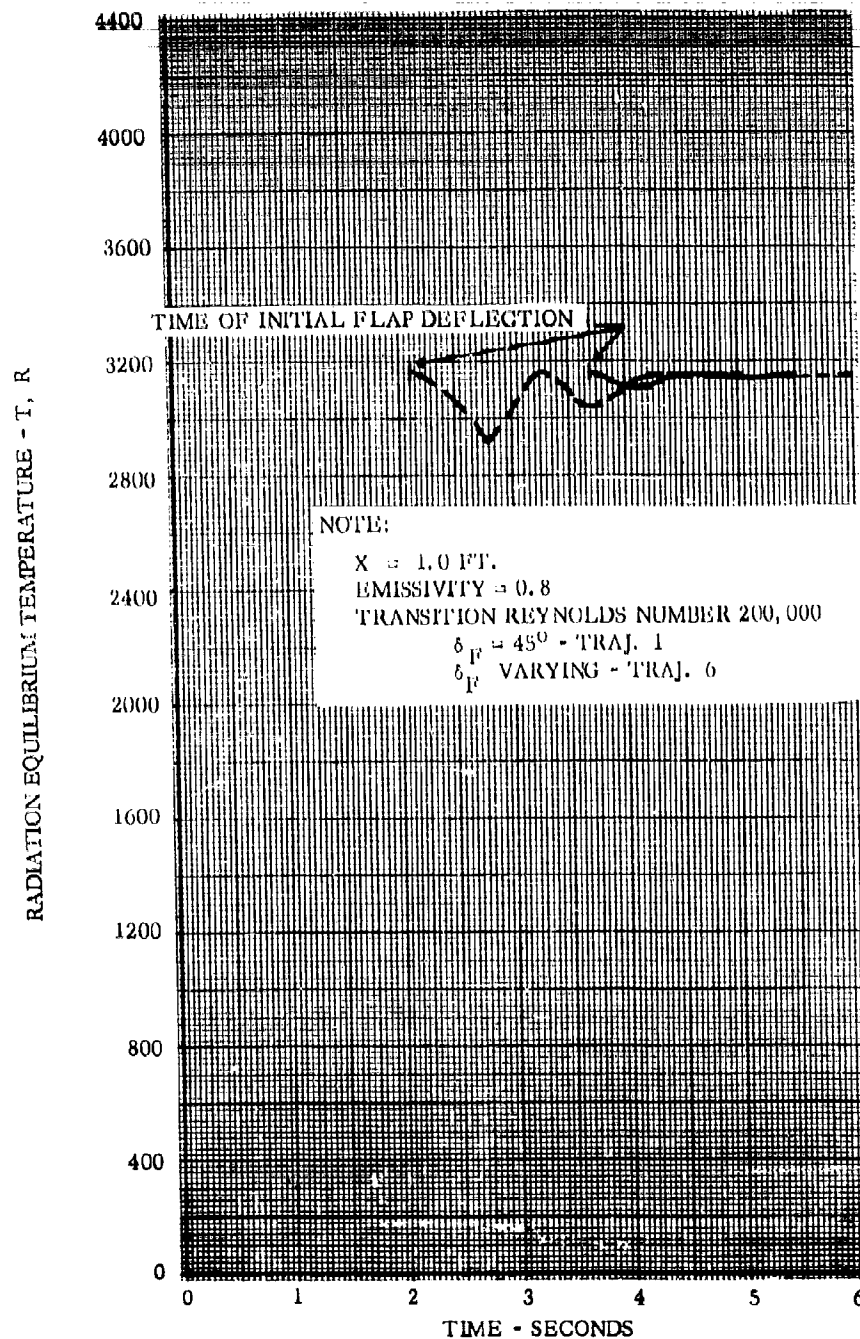


Figure 143 - Flap Temperature Histories - Run 1 and 6 - Turnaround Capsule



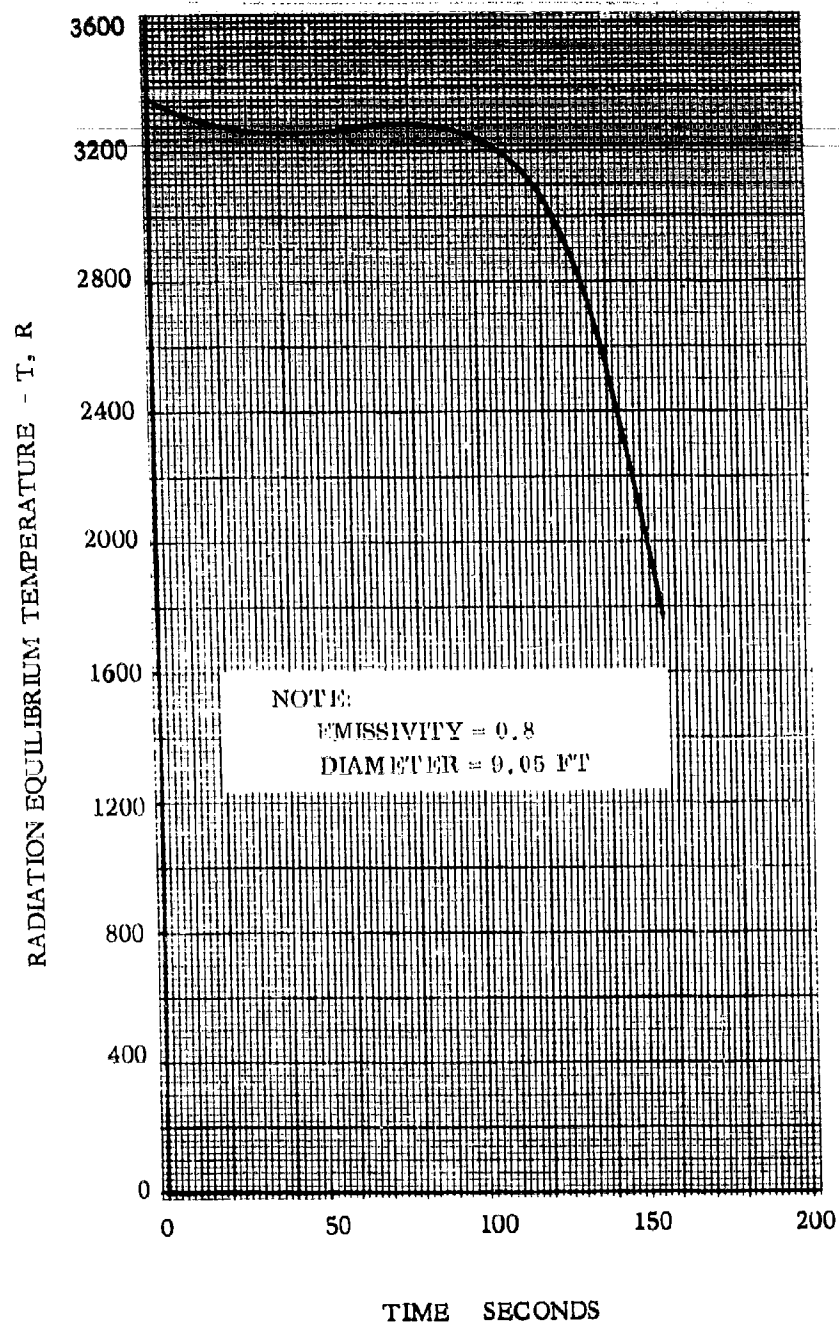


Figure 144 - Heat Shield Temperature - Long Time Trajectory Turnaround Capsule

TABLE XIX

## SUMMARY OF INITIAL CONDITIONS FOR TURNAROUND CAPSULE ORBIT TRAJECTORY RUNS

No.	$\theta_i$	$\theta_c$	$\theta_i$	REACTION	$\tau$	$\delta\theta$	THM	$\delta\theta/q$
1	180	0	-11.46	IN	25,000	40	OUT	0
2	170		0					
3	160		11.46		12,000	30	IN	.1
4	170				6,000	40		
5					25,000			
6					6,000			
7					25,000			
8					6,000			
9					25,000			
10					6,000			
11					25,000			
12								

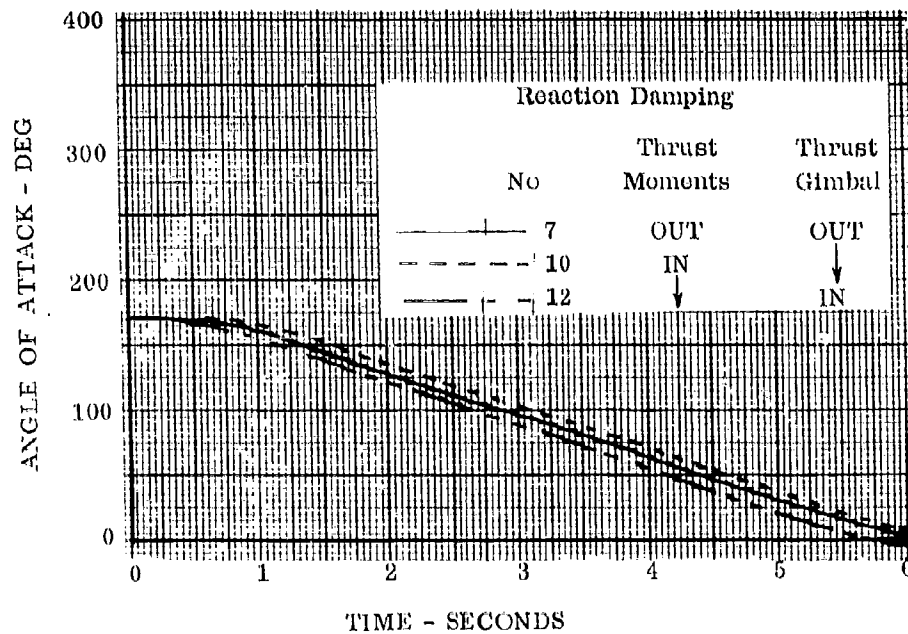


Figure 145 -Turnaround Capsule - Orbit Escape  
Trajectory Characteristics

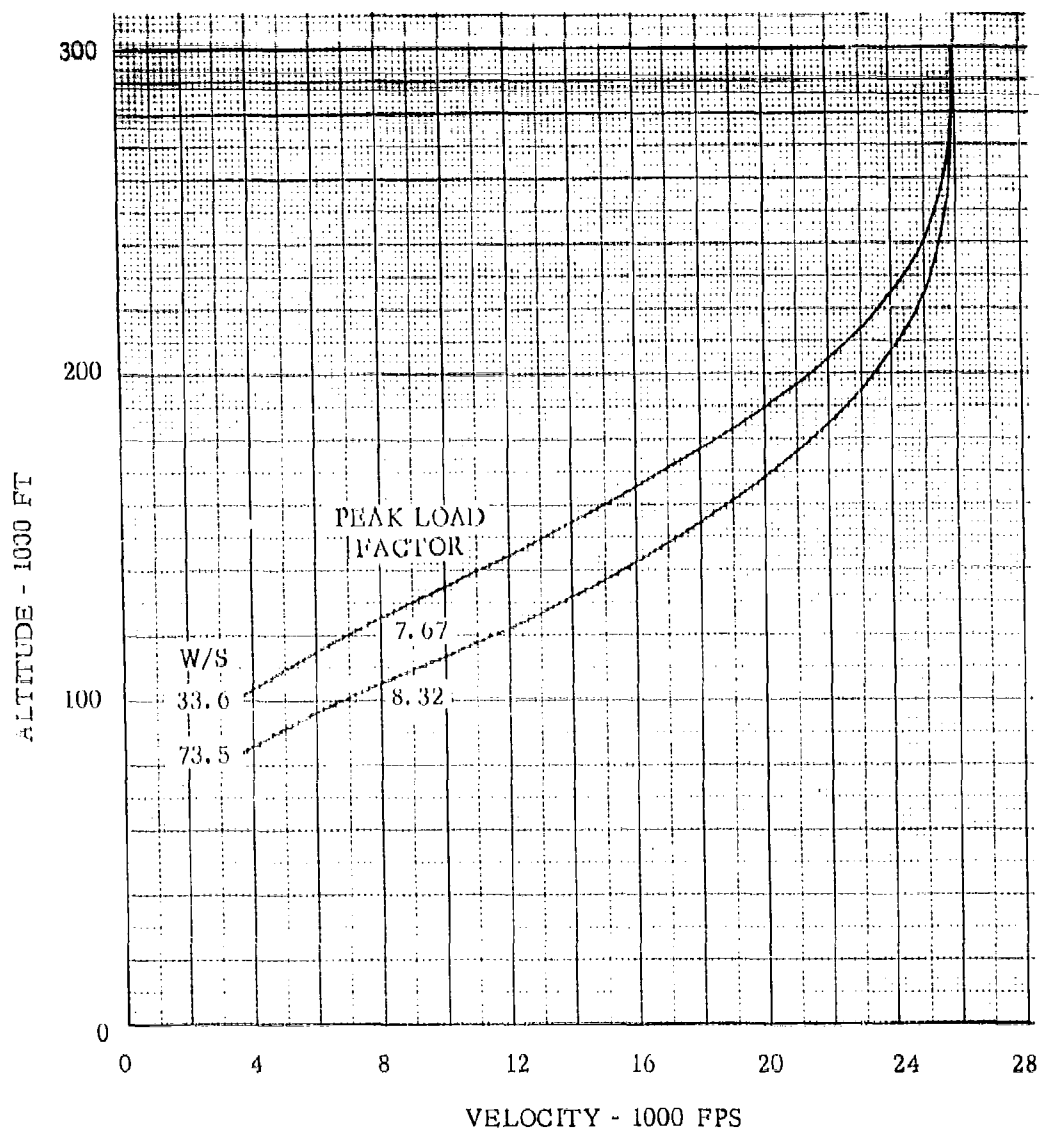


Figure 146 - Turnaround Capsule - Orbit Re-entry Trajectories

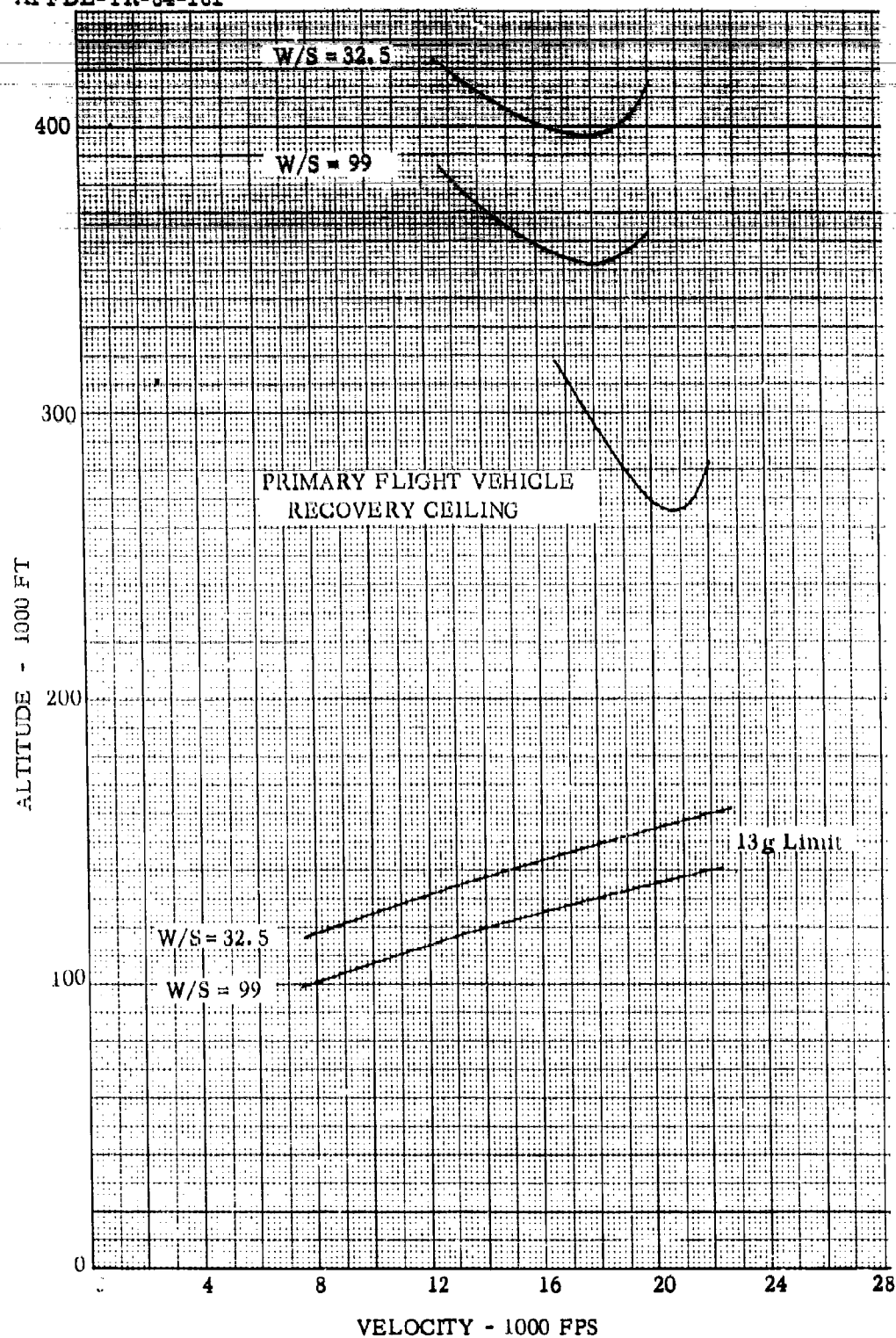


Figure 147 - Turnaround Capsule - Recovery Ceiling

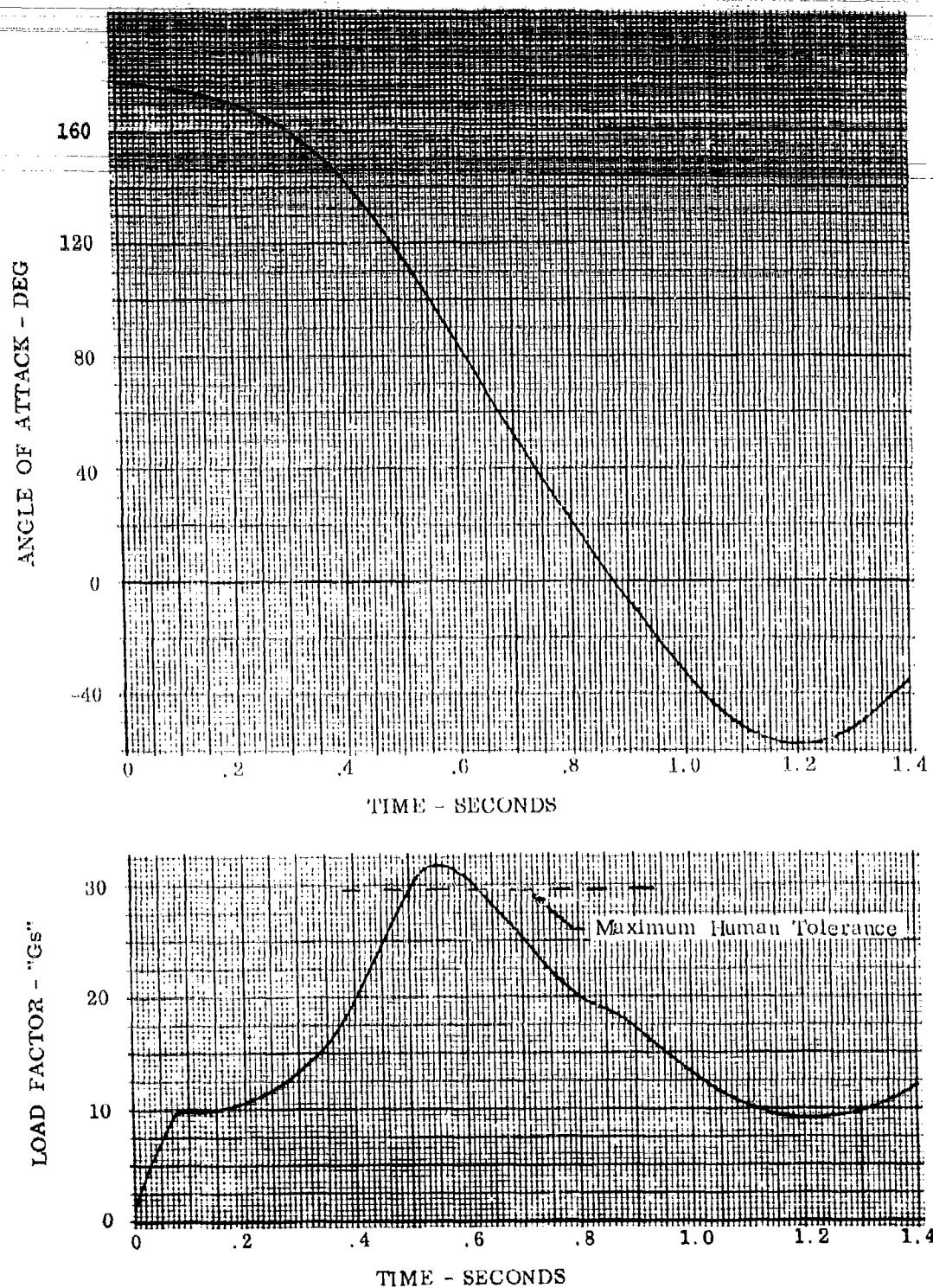


Figure 148 - Turnaround Capsule - Maximum Dynamic Pressure  
Escape Trajectory Characteristics

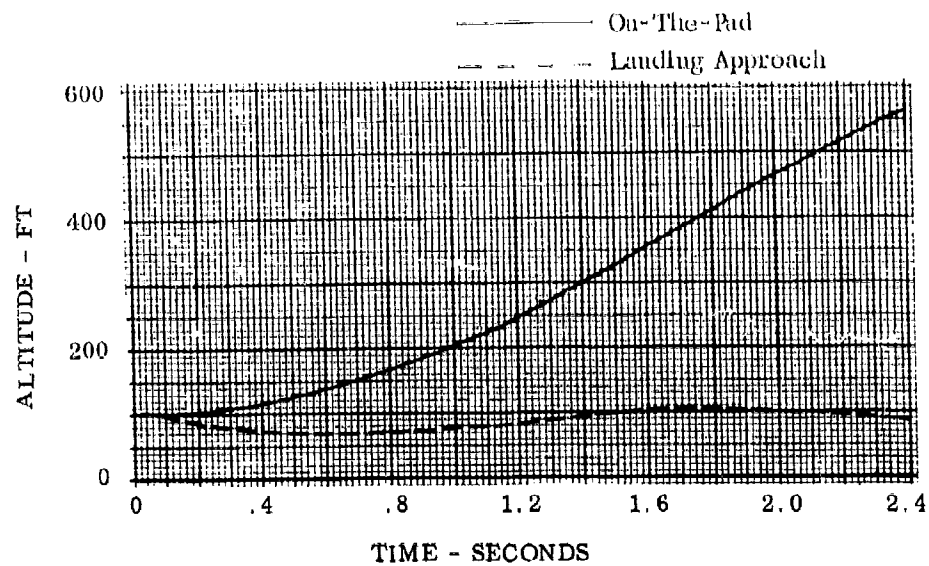
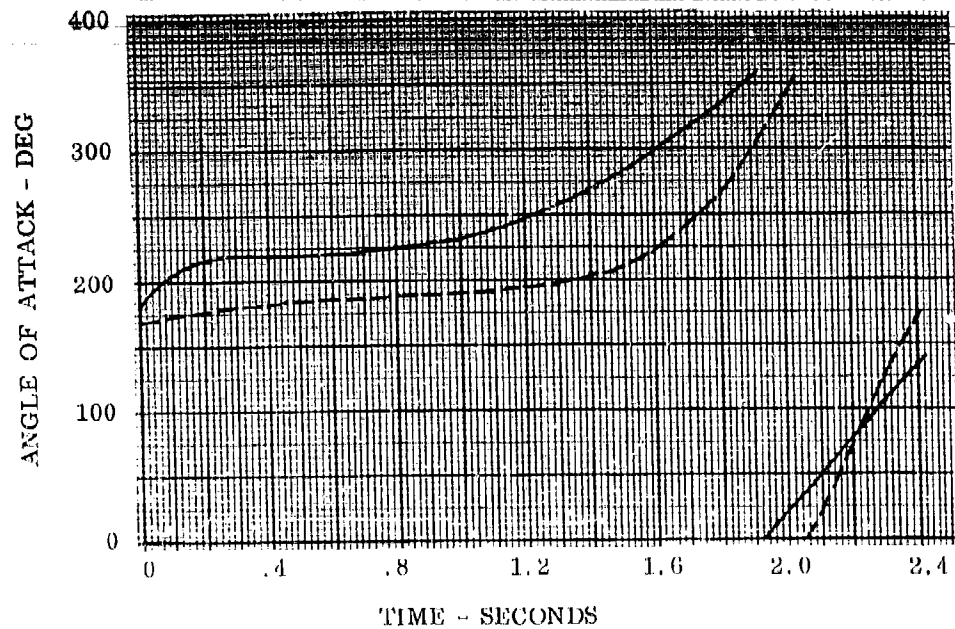


Figure 149 - Turnaround Capsule - Subsonic Escape Trajectory Characteristics

## SECTION 7

### SEPARATION INTERFACE AND DISCONNECT TECHNIQUES

This section of the report will present the results of an investigation of structural techniques applicable to the escape capsule/flight vehicle interface and associated structural and subsystem disconnects. Particular emphasis has been placed on the high temperatures associated with the re-entry into the atmosphere of the primary flight vehicle which uses a "hot truss" structure with radiation cooled external surface. Separation and disconnect devices were investigated for reliability, safety and compatibility with the high temperature environment.

In the sections which follow, general interface and disconnect criteria will be discussed and then specific applications to each of the four escape capsules will be presented.

#### 7.1 VEHICLE DEFINITIONS

7.1.1 PRIMARY FLIGHT VEHICLE. The configuration and mission of the boost-glide primary flight vehicle has been discussed in Section 2.1. The large environmental range encountered in the vehicle's operation requires the use of a wide variety of materials and structural applications. In the regime of severe heating, aerodynamic loading is relatively low but the high temperature and resulting thermal stresses impose critical design conditions at the exterior surface. Super-alloys, refractory materials and ceramics are employed to effectively withstand the temperature exposure. Radiation cooled panels are an integral part of the exterior surface. Radiation heat shielding materials are selected on the basis of low heat transfer rates when exposed for long periods at elevated temperatures.

7.1.1.1 Primary Flight Vehicle Structure. The structural concept employed in the primary flight vehicle is termed radiation cooled hot truss construction. A sketch of a typical crosssection is shown in Figure 150. The fuselage consists of two longitudinal trusses joined with cross frames and diagonals for asymmetrical loading capability. The wing spars are perpendicular to the leading edge and are of tubular truss construction. The trusses are statically determinate pin ended frames capable of transmitting axial loads, thereby relieving the bending and shear effects which occur in rigid frame structure. Fixed joints are used to reduce weight in applications where they do not create adverse structural effects.

Corrugated external skin panels transmit the aerodynamic loading to the truss members as indicated in Figure 151, and serve as radiation heat shields. These panels are not restrained along all edges which permits relative movement of the exterior surface under varying thermal conditions. Panel stiffness is provided to reduce the possibility of misalignment or gapping which can cause local hot spots, erosion, and flutter conditions. The attachment clips between the panels and the primary truss members



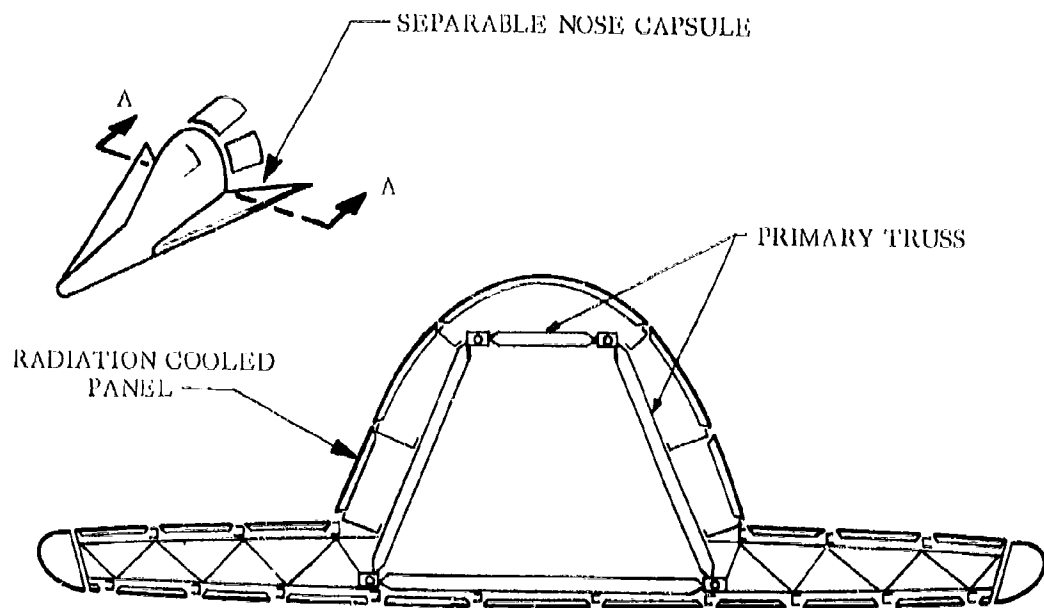


Figure 150 - Typical Hot Truss Cross Section

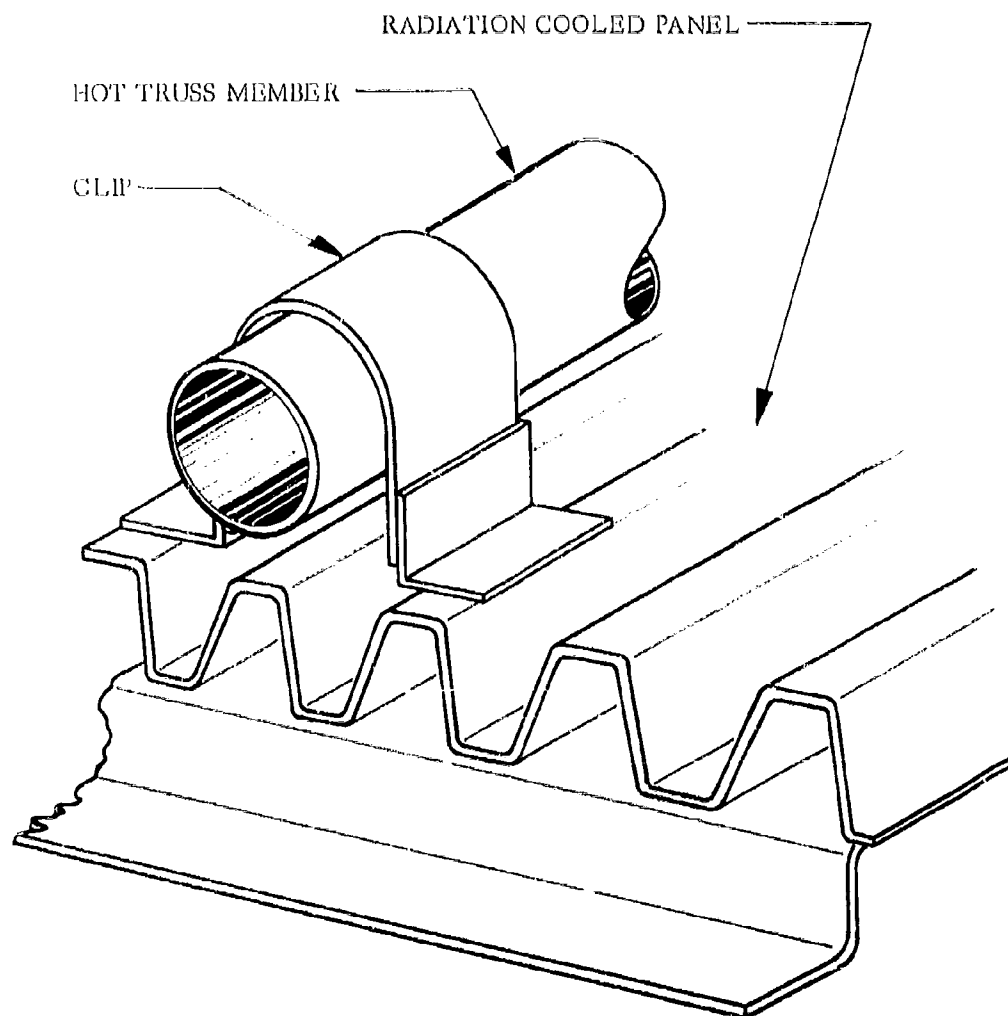


Figure 151 - Radiation Cooled Panel Attachment

provide a separation distance which aids in creating a large thermal gradient across the structure. The lower surface panels are subjected to temperatures in excess of 2000°F which requires the use of refractory alloys. These refractory alloys have high oxidization rates, well below their melting points, which requires high temperature coatings to protect them from oxidization and at the same time high surface emissivity which is the basis of the panels insulative qualities.

7.1.2 ESCAPE CAPSULE. The capsule concept provides the crew with a secondary vehicle suitable for escape at any phase of the main vehicles flight profile when required. While part of the main vehicle it serves the purpose of a control center and protective environment for the crew. For three of the capsule configurations investigated in this study it also serves as the forward portion of the main vehicle both structurally and aerodynamically. In the case of the separable pod capsule which is housed within the forward section of the main vehicle, only the upper half is subject to aerodynamic pressures and penalizes rather than contributes to the structural continuity.

7.1.2.1 Escape Capsule Structural Techniques and Criteria. The structural design philosophy is based on providing the capability of fulfilling the complete mission profile. Operational conditions expose the structure to the limits of temperature and load cycles. The critical conditions which design the capsule as a one flight item will be used to establish criteria. Stress levels used are based on an accumulated 100 hour exposure to temperature and load consistent with the main vehicle operational repeatability.

The capsule uses the same structural concept as the main vehicle, namely a determinate hot truss primary structure to which the corrugation stiffened outer radiation cooled panels are attached. The aerodynamic loads are transferred to the truss by load attachment clips as shown in Figure 151.

Attachments for all capsule concepts are made through the main vehicle structure and function as the separation disconnects, during the escape maneuver. The separable nose configurations disconnect from the primary longerons. The pod capsule and the turnaround body are amenable to alternative methods of separate carry through structure which eliminates the need for piercing ablation and heat shielding. Slip joints are formed between the capsule and main vehicle heat shields to allow disengagement at the separation interface. The thrust structure for the escape rocket is attached to the capsule primary truss and is supported to eliminate structural bending as was discussed in section 5.0. The stabilizer surface loads, and the actuator forces are reacted, into the truss structure by cross members immediately behind the pilot's compartment.

The capsule is also required to absorb the impact loads associated with the parachute landing without sustaining damage to the internal pressurized compartment or experiencing accelerations and/or load factors beyond human tolerance. This is accomplished by the use of attenuation devices such as frangible structure, inflatable bags, or shock struts.

For escape capsules the structural load factor for design is established on the basis of performance requirements which dictate the use of escape rockets applying a load factor in the range of 10 to 20 "G's". These separation loads override any maneuver or gust loads occurring either during escape or normal mission operation. The design structural load factor would therefore be the separation thrust loads increased by a factor of safety such as 1.5 which is a standard value for manned systems.

The capsule truss structure is protected from the high temperature environment either by external radiation cooled panels or ablation heat shields. The type of thermal protection can vary over the surface of the vehicle since the temperature distribution varies around the vehicle. The external surfaces experience temperature ranging from 1500°R on the upper surfaces to 4500°R on the nose. The thermal gradient across the surfaces results in truss structural temperatures between 1500°R and 2000°R.

The pilot's pressurized compartment is honeycomb construction, cooled by a transpiration insulation system which utilizes a wick blanket and passive water wall heat sink, with overboard steam venting. Radiation panels and thermal protection is provided for windows and escape hatches. This controlled environmental enclosure has stowage space for survival equipment, parachute and any propellant actuated devices. The pressurized compartment is supported from the main vehicle truss structure on a frame to minimize thermal and vibration transfer.

## 7.2 SEPARATION INTERFACE

7.2.1 DISCONNECT AND SEPARATION TECHNIQUES. During normal flight operations the escape capsule serves as a functioning portion of the primary flight vehicle. As such it is connected to the primary flight vehicle both structurally and with subsystem lines. The disconnect and separation techniques refer to the methods employed to effect separation between the escape capsule and the primary flight vehicle. The objective of these techniques is to accomplish the disconnect operation with the highest reliability, lowest weight and performance penalties without incurring damage to the escape capsule.

The primary separation force is applied by the escape rocket. This is a common element of all escape capsule systems and will not be discussed herein under disconnect and separation techniques. Details on escape rocket sizing, design and installation have been discussed in Section 5.0.

During all phases of the vehicle operation the separation and disconnect fittings transmit the structural loads across the separation interface without imposing restriction during the escape maneuver. In the escape mode structural attachments, controls, electrical power and environmental supply lines are disconnected quickly and positively.

The choice of disconnect and separation techniques is influenced by the escape capsule and primary flight vehicle configurations, the structural concept and the mission or flight environment. In the present study the primary flight vehicle is a hot truss radiation cooled boost glide vehicle. This type of construction which has been discussed in detail in Section 7.1 precludes the use of the skin as a basic structural element and dictates that the structural connection be made using the hot truss structure. The hot truss structure concept introduces cooling problems in regard to the use of explosive disconnect devices and also leads to relatively large structural deflections resulting from thermal stresses. Allowance must be made for thermal deflections in selecting disconnect and separation techniques.

The mission of the primary flight vehicle imposes three escape maneuver phases on the capsule. The re-entry phase and associated high temperature problems discussed above, on-the-pad-escape during launch, and escape when exposed to high dynamic pressure. These mission phases are related in the selection of disconnect and separation techniques since they produce critical loading conditions.

The lifting body and ballistic body escape capsules are attached to the main vehicle on a separation interface without further structural encroachment or attachment and as such reduce the adverse effects of thermal deflections in comparison with the turnaround capsule and separable pod capsule. These latter two capsules are submerged or partially surrounded by the primary vehicle structure and are affected more by thermal deflections. In addition, the use of ablation materials in the interface region on these two capsules reduces the area available for capsule/vehicle attachment.

The above paragraphs have introduced some of the problems which must be considered in selecting disconnect and separation techniques for the capsules and vehicles of the present study. The proposed solutions to these problems for each of the four escape capsules of the present study will be discussed in Section 7.3.

An important consideration in regard to separation techniques is that of separation guidance. The main advantage of separation guidance is that it insures a constant separation direction under all escape conditions thus reducing the chance of binding and consequent damage to the escape capsule. Also, with guidance the separation force can be used to disconnect subsystem lines since the separation direction is constant.

Guidance is not achieved without structural penalties. Reinforcement of the back-up structure is required to react forces normal to the guides, produced by the thrust and aerodynamic forces. Aerodynamic moments and those produced by thrust

at separation are reacted by the structure or by the rotational inertia of the capsule.

The use of guides influences the separation interface in that the guide loads can be minimized by proper orientation of the interface. The normal loads on the guides should be kept low since they produce a friction force which tends to resist separation.

The application of separation guides to the escape capsules under consideration will be discussed in Section 7.3.

**7.2.2 DISCONNECT DEVICES.** Within this program the equipment required to effect separation and disconnect of an escape capsule from the prime flight vehicle is discussed as structural or subsystem disconnect. Structural disconnects separate the structural tie between pod and primary flight vehicle. Subsystem disconnects are those which separate the controls, electrical power, and environmental supply lines at or near the interface. Disconnect devices may be either mechanical or pyrotechnic with the initiation being from mechanical, gas or pyrotechnic source.

A review of previous disconnect system studies was made, e.g. Refs. 18 and 19. The results presented in these references are not completely applicable due to differences in environmental and loading conditions. The unique factor of the present study with regard to disconnect systems is that the devices must be capable of operating in a temperature environment ranging from  $-65^{\circ}\text{F}$  to approximately  $1500^{\circ}\text{F}$ .

**7.2.2.1 Explosive Devices.** The performance reliability of explosive disconnect devices strongly influenced an investigation of their possible application as a separation device. A survey of the possible techniques which could be applied included low energy detonating chord (LEDC) and flexible linear shaped charge (FLSC). The problem involved with the use of pyrotechnic devices is the high temperature environment associated with the hot truss structural concept. Pyrotechnic devices capable of withstanding this high temperature environment are not within the present state-of-the-art. Organic explosives have temperature limits in the range of  $200^{\circ}\text{F}$  to  $400^{\circ}\text{F}$ . Development studies to increase the temperature capability are being conducted. Inorganic explosives having high temperature capability do exist however. Their use in separation devices has not been explored. Two of the principal problems of inorganic explosives are that they are difficult to ignite and react with very high temperatures.

Since the primary problem associated with explosive disconnect devices is the temperature problem, a brief investigation was made of the insulation requirements for an organic explosive. It was assumed that the temperature history of the

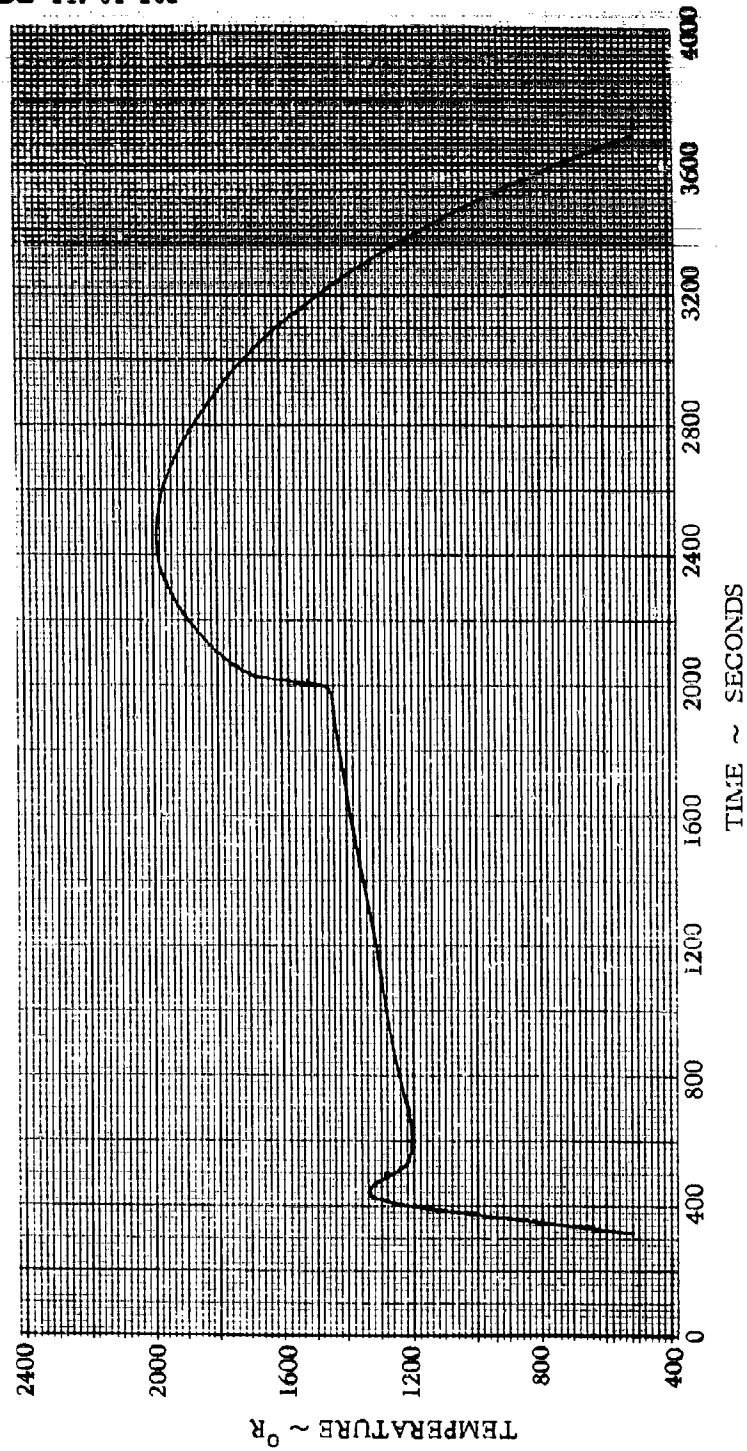


Figure 152 - Structural Temperature History at Explosive Disconnect

detachment location followed the basic Rene' 41 structure temperature history presented in Figure 152. The MinK-2000 insulation was considered in direct contact with the structural member. The shaped charge was considered as a slab. Figure 153 shows the heat transfer model.

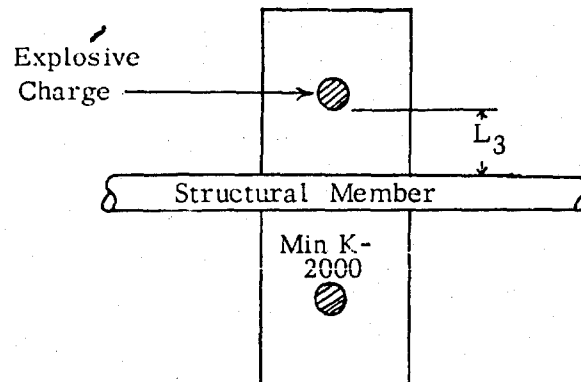


FIGURE 153. EXPLOSIVE CHARGE HEAT TRANSFER MODEL

The distance  $L_3$  which is required to protect the explosive from the hot structural member was also considered sufficient to protect the charge from radiation heat transfer from the surroundings. Hence the charge will be completely surrounded with Min K-2000 on all sides. The propellant material properties used in the rocket heating analysis discussed in Section 5.0 were also used for the explosive.

The insulation requirements analysis was performed in the same manner as the study performed for the separation rocket motors and discussed in Section 5.4. It was determined that the explosive charge should be surrounded on all sides by 1.0 inch of the Min K-2000 insulation.

These insulation requirements are not severe, however, the model which was used is typical of a shaped charge in which it is possible to isolate the charge from the structure thus greatly simplifying the insulation problem. The use of a shaped charge would eliminate the possibility of separation guidance along the primary structural members. In this case separate guides with their resultant weight penalty would be necessary. The insulation of structural disconnect devices such as explosive bolts which allow for guides on the main structural connection would be more severe due to the compact and complex nature of the design.



For the present study it was decided to exclude explosive devices from further consideration and use mechanical disconnects for structure and subsystems.

Explosives are used, however, to operate the gas generators which supply high pressure gas to the escape actuation system. The explosive would be located in the environmentally controlled crew compartment and thus protected from the high temperature environment. This system is suitable for use in either a central distribution system as shown in Figure 154 for the turnaround capsule or for application to specific mechanical functions where weight, redundancy, and thermal protection show improved reliability.

7.2.2.2 Structural Disconnects. A survey of suitable structural disconnects was made using the following postulations:

1. The adaptive sections of the disconnect form the terminal ends of the capsule and main flight vehicle, and transmit all loads across the interface.
2. Manual disconnect capability is provided for installation and ground handling.
3. Visual inspection and/or proof load testing features are desirable.
4. Systems are required to have operational repeatability consistent with the flight vehicle capability.
5. Passive and active cooling requirements are evaluated.
6. The separation equipment is compatible with the capsule loading conditions experienced throughout the mission.
7. The disconnect techniques should not interfere with or damage the heat protection surfaces of the capsule.

Latch systems provide efficient methods for mechanical type structural disconnects. These devices do not require precision manufacture to provide high degree of functional reliability, and are widely used in aerospace and industrial applications. The latches are held positively in the locked position. The applied load at the hook is reacted between the latch abutment faces to provide positive lock engagement for

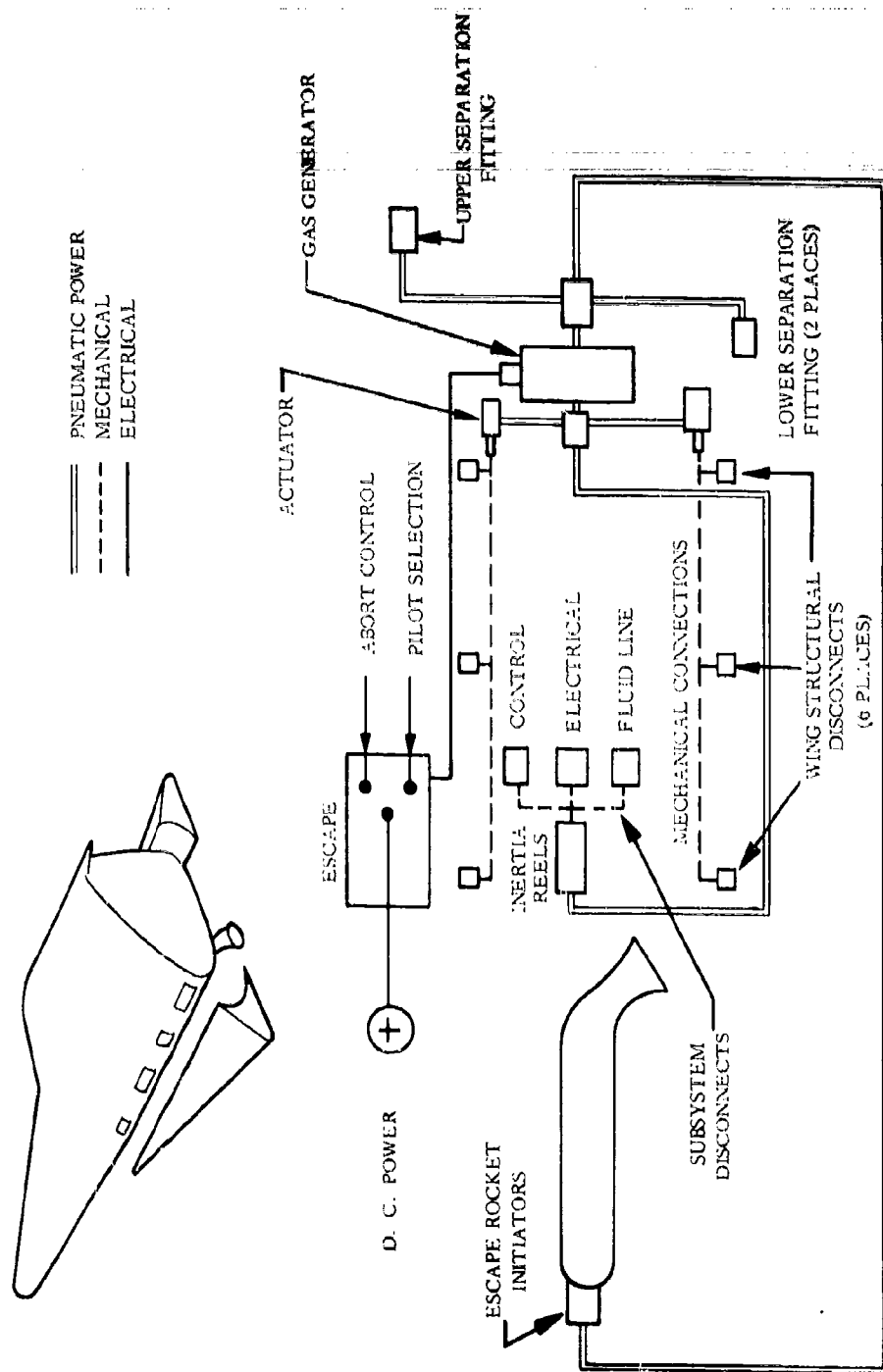


Figure 154 - Ignition System Schematic

variations in loading conditions. Spring devices maintain positive lock in the unloaded condition and protect against vibration and inadvertent release. The latch release loads are a function of the friction forces between the sliding elements.

Actuation may be accomplished manually or by power energized mechanisms. Reliance on pure mechanical devices to perform the disconnect of structure and subsystems during the initiation of the escape maneuver tends to increase the manual operating forces and time to complete the sequence. All mechanical disconnects are provided with power actuators to prevent delay in the separation sequence, and to provide efficient inter-connect between the automatic and ground controlled abort systems.

The temperature environment requires that fittings and mechanisms be manufactured from materials with properties equivalent to those used for the hot truss structure. Linear expansion of .015 inches per inch results from exposure of nickel based super-alloys to temperatures in the range of 1500 - 1800°F. Reliable mechanical operation is achievable under hot and cold conditions if particular attention is paid to material compatibility, the size of relative cross sections, and the tolerance of mating parts. Added thermal protection for critical components, cooling techniques employing water circulation, and alkali metals were considered, but appear unnecessary at this time.

Figure 155 presents a structural separation disconnect fitting, which is applied to the separable nose lifting body and ballistic body. The adjacent points of the primary flight vehicle and capsule structure terminate in an adaptor connection. A spigot formed on the flight vehicle side of the interface is housed in a socket formed by the capsule structure. A guide is machined integral with the spigot and rollers are used to reduce friction forces in the direction of the separation path. Tension is applied across the joint by an eye bolt which engages the hook of the latch mechanism. Shear is transmitted through the conical surface between the spigot and socket.

Structural disconnect is effected by retracting the plunger which retains the hook in the locked position. This mechanism is adaptable to a gas generator power system or cartridge actuator device. The actuation forces for this structural disconnect remain constant for hot and cold operation. Installation and ground handling disconnection between prime vehicle and capsule is accomplished by removal of the retaining nut. Installation adjustment is provided by the addition of shims or washers under the retaining nut. Torque loading of the joint is predicated on the strength allowable of the hook or bolt thread. The separation fittings and mechanisms are not

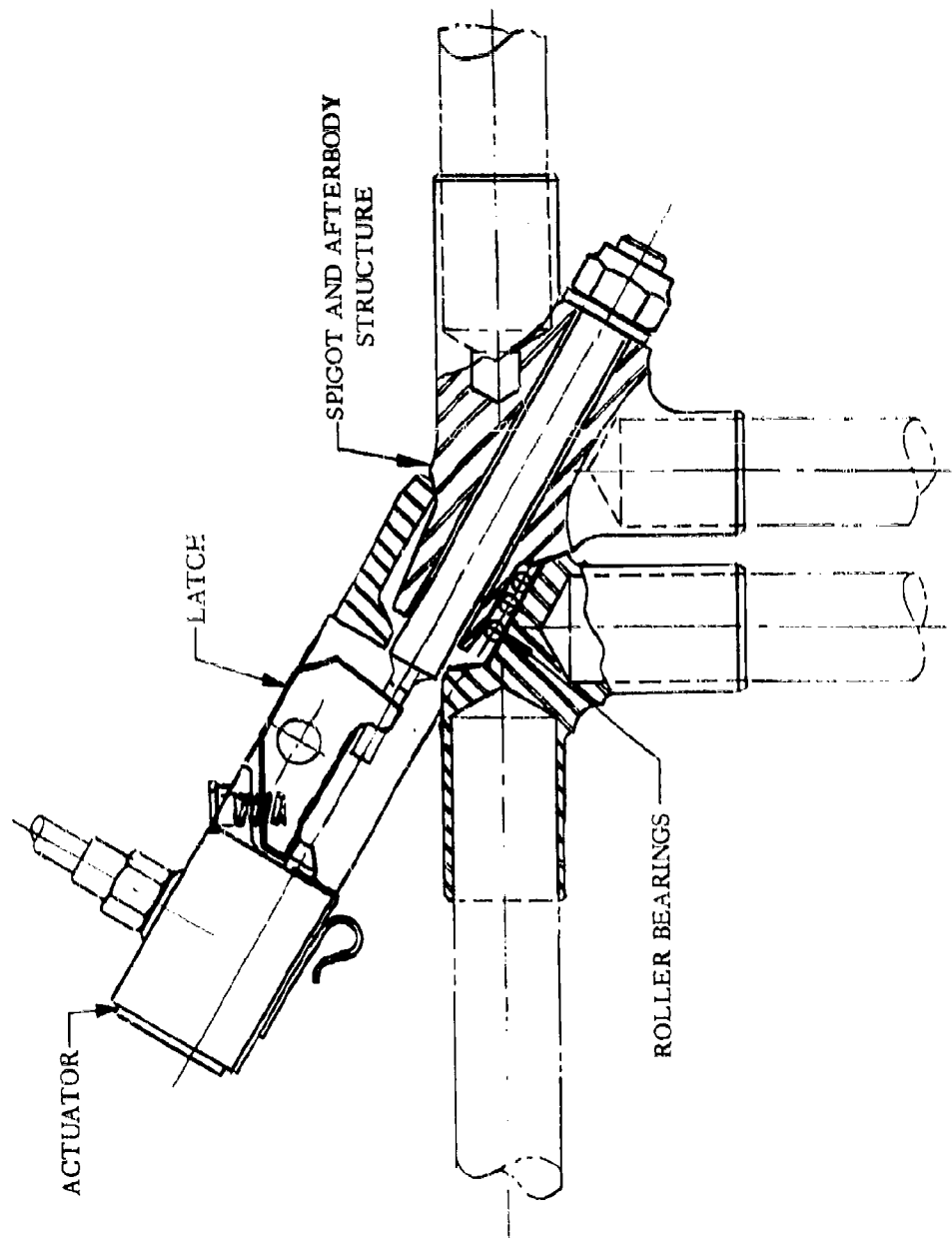


Figure 155 - Lifting Body and Ballistic Body Structural Disconnect

sensitive to inadvertent failure and are accessible for visual inspection and maintenance.

Figure 156 shows a structural disconnect adapted to the turnaround body. The latch mechanism is similar to that presented in Figure 155 with the addition of an adjustment stud and latch beam. The adjustment of the hook reduces the position tolerance between structural elements pulling the capsule and prime flight vehicle together at the interface. This fitting transmits only tension forces across the interface. Shear is distributed around the vehicle perimeter by the locating pins and fuselage ring at the interface, reference Figure 157. This structural disconnect technique is similar to that used to separate the booster stage on the Atlas Weapons System.

Structural disconnects employing a tension failure device as presented in Figure 158 were reviewed and the following comments are offered:

- (1) The force required to cause failure of the screw section varies between hot and cold conditions.
- (2) The gas pressure delivered to the piston significantly affects the ability to fail the retaining screw.
- (3) Machining tolerances, particularly the concentricity of the retaining pin diameters and hollow section, affect the failure conditions.
- (4) The cylinder, piston, segmented lock ring and bolt shank are a bench assembly. Torquing of the nut tends to apply load in the failure section of the screw. The segmented lock ring has a tendency to roll and react its load into the retaining screw through the cylinder housing.
- (5) There is no visual inspection or proof loading provision.
- (6) Guidance rollers are ideally suitable for separation and disconnect. They serve to reduce reactions at the interface and control the direction of initial separation.

Revision to the disconnect method were discussed previously and presented in Figure 155.

7.2.2.3 Subsystem Disconnects. This classification includes separation methods for functional subsystems, controls, instrumentation, electrical, fluid power and environmental supply lines. For study purposes control disconnects refer to rod and cable connections. The number and location of individual items of equipment and disconnects is not considered, however, a survey of the subsystem separation requirements for supersonic aircraft indicates the number to approach 500. It is possible to reduce the actual number of disconnects by grouping equipment in compatible packages for separation by panels and trunk lines.

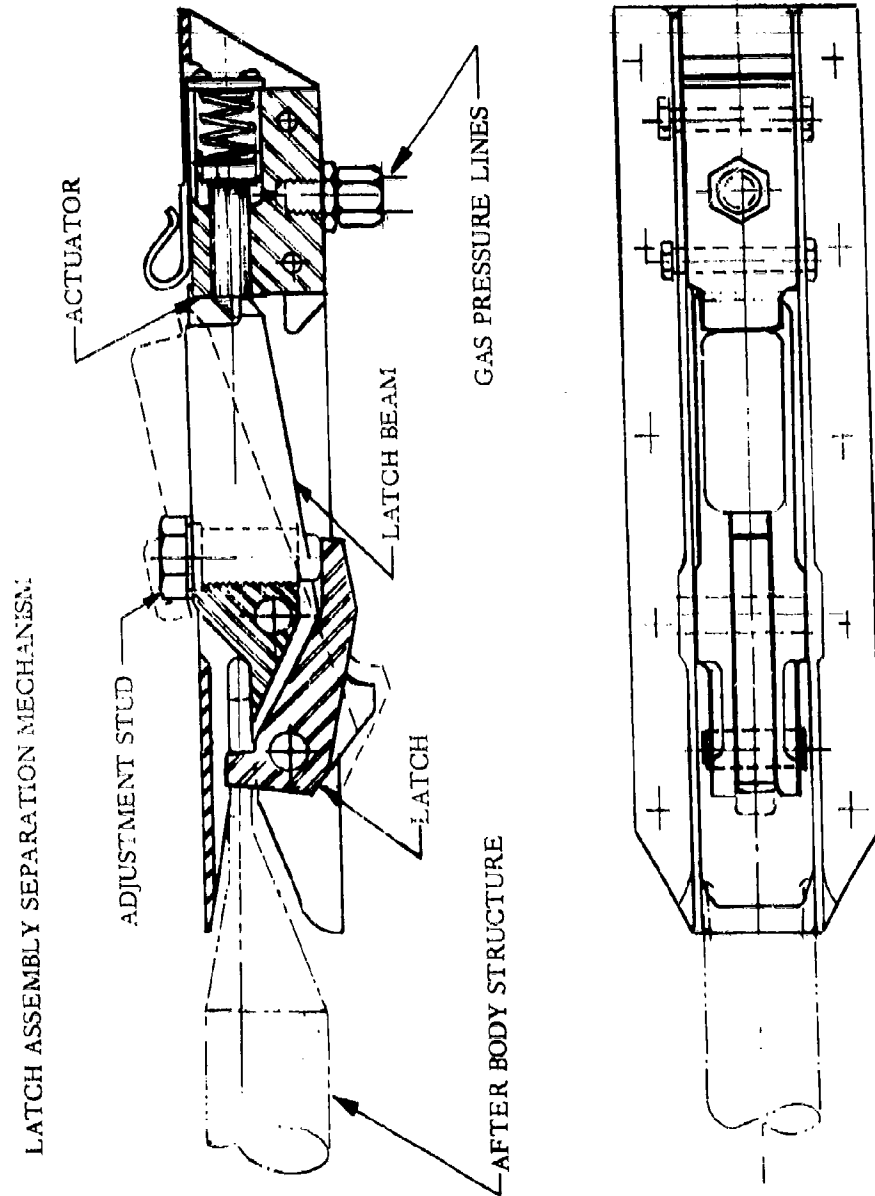


Figure 156 - Turnaround Body Structural Disconnect

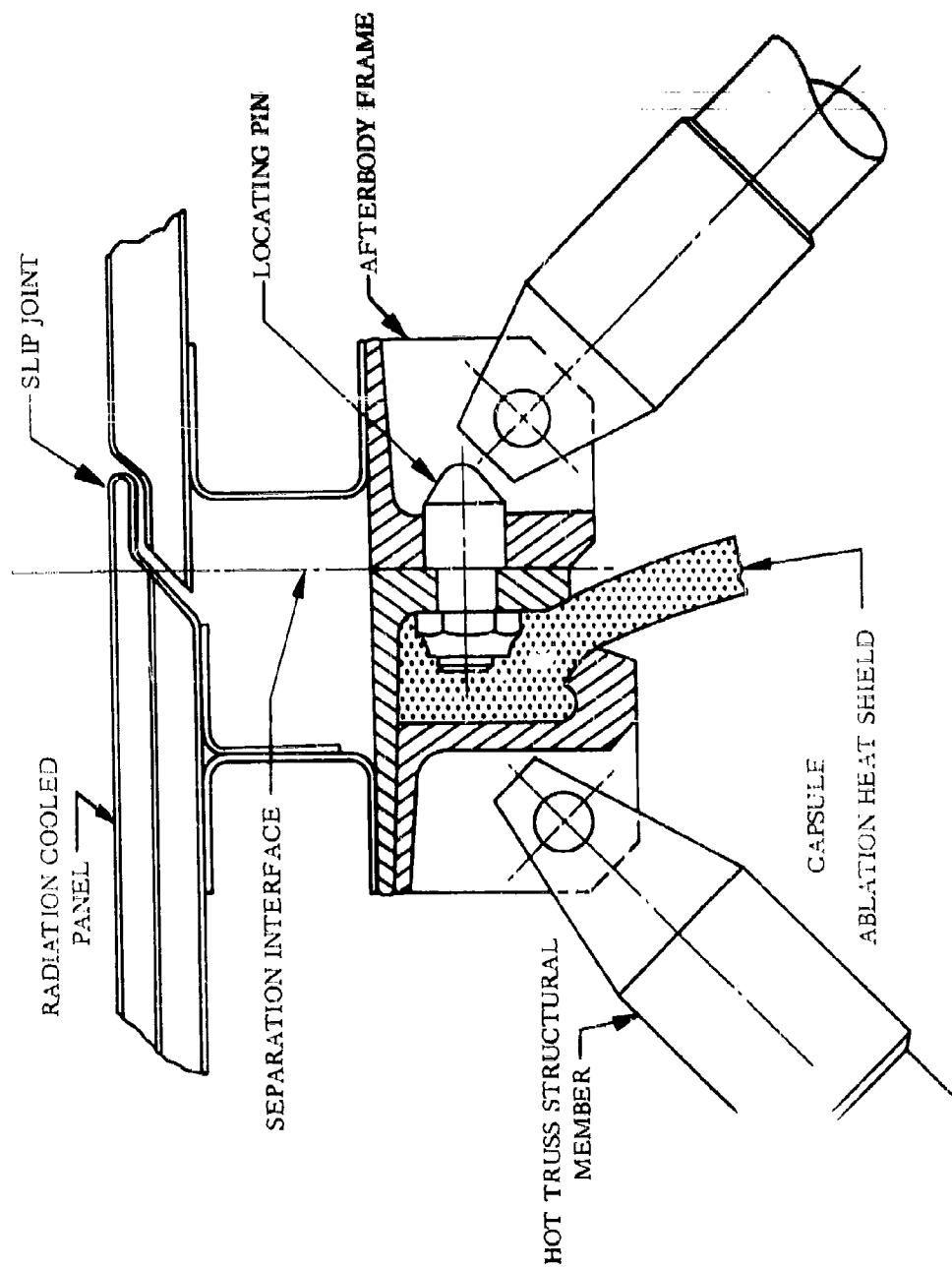


Figure 157 - Turnaround Body Shear Joint

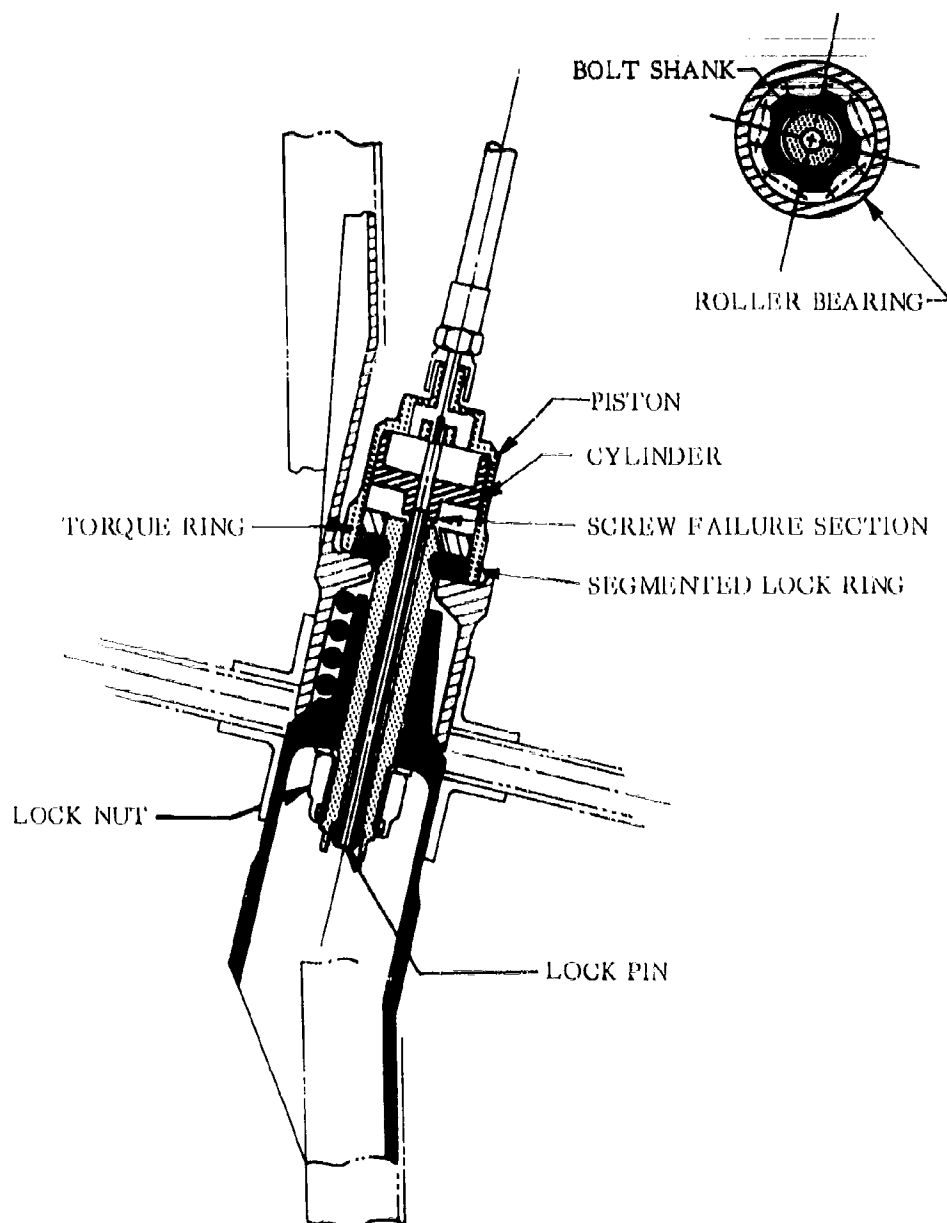


Figure 158 - Tension Failure Disconnect



The criteria listed under structural disconnect is applicable to subsystem disconnect. The use of explosive disconnects were evaluated and as previously mentioned were excluded. Mechanical type subsystem disconnects were selected.

Mechanical disconnects which operate independent of power actuation systems are desirable elements and enhance the reliability of separation. Lanyards which release spring retainers during the beginning of the guided separation are applicable in portions of this program, where directional control of the capsule separation face is maintained for a fixed distance. Hardware developed and proven reliable in missile and manned launch vehicle programs is available to meet these requirements. Figure 159 presents examples of existing electrical and electronic disconnects. Guillotine devices were examined and found to have limited cutting ability during and after possible exposure to extreme high temperature. Centrifugal clutches and brakes are adaptable to disconnect mechanisms. The outstanding features of these compact units is the great variation in torque transmitting capacity in relation to the driven speed. Harness restraints and inertia reels used in aircraft escape systems are example applications of these devices. Figure 160 shows a schematic arrangement of a centrifugal clutch used as a control separation device. The clutch remains disengaged during the normal operation of the control, and the complete assembly rotates around the pivot shaft. The control levers A and B are held together by a detent and are free to rotate about the pivot shaft. The actuator is spring loaded to the neutral position and rotates with the levers. When pressure is applied to the piston lever B rotates and engages roller C which applies force in rod D to unlatch the control disconnect E. The clutch disc F reacts the actuator force and a rapid rotational input produces centrifugal forces on the balls G causing them to lock the clutch disc and the actuator to the clutch housing H. Continued extension of the actuator piston rotates lever B and engages roller J to retract the control rod from any deflected position.

This mechanism has particular application to the separable nose turn around body capsule configuration; where controls pierce the capsule contour and connect to bell crank within the stub wing.

Fluid and environmental supply line disconnects presented in Figure 161 are state-of-the-art devices developed in sizes sufficient for the purposes of this program. They are constructed to provide sealing engagement across a separation plane within a wide range of installation tolerance. When applied to the primary flight vehicle capsule interface, the socket containing the flow shut-off element is located on the capsule, to retain the environmental control fluids aboard the capsule during the escape maneuver. The male portion of the disconnect coupling is installed on the flight vehicle separation face. The coupling halves are adaptable to an angular arrangement by manufacturing the flanges to align the coupling with the direction of the structural separation guides.

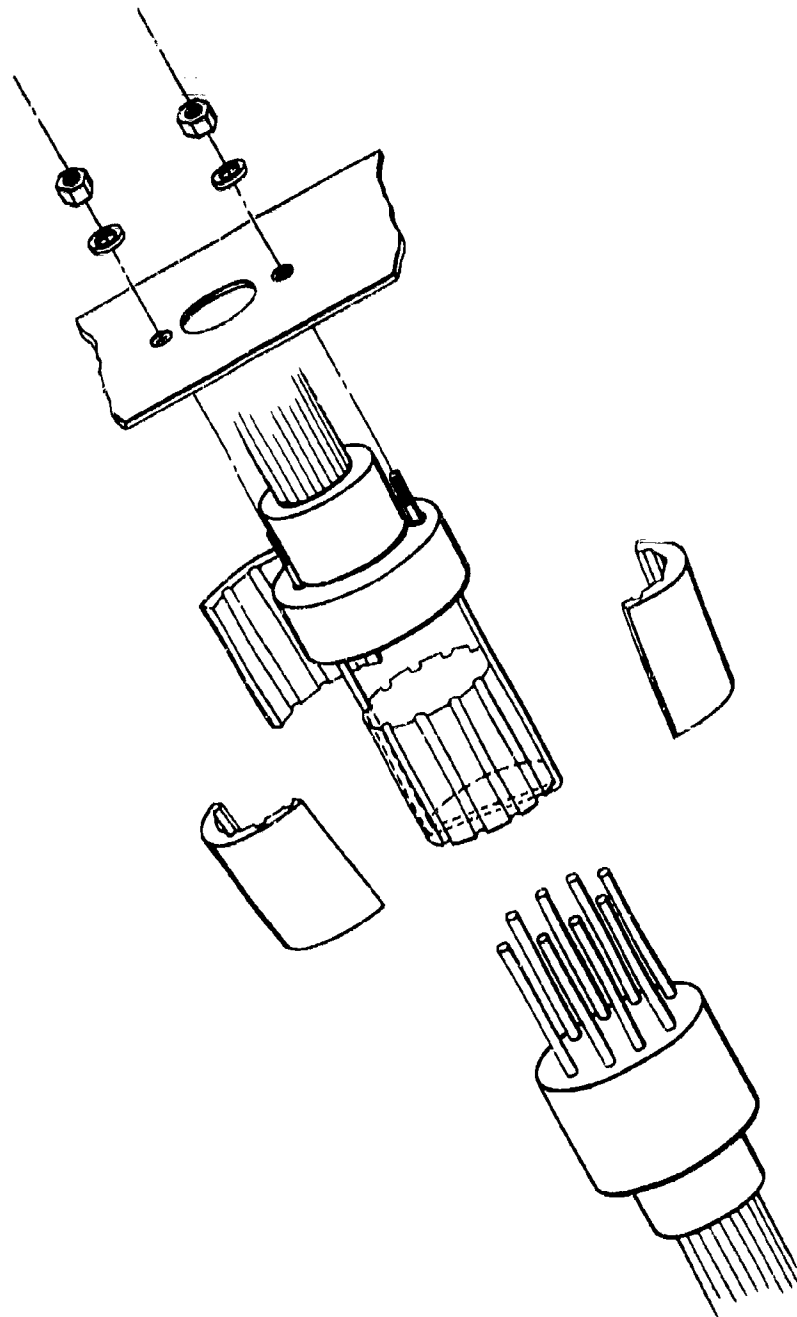


Figure 159 - Electrical & Electronic Disconnect

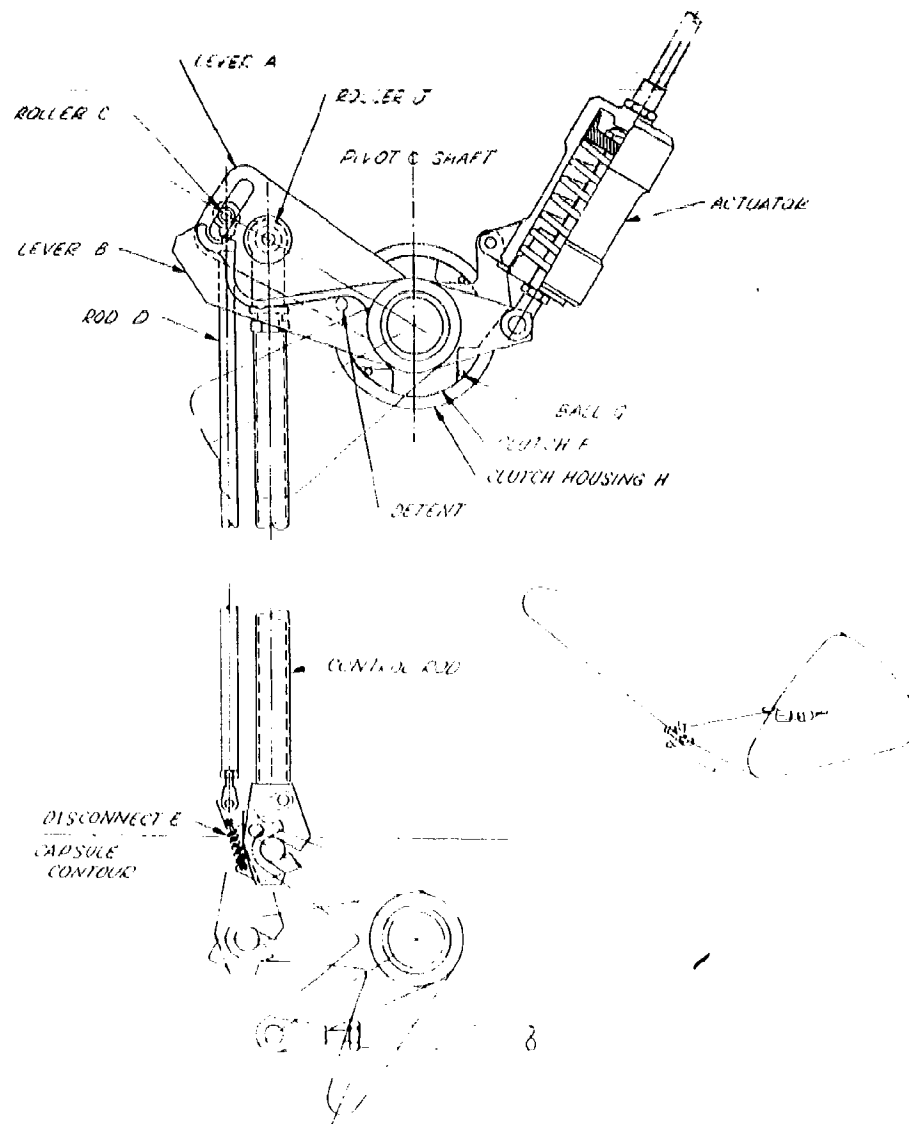


Figure 160 - Centrifugal Clutch and Control Disconnect

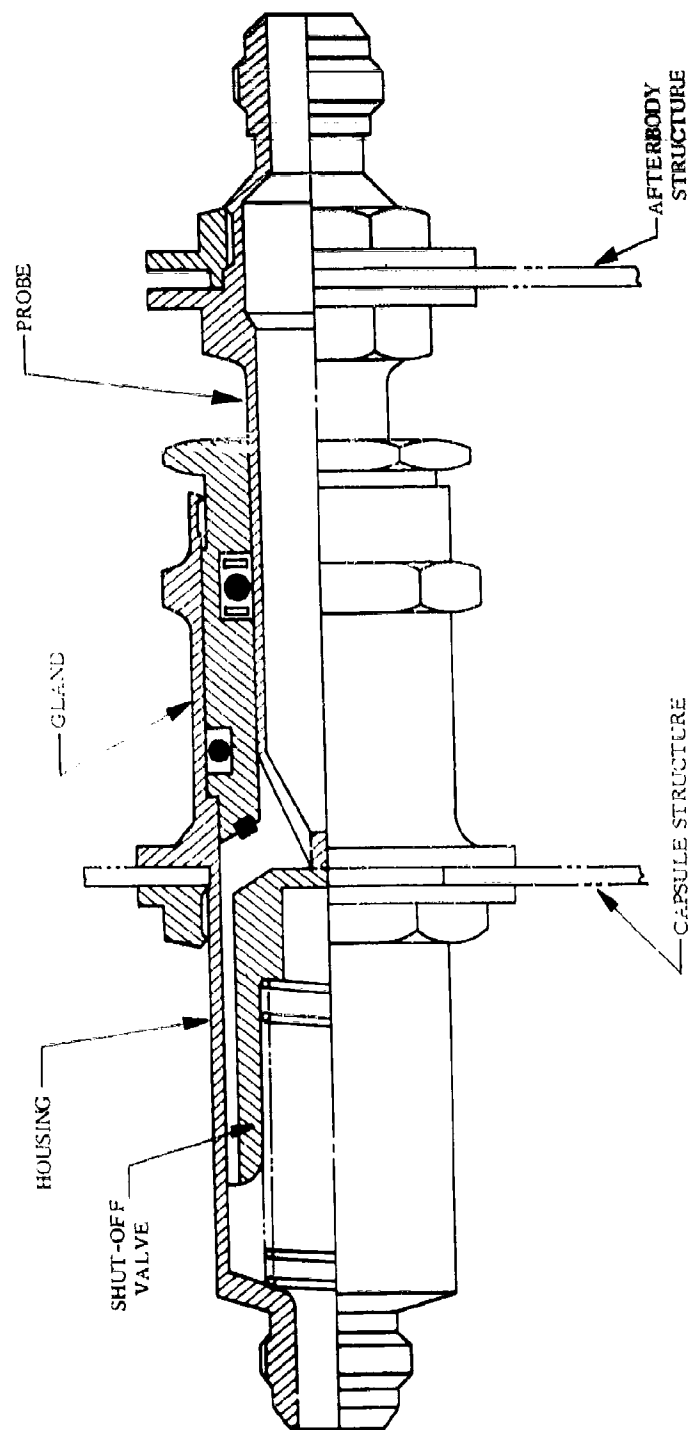


Figure 161 - Fluid and Environmental Supply Disconnect

### 7.3 ESCAPE CAPSULE APPLICATIONS

**7.3.1 SEPARABLE-NOSE BALLISTIC BODY.** This capsule configuration is attached to the prime vehicle structure by four disconnect fittings at the concentrated load points on the main longerons. A guided separation was selected for this configuration and an investigation of the loading characteristics on the guides was made in order to determine the optimum orientation of the separation interface. Figure 162 presents a sketch of this arrangement showing the various forces acting on the capsule during initial separation. It can be seen from Figure 162 that the applied forces tend to rotate the capsule about the upper guides. This would be true even in a negative lift condition since the thrust forces are much greater than the lift forces. Initially, however, in the negative lift case the capsule would tend to rotate downward since the thrust has a finite buildup time to its peak value. As the thrust builds up, however, the rotation tendency will become upward and be in that direction at separation from the guides. On this basis, therefore, there is no requirement for lower guides and only guides on the two upper longerons were considered.

The separation dynamics during the disconnect phase were calculated using an IBM 7090 digital computer program. The effects of thrust buildup rate, thrust inclination angle, separation bulkhead slope and dynamic pressure on the guide forces and capsule translation and rotation were determined. The following parameter values were considered:

Thrust buildup rate	= 550,000, 775,000 lbs/sec
Thrust inclination angle	= 30, 40 degrees
Separation bulkhead slope	= 0, 15, 30, 40 degrees
Dynamic pressure	= 0, 825 psf

The equations for the computer program were written such that the capsule could only translate along the guides and could only rotate in a nose up direction.

The separation guides were assumed to be two inches long and normal to the separation bulkhead. Figures 163 and 164 present the peak loading on the guides as a function of separation bulkhead angle. These data show that the minimum load occurs when the separation bulkhead is normal to the rocket thrust line. When using upper guides only, the same loading could be achieved by inclining only the guides and using a separation bulkhead normal to the capsule centerline.

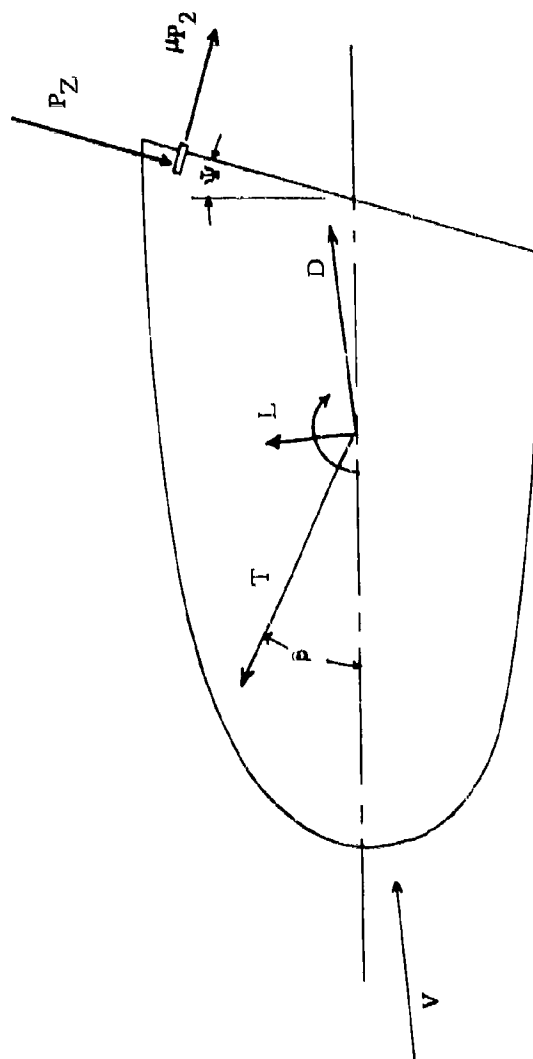


Figure 162. Ballistic Capsule Separation Forces

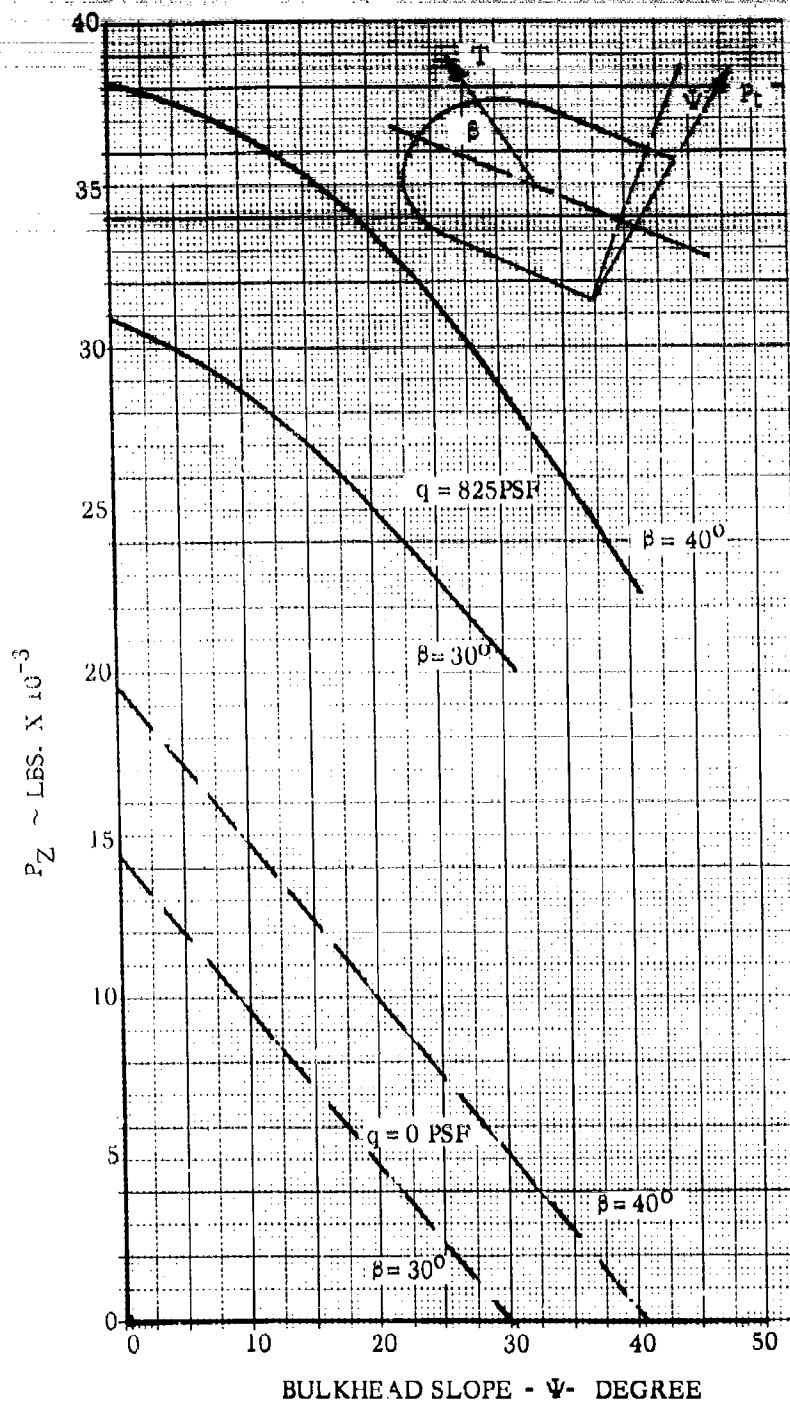


Figure 163 - Ballistic Body - Load Normal to Guides - Thrust  
Build Up = 550,000 Lb/Sec.

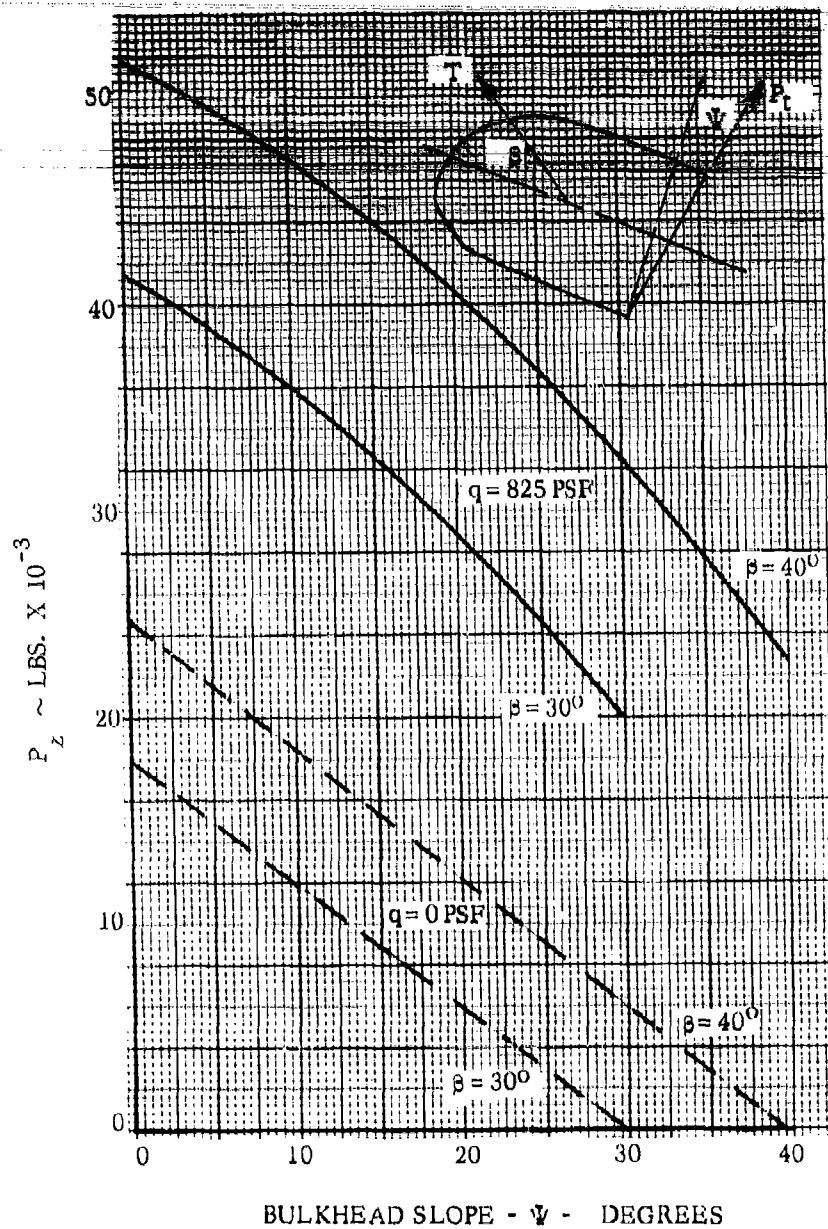


Figure 164 - Ballistic Body - Load Normal to Guides - Thrust Build-Ups = 775,000 Lbs/Sec.



The distance the capsule has traversed along the separation guides at the time the maximum thrust of 45,000 lbs. is attained is presented in Figure 165. The corresponding angle of attack characteristics are shown in Figure 166. The amount of rotation is decreased as the guides become parallel to the rocket thrust line. Allowance must be made in the disconnect mechanism for these dynamic characteristics, however they do not present any serious design problems.

Figure 167 presents a development design of the separation interface and disconnect devices of the ballistic body capsule. The drawing shows the separation interface normal to the escape rocket thrust line with an alternative arrangement in which the separation interface is normal to the centerline but the guides are parallel to the thrust line.

High pressure gas operated mechanical disconnect devices are proposed. The lower disconnect fittings form a structural tie between the structural elements. The upper fittings perform the same structural function but act to guide the capsule along a predetermined escape path at the time of separation. The friction loads in the guides are reduced by the use of baked molybdenum disulphide dry film lubricated ball or roller bearings. The connections are broken when the gas generator provides power to release a lock, which allows the capsule segment to disengage from the spigot projecting from the main vehicle structure. The controls, electrical lines, and environmental equipment are assumed to be grouped together functionally. A sprung type mechanical disconnect is used.

The separation mechanisms are designed to function under hot and cold operating conditions, and are integrated into the hot truss structural design. The cartridge actuator device (C.A.D.) gas generators are located in the crew controlled environment. The gas power source is transmitted to the mechanism by pneumatic lines on the capsule side of the separation interface, thus eliminating line disconnects at the separation fittings.

Escape rocket ignition and the ignition of the cartridge actuated gas generators occurs simultaneously. Due to the relatively long thrust buildup time in comparison with the operation time of the disconnect system, all capsule vehicle connections are severed long before maximum thrust is achieved.

7.3.2 SEPARABLE-NOSE LIFTING BODY. This configuration is quite similar to the separable-nose ballistic body with regard to the separation interface. The escape capsule, being located at the nose of the vehicle, has a relatively simple interface at the rear of the capsule.

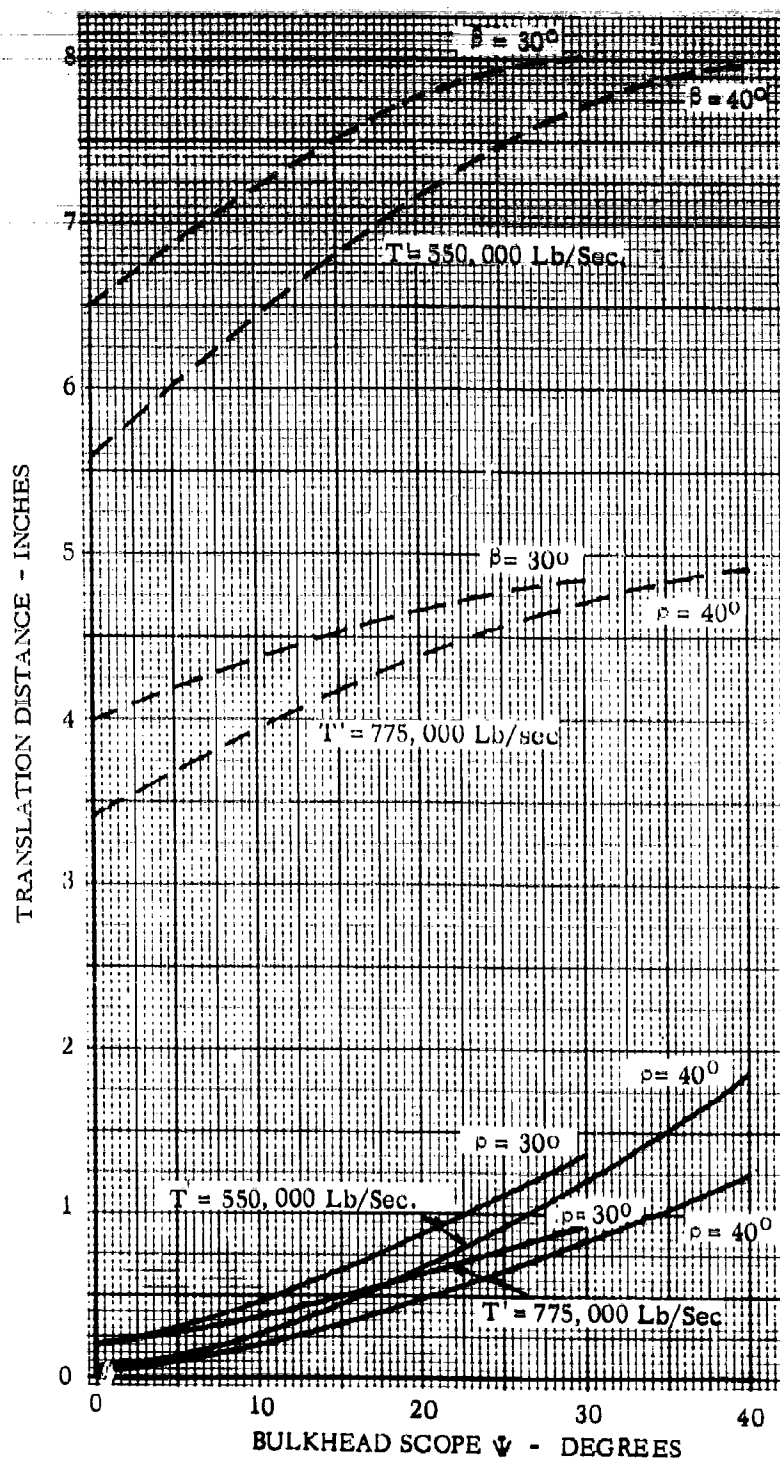


Figure 165 - Ballistic Body - Translation Distance

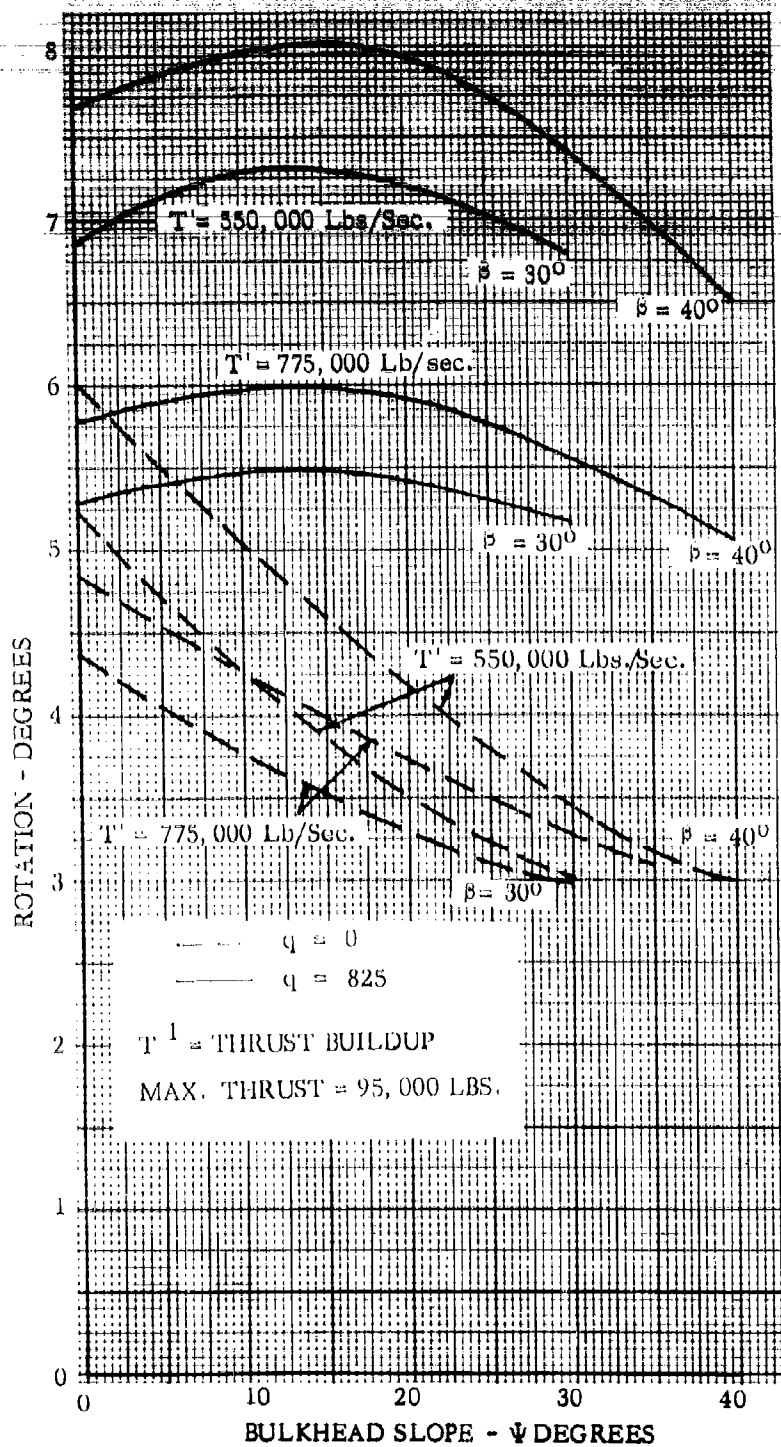


Figure 166 - Ballistic Body - Rotation Characteristics

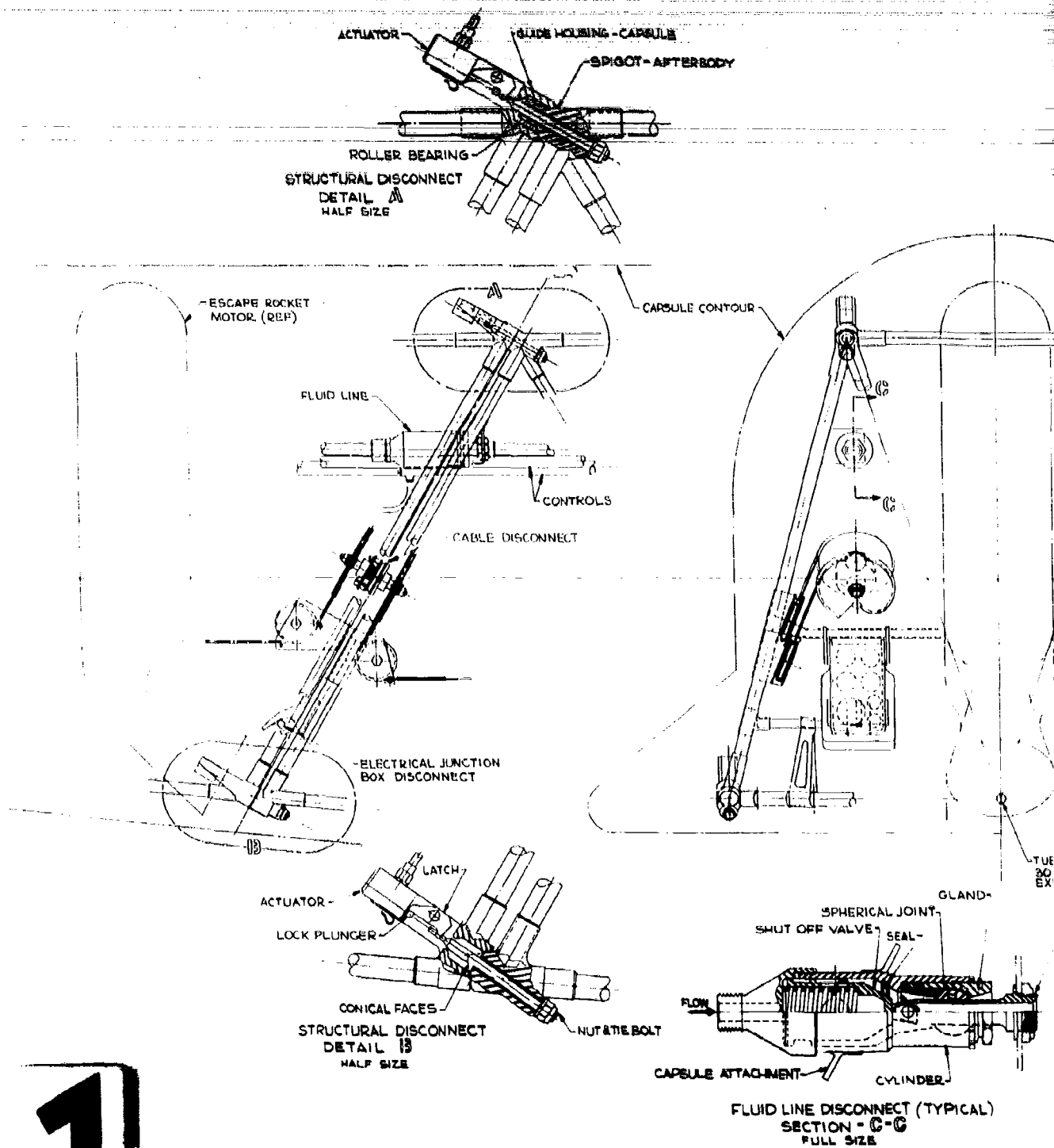
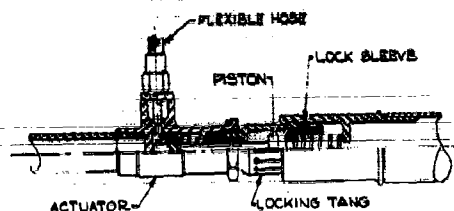


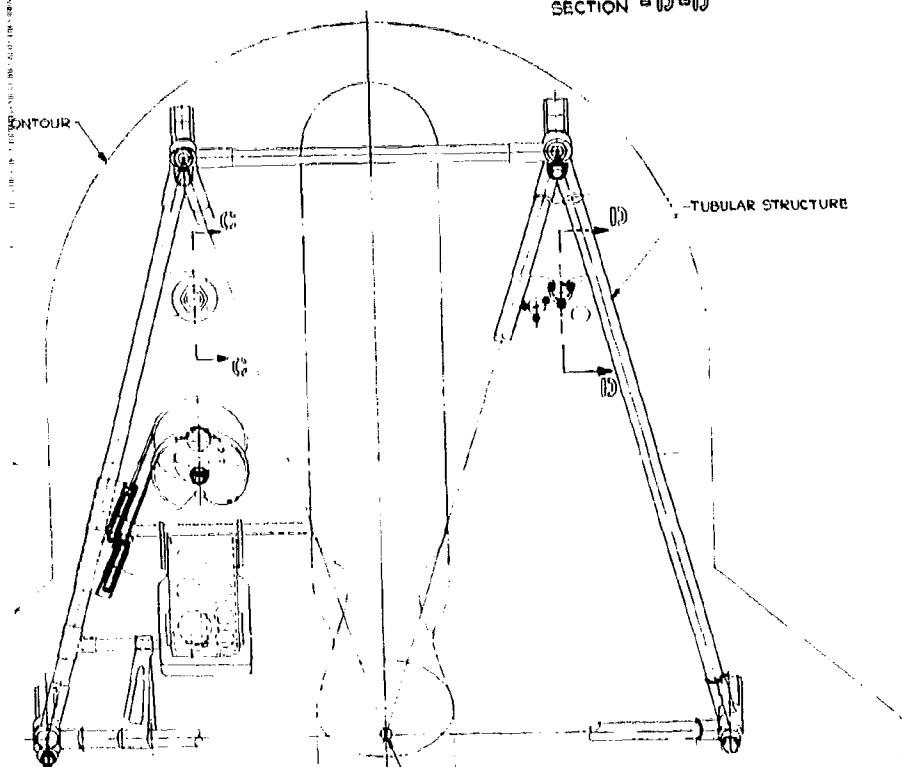
Figure 167 - Ballistic Body Capsule - Separation Inte

BODY

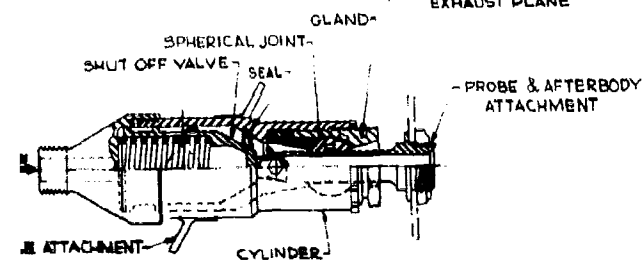


CONTROL DISCONNECT  
SECTION - D-D

CONTOUR



TUBULAR FRAME JOINT  
30 IN. AFT OF ROCKET  
EXHAUST PLANE



FLUID LINE DISCONNECT (TYPICAL)  
SECTION - C-C  
FULL SIZE

istic Body Capsule - Separation Interface Design



~~This capsule configuration is attached to the primary vehicle by four~~ disconnect fittings at the concentrated load points on the main longerons. A guided separation was selected using guides only on the upper fittings. The friction loads in these guides is reduced by the use of baked molybdenum disulphide dry film lubricated ball or roller bearings. These upper fittings with the guides form a structural tie prior to separation as do the lower fittings.

An analysis of the aerodynamic loading on the forebody was made for an angle of attack of 3 degrees at the maximum dynamic pressure condition. At this condition, the magnitude of the forces transmitted across these fittings at the separation interface are 10,000 lbs. in each of the upper fittings and 8,000 lbs. in each lower fitting.

Separation dynamics studies of the disconnect phase were conducted for this configuration as with the ballistic body capsule. The effects of the following parameter variations were investigated:

Thrust buildup rate	= 313,000, 470,000 lbs/sec
Thrust inclination angle	= 30, 40 degrees
Separation bulkhead slope	= 0, 15, 30, 40 degrees
Dynamic pressure	= 0, 825 psf

The non-dimensional loading diagram presented in Figure 162 for the ballistic body also applies to the lifting body.

The separation guides were assumed to be two inches long and normal to the separation bulkhead. Figure 168 presents the peak loading on the guides as a function of separation bulkhead angle. These data show that the minimum load occurs when the separation bulkhead is normal to the rocket thrust line. The separation forces on the guides developed at the maximum dynamic pressure condition are in the range of 15,000 to 20,000 lbs. for this orientation. The separation loading is therefore greater than the normal in flight loading, however, it is still compatible with the radiation cooled hot truss structural concept. The detrimental effects of loading on the interface during separation are reduced to some extent by the short time interval of load application and the resulting lag in effects. In some instances permanent set is tolerable particularly with respect to the primary vehicle interface structure after separation. When using upper guides only, the same separation loading condition is achieved by inclining only the guides and using a separation bulkhead normal to the capsule centerline.

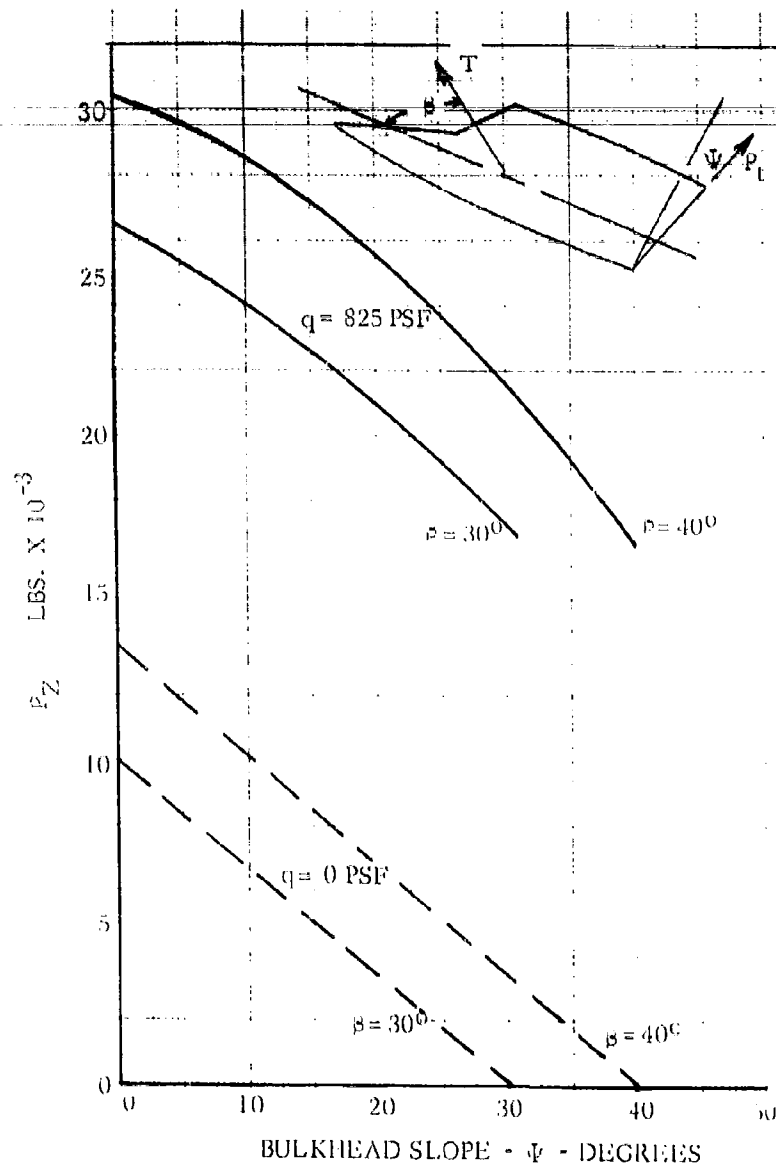


Figure 168 - Lifting Body - Load Normal to Guides

The distance the capsule has traversed along the separation guides at the time the maximum thrust of 25,000 lbs. is attained is presented in Figure 169. The corresponding angle of attack characteristics are shown in Figure 170. The amount of rotation is decreased as the guides become parallel to the rocket thrust line.

Figure 171 presents a development design for the separation interface of the lifting body capsule. The separation interface is normal to the vehicle centerline with the guides inclined so that they are parallel to the rocket thrust line. The structural and subsystem disconnect fittings are identical to those proposed for the ballistic body in Section 7.3.1.

7.3.3 SEPARABLE NOSE TURNAROUND CAPSULE. This capsule configuration consists of the forward part of the fuselage of the primary flight vehicle with an ablation heat shield at the aft end. A design for the disconnect and separation mechanism for this configuration using available technology appears to be feasible though not without complications.

This configuration presents a difficult problem at the interface since the structural tie between the capsule and the primary flight vehicle should not pierce the ablation heat shield. Discontinuities in an ablation surface tend to burn out and lead to local failure of the ablative material. In addition, the vehicle utilizes a radiation cooled hot truss structural concept in which the skin is not a main structural component and hence cannot serve as the structural connection between the primary flight vehicle and the capsule.

The structural connections are made external to the basic capsule contour. This requires structural hard points at the surface to connect and brace these external fittings. This approach is not basically compatible with the structural concept being used.

Figure 172 presents the design concept for the separation interface of this configuration. There is little flexibility in selecting the interface slope on this configuration due to the large ablation heat shield. The interface must be such that there is clearance for this heat shield during separation.

The structural attachment for this configuration is made external to the capsule contour at three points. One on the upper surface of the longitudinal centerline of the vehicle, and one in each of the lower quadrants within the wing root. The upper disconnect is made between the vehicle longeron and an external member connected



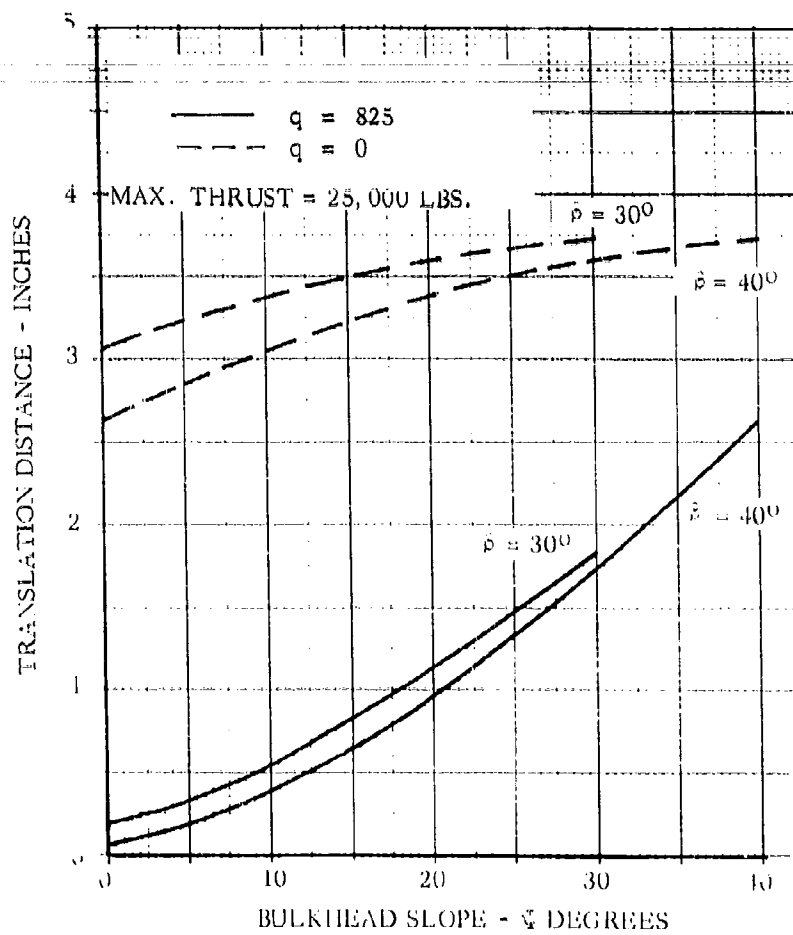


Figure 169 - Lifting Body - Translation Distance

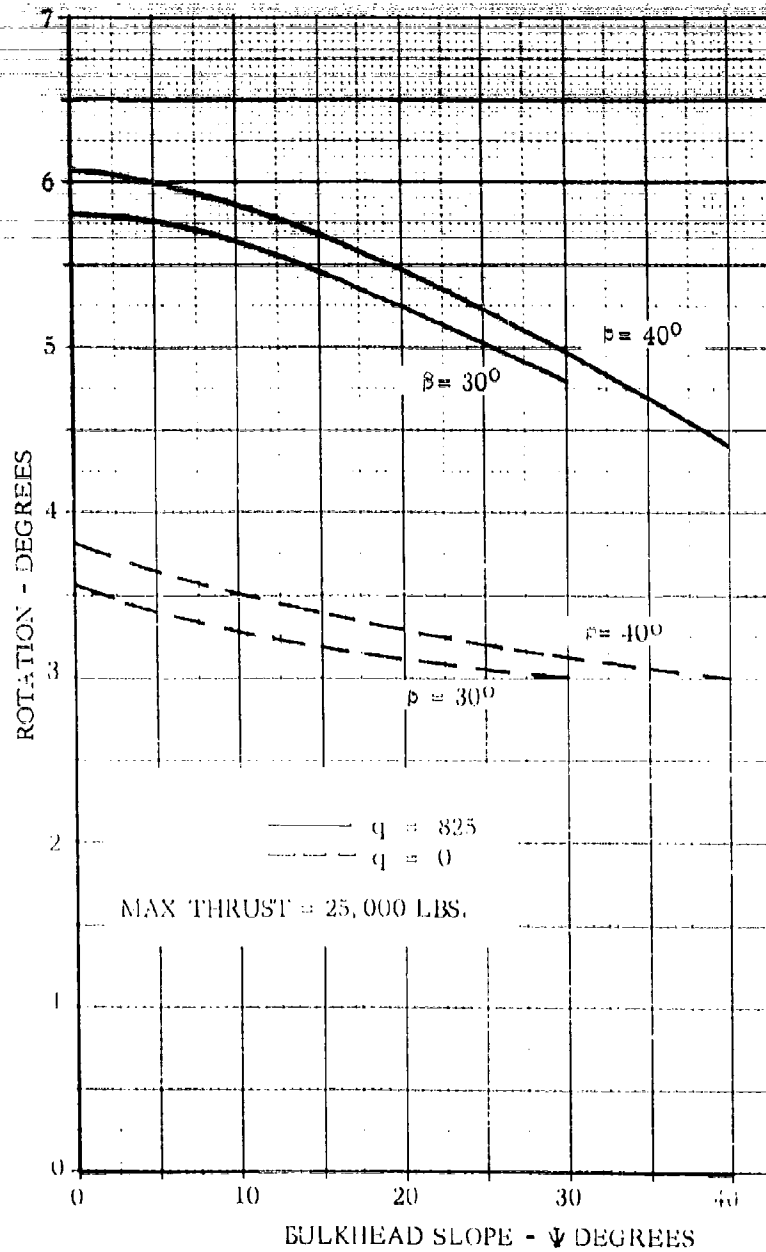


Figure 170 -Lifting Body - Rotation Characteristics

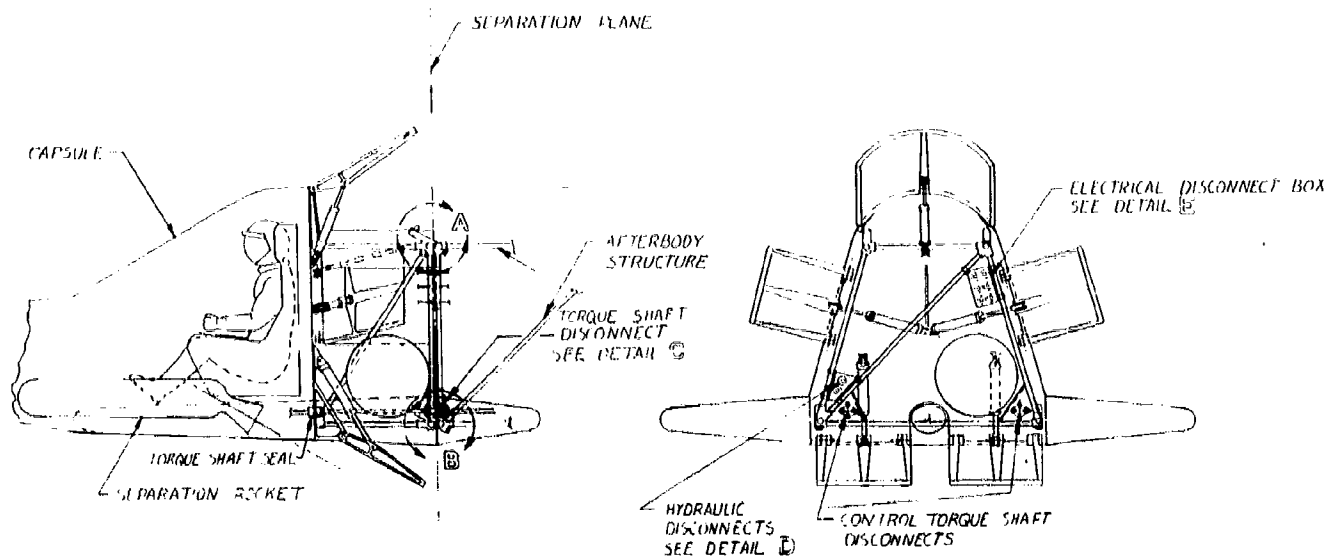
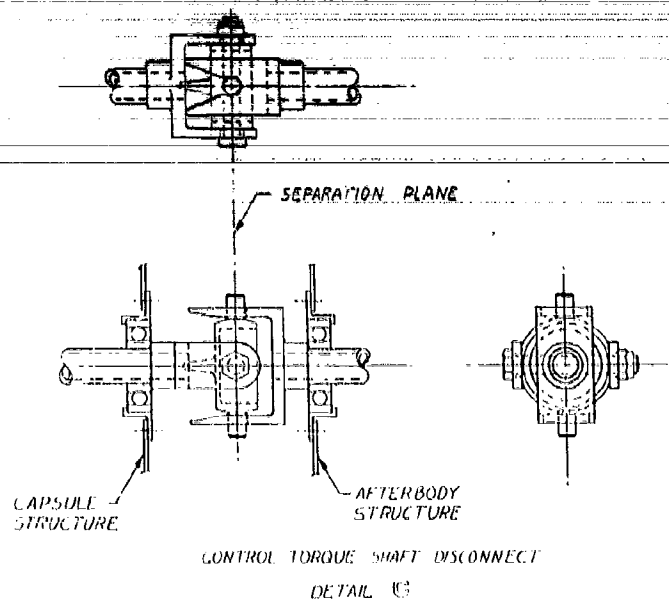
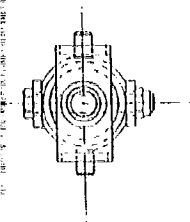
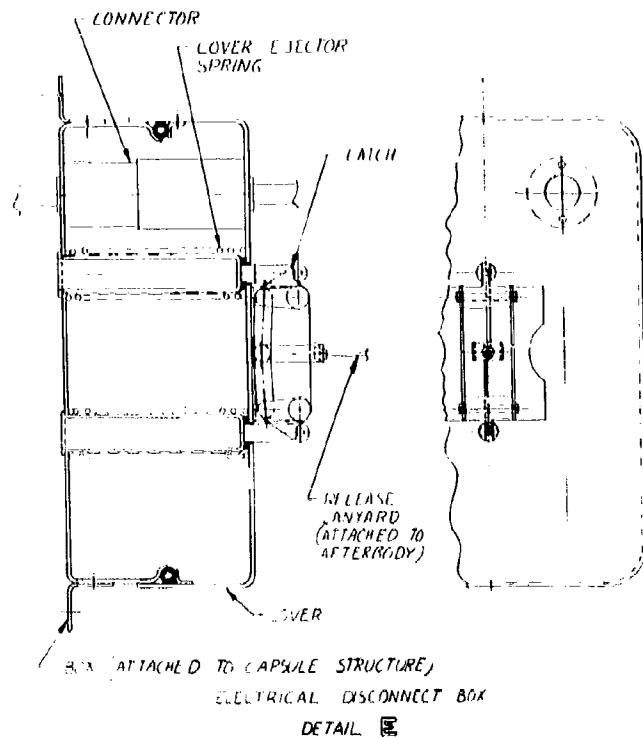
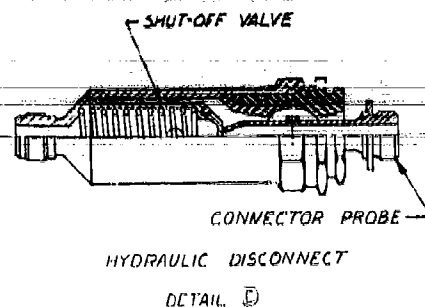
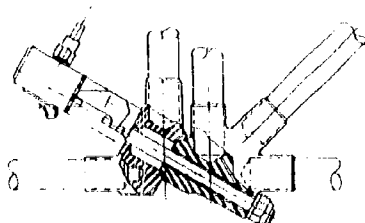
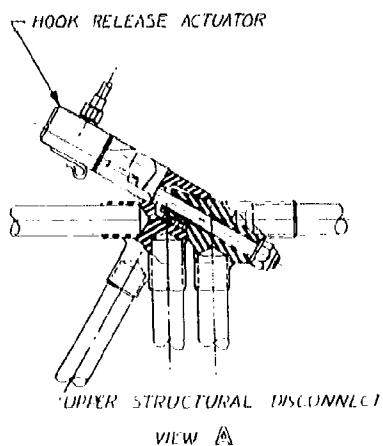


Figure 171 - Lifting Body Capsule - Separation



NNLCI

ELECTRICAL DISCONNECT BOX  
SEE DETAIL E



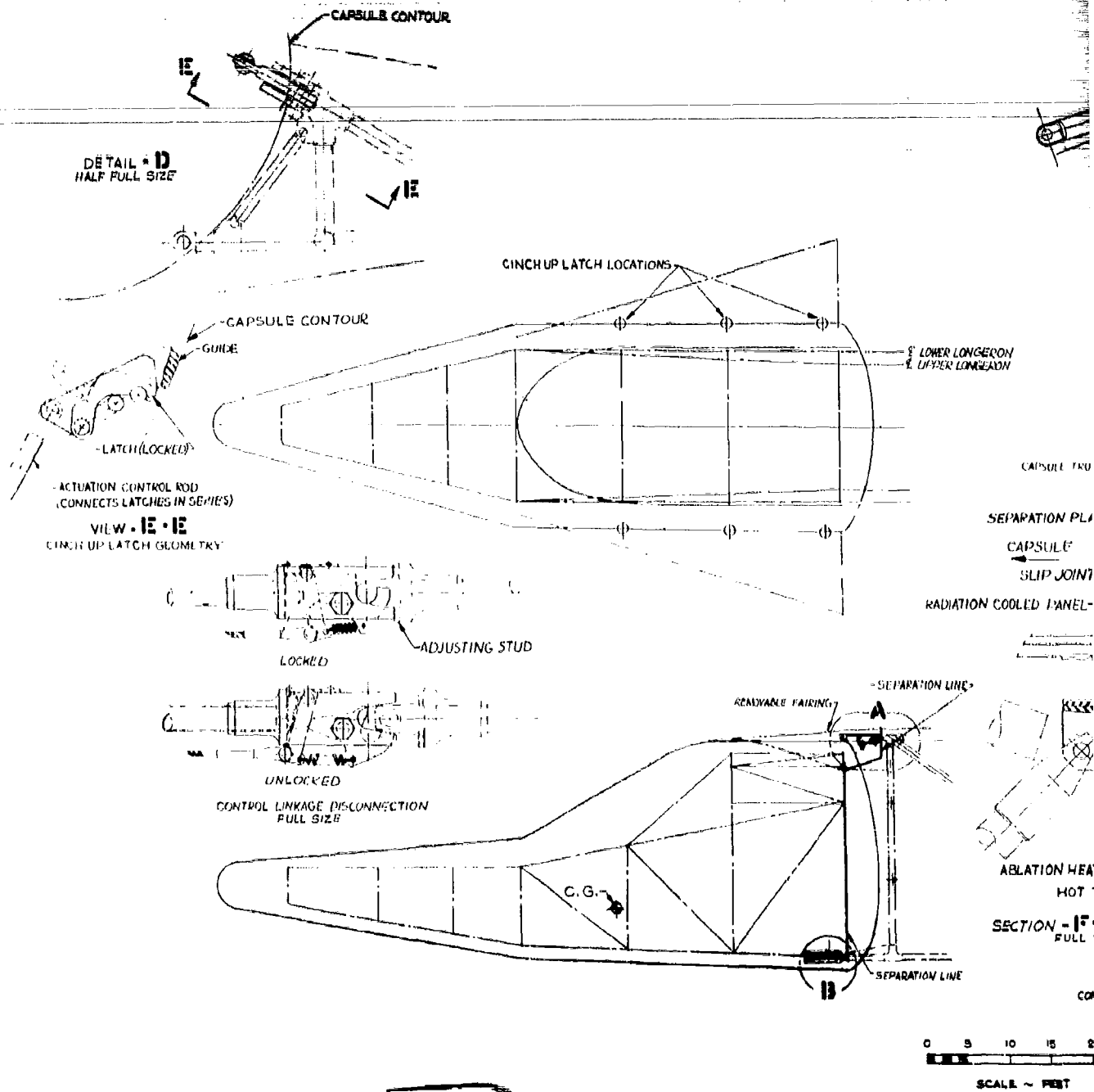


Figure 172 - Turnaround Capsule - S

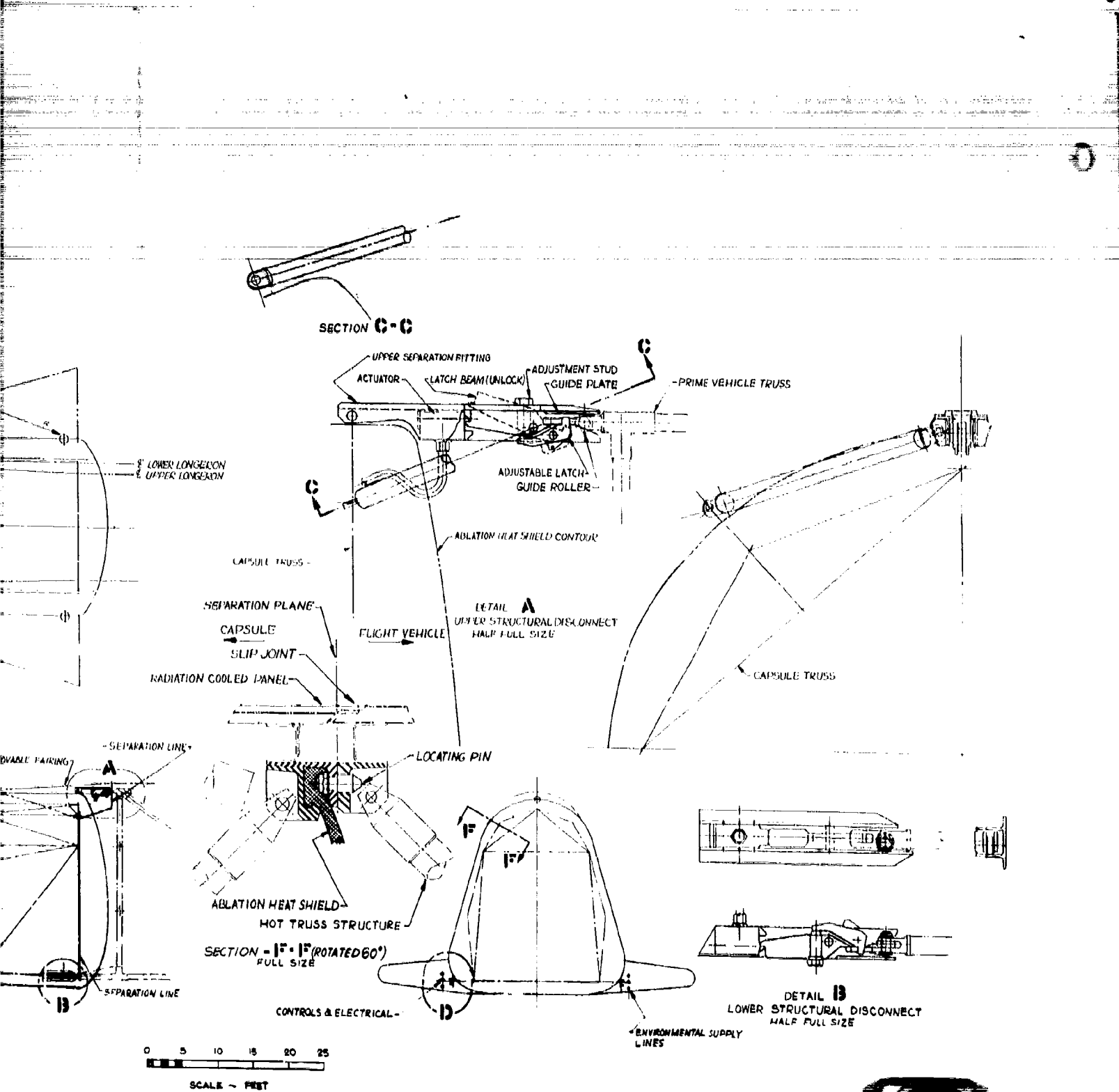


Figure 172 - Turnaround Capsule - Separation Interface Design

through the contour into the capsule structure, with provision to clear the dome contour of the ablation heat shield during the separation maneuver. Detail A shows the complication of the upper structural disconnect required to carry the structure across the separation interface and avoid piercing the ablation heat shield. The attachments on the lower surface are tension ties, which project from the main vehicle and are latched to the capsule by fittings similar to the upper disconnect. A guided separation has been selected for this configuration with the guides contained as part of the three structural disconnect fittings. Rollers are used within the guides to minimize friction.

The lower mechanical disconnects are protected from the extreme temperature, being housed in the wing root. The geometry for the external structure supporting the upper disconnect is protected by an external fairing which is released during the turnaround maneuver. In addition to releasing the fairing over the upper disconnect, it is also necessary to release the exposed disconnect devices so that there are no local hot spots due to protuberances.

The alignment of the capsule and primary flight vehicle is maintained by a series of locating pins projecting from the capsule terminal frame around the ablation shield, which engage in matching holes on the flight vehicle frame. Section FF shows this feature.

The capsule and forward wing root section are attached by cinch up latches at three locations on each side of the vehicle. Detail D shows a method of hinging the lower wing surface and latching the stub wing and capsule structure. The latches are connected by rods and linkages to a gas powered actuator. Spring loaded cover plates are considered to seal the capsule surface breaks to reduce the effects of turbulence and local heating. A similar arrangement could be used for the three main structural fittings.

The flight controls, electrical wiring, and environmental controls are functionally grouped and cross the separation interface through the wing root. Typical subsystem disconnects applicable to this configuration are shown in Figures 159 through 161. All the disconnect fittings are operated by a high pressure gas from a cartridge actuator. The structural attachments and controls are disconnected simultaneously with the escape rocket motor ignition.

The capsule dynamics during disconnect for this configuration are similar to the lifting body discussed in Section 7.3.2. However, the loads at the interface are redistributed as a result of the disconnect technique selected.

Figure 173 shows the disconnect forces as a function of time from rocket thrust initiation for maximum dynamic pressure separation. The loads were calculated assuming the capsule to be connected throughout rocket thrust buildup.  $P_U$  and  $P_L$  are the loads in the upper and lower attachments respectively,  $F$  is the shear force in the locating pins at the separation interface. If the structural attachments are released at the time of rocket initiation, the longitudinal loads  $P_U$  and  $P_L$  will no longer exist and the capsule is free to rotate and translate forward. The pitch up moment characteristics indicated in Figure 173 will significantly reduce the longitudinal load in the lower fittings. Due to the finite thrust buildup time, the capsule will not translate until the thrust forces overcome the aerodynamic drag forces. During this period longitudinal forces will exist in the upper fitting. The capsule translation as a function of time is also given in Figure 173. Translation does not begin until .033 seconds after rocket initiation. During translation there are no longitudinal forces in the guide fittings, however, as the capsule comes off the shear pins the normal force,  $P$ , must be absorbed in the guides.

Assuming a guide length of 1.6 inches, separation is complete 0.05 seconds after escape rocket thrust initiation. At this time the normal load in the guides is 12,000 lbs. The in-flight loading conditions at the separation face were examined for an angle of attack of three degrees at the maximum dynamic pressure condition. The forces at the upper and lower attachments were 6,100 lbs. in the upper and 4,300 lbs. distributed between the two lower attachments. A shear force of 2,000 lbs. is developed at the interface and reacted by the locating pins.

In summary, the turnaround configuration presents a very difficult and complex interface. Structural and disconnect techniques are feasible, however, they are complex and consequently penalize reliability, and escape system weight much more than any of the other configurations.

7.3.4 POD CAPSULE. This configuration consists of the pilot compartment portion of the forward fuselage. It utilizes the re-radiative structure of the primary vehicle for its upper surface and has an ablation heat shield on its lower surface which is enclosed within the primary vehicle fuselage during normal flight.

The advantages of a pod capsule when compared to separable nose capsules are a decrease in capsule weight and size, a reduction on stabilizing surface area required and smaller escape rocket requirements.

The use of a pod type escape capsule requires a cut out in the primary flight vehicle and introduces a problem, in the area of structural continuity between the



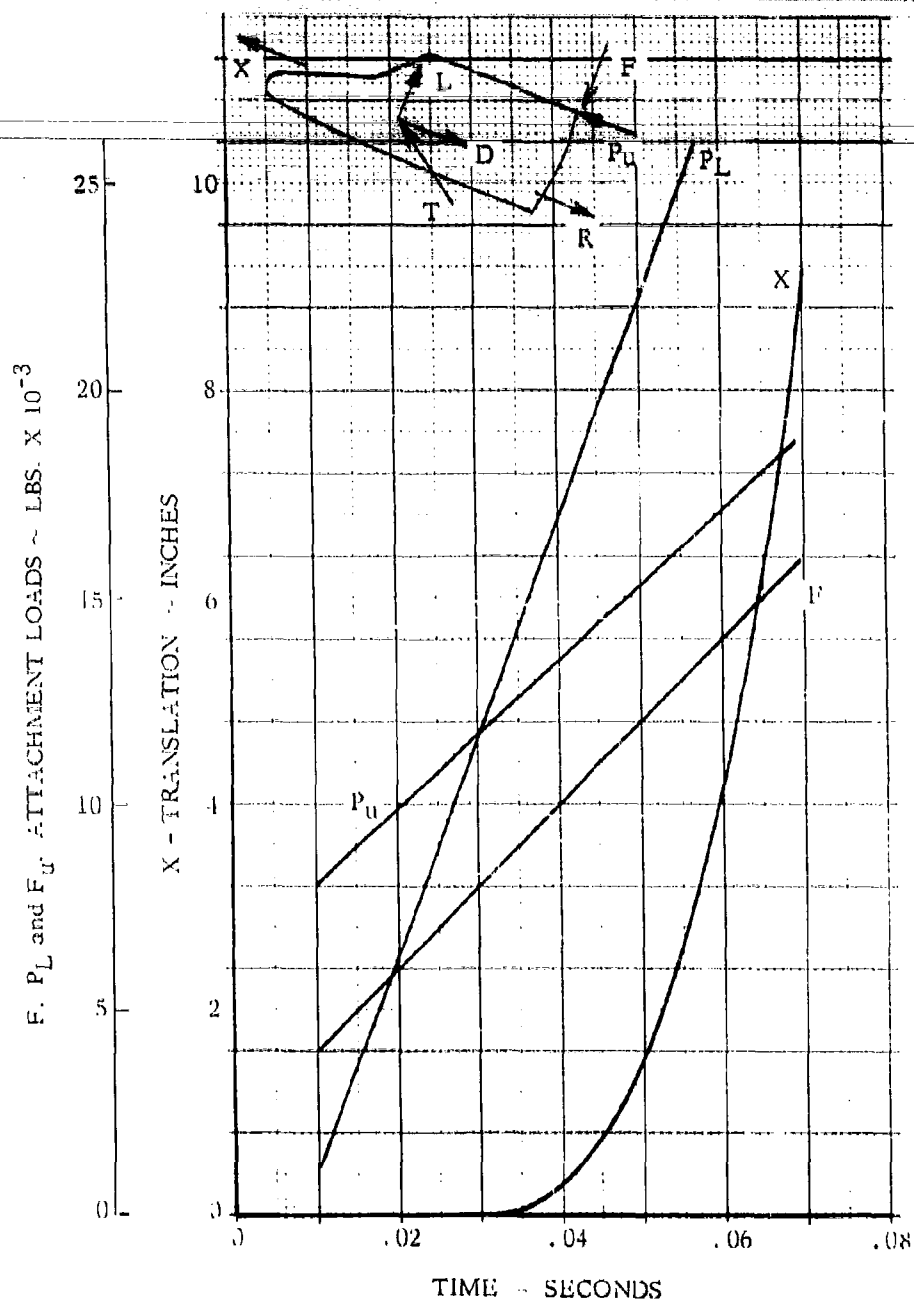


Figure 173 - Turnaround Capsule - Load Time History

nose and the afterbody. A continuous structural attachment was examined and found impractical due to the incomparability of pyrotechnic rupture devices with the hot truss structural concept. This was discussed in Section 7.2.2.1. In pod capsules such as the F-111, which utilize a monocoque construction, continuity of the flight vehicle and capsule are maintained up to the time of separation. Upon severance of the skin the lag in structural collapse of the forebody permits successful separation of the capsule. The radiation cooled panels and hot truss structure concept of the vehicles presented in this study is not compatible with this technique. In the present vehicle under study the structural frames of the capsule and the primary flight vehicle work independently of each other at all times.

The cutout in the primary vehicle structure reduces the beam depth of the primary vehicle forebody and therefore requires strengthening of the structure with a resultant weight penalty. An analysis of this weight penalty was made. Aerodynamic and inertia loads were determined for a three degree angle of attack at the maximum dynamic pressure condition. The geometry of the side frames and the force diagram is shown in Figure 174. The loads, sizes and weight estimate for the side frame members are presented in Table XX.

Side bracing is similar to that used in the separable nose concept and is not considered a weight penalty. The additional frame members present a minimum structural weight penalty applied to the pod capsule when compared with separable nose configuration which uses the capsule structure for the dual purpose of normal inflight and escape maneuver conditions.

The capsule is attached at the rear interface by four disconnect fittings on the main longerons which transmit loads between the capsule and the primary vehicle structure. In order to reduce the deflections between the capsule and the fuselage forebody an attachment between the forward part of the capsule and the primary vehicle structure is desirable. This attachment cannot be through the lower surface because of the ablation material. A single attachment is made from the foremost point of the pod truss structure through to the adjacent nose truss of the vehicle. Five main connections, make use of available structure without penetrating the lower surface heat shields.

The choice of pod geometry is influenced by the geometry of the main vehicle. In the present configuration the primary vehicle must shroud the pod lower surface in a smooth manner to prevent adverse aerodynamic heating effects during normal mission operation. These fairings must be such that they do not interfere with the separation.

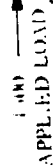


TABLE XX

## FRAME WEIGHT ESTIMATE

## PRIMARY VEHICLE WITH POD CAPSULE

Reference - Figure 174

MEMBER	LOAD	SIZE OF MEMBER	LENGTH	EST. WT.
B-1	- 3750	1.25 <sup>0</sup> /D x .035 Wall	34.2	1.30
1-H	- 600	.75 <sup>0</sup> /D x .022 Wall	29.0	.60
1-2	+16100	1.5 <sup>0</sup> /D x .035 Wall	36.0	1.37
2-C	-14505	2.0 <sup>0</sup> /D x .035 Wall	33.0	2.00
2-3	+23750	1.38 <sup>0</sup> /D x .058 Wall	10.0	.68
3-II	+22700	1.38 <sup>0</sup> /D x .058 Wall	24.0	1.70
3-4	- 4000	1.0 <sup>0</sup> /D x .028 Wall	18.0	.54
4-C	-30200	2.0 <sup>0</sup> /D x .083 Wall	36.0	5.10
4-5	- 4250	1.25 <sup>0</sup> /D x .049 Wall	22.0	1.15
5-II	+30400	1.75 <sup>0</sup> /D x .058 Wall	41.5	3.00
5-6	- 7100	1.50 <sup>0</sup> /D x .049	23.0	1.45
6-D	-40800	3.0 <sup>0</sup> /D x .083	40.0	8.60
6-7	- 5300	1.25 <sup>0</sup> /D x .049 Wall	22	1.15
7-II	+41680	2.0 <sup>0</sup> /D x .083 Wall	19	2.86
		Left Side		31.49
		Right Side		31.49

Total for Longitudinal Frame	62.98
Bolts and Pins	12.16
End Fittings (56 total) .55 Lb. each	30.80
Miscellaneous	12.00
<b>TOTAL FRAME WEIGHT</b>	<b>117.94</b>

To avoid the need to eject all these fairings, it is possible to provide sliding fillet joints which overlap the capsule outer radiation panels. It is also feasible to rotate the fillet around the capsule nose during the escape maneuver, without incurring damage to the capsule radiation structure.

Figure 175 presents a design of the separation interface for the pod capsule. A guided separation has been selected to prevent interference and binding. The guide which is located at the aft separation bulkhead is oriented such that the capsule moves up initially. As with the other escape capsules, the use of a guided separation insures the orderly disconnect of functional equipment, e.g., controls, environmental and fluid lines and electrical wiring, between the capsule and the primary flight vehicle. The rollers traverse up the guides during the time of escape rocket thrust buildup. When the lower rollers disengage from the capture section, the capsule is free to leave the knife edge rails along the line of the resultant force vector.

Mechanical latch type disconnects are used for the structural disconnects as shown in Figure 155. The disconnect devices are actuated by high pressure gas which activates all disconnect devices simultaneously. The escape rocket is ignited simultaneously with the operation of the disconnect devices.

A turnbuckle linkage at the nose latch is used to apply tension in the attachments thereby reducing installation tolerances between the pins and latches. The location of the latch release mechanisms within the controlled environment of the pilot compartment obviates the need for additional or alternative cooling techniques. The latches at the aft separation bulkhead are within the main vehicle contour and are protected during the normal mission operation by the radiation cooled outer surface, and are not exposed until the separation maneuver is initiated. The nose latch is afforded similar protection by the main vehicle structure. Provision is made to allow the nose latch assembly to rotate in order to align the "open jaw" gap with the direction of separation. Further provision is made to permit the outer radiation cooled panel at the nose to be displaced, it being attached to the turnbuckle linkage is rotated as the capsule is ejected.

The loading on the capsule was analyzed for both the normal flight condition and for separation at maximum dynamic pressure. For normal flight the maximum loading on the nose linkage is 10,000 lbs. The forces on the capsule during maximum dynamic pressure separation are shown schematically in Figure 176. The time history of the resultant forces normal and along the separation guide is given in Figure 177. The force  $P_z$  acts to move the capsule up the guides while the normal force  $P_T$  is reacted

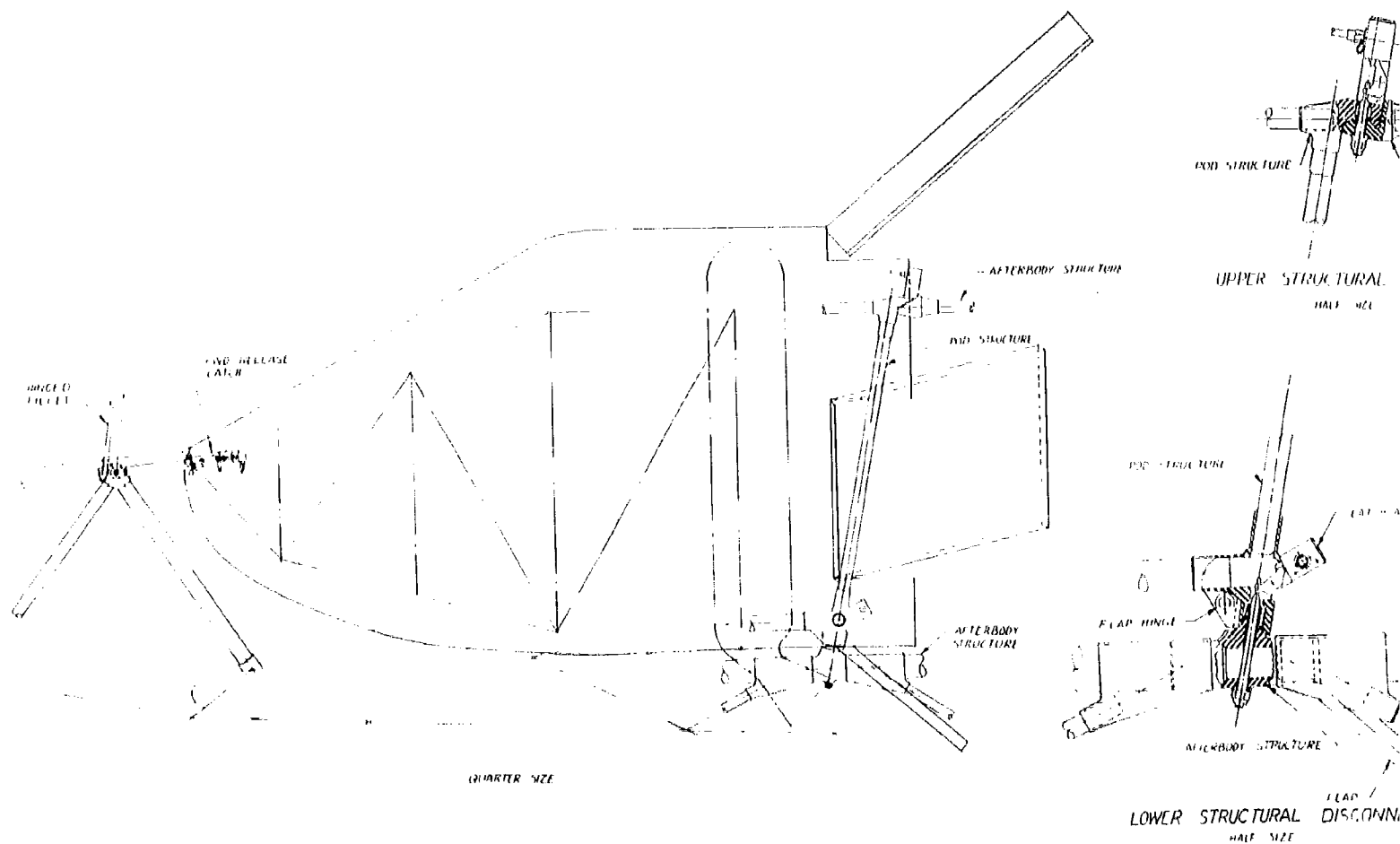


Figure 175 - Pod Capsule-Separation Interface Design

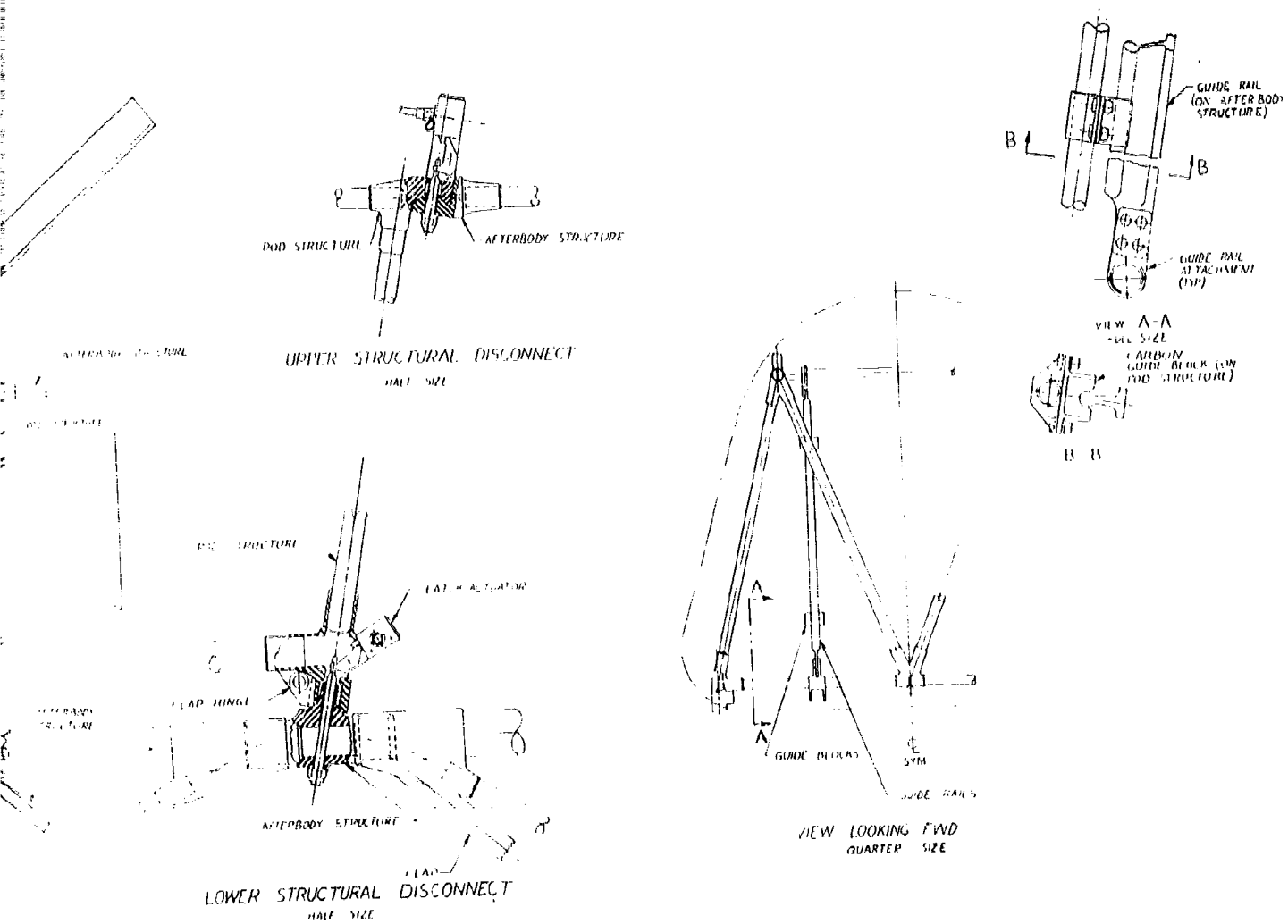


Figure 1-5 - Pod Capsule-Separation Interface Design

by the guides. The data in Figure 177 is presented for a guide length of 3.2 inches. Actually, the proposed guides for the pod capsule as shown in Figure 175 are only 2 inches long. The maximum load normal to the guide is 18,500 lbs. The disengagement of all functional equipment, controls, electrical lines and fluid lines between the capsule and main vehicle is accomplished during the guided disconnect phase. After clearing the guides, the capsule separates in the direction of the resultant force.



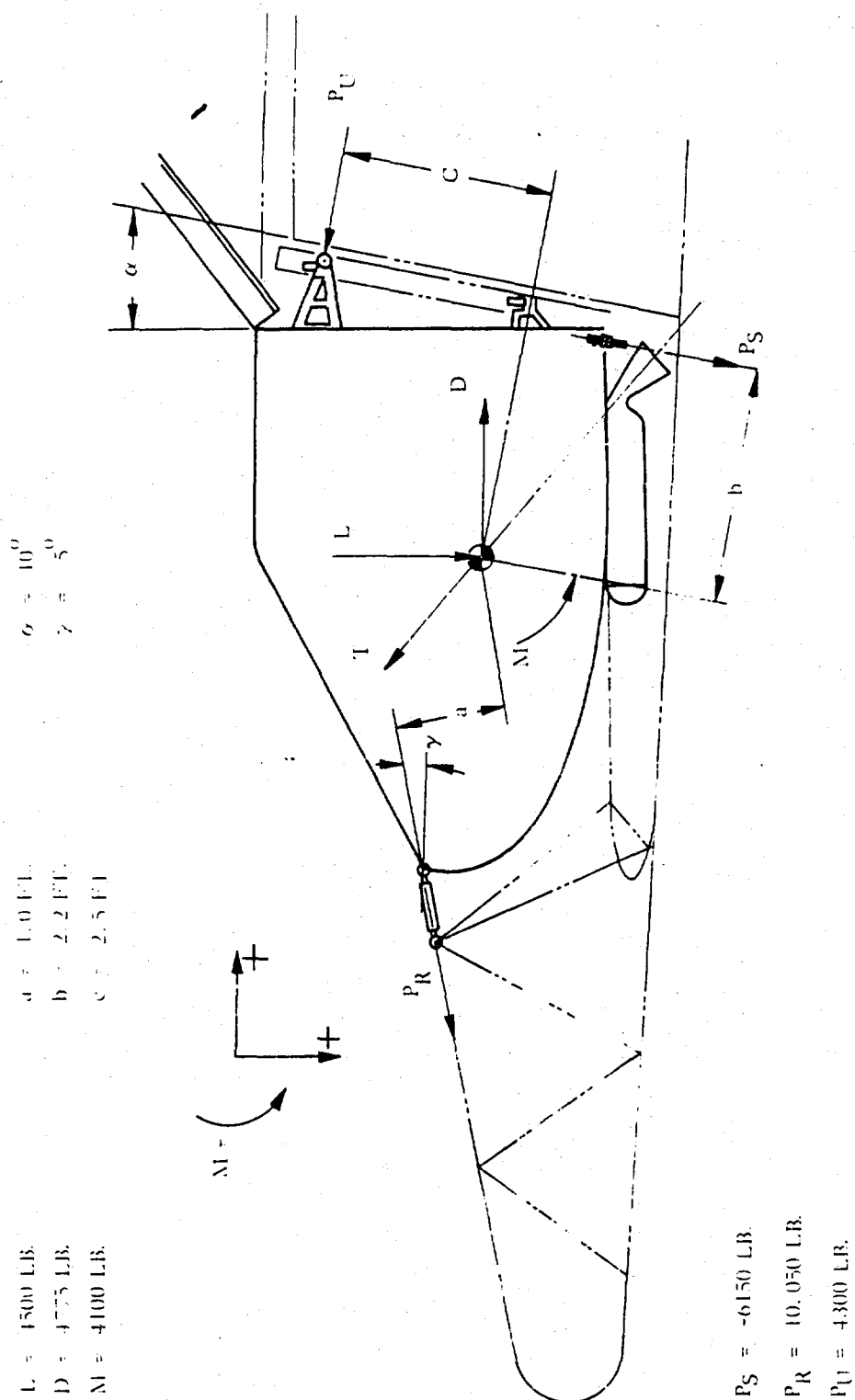


Figure 176 - Pod Capsule Loading Diagram

Best Available Copy

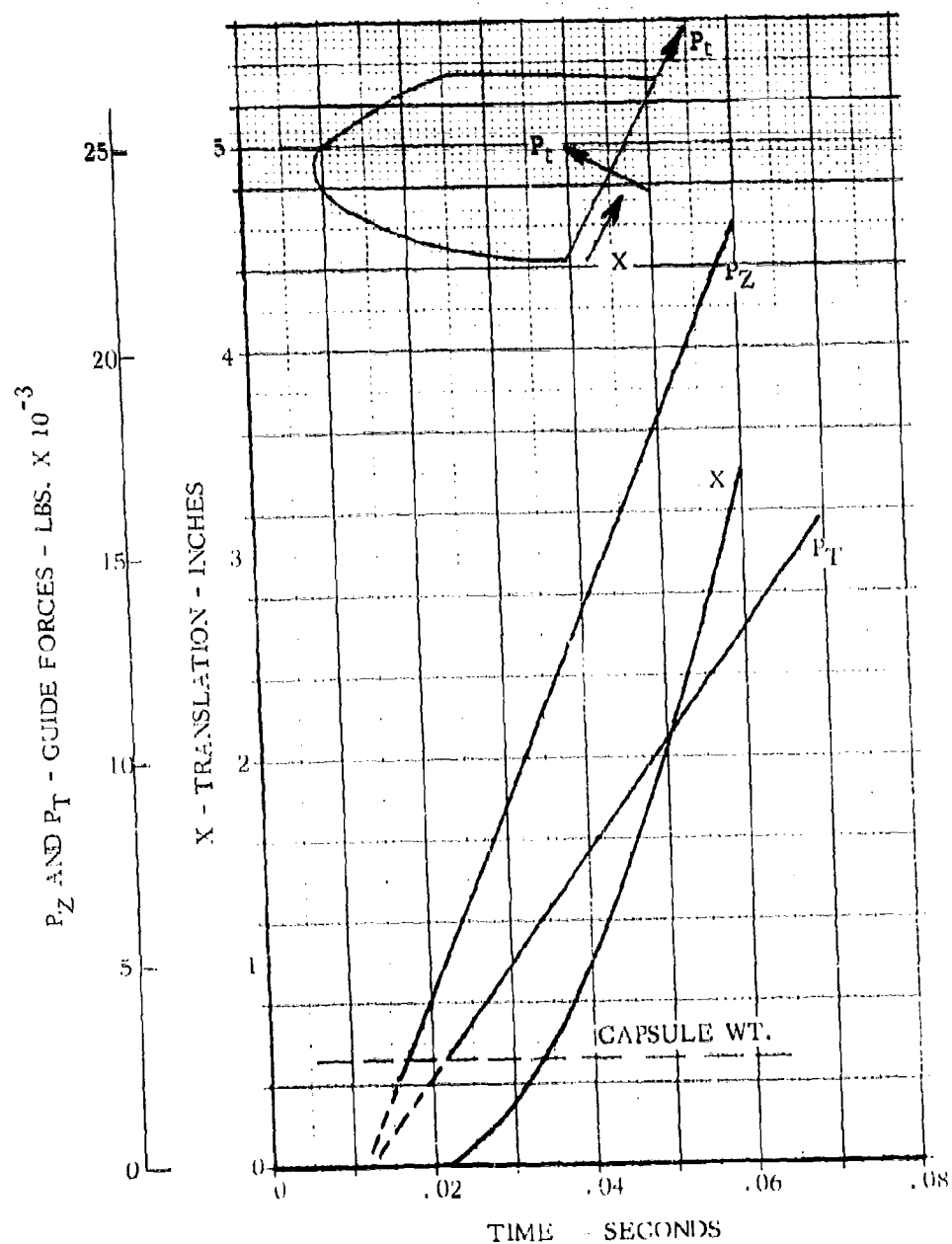


Figure 177 - Pod Capsule - Load Time History

## SECTION 8

### CONCLUSIONS

#### 8.1 CONCLUSIONS

1. The ballistic body, lifting body and pod capsules can achieve adequate escape performance throughout the mission profile of the primary flight vehicle.
2. The lifting body capsule attains temperatures in excess of the nominal allowable temperatures for wing loadings greater than approximately 35 psf. By taking advantage of the altitude margin generally associated with a lifting re-entry vehicle higher wing loading escape capsules could be utilized. Aerodynamic heating performance of the lifting body capsule is improved by lift modulation.
3. The high flap temperatures attained on all capsules would probably require the use of an ablation material. The desired material would be one which would only ablate during escape when the flaps are deflected.
4. Satisfactory performance can be achieved with either reaction or aerodynamic controls. The damping characteristics attained with reaction controls are poorer than with aerodynamic controls, however the load factors do not exceed human tolerance limits.
5. The ballistic body and turnaround capsules have recovery ceilings greater than the primary flight vehicle. The recovery ceilings of the lifting body and pod capsules are less than the primary flight vehicle.
6. Aerodynamic interference effects as measured by initial pitch rate are adequately handled by the control system.
7. The turnaround capsule exceeds human tolerance limits to acceleration during maximum dynamic pressure escape. At the low altitude escape conditions, unsatisfactory recovery conditions are attained.
8. The choice of the number of separation rockets is dependent upon the specific vehicle, its mission and a reliability analyses of both the vehicle and the separation rockets. Multiple rockets offer the advantage of using a single system to provide both separation impulse and de-orbit retro for orbit escape.

9. The escape rockets must be installed so that:
  - a. The resultant thrust goes through the C. G.
  - b. The loads are transferred to the primary structure
  - c. The rocket is thermally protected so that the propellant temperature does not exceed the allowable temperature.
  - d. The rocket thrust can be ducted out of the capsule.
10. Thrust gimbaling is not a necessity since the adverse effects of thrust misalignment do not lead to load factors in excess of human tolerance limits. Although some of the low altitude separation trajectories gave poor altitude performance due to thrust moment effects, it is believed that adjustments in trim angle of attack would eliminate this problem.
11. Separation interface and disconnect techniques which satisfy the requirement for escape during all mission phases were designed and have application to future configurations.
12. The high temperature environment associated with the radiation cooled hot truss structure makes the use of explosive disconnect devices extremely difficult. Isolated explosives such as shaped charges can be easily insulated, but the insulation of devices such as explosive bolts is quite complicated.
13. Mechanical disconnects can be designed to operate in the high temperature environment and were selected for the capsules of this study. A propellant actuated gas generator is used to supply high pressure gas to the disconnect devices as a means of actuation.
14. Realistic structural design techniques are applicable to all escape capsule concepts. The turnaround and pod capsule concepts cause structural complications with resultant weight penalties.
15. The optimum capsule configurations from the standpoint of structural and disconnect techniques at the separation interface are the separable nose concepts. These are optimum since the interface is a single plane which simplifies all disconnect problems.
16. The pod capsule concept and radiation cooled hot truss structure are not an ideal combination. It imposes a structural weight penalty on the frames of the forebody.

## GENERAL DYNAMICS | CONVAIR

17. The turnaround capsule configuration presents a very difficult and complex interface. Structural and disconnects techniques are feasible, however, they are complex and consequently penalize reliability and escape system weight much more than any of the other configurations.
18. Preliminary design studies including a structural design phase are required to establish a good weight comparison between the various capsule concepts.
19. A general analysis of primary flight vehicle attitude deviations prior to separation and flight path characteristics after separation should be made. The altitude prior to separation influences the loading during the disconnect phase. The primary vehicle flight path characteristics after separation determine what are good separation trajectories in terms of separation distance. This is especially significant in the boost phase where the thrust can vary from zero to full thrust and the altitude can vary including tumbling.
20. A study is required of the effect of vehicle structural concept on the structural criteria and disconnect techniques. The three basic structural concepts would be:
  - a. Truss
  - b. Semi-Monocoque
  - c. Monocoque Sandwich

Associated with the variable of structural concept is the additional variable of thermal protection. There are three possibilities.

- a. Hot
  - b. Passively Insulated
  - c. Ablation Cooled
21. An experimental investigation is necessary to determine the design criteria applicable to mechanical disconnect devices for operation in a high temperature environment. Data regarding materials, size and tolerances between moving parts should be determined.
22. A firm requirement exists for the development of explosives capable of operating in a high temperature environment.

## REFERENCES

1. Technical Documentary Report ASD-TDR-62-243, "Investigation of Stabilization and Control Systems for Application to Aerospace Vehicle Escape Capsules", June 1962.
2. Hoak, D. E., Carlsen, J. W., and Malthan, L. V., "USAF Stability and Control Datacom", Douglas Aircraft Company, Inc., October 1960, Revised July 1963.
3. Sarabia, Michael, F., "Aerodynamic Characteristics of a Blunt Half-Cone Entry Configuration at Mach Numbers from 3 to 6", NASA TMX-393, October 1950 (Confidential).
4. McShera, John T. Jr., and Wassum, Donald L., "Stability and Control Characteristics of a Low-Lift-Drag-Ratio Re-Entry Vehicle at Mach Numbers from 2.3 to 4.65", NASA TMX-891, July 1963 (Confidential).
5. Holtzclaw, Ralph W., "Static Stability and Control Characteristics of a Half-Cone Entry Configuration at Mach Numbers from 2.2 to 4.7", NASA TMX-619, March 1962 (Confidential).
6. Reed, James D. and Shaw, David S., "Static Stability and Control Characteristics of a Proposed Winged Re-Entry Vehicle at Mach Numbers of 1.5, 2.96, and 4.63", NASA TMX-676, April 1962 (Confidential).
7. Allen, Clyde, Q., "Low Speed Aerodynamic Characteristics of a Model of the DS-1 Glider", NASA TMX-573, August 1961 (Confidential).
8. Hassel, James L., Jr., "Investigation of the Low-Subsonic Stability and Control Characteristics of a 1/3 Scale Free-Flying Model of a Lifting-Body Re-Entry Configuration", NASA TMX-297, July 1960 (Confidential).
9. Air Force Office of Scientific Research Technical Report, AFOSR-109, Dynamics of Separating Bodies, Volume 1, Theoretical Analysis, AFOSR-106, Dynamics of Separating Bodies, Volume 2, Measurements at Mach 2, 4 and 5.
10. Thiokol Chemical Corporation "Rocket Propulsion Data (U)", September 1963 (Confidential).

11. Rocket Power Incorporated "Rocket Motors and Propellants", June 1962.
12. Chagaris, W. J., "Analysis of an Integrated Spacecraft Escape System", Douglas Aircraft Co. Paper #1860, April 1964.
13. McAdams, W. H. "Heat Transmission", McGraw-Hill, New York, N. Y., Third Edition 1954, 532 pp., Page 78.
14. Koelle, H. H. "Handbook of Astronautical Engineering", McGraw-Hill, New York, N. Y., First Edition 1961, page 19-13.
15. "Preliminary Thermal Analysis of the Dyna-Soar Glider", Boeing Airplane Company - Document No. D2-8113 - July 1961 (Confidential)
16. Seegmiller, H. L. and Reller, J. O. "An Experimental Investigation of the Convective Heat Transfer to a Blunt Lifting Body with Controls", NASA TMX-785, April 1963 - (Confidential)
17. Bertram, M. H., and Everhart, P. B., "An Experimental Study of the Pressure and Heat Transfer Distribution on a 70° Sweep Slab Delta Wing in Hypersonic Flow", NASA TR-R-153, 1963.
18. Newquist, B. A., Cassidy, M. D., Lindblom, C. W., and Sullivan, P. J., "Development of an Ejectable Nose Escape Capsule", WADC TR-59-493, ASTIA AD 241-590, June 1959.
19. Technical Report No. ASD-TR-61-671 "Structural Design Criteria for Stage Separation", January 1963.

**BIBLIOGRAPHY**

1. Kops, E. A., Mooney, W. E., Campbell, G. F., Webster, H. T., and Cohan, C. J., "Investigation of Crew Escape Techniques for Aerospace Vehicles Which Include Re-Entry and High Dynamic Pressure Phases", Air Force Report ASD-TDR-62-824, August 1962.
2. Mavriplis, F., "Investigation of Emergency Escape and Rescue Techniques for Multicrew Earth Orbital Vehicles". Air Force Report ASD-TDR-297, October 1962.
3. "Penetration Ballistics for a Shaped Charge Jet Forming Explosive Device", Ballistic Research Laboratory Report BRL-1184.
4. Romaine, Octave, "Why Explosive Devices", Space/Aeronautics, March 1963, pp. 96.
5. ASD-TDR-62-050, "Space Vehicle Attachment and Connection", November 1962.
6. Islinger, J. S., Armour Research Foundation, "Sealing Against Vacuum", Institute of Environmental Sciences, 1963 Annual Technical Meeting, pp. 481-490.
7. Redivine, D. A., "Design Study to Modify an MB-1 Pod into a Test Vehicle for Escape Capsules", WADD Technical Report 60-569, August 1960.



UNCLASSIFIED

AFFDL-TR-64-161

## Security Classification

## DOCUMENT CONTROL DATA - R&amp;D

(Security classification of title, body of abstract and indexing information must be entered when the overall report is classified)

## 1. ORIGINATING ACTIVITY (Corporate author)

General Dynamics/Astronautics

## 2a. REPORT SECURITY CLASSIFICATION

UNCLASSIFIED

## 2b. GROUP

N/A

## 3. REPORT TITLE

High Temperature Investigation of Various Crew Escape Concepts for the Reentry Flight Regime

## 4. DESCRIPTIVE NOTES (Type of report and inclusive dates)

Final Technical Report

## 5. AUTHOR(S) (Last name, first name, initial)

Cohan, C. J.

## 6. REPORT DATE

December 1964

## 7a. TOTAL NO. OF PAGES

283

## 7b. NO. OF REFS

19

## 8a. CONTRACT OR GRANT NO.

AF 33(615)-1131

## b. PROJECT NO.

1362

## c.

## d.

## 9a. ORIGINATOR'S REPORT NUMBER(S)

AFFDL-TR-64-161

## 9b. OTHER REPORT NO(S) (Any other numbers that may be assigned this report)

GD/A-DCB-64-076

## 10. AVAILABILITY/LIMITATION NOTICES

1. Qualified requesters may obtain copies of this report from DDC. 2. This report is not releasable to OTS.

## 11. SUPPLEMENTARY NOTES

NONE

## 12. SPONSORING MILITARY ACTIVITY

AF Flight Dynamics Laboratory  
Wright-Patterson AFB, Ohio

## 13. ABSTRACT

This report presents the results of an analysis of escape system separation techniques from a maximum heating re-entry trajectory. Four escape capsule concepts applicable to a lifting type flight vehicle were considered. These are (1) a separable-nose ballistic body; (2) a separable-nose lifting body; (3) a pod capsule; (4) a turnaround capsule. The objective of the study was to determine the applicability of these capsules and various thermal protection schemes to providing escape capability from the maximum heating point of a typical lifting re-entry trajectory. The compatibility of escape techniques developed at the maximum heating point with providing escape capability throughout the complete mission profile was also investigated. It was determined that all concepts except the turnaround capsule could provide escape capability throughout the mission. Separation interface structural criteria and disconnect techniques applicable to the four capsule configurations are presented.

DD FORM 1473  
1 JAN 64

284

UNCLASSIFIED

Security Classification

14. KEY WORDS		LINK A		LINK B		LINK C	
		ROLE	WT	ROLE	WT	ROLE	WT
1. Crew Escape							
2. Reentry Flight Regime							
3. High Temperature Requirements							

## INSTRUCTIONS

1. **ORIGINATING ACTIVITY:** Enter the name and address of the contractor, subcontractor, grantee, Department of Defense activity or other organization (*corporate author*) issuing the report.
- 2a. **REPORT SECURITY CLASSIFICATION:** Enter the overall security classification of the report. Indicate whether "Restricted Data" is included. Marking is to be in accordance with appropriate security regulations.
- 2b. **GROUP:** Automatic downgrading is specified in DoD Directive 5200.10 and Armed Forces Industrial Manual. Enter the group number. Also, when applicable, show that optional markings have been used for Group 3 and Group 4 as authorized.
3. **REPORT TITLE:** Enter the complete report title in all capital letters. Titles in all cases should be unclassified. If a meaningful title cannot be selected without classification, show title classification in all capitals in parentheses immediately following the title.
4. **DESCRIPTIVE NOTES:** If appropriate, enter the type of report, e.g., interim, progress, summary, annual, or final. Give the inclusive dates when a specific reporting period is covered.
5. **AUTHOR(S):** Enter the name(s) of author(s) as shown on or in the report. Enter last name, first name, middle initial. If military, show rank and branch of service. The name of the principal author is an absolute minimum requirement.
6. **REPORT DATE:** Enter the date of the report as day, month, year, or month, year. If more than one date appears on the report, use date of publication.
- 7a. **TOTAL NUMBER OF PAGES:** The total page count should follow normal pagination procedures, i.e., enter the number of pages containing information.
- 7b. **NUMBER OF REFERENCES:** Enter the total number of references cited in the report.
- 8a. **CONTRACT OR GRANT NUMBER:** If appropriate, enter the applicable number of the contract or grant under which the report was written.
- 8b, c, & 8d. **PROJECT NUMBER:** Enter the appropriate military department identification, such as project number, subproject number, system numbers, task number, etc.
- 9a. **ORIGINATOR'S REPORT NUMBER(S):** Enter the official report number by which the document will be identified and controlled by the originating activity. This number must be unique to this report.
- 9b. **OTHER REPORT NUMBER(S):** If the report has been assigned any other report numbers (*either by the originator or by the sponsor*), also enter this number(s).
10. **AVAILABILITY/LIMITATION NOTICES:** Enter any limitations on further dissemination of the report, other than those

imposed by security classification, using standard statements such as:

- (1) "Qualified requesters may obtain copies of this report from DDC."
- (2) "Foreign announcement and dissemination of this report by DDC is not authorized."
- (3) "U. S. Government agencies may obtain copies of this report directly from DDC. Other qualified DDC users shall request through \_\_\_\_\_."
- (4) "U. S. military agencies may obtain copies of this report directly from DDC. Other qualified users shall request through \_\_\_\_\_."
- (5) "All distribution of this report is controlled. Qualified DDC users shall request through \_\_\_\_\_."

If the report has been furnished to the Office of Technical Services, Department of Commerce, for sale to the public, indicate this fact and enter the price, if known.

11. **SUPPLEMENTARY NOTES:** Use for additional explanatory notes.
12. **SPONSORING MILITARY ACTIVITY:** Enter the name of the departmental project office or laboratory sponsoring (paying for) the research and development. Include address.
13. **ABSTRACT:** Enter an abstract giving a brief and factual summary of the document indicative of the report, even though it may also appear elsewhere in the body of the technical report. If additional space is required, a continuation sheet shall be attached.

It is highly desirable that the abstract of classified reports be unclassified. Each paragraph of the abstract shall end with an indication of the military security classification of the information in the paragraph, represented as (TS), (S), (C), or (U).

There is no limitation on the length of the abstract. However, the suggested length is from 150 to 225 words.

14. **KEY WORDS:** Key words are technically meaningful terms or short phrases that characterize a report and may be used as index entries for categories regarding the report. Key words must be selected so that no additional classification is required. Identifiers, such as equipment model designation, trade name, military project code name, geographic location, may be used as key words but will be followed by an indication of technical context. The assignment of links, rules, and weights is optional.